

# P2X7 Receptor Function in Microglia in Relation to Glaucoma

**Matthew Felgate**

**A THESIS PRESENTED FOR THE DEGREE OF DOCTOR OF  
PHILOSOPHY AT THE UNIVERSITY OF EAST ANGLIA  
NORWICH, UK**

**SCHOOL OF PHARMACY**

**2019**

® This copy of the thesis has been supplied on the condition that anyone who consults it is understood to recognise that its copyright rests with the author and the use of any information derived there from must be in accordance with current UK copyright Law. In addition, any quotation or extract must include full attribution.

## Abstract

**Purpose:** The purpose of this research was to investigate the role of P2X7 in microglial function, in relation to glaucoma. Specifically, a P2X7 knockout (K/O) microglial cell line was generated and used to explore the responses of purinergic stimulation, including  $[Ca^{2+}]_i$  signalling, cytotoxicity, and IL-1 $\beta$  production and release. Purinergic mediated consequences of oxygen glucose deprivation were also briefly explored.

**Methods:** P2X7 K/O microglial cells were generated using CRISPR gene editing technology on BV-2 microglia, and tested for P2X7 expression using flow cytometry, gDNA PCR, qRT-PCR and Western blotting.  $[Ca^{2+}]$  responses to purinergic agonist stimulation were measured in Fura-2 loaded BV-2 and P2X7 K/O cells. Viability and cytotoxicity of purinergic stimulated BV-2 cells were assessed with MTS, LDH and caspase-3/7 staining assays. IL-1 $\beta$  mRNA and protein expression was measured with qRT-PCR and ELISAs respectively. BV-2 cells were subject to OGD using a custom incubator

**Results:** CRISPR modification generated a cell line, which upon analysis demonstrated knockout of P2X7 protein expression. Purinergic agonists demonstrated a multifaceted  $[Ca^{2+}]_i$  response mediated by multiple receptors including P2X7, P2X4, P2Y2 and P2Y6, with P2X7 giving a sustained rise in  $[Ca^{2+}]_i$ . Microglia were sensitive to ATP-induced cytotoxicity mediated by P2X7. An initial lower level of ATP-induced toxicity was P2X7-independent and mediated by ADP. ATP treatment was a sufficient priming stimulus for IL-1 $\beta$  mRNA and protein and P2X7 was responsible for IL-1 $\beta$  release upon subsequent, in a P2X7-dependent manner.

**Conclusions:** The generation of a P2X7 K/O microglial cell line has provided a wealth of information that can contribute to the understanding of the role of microglia in the pathophysiological mechanisms in glaucoma.

## **Access Condition and Agreement**

Each deposit in UEA Digital Repository is protected by copyright and other intellectual property rights, and duplication or sale of all or part of any of the Data Collections is not permitted, except that material may be duplicated by you for your research use or for educational purposes in electronic or print form. You must obtain permission from the copyright holder, usually the author, for any other use. Exceptions only apply where a deposit may be explicitly provided under a stated licence, such as a Creative Commons licence or Open Government licence.

Electronic or print copies may not be offered, whether for sale or otherwise to anyone, unless explicitly stated under a Creative Commons or Open Government license. Unauthorised reproduction, editing or reformatting for resale purposes is explicitly prohibited (except where approved by the copyright holder themselves) and UEA reserves the right to take immediate 'take down' action on behalf of the copyright and/or rights holder if this Access condition of the UEA Digital Repository is breached. Any material in this database has been supplied on the understanding that it is copyright material and that no quotation from the material may be published without proper acknowledgement.

## List of Contents

<b>Chapter 1</b> .....	<b>1</b>
<b>Introduction</b> .....	<b>1</b>
<b>1.1 The Retina</b> .....	<b>1</b>
1.1.1 Non neuronal retinal cells .....	3
1.1.2 Retinal glia .....	4
1.1.3 The neuronal retina .....	5
<b>1.2 Glaucoma</b> .....	<b>8</b>
<b>1.3 Microglia</b> .....	<b>10</b>
1.3.1 Retinal microglia .....	13
1.3.2 Retinal microglia in glaucoma .....	14
<b>1.4 Purinergic signalling</b> .....	<b>17</b>
1.4.1 Purinergic receptors .....	20
1.4.2 Adenosine receptor family .....	21
1.4.3 P2Y receptor family .....	22
1.4.4 P2X receptor family .....	30
1.4.5 Purinergic receptors in microglia .....	41
1.4.6 Purinergic signalling in glaucoma .....	43
<b>1.5 Calcium Signalling</b> .....	<b>45</b>
1.5.1 Intracellular calcium homeostasis .....	45
1.5.2 Calcium second messenger signalling .....	45
1.5.3 Purinergic mediated Ca <sup>2+</sup> signalling .....	49
<b>1.6 Cytokines</b> .....	<b>49</b>
1.6.1 Interleukin-1 $\beta$ .....	50
1.6.2 IL-1 $\beta$ in microglia .....	53
1.6.3 IL-1 $\beta$ in glaucoma .....	54
<b>1.7 Cell death</b> .....	<b>55</b>
1.7.1 Apoptosis .....	56
1.7.2 Necrosis .....	58
1.7.3 Pyroptosis .....	59
1.7.4 Necroptosis .....	61
1.7.5 P2X7R mediated cell death .....	62
1.7.6 Cell death in Glaucoma .....	63
1.7.7 Cell death in microglia .....	64
<b>1.8 Aims and Objectives</b> .....	<b>65</b>
<b>Chapter 2</b> .....	<b>67</b>
<b>Materials and methods</b> .....	<b>67</b>
<b>2.1 Cell culture</b> .....	<b>67</b>
<b>2.2 Transfection</b> .....	<b>69</b>
<b>2.3 Single cell clonal expansion</b> .....	<b>70</b>
<b>2.4 Real time Ca<sup>2+</sup> response measurements</b> .....	<b>71</b>
<b>2.5 MTS</b> .....	<b>73</b>
<b>2.6 LDH</b> .....	<b>75</b>
<b>2.7 Caspase 3/7 activation live cell imaging</b> .....	<b>77</b>
<b>2.8 Hoescht &amp; Caspase 3/7 positive cell counting</b> .....	<b>78</b>
<b>2.9 Genomic DNA extraction</b> .....	<b>79</b>
<b>2.10 Non-quantitative gDNA PCR</b> .....	<b>80</b>
<b>2.11 RNA extraction</b> .....	<b>80</b>

2.12 cDNA synthesis .....	81
2.13 Rotorgene qRT-PCR .....	82
2.14 Taqman® qRT-PCR.....	84
2.15 ELISA.....	85
2.16 Flow cytometry.....	87
2.17 BCA.....	88
2.18 Western Blot.....	88
2.19 Oxygen glucose deprivation.....	90
2.20 Data Analysis.....	90
<b>Chapter 3 .....</b>	<b>91</b>
<b>Generation and characterisation of a P2X7 receptor knockout microglial cell line.....</b>	<b>91</b>
<b>3.1 Introduction.....</b>	<b>91</b>
<b>3.2 Results.....</b>	<b>94</b>
3.2.1 Optimisation of transfection conditions for BV-2 microglia.....	94
3.2.2 Design of mP2X7 exon2 targeting crRNA sequences.....	98
3.2.3 P2X7R flow cytometry screening of blasticidin resistant CRISPR treated BV-2 cells.....	101
3.2.4 Single cell clonal expansion of P2X7 deficient BV-2 populations .....	102
3.2.5 P2X7 flow cytometry screening of single cell clones .....	103
3.2.6 P2X7 mediated Fura-2 Ca <sup>2+</sup> screening of generated clone populations.....	106
3.2.7 P2X7R Genomic DNA region sequencing.....	107
3.2.8 qRT-PCR analysis of purinergic receptor expression in BV-2 and BV-2 P2X7 K/O cells .....	113
3.2.9 Western Blot analysis of total cell P2X7 protein .....	115
<b>3.3 Discussion .....</b>	<b>116</b>
<b>Chapter 4 .....</b>	<b>122</b>
<b>P2X7, along with P2X4 and P2Y2 receptors mediate ATP stimulated intracellular Ca<sup>2+</sup> responses in resting microglia.....</b>	<b>122</b>
<b>4.1 Introduction.....</b>	<b>122</b>
<b>4.2 Results.....</b>	<b>124</b>
4.2.1 ATP mediated Ca <sup>2+</sup> responses in BV-2 microglia.....	124
4.2.2 ATP mediated Ca <sup>2+</sup> responses in P2X7 K/O Clone-14 microglia .....	126
4.2.3 AZ10606120 antagonism of ATP mediated Ca <sup>2+</sup> responses in BV-2 microglia .....	128
4.2.4 BzATP mediated Ca <sup>2+</sup> responses in BV-2 microglia.....	130
4.2.5 BzATP mediated Ca <sup>2+</sup> responses in P2X7 K/O Clone-14 microglia.....	130
4.2.6 AZ10606120 antagonism of BzATP mediated Ca <sup>2+</sup> responses in BV-2 microglia .....	133
4.2.7 PSB12062 antagonism of ATP mediated Ca <sup>2+</sup> responses in P2X7 K/O Clone-14 microglia.....	135
4.2.8 5-BDBD antagonism of ATP mediated Ca <sup>2+</sup> responses in P2X7 K/O Clone-14 microglia.....	137
4.2.9 AR-C 118925XX antagonism of UTP mediated Ca <sup>2+</sup> responses in BV-2 microglia .....	139
4.2.10 ADP mediated Ca <sup>2+</sup> responses in BV-2 microglia.....	141
4.2.11 ADP mediated Ca <sup>2+</sup> responses in P2X7 K/O Clone-14 microglia .....	141
4.2.12 MRS2179 antagonism of ADP mediated Ca <sup>2+</sup> responses in BV-2 microglia..	144
4.2.13 MRS2578 antagonism of ADP mediated Ca <sup>2+</sup> responses in BV-2 microglia..	144
4.2.14 PSB0739 antagonism of ADP mediated Ca <sup>2+</sup> responses in BV-2 microglia...	147
<b>4.3 Discussion .....</b>	<b>149</b>

<b>Chapter 5 .....</b>	<b>157</b>
<b>P2X7 receptor mediates viability and cell death of resting microglia .....</b>	<b>157</b>
<b>5.1 Introduction .....</b>	<b>157</b>
<b>5.2 Results .....</b>	<b>159</b>
5.2.1 Cell viability/death in response to ATP in BV-2 microglia .....	159
5.2.2 Caspase 3/7 activation in response to ATP in BV-2 microglia.....	160
5.2.3 Cell viability/death in response to ATP P2X7 K/O Clone-14 microglia .....	162
5.2.4 BzATP dose response in BV-2 microglia .....	164
5.2.5 P2X7 receptor antagonism with ATP stimulation in BV-2 microglia.....	165
5.2.6 P2X4 receptor antagonism with ATP stimulation in BV-2 microglia.....	167
5.2.7 P2Y2 receptor antagonism with ATP stimulation in BV-2 microglia.....	170
5.2.8 ATPyS dose response in BV-2 microglia .....	171
5.2.9 ATP metabolite dose responses in BV-2 microglia.....	172
5.2.10 P2Y1 receptor antagonism with ADP stimulation in BV-2 microglia.....	173
5.2.11 P2Y12 receptor antagonism with ADP stimulation in BV-2 microglia .....	174
5.2.12 Uracil-nucleotide dose responses in BV-2 microglia.....	175
<b>5.3 Discussion .....</b>	<b>177</b>
<b>Chapter 6 .....</b>	<b>187</b>
<b>Prole of P2X7 receptor in purinergic mediated IL-1<math>\beta</math> mRNA expression, protein processing and release in microglia .....</b>	<b>187</b>
<b>6.1 Introduction .....</b>	<b>187</b>
<b>6.2 Results .....</b>	<b>189</b>
6.2.1 LPS priming of BV-2 microglia .....	189
6.2.2 P2X7 in IL-1 $\beta$ release in BV-2 and clone-14 microglia.....	192
6.2.3 Purinergic priming of BV-2 microglia .....	195
<b>6.3 Discussion .....</b>	<b>201</b>
<b>Chapter 7 .....</b>	<b>206</b>
<b>P2X7 role in viability and IL-1<math>\beta</math> regulation in simulated oxygen glucose deprived (OGD) microglia .....</b>	<b>206</b>
<b>7.1 Introduction .....</b>	<b>206</b>
<b>7.2 Results .....</b>	<b>208</b>
7.2.1 OGD stimulated MTS viability and LDH release in BV-2 microglia .....	208
7.2.2 MTS viability in BV-2 and Clone-14 microglia following 3hr OGD stimulation .....	209
7.2.3 IL-1 $\beta$ mRNA expression in BV-2 microglia following 3 hours of complete OGD .....	210
<b>7.3 Discussion .....</b>	<b>211</b>
<b>Chapter 8 .....</b>	<b>213</b>
<b>General Discussion .....</b>	<b>213</b>
<b>Conclusions .....</b>	<b>220</b>
<b>List of Abbreviations .....</b>	<b>221</b>
<b>References .....</b>	<b>227</b>

## LIST OF FIGURES AND TABLES

### Chapter 1

<b>Figure 1.1</b>	Topographical view of the human retina	2
<b>Figure 1.2</b>	Diagram of the functional organisation of retinal layers and retinal cell types	3
<b>Figure 1.3</b>	Diagram of human rod and cone cells	6
<b>Figure 1.4</b>	Diagram of the flow of humor and the iridocorneal angle in glaucoma	9
<b>Figure 1.5</b>	Molecular structure of ATP	18
<b>Figure 1.6</b>	Overview of receptor families, endogenous ligands and ectonucleotidases that constitute purinergic signalling	20
<b>Figure 1.7</b>	X-ray crystal structure of P2Y <sub>12</sub> with antagonist AZD1283 bound	23
<b>Figure 1.8</b>	Representation of the P2XR superfamilies characteristic trimeric structure, in its closed channel and open channel forms with ATP bound	32
<b>Figure 1.9</b>	Schematic view of exons expressed (1-13) in known P2X <sub>7</sub> splice variants	39
<b>Figure 1.10</b>	Diagram of cellular Ca <sup>2+</sup> homeostasis and mobilisation mechanisms	48
<b>Figure 1.11</b>	Schematic diagram of NLRP3 inflammasome assembly	51
<b>Figure 1.12</b>	Diagram of the canonical and non-canonical inflammasome pathways involved in pyroptosis	60

### Chapter 2

<b>Table 2.1</b>	Experimental seeding densities	68
<b>Figure 2.1</b>	96 well plate clonal expansion dilution method	70
<b>Figure 2.2</b>	Fura-2 ratiometric emission profile	72
<b>Table 2.2</b>	ETotal buffer composition	72
<b>Figure 2.3</b>	MTS oxidization pathway	74
<b>Figure 2.4</b>	Linear absorption of MTS in BV-2 cells	75
<b>Figure 2.5</b>	LDH/Formazan production pathway	76
<b>Figure 2.6</b>	Diagrammatic representation of Caspase 3/7 imaging	77
<b>Figure 2.7</b>	Cell counting using Fiji software	78
<b>Table 2.3</b>	Rotorgene qRT-PCR custom primer sequences	82
<b>Figure 2.8</b>	Rotorgene qRT-PCR custom primer validation	83
<b>Table 2.4</b>	Taqman qRT-PCR reaction mixture components	84
<b>Table 2.5</b>	Taqman qRT-PCR primer sequence IDs	85
<b>Figure 2.9</b>	Flow cytometry gating method	87

### Chapter 3

<b>Figure 3.1</b>	Representative diagram of CRISPR/Cas9 assembly	92
<b>Table 3.1</b>	Table of transfection reagents tested	94
<b>Figure 3.2</b>	BV-2 cell resting morphology	95
<b>Figure 3.3</b>	Representative images of BV-2 morphology following transfection reagent testing	96
<b>Figure 3.4</b>	Brightfield and fluorescent images of rP2X <sub>7</sub> -GFP expressing BV-2 microglia	97
<b>Figure 3.5</b>	pHCSVblast-Cas9 plasmid map	98
<b>Table 3.2</b>	Predicted crRNA sequences	99
<b>Figure 3.6</b>	Base sequence of mP2X <sub>7</sub> exon 2	100

<b>Figure 3.7</b>	P2X7 flow cytometry of blasticidin resistant BV-2 microglia	101
<b>Figure 3.8</b>	P2X7 flow cytometry of single cell clone colonies	103
<b>Table 3.3</b>	Surface expression of P2X7 on single cell colonies	105
<b>Figure 3.9</b>	Area under the curve Fura-2 Ca <sup>2+</sup> responses in P2X7 stimulate knockout clones	106
<b>Figure 3.10</b>	Gel separation of mP2X7 PCR products from BV-2 and clone-14 cells	107
<b>Figure 3.11</b>	BV-2 mP2X7 exon 2 gDNA chromatogram	109
<b>Figure 3.12</b>	Aligned sequences of BV-2 and <i>Mus musculus</i> (mm10) P2X7 exon2 gDNA	110
<b>Figure 3.13</b>	Clone-14 mP2X7 exon 2 gDNA chromatogram	111
<b>Figure 3.14</b>	Expression of purinergic receptor mRNA in BV-2 and clone-14 microglial cells	112
<b>Table 3.5</b>	Aligned sequences of clone-14 and BV-2 P2X7 exon2 gDNA	114
<b>Figure 3.15</b>	Western blot of P2X7 and $\beta$ -actin protein in BV-2 and clone 14 microglial cells and J774 macrophages	115
 <b>Chapter 4</b>		
<b>Figure 4.1</b>	ATP mediated Ca <sup>2+</sup> responses in BV-2 microglia	125
<b>Figure 4.2</b>	ATP mediated Ca <sup>2+</sup> responses in P2X7 K/O clone-14 microglia	127
<b>Figure 4.3</b>	AZ10606120 antagonism of ATP mediated Ca <sup>2+</sup> responses in BV-2 microglia	129
<b>Figure 4.4</b>	BzATP mediated Ca <sup>2+</sup> responses in BV-2 microglia	131
<b>Figure 4.5</b>	BzATP mediated Ca <sup>2+</sup> responses in P2X7 K/O clone-14 microglia	132
<b>Figure 4.6</b>	AZ10606120 antagonism of ATP mediated Ca <sup>2+</sup> responses in P2X7 K/O clone-14 microglia	134
<b>Figure 4.7</b>	PSB12062 antagonism of ATP mediated Ca <sup>2+</sup> responses in P2X7 K/O clone-14 microglia	136
<b>Figure 4.8</b>	5-BDBD antagonism of ATP mediated Ca <sup>2+</sup> responses in P2X7 K/O clone-14 microglia	138
<b>Figure 4.9</b>	UTP mediated Ca <sup>2+</sup> responses in BV-2 microglia	139
<b>Figure 4.10</b>	AR-C118925XX antagonism of UTP mediated Ca <sup>2+</sup> responses in BV-2 microglia	140
<b>Figure 4.11</b>	ADP mediated Ca <sup>2+</sup> responses in BV-2 microglia	142
<b>Figure 4.12</b>	ADP mediated Ca <sup>2+</sup> responses in P2X7 K/O clone-14 microglia	143
<b>Figure 4.13</b>	MRS2179 antagonism of ADP mediated Ca <sup>2+</sup> responses in BV-2 microglia	145
<b>Figure 4.14</b>	MRS25789 antagonism of ADP mediated Ca <sup>2+</sup> responses in BV-2 microglia	146
<b>Figure 4.15</b>	PSB0739 antagonism of ADP mediated Ca <sup>2+</sup> responses in BV-2 microglia	148
 <b>Chapter 5</b>		
<b>Figure 5.1</b>	MTS cell viability in BV-2 microglia in response to ATP stimulation	159
<b>Figure 5.2</b>	LDH release in BV-2 microglia in response to ATP stimulation	160
<b>Figure 5.3</b>	% of Caspase-3/7 positively stained BV-2 microglia in response to ATP stimulation	161

<b>Figure 5.4</b>	MTS cell viability in BV-2 and clone-14 microglia in response to ATP stimulation	162
<b>Figure 5.5</b>	% of Caspase-3/7 positively stained clone-14 microglia in response to ATP stimulation	163
<b>Figure 5.6</b>	MTS cell viability in BV-2 microglia in response to BzATP stimulation	164
<b>Figure 5.7</b>	LDH release in BV-2 microglia in response to BzATP stimulation	165
<b>Figure 5.8</b>	MTS cell viability in BV-2 microglia in response to AZ10606120 stimulation	166
<b>Figure 5.9</b>	MTS cell viability in BV-2 microglia in response to ATP stimulation with AZ10606120 antagonism	167
<b>Figure 5.10</b>	MTS cell viability in BV-2 microglia in response to ATP stimulation with PSB12062 antagonism	168
<b>Figure 5.11</b>	MTS cell viability in BV-2 microglia in response to ATP stimulation with 5-BDBD antagonism	169
<b>Figure 5.12</b>	MTS cell viability in BV-2 microglia in response to ATP stimulation with AR-C118925XX antagonism	170
<b>Figure 5.13</b>	MTS cell viability in BV-2 microglia in response to ATP <sub>γ</sub> S stimulation	171
<b>Figure 5.14</b>	MTS cell viability in BV-2 microglia in response to ADP stimulation	172
<b>Figure 5.15</b>	MTS cell viability in BV-2 microglia in response to adenosine stimulation	173
<b>Figure 5.16</b>	MTS cell viability in BV-2 microglia in response to ADP stimulation with MRS2179 antagonism	174
<b>Figure 5.17</b>	MTS cell viability in BV-2 microglia in response to ADP stimulation with PSB0739 antagonism	174
<b>Figure 5.18</b>	MTS cell viability in BV-2 microglia in response to UTP stimulation	175
<b>Figure 5.19</b>	MTS cell viability in BV-2 microglia in response to UDP stimulation	176
 <b>Chapter 6</b>		
<b>Figure 6.1</b>	LDH release time course in BV-2 microglia in response to LPS stimulation	189
<b>Figure 6.2</b>	IL-1 $\beta$ mRNA expression time course in LPS stimulated BV-2 microglia	190
<b>Figure 6.3</b>	IL-1 $\beta$ mRNA expression in LPS stimulated BV-2 microglia after 24 hours	191
<b>Figure 6.4</b>	Intracellular IL-1 $\beta$ protein expression in LPS primed BV-2 and P2X7 K/O clone-14 microglia after 4 hours	191
<b>Figure 6.5</b>	IL-1 $\beta$ release from LPS primed and ATP stimulated BV-2 microglia	192
<b>Figure 6.6</b>	IL-1 $\beta$ release from LPS primed and ATP stimulated P2X7 K/O clone-14 microglia	193
<b>Figure 6.7</b>	AZ10606120 antagonism of IL-1 $\beta$ release LPS primed and ATP stimulated BV-2 microglia	194
<b>Figure 6.8</b>	IL-1 $\beta$ mRNA expression in purinergic stimulated BV-2 microglia over 24 hours	196
<b>Figure 6.9</b>	IL-1 $\beta$ mRNA expression in purinergic stimulated P2X7 K/O clone-14 microglia at 24 hours	197

<b>Figure 6.10</b>	AZ10606120 antagonism of IL-1 $\beta$ release ATP primed and ATP stimulated BV-2 microglia	198
<b>Figure 6.11</b>	Intracellular IL-1 $\beta$ protein in BV-2 microglia following ATP priming	199
<b>Figure 6.12</b>	IL-1 $\beta$ release from LPS primed and ATP stimulated BV-2 microglia	200
<b>Chapter 7</b>		
<b>Figure 7.1</b>	MTS cell viability and LDH release in BV-2 microglia in response to OGD treatment time course	208
<b>Figure 7.2</b>	MTS cell viability in BV-2 and P2X7 K/O clone-14 microglia in response to 3hr OGD treatment	209
<b>Figure 7.3</b>	IL-1 $\beta$ mRNA expression in BV-2 microglia following 3hr OGD treatment	210

## **Acknowledgements**

Undertaking a PhD is both the challenge and opportunity of a lifetime, one that I was lucky enough to pursue. My time at UEA was not without difficulty, but ultimately proved extremely rewarding, thanks to the support of many close friends and colleagues who I would now like to take the opportunity to acknowledge.

Firstly, Dr Julie Sanderson, for granting me such an opportunity, as well as her wisdom and unwavering guidance throughout my research. I would also like to thank Dr Leanne Stokes, who exceeded her duties of secondary supervisor, and provided me with a host of additional opportunities to improve my research immeasurably. Rounding off my supervisor panel was Professor David Broadway, whose calm support and insight was always appreciated. Not all PhD students are lucky enough to have a role model for a supervisor, very few are blessed with three. I would like to thank all previous and current members of both Sanderson and Stokes lab groups, for creating a friendly and enjoyable working environment. Special mentions for Dr Philip Wright for his patient guidance in teaching lab techniques, and for Dr Sofie Habib and Noelia Domínguez Falcón for keeping me sane.

I would also like to thank all my friends and family, in particular my parents, whose sacrifices provided me with an upbringing that allowed me to pursue my dreams.

Finally, to my soulmate Elleigh. I was anxious to move halfway across the country, but I shouldn't have been, because you were right there with me ready to take on the challenge together. You sacrificed so much to help me, and I couldn't have done it without you.

Elleigh Ranns, will you marry me?

### **Declaration by Candidate**

I hereby declare that this thesis is my own work and includes nothing which is the outcome of work done in collaboration. Where other sources of information have been used, they have been acknowledged. This thesis has not been submitted for another degree or qualification in this or any other university or institution and douse not exceed the word limit.

Signature:

# Chapter 1

## Introduction

### 1.1 The Retina

The retina is a highly specialised tissue that lines the majority of the posterior of the vitreous cavity of the eye and is held in place by the outward pressure exerted on it from the vitreous humor, RPE interdigitation and other fluid pressures (Marmor, 1993). The retina has a number of important regional morphological features (Figure 1.1). The central retina or posterior pole is a circular zone with an approximate 5mm diameter, situated between the two temporal retinal arteries. Within the central retina lies a carotenoid-pigmented yellow disc, 1.5mm in diameter, known as the macula, and further within lies the fovea and the foveolar. The foveolar is a circular depression containing the highest density of cone photoreceptors in the retina for greatest visual acuity.

The optic disc, also known as the optic nerve head, is a region 1.8mm in diameter situated 3-4mm to the nasal side of the fovea with a slightly raised rim. It is anatomically unique as it is the only white matter tract of the central nervous system (CNS) that leaves the cranial cavity, and as such is useful in various forms of clinical diagnostics. There is a complete absence of normal retinal layers in this zone, meaning no visual detection can occur here giving rise to a blind spot. Instead of normal retinal layers, the optic disc contains on average 1.2 million retinal ganglion cell axons (Jonas *et al*, 1990) that transport visual information as action potentials out of the eye and into the brain. When the ganglion cell axons have left the eye, they perforate the *lamina cribrosa*, and form the optic nerve.

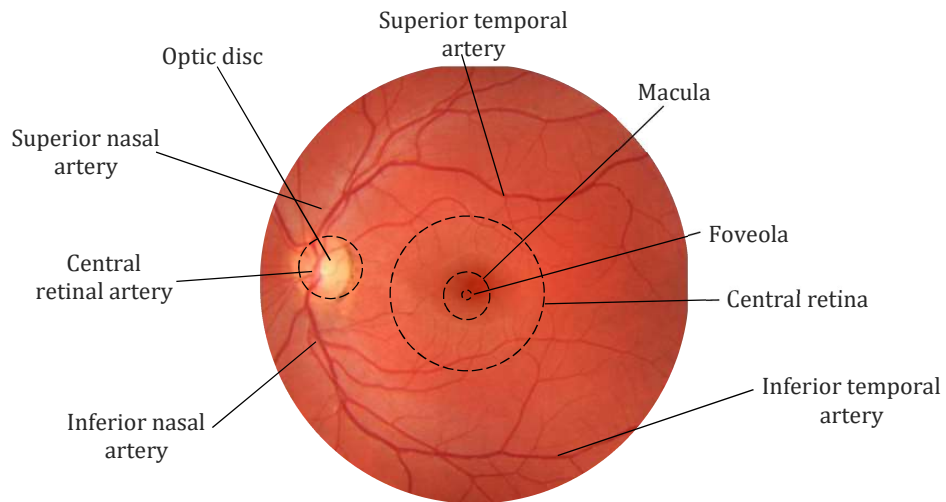


**Figure 1.1:** Topographical view of the human retina. Adapted from: [https://upload.wikimedia.org/wikipedia/commons/4/48/Fundus\\_photograph\\_of\\_normal\\_left\\_eye.jpg](https://upload.wikimedia.org/wikipedia/commons/4/48/Fundus_photograph_of_normal_left_eye.jpg)

The retina has the highest oxygen consumption per weight of any tissue in the human body (Yu & Cringle, 2001) and therefore requires an extensive blood supply to maintain visual function. The retina has a dual blood supply: the central retinal artery, a branch of the ophthalmic artery, supplies the inner two thirds; the choroidal circulation/vascular bed, supplies the remaining outer retinal segment. The central retinal artery enters the retina at the optic disc, and branches several times, firstly into superior and inferior branches which then subdivide into nasal and temporal arteries. Finally, these divide into a vast network of capillaries, the distribution of which is unique to every individual (Kaufman & Alm, 2003).

The role of the tissue is to sense the incoming light stimulus and convert it to electrical and chemical signals that finally project to higher cortical regions of the brain for interpretation. Due to its role, the retina contains many specialised and unique cells, which are organised into ten distinct layers (Figure 1.2). The nuclear layers contain the cell bodies of the residing neuronal and glial cells and the plexiform layers are predominately the synaptic region.

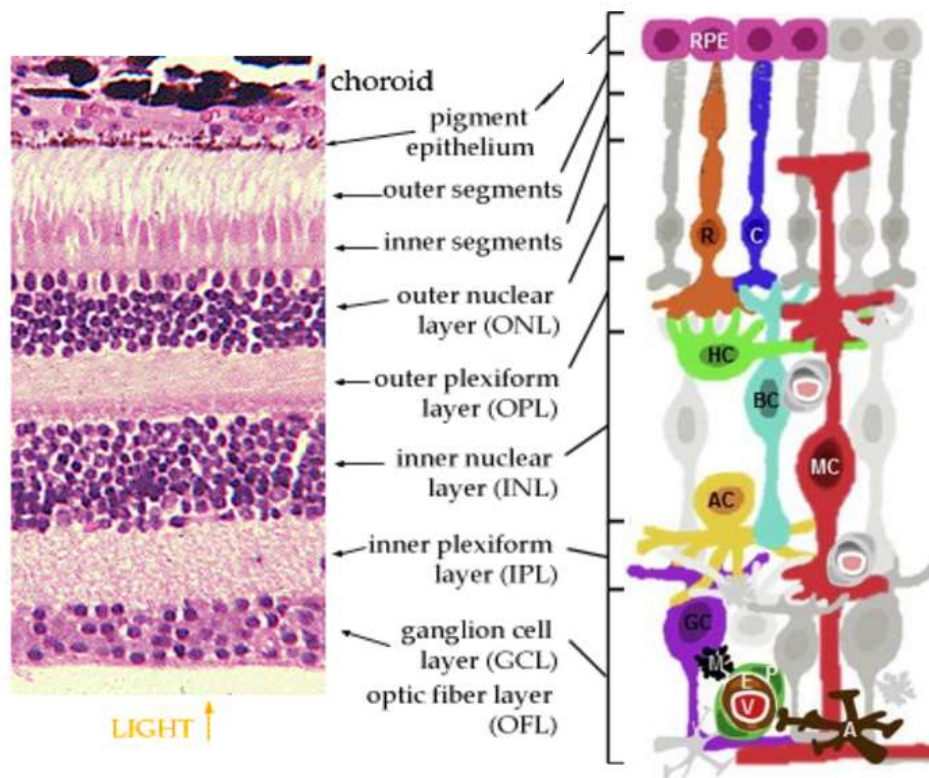


**Figure 1.2:** Diagram of the functional organisation of the retinal layers cells (left) and retinal cell types (right). Cell types shown: Retinal pigmented epithelium (RPE), Rod (R), Cone (C), Horizontal cell (HC), Bipolar cell (BC), Müller cell (MC), Amacrine cell (AC), Ganglion cell (GC), Astrocyte (A), Blood vessel (V), Endothelial cell (E), Pericyte (P), Microglia (M). Adapted from: <http://eyeseeyetalk.blogspot.co.uk/2007/12/231-worn-and-torn-retina.html> and Santos-Carvalho *et al* (2014)

### 1.1.1 Non neuronal retinal cells

#### 1.1.1.1 Retinal pigment epithelia

The RPE is a monolayer of hexagonal shaped cuboidal epithelial cells that lies at the base of the retina. Each RPE cell is asymmetric in structure, which allows for specialised directional function with the different neighbouring environments of the cell. The RPE cells apical surface borders and interacts with the interphotoreceptor matrix (IPM) within the subretinal space, in which RPE cells have important roles in retinal adhesion (Marmor, 1993), storage, regulation and transport of nutrients, (vitamin A is of particular importance) (Steinberg, 1985) and phagocytosis of shed outer segment photoreceptor discs (Bosch *et al*,

1999; Nguyen-Legros & Hicks, 2000). In general terms, RPE cells are required for the homeostasis of the photoreceptors and can be thought of as forming the blood-retinal barrier. The RPE monolayer originates beside the optic nerve head and extends to a serrated junction between the retina and the ciliary body known as the *ora serrata*. The average human eye contains 4-6 million RPE cells (Kaufman & Alm, 2003) with variable size and shape depending on the spatial distribution in the retina, being thinner and more concentrated in the central retina, but wider and slightly flattened in the peripheral retina (Forrester *et al*, 2016).

### **1.1.2 Retinal glia**

#### **1.1.2.1 Müller cells**

Müller cells are specialised radial glial cells and the most abundant of all retinal glial cells. Müller cells provide structural stabilization of the retina and span the entire thickness of the retina (Figure 1.2), with their foot processes forming the inner limiting membrane (ILM) of the retina, and by having adherens junctions with photoreceptors, form the external limiting membrane (ELM) of the retina. Müller cells are involved in forming glial sheaths around many retinal cells and synapses. Unlike other retinal cell, Müller cells are very resistant to insult (Anderson & Davis, 1975), in particular hypoxic environments (Silver *et al*, 1997), which is likely due to their primary energy metabolism being derived from anaerobic glycolysis (Winkler *et al*, 2000). Following cellular insults, Müller cells interact with microglia to undergo gliosis and become activated (Bringmann *et al*, 2009; Vecino *et al*, 2016). Examples of gliotic Müller cell function include cytokine production (Kumar *et al*, 2012) and phagocytosis of foreign substances (Mano & Puro, 1990). Müller cells also ensheath RGCs, which helps protect them against neurotoxic insults (Kawasaki *et al*, 2000) and isolate the impulses being sent to higher processing centres in the brain.

### **1.1.2.2 Astrocytes**

Astrocytes are glial cells of peripheral origin that migrate to the retina during development. Astrocytes have a characteristic flattened cell body morphology with radiating processes. Astrocytes are located in the inner retina, predominately the nerve fibre layer and their presence correlates with the presence and distribution of retinal blood vessels. The main function of retinal astrocytes is to form ensheathing membranes around retinal neurons, but also have roles in neurotrophic support and maintenance of the blood-retina barrier (Vecino *et al*, 2016).

### **1.1.2.3 Microglia**

Microglia are the resident immune cells of the retina, located throughout the retinal layers, and have a number of roles retinal homeostatic functions. Microglia will be discussed in more detail (1.3)

## **1.1.3 The neuronal retina**

### **1.1.3.1 Photoreceptors**

Photoreceptors are highly specialised light sensitive cells, responsible for the detection of the electromagnetic radiation in the visible light spectrum (390-700nm wavelengths). Human eyes contain two types of photoreceptor, rods and cones. Overall both types of photoreceptor have similar structure (Figure 1.3), but the subtle differences in structure and contents allow them to perform different roles in the phototransduction cascade.

Rods are much more abundant in the human retina than cones, there being approximately 125 million rods in each eye (Osterberg, 1935). Spatially, rods are much more concentrated in regions of the peripheral retina. Rod photoreceptor functions in visual detection are related to contrast, brightness and motion detection (Forrester *et al*, 2016). In comparison with cones, rods are more sensitive in low-light conditions, and do not discriminate between colours, the pigment rhodopsin having peak absorption in the blue-green wavelengths of the

visible light spectrum (Willoughby *et al*, 2010), resulting in them being the primary photoreceptor used in low light conditions. The distribution and properties of rod photoreceptors result in poorer visual acuity in the peripheral visual field in comparison with that of the fovea with its low rod count and high density of cone photoreceptors. In contrast to rods, cone photoreceptors require higher levels of light stimulation and are sensitive to three different peak absorptions (red, green and blue) (Wassel & Boycott, 1991). Cones are most highly concentrated in the fovea and are responsible for high acuity vision and colour discrimination. The nuclei of photoreceptor cells are situated in the outer nuclei layer, and their outer segments are situated close to the RPE.

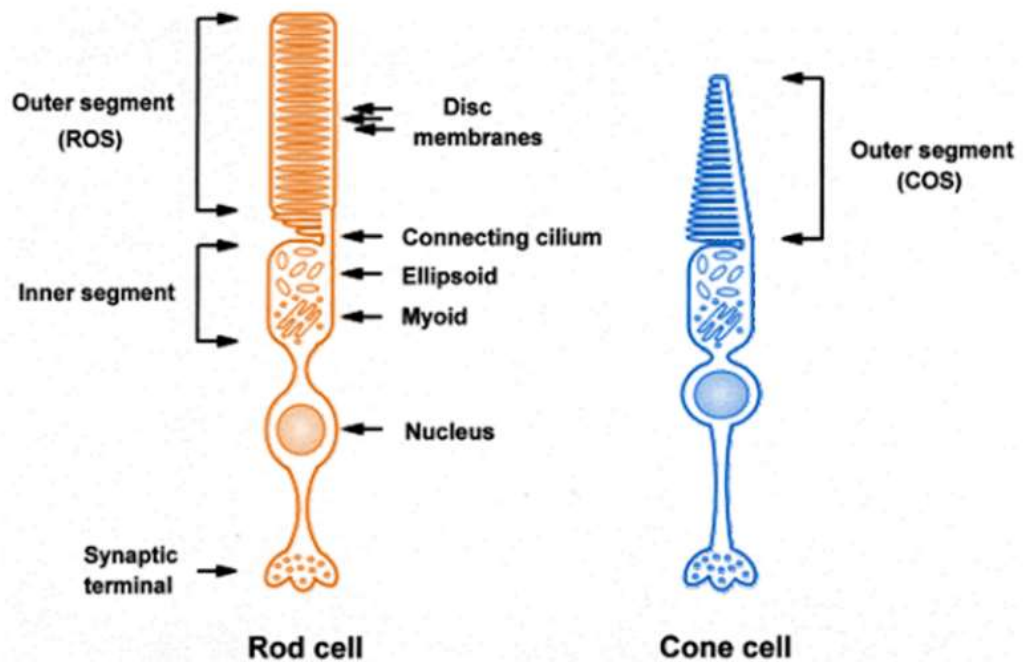


**Figure 1.3:** Diagram of human rod and cone photoreceptors. Adapted from: DeMar *et al* (1999).

### 1.1.3.2 Bipolar cells

Bipolar cells are second order neuronal cells that are responsible for the transmission of signals from photoreceptors and horizontal cells to amacrine cells and RGCs. Different types of bipolar cell are responsible for scotopic (low light/rod mediated) and photopic (bright light/cone

mediated) vision, with rod photoreceptors making synaptic connections to only one type of bipolar cell, but as many as 10 different type of bipolar cell being associated with photopic signalling (Wu, 2009). The ratio of bipolar cell connection to photoreceptors also varies greatly with location across the retina. Often in the fovea and central retina there is a 1:1 ratio of bipolar cell to photoreceptor, whereas bipolar cells in the peripheral retina can form synaptic connections with up to 100 rods (Forrester, 2016). Consequently, the size of bipolar cell dendritic tree also varies depending on position in the retina, being much larger in the peripheral retina.

#### **1.1.3.3 Horizontal cells**

Horizontal cells are interneurons that connect laterally in the inner nuclear layer (INL) of the retina. Horizontal cells can be classified into 3 distinct types, HI, HII & HIII depending on their ability to connect to the different sub classes of cone photoreceptors and also rods in the case of HII cells (Kolb *et al*, 1994). The functional role of horizontal cells is regulation of the electrical firing rate of their connected bipolar cells.

#### **1.1.3.4 Amacrine cells**

Amacrine cells are interneurons that project their dendrites into the inner plexiform layer (IPL) at the synapses between bipolar cells and RGCs. Multiple subtypes of amacrine cell exist with a diverse range of functions to modulate the responses of bipolar cells and RGCs, which is achieved by the release of excitatory neurotransmitters such as glutamate and acetylcholine or conversely by release of inhibitory neurotransmitters such as glycine and GABA.

#### **1.1.3.5 Retinal ganglion cells**

Retinal Ganglion cells (RGCs) are the neurones of the retina that receive information from the photoreceptors via the bipolar and amacrine cells. They contain a single axon, which emerges from the

cell body and forms the inner nerve fibre layer of the retina. The RGC axons run parallel to the inner surface of the retina and accumulate with all RGC axons at the optic disc. As a result, the density of the RGC layer is thickest at the optic disc (Forrester *et al*, 2016). The total number of RGCs for each eye has a reported 800,000 – 1.5million cells (Jonas *et al*, 1990). The nerve fibres then leave the eye, passing through the *lamina cribrosa* and forming the optic nerve.

There are multiple different forms of retinal ganglion cells and each type has their own classification based on the morphology and spread of their dendritic tree, the level of branching in the inner plexiform layer and the size of their cell body.

## **1.2 Glaucoma**

Glaucoma is the term for a group of progressive and irreversible optic neuropathies that lead to loss of RGCs in the inner retina and their axonal projections. The result is a gradual reduction in the visual field, starting at the periphery before progressing to the centre, which can lead ultimately to total blindness. It is estimated that more than 60 million people worldwide suffer from glaucoma and it is the second leading cause of global blindness after cataract (Flaxman, 2017), which makes glaucoma the world leading cause of irreversible blindness.

Due to glaucoma being a term that encompasses a group of retinal neuropathies, it can be classified into different sub-types depending on cause and pathophysiology. It is divided into primary and secondary glaucoma, where secondary glaucoma occurs as the result of another condition such as uveitis (Panek *et al*, 1990), or as a result of ocular trauma, drugs or injury (Girkin *et al*, 2005). Primary glaucoma can then be subdivided into open-angle or closed angle, depending on the acute angle situated between the iris and the cornea at the periphery of the anterior chamber, the iridocorneal angle (Figure 1.4).

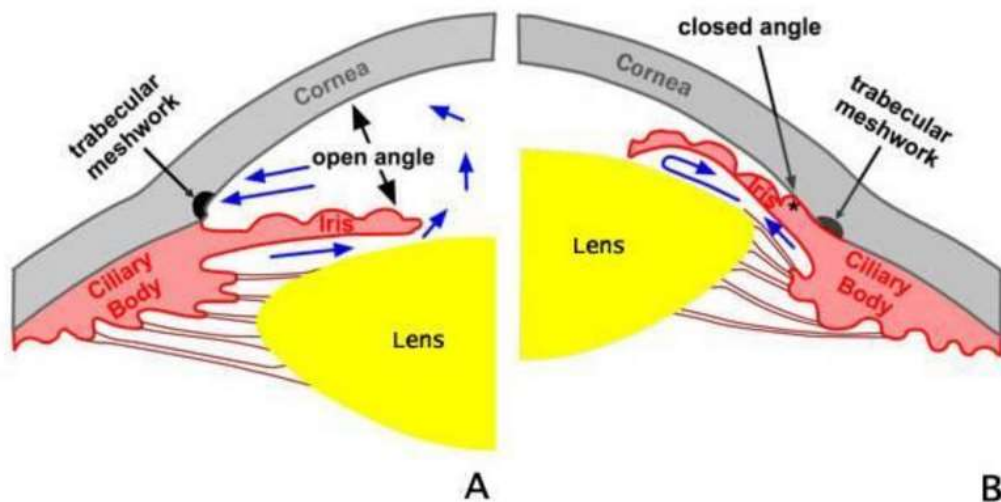


**Figure 1.4:** Diagram of the flow of humor and the iridocorneal angle in **A**-Open angle Glaucoma, **B**-Closed angle glaucoma. Available from: [https://classconnection.s3.amazonaws.com/33/flashcards/602033/jpg/open\\_angle\\_vs\\_closed\\_angle\\_glaucoma1330585756893.jpg](https://classconnection.s3.amazonaws.com/33/flashcards/602033/jpg/open_angle_vs_closed_angle_glaucoma1330585756893.jpg)

Estimates suggest both types have roughly equal prevalence (Flaxman, 2017). Of the two primary forms, both have the characteristic feature of raised intraocular pressure (IOP), which is a major modifiable risk factor in disease progression. However, in many cases, glaucoma presents without increased IOP, a category known as normal tension glaucoma (NTG).

Despite being extensively investigated, current knowledge of the exact mechanism of RGC death in glaucoma remains unknown, there is increasing evidence that neuroinflammation plays an important role (Mac Nair & Nickells, 2015; Williams *et al*, 2017). Microglia, as resident immune cells of the retina are central to the process of neuroinflammation, with understanding of microglial function being of great importance in the understanding of glaucomatous pathophysiology.

### 1.3 Microglia

Microglia are resident mononuclear phagocytic cells, distributed widely throughout the central nervous system (CNS). Microglia derive from myeloid progenitor cells in the primitive yolk sac and proceed to migrate to the brain and associated CNS parenchyma during early embryonic development (Ginhoux *et al*, 2013, Kierdorf *et al*, 2013). Once migrated to the CNS, microglia continue to locally self-regulate and renew their population throughout adult life by a balance of proliferation and apoptosis (Bruttger *et al*, 2015), without any further contribution from peripheral immune cells (Askew *et al*, 2017). It is estimated that microglia represent between 10-15% of the total cell population of the brain (Lawson *et al*, 1992), and also display a diverse range of morphologies across the various regions they reside in. Additionally, as the retina is a CNS tissue, microglia are located throughout, residing predominantly at the nerve fibre layer-ganglion cell layer interface, the inner nuclear layer and the outer plexiform layer (Hume *et al*, 1983). Microglial cells have a diverse range of functions throughout the CNS, related to CNS development, regulating homeostasis and as responders to immune and pathogenic challenges.

As they share a common lineage with macrophages and other immune cells, it can be difficult to selectively distinguish microglia experimentally. One of the first microglial detection methods was with weak silver carbonate stain (McCarter, 1940). Since then multiple more markers with increased selectivity for resting microglia have been discovered, including transmembrane protein 119 (TMEM119) (Satoh *et al*, 2016), the purinergic P2Y12 receptor (P2Y12R), and, exclusively to murine microglia, Fc receptor-like scavenger S (FCRLS) (Butovsky *et al*, 2014).

It has been demonstrated that microglia have a range of critical roles in early CNS development (Frade & Barde *et al*, 1998). Microglia

are also involved in various aspects of synaptic health and homeostasis, including their formation (Lim *et al*, 2013) and remodelling (Weinhard *et al*, 2018), including the regulation of synaptic plasticity (Rogers *et al*, 2011) and the process of synaptic pruning critical for correct brain function (Bruce-Keller, 1999, Paolicelli *et al*, 2011; Schafer *et al*, 2012). Outside of their synaptic duties, microglia are also involved in embryonic neurogenesis (Walton *et al*, 2006; Cunningham *et al*, 2013), reorganisation of neuronal networks via phagocytosis (Sierra *et al*, 2010; Tremblay *et al*, 2010) and supporting the remyelination of axons (Olah *et al*, 2012). The roles microglia play in early CNS development are perhaps best highlighted by studies of microglial dysfunction or absence, which results in the subsequent dysfunction of neuronal networks (Zhan *et al*, 2014) and general disrupted brain development (Erblich *et al*, 2011; Paolicelli *et al*, 2011).

As well as their neuronal remodelling and synaptic functions, under normal “resting” conditions, microglia contribute to a signalling network system with neurons, in order to modify function and promote neuronal survival. For instance, healthy neurons tonically release the chemokine CX3CL1 (fractalkine), which binds to its corresponding receptor (CX3CR1) on resting microglia to induce the release of adenosine, which in turn acts on neuronal A1 receptors to activate survival pathways (Lauro *et al*, 2008; 2010). The microglial/neuronal CX3CL1 pathway has also been implicated in the process of synaptic pruning (Kettenmann *et al*, 2013), whereby deficiency in the chemokine leads to reduced microglial surveillance (Pagani *et al* 2015). There is also a wealth of evidence that microglia regulate inhibitory transmission of neuronal networks via the release of brain derived neurotrophic factor (BDNF), which interacts with Tropomyosin receptor kinase B (TrkB) (Tanaka *et al*, 1997; Frerking *et al*, 1998; Baldelli *et al*, 2005).

Perhaps the most important role of microglia, is monitoring the CNS parenchyma for pathological stimuli, in order to react and mount a protective response. Signalling molecules that stimulate a microglial immune response are often grouped into two categories, pathogen-associated molecular patterns (PAMPs) and danger-associated molecular patterns (DAMPs) based on their source of origin (Bianchi, 2007). PAMPs, as their name would suggest, are derived from infectious microorganisms and include the bacterial cell wall component lipopolysaccharide (LPS). In contrast, DAMPs are derived from host cell components as a result of damage/stress and cell death. Microglial surveillance of their environment is achieved utilising fine motile processes which sample their surroundings (Davalos *et al*, 2005; Nimmerjahn *et al*, 2005). In order to detect a wide range of stimuli, microglia are endowed with a large array of immune receptors such as toll-like receptors (TLRs), nucleotide-binding oligomerization domains (NODs) and various scavenger receptors (SRs) (Chen *et al*, 2009; Bell *et al*, 1994; Ransohoff & Perry, 2009; Kettenmann *et al*, 2011).

When microglia are stimulated, they respond based on the specific nature of the stimulus, to either promote or suppress inflammation, in order to prevent tissue damage, promote tissue repair, and return the surrounding microenvironment back to homeostatic control (Nakajima & Kohsaka, 1993). After activation, in order to elicit an appropriate response microglia must undergo morphological transformation into functional phenotypes, a process known as microgliosis. It is now recognised that activated microglia exist in two broad distinct states; M1 or “classically” activated, responsible for pro-inflammatory responses and M2 or “alternatively” activated, responsible for an anti-inflammatory response. Although this nomenclature and classification originally referred to activation states recognised in peripheral macrophages, activated CNS microglia undergo similar profiles, and much of the evidence for macrophage profiles can be extrapolated to that of microglia.

### 1.3.1 Retinal microglia

During development, migration of microglia to the retina is thought to occur from two sources, the optic nerve head and the ciliary body. The lineage of optic nerve head derived microglia is thought to be macrophagic (Ginhoux *et al*, 2010), whereas the ciliary body derived microglia show markers of dendritic lineage (Diaz-Araya *et al*, 1995a; 1995b). In the developing retina, microglia inhabit all layers of the retina (Ashwell *et al*, 1989), however as the retinal layers develop, microglia settle in the plexiform layers (Santos *et al*, 2008), albeit with a highly branched morphology, with branches that can span the entire retina (Karlsetter *et al*, 2015). This is consistent with the resting state of other CNS microglia.

Like their brain counterparts, retinal microglia have a range of physiological roles in retinal development, homeostasis and inflammation/disease. As activation of retinal microglia by changes in the retinal environment can lead to deleterious effects (Dick *et al*, 2003), several mechanisms are utilised in maintaining microglia in a resting state for retinal homeostasis. This process involves contribution from multiple retinal cell types, such as RPE cells (Liversidge *et al*, 1994), retinal neurons (Liang *et al*, 2009) and Müller cells (Wang & Wong, 2014; Gallina *et al*, 2015), which release a variety of signalling molecules that modulate microglial activity. Such signalling molecules include CX3CL1 (Liang *et al*, 2009; Huang *et al*, 2013), CD200 (Carter & Dick, 2004), diazapam binding inhibitor (DBI) (Wang *et al*, 2014), NO and Prostaglandin E2 (Liversidge *et al*, 1994), and ATP (Wang & Wong), 2014. During development, microglial phagocytosis is thought to play a major role in the clearance of dying neurons in the GCL and INL of the retina (Hume *et al*, 1983). As previously described, microglia play a key role in synaptic pruning, a process that involves the associated protein C1q (Stevens *et al*, 2007). Since expression of C1q is concentrated at synapses of RGCs in the IPL, and that expression negatively correlates with maturation of the

retina (Stevens *et al*, 2007), it is assumed that retinal microglial synaptic pruning occurs in the retina as part of the development process in this layer. Microglial phagocytotic function is retained in the developed retina, and contributes to the clearance of dead cells and debris in pathological conditions (Thanos, 1991; Khono *et al*, 2013; Yuan *et al*, 2015). The role of microglial phagocytosis was further demonstrated with neutralisation of the microglial c-type lectin protein dectin-1, causing a reduction in the clearance of *Candida albicans* (Maneu *et al*, 2011).

### **1.3.2 Retinal microglia in glaucoma**

Microglia are often the primary responding cell type to pathophysiological events, and as such investigation into microglial activity may provide a wealth of information into early stages of glaucoma development. Primary isolated retinal microglia represent an excellent tool for research, however their limited lifespan and difficulty in isolating from native tissue are also limiting factors. Alternatively, CNS derived, retrovirally immortalised microglial cell lines are also commercially available including BV-2 and N9 murine microglia, which mitigate some of the disadvantages associated with the use of primary microglia. Immortalised cell lines also have associated disadvantages including their susceptibility to dedifferentiation. Investigation of microglial responses, whether isolated primary cells or immortalised cell lines, in the absence of additional cell types and native tissue architecture however is not the same as experimental modelling of glaucoma, and caution should be taken when interpreting results of such experiments.

As with other neurodegenerative diseases of the CNS such as Parkinson's and Alzheimer's disease, there is much interest in the role of microglia in the pathophysiology of glaucoma, however it remains poorly understood. Microglial activation in the optic nerve head (ONH) and the retina is reported as one of the first detectable events in

glaucoma, preceding RGC death (Neufeld, 1999; Yuan & Neufeld, 2001; Johnson & Morrison, 2009; Ebner *et al*, 2010; Bosco *et al*, 2011; Taylor *et al*, 2011). Evidence of early microglial activation in glaucoma is based on numerous studies.

For example, in human subjects with glaucoma, microglia have been demonstrated to undergo morphological changes to an amoeboid M1 state coupled with increased proliferation (Yuan & Neufeld, 2001). Several other morphological changes have also been observed, including, an upregulation of several immune related receptors, such as TLRs (Luo *et al*, 2004), MHC classes I and II (Kreutzberg, 1996; Streit *et al*, 1999) and CD68, which is coupled to enhanced phagocytic activity (Rojas *et al*, 2014; Yuan & Neufeld, 2001). Additionally, these phagocytic microglia express pro-inflammatory molecules such as complement cascade proteins, Tumor necrosis factor alpha (TNF $\alpha$ ), and several metalloproteases (Yuan & Neufeld, 2000; Yuan & Neufeld, 2001). Based on the microglial profile expressed in the early stages of glaucoma, the stimuli responsible are likely to be one of many DAMPS or heat shock proteins (HSPs). Interestingly, proteomic analysis of human glaucomatous retina has shown increased expression of HSP-60 and HSP-70, as well as TLR2, TLR4 and TLR7 (Luo *et al*, 2010), although this is a tissue-wide phenomenon and not isolated to microglia.

Due to the difficulties associated with human tissue, animal models of glaucoma are much more prevalent and thus a much wider body of data on microglia in animal glaucomatous models is available (Bouhenni *et al*, 2012), with the majority of studies conducted in rodent models (Pang & Clark, 2007). Experimental increase of IOP by cauterization of episcleral veins in rats demonstrated the death of RGCs (Naskar *et al*, 2002), and their ingestion by activated microglia. In this study, activated microglia with phagocytosed RGC contents were observed at the site of degeneration after just 3 days of increased

IOP. Similarly, in a model of acute IOP increase in C57BL/6J mice, the migration and proliferation of amoeboid microglia was observed after a week (Kezic *et al*, 2013). In a study utilising CX3CR1-GFP reporter mice, similar patterns of activation, proliferation and migration were observed, which were parallel to a decline in the number of total RGCs (Liu *et al*, 2012). Another procedure used to study glaucoma in a mouse model is unilateral laser induced ocular hypertension, in which the untreated eye serves as a negative control. In studies utilising this model, microglial activation was demonstrated in the ganglion cell layer of the optic nerve head, as well as the outer regions of the retina (Gallego *et al*, 2012; de Hoz *et al*, 2013; Rojas *et al*, 2014).

One model commonly used to study glaucomatous progression is the DBA/2J (D2) mouse model. DBA/2J (D2) mice have genetic mutations in the melanosomal protein glycosylated protein NMB (GPNMB) and tyrosine-related protein-1 (TYRP1), which leads to an increase in IOP secondary to systemic pigment dispersion syndrome, presenting between 6-8 months in age (Anderson *et al*, 2002). With DBA/2J (D2) mice, these mutations do not always fully develop due to low mutation penetrance (Libby *et al*, 2005), meaning mice with regular IOP after 6 months can be used as a negative control in these studies. Temporal analysis of microglia in the DBA/2J (D2) via staining with Iba1 marker demonstrated early microgliosis and the clustering of Iba1 positive cells (presumably microglia) in the inner central retina and unmyelinated optic nerve sections at only 3 months (Bosco *et al*, 2011). Analysis of DNA microarrays of microglia from the optic nerve head region of DBA/2J (D2) mice have shown high expression of C1qa, endothelin 2 and components of the complement cascade (Howell *et al*, 2011). To validate these observations, dietary administration with the endothelin receptor antagonist bosentan protected against neurodegeneration (Howell *et al*, 2014).

#### **1.4 Purinergic signalling**

Purine nucleosides such as adenosine, and nucleotides such as adenosine-5'-triphosphate (ATP) and adenosine-5'-diphosphate (ADP), are part of a family of chemical mediators which are most well known for their role in cellular energy metabolism, however they also have a diverse range of functions in extracellular signalling, including within the peripheral and central nervous system (Figure 1.5). The role of purines as cell signalling molecules was originally discovered in relation to the effects of adenosine on the cardiovascular system (Drury & Szent-Györgyi, 1929). This discovery led to the idea that purine nucleotides and nucleosides could act as a signalling molecule between cells. The role of purine nucleotides and nucleosides (in particular ATP) as neurotransmitters was discovered in early electro-stimulation experiments (Holton, 1959), and is now understood to be present and modulatory in almost all neurons. This theory was long contested among the scientific community, but today is accepted universally.

It was from pioneering work in the early 1970s by Burnstock (*et al*, 1970; Burnstock, 1972), where the discovery was made that ATP is also released at many neurons as a co-transmitter, that the term purinergic signalling was first coined. ATP is often co-packaged with neurotransmitters such as acetylcholine and noradrenaline (Silinsky, 1975 Unsworth & Johnson, 1990) and has also been shown to be co-released alongside various neurotransmitters including GABA, glutamate, 5-hydroxytryptamine (5-HT) and dopamine (Burnstock, 2007).

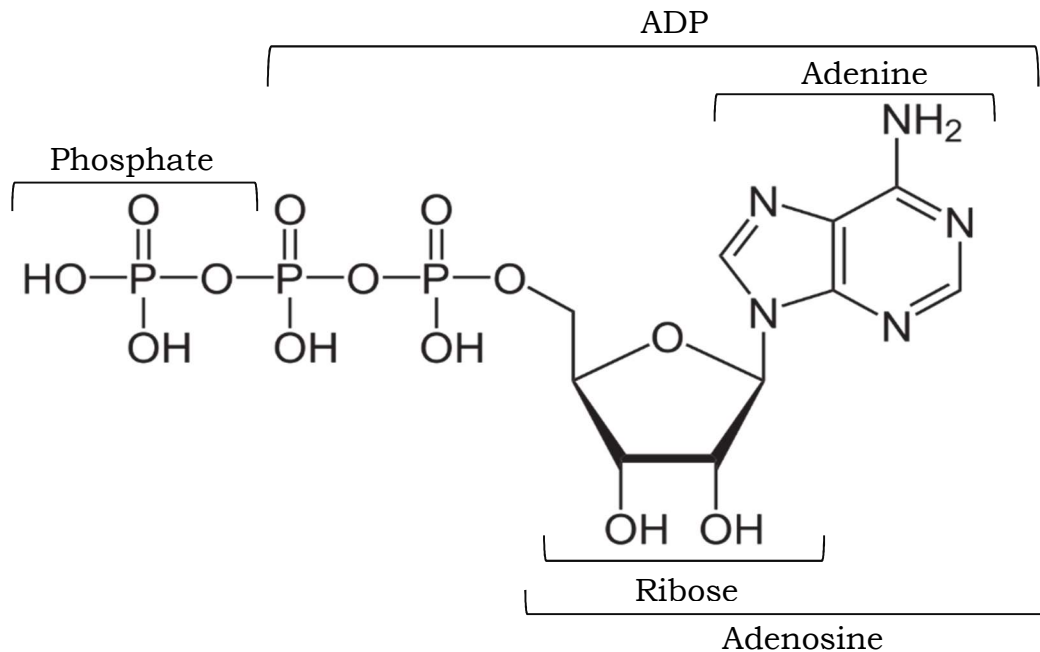


**Figure 1.5:** Molecular structure of ATP

As well as ATP being in synaptic vesicles in neurons, ATP is stored in secretory vesicles in other cells, which can be stimulated to release via exocytosis (Praetorius & Leipziger, 2009). The packaging of ATP into synaptic or secretory vesicles is regulated by the vesicular nucleotide transporter (VNUT), which utilises an intracellular proton gradient generated by V-ATPase (Sawada *et al*, 2008). Exocytosis of ATP from vesicles is a highly regulated process involving the soluble N-ethylmaleimide-sensitive factor attachment protein receptor (SNARE) family of proteins, as well as associated accessory factors (Sudhof & Rothman, 2009). A key stimulus of vesicle exocytosis is increased levels of intracellular calcium ( $[Ca^{2+}]_i$ ) (Messenger *et al*, 2014).

Free cytosolic ATP is also released by plasma membrane channels, primarily via a pannexon pore, formed as a homohexamer of pannexin-1 subunits (Dahl, 2015). The pannexon channel has two open conformations, whereby the larger open state is non-selectively permeable to molecules with a molecular weight of less than 1.5kD, including ATP (Dahl, 2015). Pannexin channel involvement in non-vesicular ATP release has been demonstrated after a range of

stimulating factors, including mechanical stress, hypoxia, elevated  $[Ca^{2+}]_i$  and the binding of several ligands to their respective receptors, including glutamate and angiotensin II (Bruzzzone *et al*, 2005; Ransford *et al*, 2009; Dahl, 2015). Furthermore, ATP stimulation of purinergic receptors is able to induce pannexin mediated ATP release in a positive feedback mechanism termed ATP-induced ATP release (Locovei *et al*, 2006; Locovei *et al*, 2007), which acts to amplify ATP signals. Cellular ATP release also occurs during cellular injury and death (Martins *et al*, 2014). In cell death that features disruption of the cell membrane, such as necrosis, intracellular contents including ATP are passively released into the extracellular milieu.

Upon release, ATP is degraded by extracellular ectonucleotidases to related purinergic signalling ligands, such as ADP, adenosine monophosphate (AMP) and adenosine, which are pharmacologically active, providing ligands for all classes of purine receptor (Abbracchio *et al*, 2009). These pathways are summarised in Figure 1.6. Ectonucleoside triphosphate diphosphohydrolase-1 (NTPDase1), more commonly known as Cluster of Differentiation 39 (CD39), is a key enzyme in the degradation of ATP, which catalyses the hydrolysis of  $\gamma$  and  $\beta$  phosphate groups, to produce ADP and AMP respectively, in a  $Ca^{2+}$  and  $Mg^{2+}$  dependent manner (Heine *et al*, 2001). Ectonucleotide pyrophosphatase/phosphodiesterase 1 (ENPP1) is another ectonucleotidase enzyme that catalyses the cleavage of 5'-phosphodiester bonds of a broad range of nucleotide substrates, including ATP, UTP and cyclic AMP (cAMP) (Namasivayam *et al*, 2017), albeit with preference towards ATP as a substrate (Kato *et al*, 2012). Catalysis of ATP by ENPP1 generates AMP without the formation of intermediary ADP due to the hydrolysis of the phosphodiester bond between the  $\alpha$  and  $\beta$  phosphate groups (Kato *et al*, 2012). Adenosine is subsequently formed from the degradation of AMP, primarily by activity of the dimeric enzyme cluster of differentiation 73 (CD73), alternatively known as Ecto-5'-nucleotidase (Latini & Pedata, 2001).

Another source of production of intracellular adenosine is from the hydrolysis of *S*-adenosylhomocysteine (SAH) by the enzyme SAH hydrolase, a process which is thought to provide the cell with up to a third of its adenosine production (Lloyd *et al*, 1988).

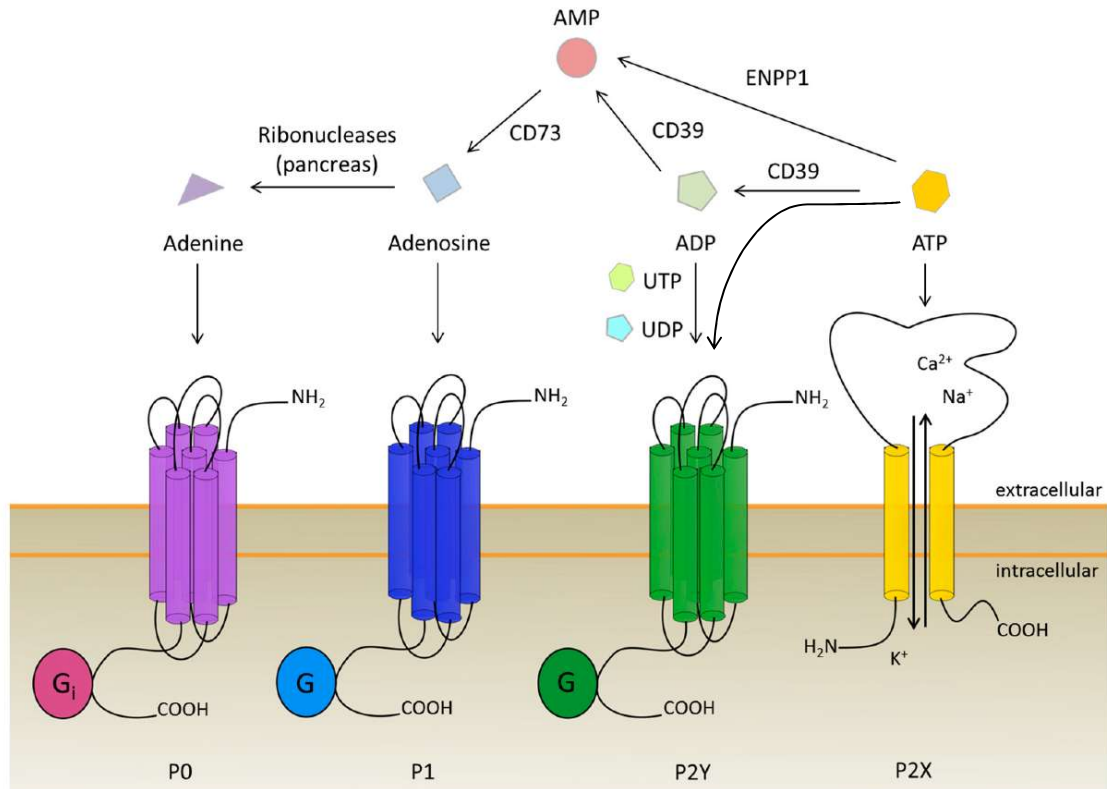


**Figure 1.6:** Overview of receptor families, endogenous ligands and ectonucleotidases that constitute purinergic signalling. Adapted from Ottensmeyer *et al*, 2018.

### 1.4.1 Purinergic receptors

The effects of signalling via nucleotides and nucleosides ligands are exerted at families of purinergic receptors. A system of purinoceptor classification was first established based on a combination of structural characteristics and pharmacological properties (Burnstock, 1978; Burnstock & Kennedy, 1985). Although experimental evidence for purinergic receptors had existed for some time, widespread acceptance of their existence was determined by the cloning and characterization of purine and pyrimidine sensitive receptors, of which four P1, eight P2Y (1,2,4,6,11-14) and seven P2X receptor subtypes (1-7) have been discovered in humans.

### 1.4.2 Adenosine receptor family

Receptors sensitive to adenosine, originally termed P1 receptors, were the first to be cloned (Libert *et al*, 1991). There are currently four recognised adenosine receptor subtypes, A<sub>1</sub>, A<sub>2a</sub>, A<sub>2b</sub> and A<sub>3</sub>, all of which are members of the G protein-coupled receptor (GPCR) superfamily. They are all linked to adenylate cyclase which governs the majority of their effects. Adenosine receptors have been shown to play critical roles in cardiac muscle regulation, neuronal function, pain and sleep, as well as inflammation (Blackburn *et al*, 2009; Sawynok, 2016). The pro-inflammatory effects of adenosine are largely attributed to the A<sub>1</sub> receptor, whereas anti-inflammatory effects are mediated via the A<sub>2a</sub> receptor (Blackburn *et al*, 2009). The crystal structures of A<sub>1</sub> and A<sub>2a</sub> receptor subtypes have been published (Cheng *et al*, 2017). Of the four receptor subtypes, A<sub>1</sub> and A<sub>3</sub> share ~49% sequence homology and couple to G<sub>α<sub>i/o</sub></sub> (Cordeaux *et al*, 2004; Zhou *et al*, 1992). A<sub>1</sub> can also couple to G<sub>α<sub>s</sub></sub> and G<sub>q</sub>/G<sub>11</sub> demonstrating ligand specific G-protein selectivity (Cordeaux *et al*, 2004). A<sub>2a</sub> and A<sub>2b</sub> share ~59% sequence homology and couple to G<sub>α<sub>s</sub></sub> (Olah, 1997; Feoktistov & Biaggioni, 1995). Expression of adenosine receptors is ubiquitous throughout the body and has been shown on all immune cells (Haskó *et al*, 2008), including the presence of all receptor subtypes on microglia (Fredholm *et al*, 2001).

The endogenous ligand of all adenosine receptors is its namesake purinergic-signalling molecule. Compounds of the methylxanthine class of drugs are non-selective antagonists of adenosine receptors, including theophylline, istradefyline and (the most widely consumed drug worldwide), caffeine, all of which are approved therapeutic drugs. Numerous subtype selective agonists and antagonists have also been developed.

### 1.4.3 P2Y receptor family

The P2Y receptor family (P2YR) are all G protein-coupled, but with a relatively high diversity in amino acid sequence amongst the eight recognised mammalian subtypes. Despite this diversity in subtype sequences, all P2YRs belong to the  $\delta$ -branch of class A GPCRs (Fredriksson *et al*, 2003; Lagerström & Schiöth, 2008). The first P2YR was successfully cloned from chick brain cDNA was P2Y1 (Webb *et al*, 1993). Soon after, all eight mammalian subtypes were cloned and characterised as well as a number of orphan receptors and predicted non-mammalian nucleotide G protein-coupled receptors that are structurally similar, but have yet to be proven functional, (denoted as p2y lowercase) (Vanhoutte *et al*, 1996; King *et al*, 2000).

The early GPCR structural prediction was based on genetic structural analysis coupled to molecular modelling approaches with the similarly related rhodopsin GPCR (Costanzi *et al*, 2004; Jacobson *et al*, 2013), and was eventually supported by the recent publication of the crystal structures for P2Y12 (Zhang *et al*, 2014a; Zhang *et al*, 2014b) and P2Y1 (Zhang *et al*, 2015) which demonstrated multiple GPCR structural characteristic features including seven hydrophobic  $\alpha$ -helical transmembrane regions (TM1-7) interspersed with alternating intracellular and extracellular loops (three of each in total) (Figure 1.7). Clarification of the ligand binding site was achieved initially by searching for conserved sequences combined with mutagenesis of likely candidates (Erb *et al*, 1995; Jacobson *et al*, 2013; Schmidt *et al*, 2013). Eventually, clarification of the ligand-binding site was supported with crystal structure publications, identifying that regions in TM3,6 & 7 appear to be involved (Schmidt *et al*, 2013; Zhang *et al*, 2015). P2YR receptors can be subdivided into two groups based on their more similar sequence homology. P2YRs 1, 2, 4, 6 & 11 comprise the first subgroup and couple to G<sub>q</sub>, exerting their effect via

phospholipase C (PLC) activation and subsequent IP<sub>3</sub> signalling and release of intracellular calcium stores. Conversely, the P2YRs 12, 13 & 14 of the second subgroup couple to G<sub>i</sub> to inhibit adenylate cyclase or modulate activity of ion channels. Uniquely among P2YRs is P2Y<sub>11</sub>, which has also been shown to couple to G<sub>s</sub> and increase activity of adenylate cyclase.

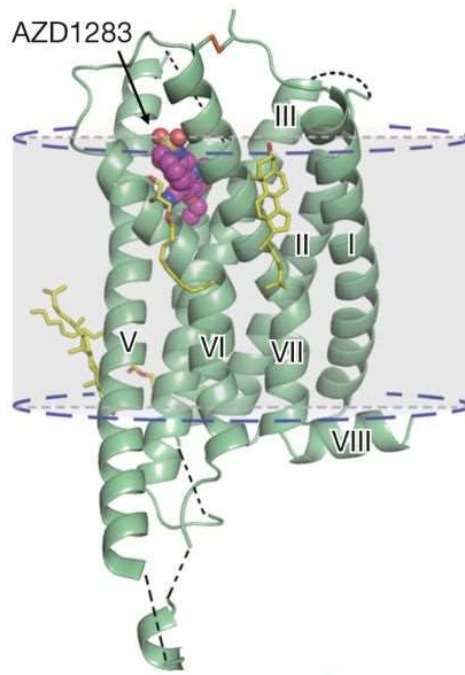


**Figure 1.7** X-ray crystal structure of P2Y<sub>12</sub> with antagonist AZD1283 bound, showing the characteristic structural features of the P2YR family of GPCRs. Cell membrane is represented by the shaded region and  $\alpha$ -helical transmembrane regions are labelled I-VII. Adapted from Zhang *et al*, 2014b.

As well as structural diversity, there is large diversity in endogenous agonists for the P2YR subtypes, including adenine nucleotides, (predominantly ADP, but also ATP to a lesser extent), the uracil nucleotides UTP, UDP and the sugar linked UDP-glucose.

#### 1.4.3.1 P2Y<sub>1</sub>

The first P2YR to be cloned, P2Y<sub>1</sub> was isolated from chick brain tissue (Webb *et al*, 1993), and the human homologue was isolated shortly afterwards (Ayyanathan *et al*, 1996). The human P2Y<sub>1</sub> receptor gene

(P2RY1) contains no intron regions and is located on chromosome 3. Human P2Y1 is expressed extensively throughout the body and in the CNS. It is distributed across a number of brain regions (most notably the nucleus accumbens) as well as in the spinal cord, (Moore *et al*, 2001) and in retinal Müller cells (Grosche *et al*, 2013) and RPE cells (Tovell & Sanderson, 2008). In immune cells, P2Y1 is shown to be expressed in human macrophages (Moore *et al*, 2001) and additionally mouse microglial cells (Light *et al*, 2006; Fukumoto *et al*, 2018), although receptor expression in microglia is reportedly weak. Human, rat and mouse P2Y1 all form a 373 amino acid protein, with a 97.1% sequence homology between the two rodent receptors (Tokuyama *et al*, 1995). P2Y1 belongs to the first subfamily of P2YRs that couple to  $G\alpha_q/G\alpha_{11}$  as well as modulating the inhibition of  $K^+$  channels (Filippov *et al*, 2006; Erb & Weisman, 2012).

Both adenine based nucleotides ADP and ATP act as endogenous ligands at P2Y1, where ADP is a full and ATP a partial agonist (Palmer *et al*, 1998; Waldo *et al*, 2002; von Kügelen, 2019). Further P2Y1 ligands include methylthionated analogues of ADP, as well as the highly selective and potent MRS2365 (Chhatriwala *et al*, 2004) which mimic the pharmacology of their endogenous counterparts (Schachter & Harden, 1997; Waldo *et al*, 2002). P2Y1 is blocked at low affinity by pan P2-antagonists PPADS and suramin (Waldo *et al*, 2002), however the competitive antagonist MRS2179 is both more potent and highly selective for P2Y1 receptors (Boyer *et al*, 1998).

#### **1.4.3.2 P2Y2**

P2Y2 was originally referred to as the  $P_{2U}$  receptor before being renamed under nomenclature guidelines. Discovered shortly after P2Y1, P2Y2 was originally cloned from murine neuroblastoma cells (Lustig *et al*, 1993) followed by the human homologue from human epithelial airway cells (Parr *et al*, 1994), where its gene was located to chromosome 11. P2Y2 expression has been detected in many tissues

including extensively in the CNS in various brain regions (Moore *et al*, 2001), RPE cells (Tovell & Sanderson, 2008), as well as macrophages (Abbracchio *et al*, 2006) and microglia (Tozaki-Saitoh *et al*, 2012). The translated human receptor protein is 377 amino acids in length, and couples directly to PLC $\beta$ <sub>1</sub> via G $\alpha$ <sub>q/11</sub> (Erb & Weisman, 2012).

Both endogenous UTP and ATP are full agonists of P2Y<sub>2</sub>, with the former having stronger potency (Lazarowski *et al*, 1995), whereas the receptor is insensitive to ADP and UDP. Additional selective agonists have been developed including MRS2698 (Ivanov *et al*, 2007) and PSB1114, which is 60-fold more selective over P2Y<sub>4</sub> and P2Y<sub>6</sub> (El-Tayeb *et al*, 2011). Another class of agonists include analogues of UTP with a thiol group at different positions on the uracil base (Brunschweiler & Müller, 2006; El-Tayeb & Müller 2006). Although insensitive to pan purinergic antagonists PPADS and Reactive blue 2 (RB2), P2Y<sub>2</sub> is sensitive to suramin (Janssens *et al*, 1999). The selective competitive antagonist AR-C118925XX is also used experimentally (Kemp *et al*, 2004).

#### **1.4.3.3 P2Y<sub>4</sub>**

Previously known as the pyrimidinoceptor, P2Y<sub>4</sub> was isolated from a human genomic cDNA library (Communi *et al*, 1995; Nguyen *et al*, 1995) independently by two groups at roughly the same time. The location of the gene (P2RY4) was determined to be at region q13 on the X chromosome (Nguyen *et al*, 1995). Human P2Y<sub>4</sub> has been demonstrated as widely expressed in tissues including the intestine, liver, kidneys, pancreas and brain (Moore *et al*, 2001). In terms of immune cells human macrophages show P2Y<sub>4</sub> expression (Moore *et al*, 2001) and low levels of P2Y<sub>4</sub> mRNA have been detected in microglia (Light *et al*, 2006) along with protein expression (Li *et al*, 2013). There is evidence of expression in rat retinal Müller cells (Wurm *et al*, 2009) and RPE cells (Tovell & Sanderson, 2008). Translated hP2Y<sub>4</sub> receptor protein is 365 amino acids in length (both murine are 361) and only

shows 51% sequence homology to human P2Y2 receptor (Communi *et al*, 1995). Like P2Y1 and P2Y2, P2Y4 couples to PLC $\beta$ <sub>1</sub> via G $\alpha$ <sub>q/11</sub> (Erb & Weisman, 2012).

There are prominent species specificity differences for the endogenous ligands of P2Y4. UTP is a full agonist at the hP2Y4 but only a partial agonist at the rP2Y4, whereas ATP, which is a full agonist at rP2Y4 and an antagonist at hP2Y4 (Kennedy *et al*, 2000, Jacobson *et al*, 2002). Similarly to ATP, diadenosine tetraphosphate (AP4A) acts as an agonist at rP2Y4, but as an antagonist at hP2Y4 (Kennedy *et al*, 2000). ATP/UTP analogues with alternative nucleoside groups such as inosine-5'-triphosphate (ITP), guanosine-5'-triphosphate (GTP) and cytidine-5'-triphosphate (CTP) all act as partial agonists at both human and rat P2Y4 (Bogdanov *et al*, 1998, Kennedy *et al*, 2000). Relatively recently, synthetic selective P2Y4 agonists have emerged including MRS2927 and MRS4062 (Maruoka *et al*, 2011). There are currently very few antagonists for P2Y4, with the P2Y4 selective antagonist PSB-16133 having been developed only recently (Rafehi *et al*, 2017). The pan-antagonists PPADS and RB2 are antagonists at hP2Y4 and rP2Y4 respectively (Jacobson *et al*, 2009; Bogdanov *et al*, 1998).

#### **1.4.3.4 P2Y6**

P2Y6 was first cloned from aortic smooth muscle (Chang *et al*, 1995), with cloning of the human homologue from a placenta cDNA library occurring shortly after (Communi *et al*, 1996), where it was located to chromosome 11 (Pidlaoan *et al*, 1997). Reverse transcription polymerase chain reaction (RT-PCR) studies have revealed extensive expression of P2Y6 across multiple brain regions, with highest expression located in the cingulate gyrus (Moore *et al*, 2001). Notable P2Y6 expression outside the CNS includes the high levels in the spleen, as well as; macrophages and Müller cells (Moore *et al*, 2001; Fries *et al*, 2005). Evidence also suggests P2Y6 to be the most highly expressed purinergic receptor in microglia (Light *et al*, 2006). The

translated P2Y6 receptor is only 328 amino acids long for human and both rodent homologues (Bailey *et al*, 2001; Lazarowski *et al*, 2001). As a member of the first subgroup of P2YRs, P2Y6 couples to PLC $\beta$ <sub>1</sub> via G $\alpha$ <sub>q/11</sub> (Erb & Weisman, 2012), but also shows evidence of G<sub>12</sub> coupling in some cell types (Nishida *et al*, 2008).

The only endogenous full agonist for P2Y6 is UDP, however UTP and ADP are also less potent partial agonists (Communi *et al*, 1996). Several synthetic selective P2Y6 agonists have been developed including MRS2693 (Besada *et al*, 2006), MRS2782 (Ko *et al*, 2008) and MRS2957 (Maruoka *et al*, 2010). Non-competitive antagonist MRS2578 is P2Y6 selective (Mamedova *et al*, 2004). P2Y6 is also blocked by purinergic receptor pan-inhibitors PPADS, RB2 and suramin (von K $\ddot{u}$ gelgen & Hoffmann, 2016).

#### **1.4.3.5 P2Y11**

The human P2Y11 receptor was first cloned from placental tissue (Communi *et al*, 1996) and is unique among P2YRs in many aspects. Notably, the P2Y11 gene (P2RY11), found on chromosome 19, contains an intron in its coding sequence (Communi *et al*, 2001). No ortholog from rat or mouse has been cloned, although experimental evidence for a functional murine P2Y11 has been demonstrated in mouse cardiomyocytes (Balogh *et al*, 2005). P2Y11 is expressed extensively in the central nervous system, notably highly in the parahippocampal gyrus, putamen, nucleus accumbens and striatum brain regions, as well as the spinal cord, pituitary gland. It is also expressed in lymphocytes and macrophages (Moore *et al*, 2001). Structurally P2Y11 is a 374 amino acid length protein which contains much larger second and third extracellular loops than other P2YRs (Communi *et al*, 1997; Communi *et al*, 2001). P2Y11 also dually couples to G<sub>q</sub> and G<sub>s</sub> proteins (Communi *et al*, 1997; Communi *et al*, 1999; Qi *et al*, 2001). Evidence of co-expression and interaction between P2Y11R with P2Y1R has also

been demonstrated (Haas *et al*, 2014), including in functional evidence in rat microglia (Seo *et al*, 2004; Seo *et al*, 2008).

P2Y<sub>11</sub>R displays sensitivity to the endogenous ligands ATP and UTP with similar affinities (Communi *et al*, 1999; White *et al*, 2003), but not ADP. A number of synthetic agonists also have activity at P2Y<sub>11</sub>R, including BzATP, 2MeSATP, ADP $\beta$ S (Communi *et al*, 1999). Highly potent P2Y<sub>11</sub> selective agonists have also been developed, namely NF546 (Meis *et al*, 2010), and AR-C67085 (Balogh *et al*, 2005), which also displays antagonistic activity at P2Y<sub>12</sub> (Kennedy *et al*, 2013).

#### **1.4.3.6 P2Y<sub>12</sub>**

Cloned from a human platelet cDNA library (Hollopter *et al*, 2001), the human P2Y<sub>12</sub> gene (P2YR12) is located on chromosome 3. P2Y<sub>12</sub>R is expressed highly in various brain regions (Hollopter *et al*, 2001; Sasaki *et al*, 2003), as well as on lymphocytes, leukocytes and platelets (Wang *et al*, 2004). Interestingly, microglia express P2Y<sub>12</sub>R at such a high level, that it is often used as cell marker for identifying microglial cells over macrophages (Kobayashi *et al*, 2008; Zhu *et al*, 2017). The hP2Y<sub>12</sub>R structure is fairly typical for that of a P2YR, forming a 342 length amino acid protein, albeit with a distinct straight conformation of helix V (Figure 1.7; Zhang *et al*, 2014b). Murine orthologs are 343 and 347 amino acids in length for rat and mouse species respectively (Simon *et al*, 2002; Pausch *et al*, 2004). Similarly to P2Y<sub>13</sub> and P2Y<sub>14</sub> subtypes, P2Y<sub>12</sub>R signals predominately via G<sub>i</sub>/G<sub>o</sub> and inhibits adenylate cyclase activity (Sasaki *et al*, 20003; Bodor *et al*, 2003).

The principal endogenous agonist at P2Y<sub>12</sub> is ADP (Herbert & Savi, 2003), although 2MeSADP and ADP $\beta$ S are also agonists (Takasaki *et al*, 2001). Due to P2Y<sub>12</sub>R's clinical role in the regulation of blood clotting (Dorsam & Kunapuli, 2004), a number of selective synthetic irreversible antagonists for P2Y<sub>12</sub>R have been developed to prevent platelet aggregation. Of the thienopyridine class, clopidogrel and

prasugrel are prodrugs and require two sequential catalytic conversions by hepatic cytochrome enzymes to generate their pharmacologically active metabolites (Savi *et al*, 2000; Kazui *et al*, 2010). A number of experimentally used high affinity P2Y<sub>12</sub>R selective synthetic antagonists are also available that do not require metabolic activation including AZD1283 (Bach *et al*, 2013), AR-C67085 (Kennedy *et al*, 2013) and PSB0739 (Hoffmann *et al*, 2009).

#### **1.4.3.7 P2Y<sub>13</sub>**

The P2Y<sub>13</sub> receptor subtype, initially known as the orphan receptor GPR86 (Wittenberger *et al*, 2001) was first cloned from the human astrocytoma cell line 1321N1 (Communi *et al*, 2001), followed shortly by cloning of the mouse and rat orthologs (Zhang *et al*, 2002; Fumagalli *et al*, 2014). The human P2Y<sub>13</sub> gene (P2RY13) is located on chromosome 3, clustered with six closely related GPCRs, including P2Y<sub>1</sub> (Wittenberger *et al*, 2001). Expression of P2Y<sub>13</sub> has been exhibited in various cell types and tissues including platelets (Zhang *et al*, 2002), monocytes (Wang *et al*, 2004), epidermal keratinocytes (Inoue *et al*, 2007) and megakaryocytes (Balduini *et al*, 2012). Mature human P2Y<sub>13</sub> protein is 354 amino acids in length, slightly larger than both murine homologues (Zhang *et al*, 2002) and signals predominately via G<sub>i</sub>/G<sub>o</sub> (Communi *et al*, 2001)

Both ADP and ATP are endogenous agonists for P2Y<sub>13</sub>R, although the former is considerably more potent (Marteau *et al*, 2003). There are currently no P2Y<sub>13</sub>R selective agonists, however the synthetic compounds 2MeADP and 2MeATP are significantly more potent than their endogenous counterparts (Marteau *et al*, 2003). A number of synthetic P2Y<sub>13</sub>R selective antagonists have been developed, including the pyridoxal phosphate derivative compounds MRS2211 and MRS2603 (Kim *et al*, 2005), as well as the clinically used antiplatelet drug cangrelor (Marteau *et al*, 2003). The non-selective pan inhibitors suramin, PPADS and reactive blue 2 are also antagonists of P2Y<sub>13</sub>R

(Marteau, 2003), albeit with lower affinity than the selective compounds.

#### **1.4.3.8 P2Y14**

Originally cloned from human myeloid cells as the orphan receptor KIAA0001 (Nomura *et al*, 1994), P2Y14 was eventually re-classified as a P2YR subtype due to its unique pharmacological profile (Chambers *et al*, 2000). Cloning of murine orthologs followed shortly after (Freeman *et al*, 2001). The human and mouse P2Y14 receptor transcripts differ significantly but transcribe the same 338 amino acid length mature receptor (Carter *et al*, 2009), whereas the rat ortholog is significantly truncated at only 305 amino acids (Freeman *et al*, 2001). All P2Y14 homologues signal predominately via  $G_i/G_o$ . P2Y14 is fairly ubiquitously expressed, but is prominently associated with immune cells (including microglia) and epithelial cells (Abbrachio *et al*, 2006).

P2Y14 is activated by endogenous UDP-sugars, of which UDP-glucose is the most potent (Fricks *et al*, 2008). The related purine sugar compounds UDP-galactose, UDP-glucuronic acid and UDP N-acetyl-glucosamine (Fricks *et al*, 2009) are also endogenous agonists at P2Y14. There are conflicting reports of UDP acting as an agonist and as a competitive antagonist (Carter *et al*, 2009; Fricks *et al*, 2008). The first P2Y14 selective synthetic antagonist to be developed was PPTN (Barrett *et al*, 2013). The structurally related synthetic antagonists MRS4458 and MRS4478 (Yu *et al*, 2018) have since been developed with similar affinities.

#### **1.4.4 P2X receptor family**

Unlike P2Y receptors, all seven subtypes of P2X receptor are ligand gated ion channels (LGICs), with shared structural characteristics. The P2X family of receptors (P2XRs) are structurally distinct from other super-families of LGICs such as tetrameric glutamate and pentameric

Cys-loop receptors, and consist of a trimeric assembly of 3 subunits around a central non selective ion conductance pore (Jiang *et al*, 2003; Hattori & Gouaux, 2012) in a three-fold axes of symmetry. Whilst homomeric assembly of the trimeric subunits is most common, there is evidence of heteromeric trimer assembly (Saul *et al*, 2013). The topology of each subunit consists of intracellular N- and C-termini with two transmembrane spanning regions, the first of which (TM1) is linked to gating of the channel, whilst the second (TM2) forms the interior lining of the central conductance pore (Burnstock, 2007). Another characteristic feature of P2XR subunits is a large extracellular loop (the ectodomain) between TM1 and TM2 (Clyne *et al*, 2002; Ennion & Evans, 2002; Rokic *et al*, 2010).

The endogenous ligand for all P2XRs is ATP. Despite this P2XRs do not contain a Walker motif characteristic of proteins that bind ATP (Walker *et al*, 1982). Initially experimental evidence (Nagaya *et al*, 2005), followed by experiments combining mutagenesis and electrophysiology on eight highly conserved amino acid residues of the ectodomain of zfP2X4 (K70, K72, N96, F188, T189, F297, R298 and K316) (Ennion *et al*, 2000; Wilkinson *et al*, 2006; Fischer *et al*, 2007; Marquez-Klaka *et al*, 2007; Roberts & Evans, 2007), led to the hypothesised ATP binding site for P2XRs as a positively charged pocket at an interface between two adjacent subunits, with three sites in total per assembled trimeric receptor (Marquez-Klaka *et al*, 2007). With the publication of the X-ray crystal structure of the zebrafish P2X4 receptor (zfP2X4) in its closed state (Kawate *et al*, 2009), followed soon after in its open pore state with ATP bound (Hattori & Gouaux, 2012), and more recently the crystal structure of P2X3 at three different stages of the gating cycle (Mansoor *et al*, 2016), confirmation of the ATP binding site location in P2XRs, as well as the mechanisms of conformational changes associated with its binding followed (Figure 1.8). Due to the existence of three ATP binding sites per trimeric receptor, it was initially unclear whether one ATP molecule bound was sufficient stimulus to open the

ion channel pore. It has subsequently been recognised that whilst the binding of one ATP molecule is not sufficient for channel opening, it does induce a receptor conformation change, resulting in an alteration of the second and third ATP binding sites, demonstrating positive cooperative binding for the subsequent ATP molecules (Jiang *et al*, 2012).

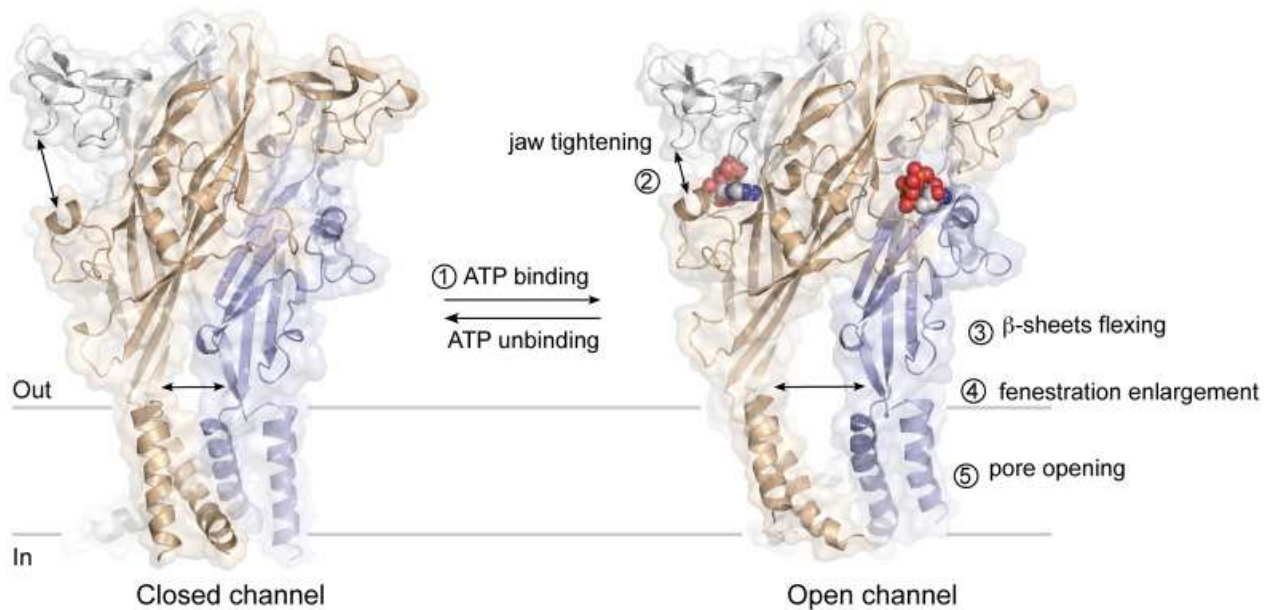


**Figure 1.8:** Representation of the P2XR superfamilies characteristic trimeric structure, in its closed channel and open channel forms with ATP bound. Proposed sequence of channel opening in response to ATP binding is labelled 1-5. From Chataigneau *et al*, 2013.

Despite the approximate 30-50% peptide sequence homology across the seven P2XR subtypes (North, 2002; Stojilkovic *et al*, 2005), there exists a reasonably large variation in P2XR channel dynamics and tissue distribution, which in turn implicates different subtypes in a vast range of homeostatic functions throughout the body.

#### 1.5.4.1 P2X1

The first cloned receptor of the P2XR class was isolated from rat vas deferens tissue (Valera *et al*, 1994), and was named P2X1. Shortly after, the human P2X1 ortholog was cloned from a urinary bladder cDNA library (Longhurst *et al*, 1996). The human P2X1 gene (P2RX1) is

located near that of P2X5 (and the vanilloid receptor, VR1) on the short arm of chromosome 17 (Longhurst *et al*, 1996). As well as bladder tissue that it was originally cloned from, human P2X1 is also highly expressed in the vas deferens (similar to rat expression) (Banks, *et al*, 2006), smooth muscle cells (Wang *et al*, 2002), arteries (Bo *et al*, 1998) and moderately expressed in platelets (Scase *et al*, 1998; Vial *et al*, 1997), lymphocytes (Sluyter *et al*, 2001), mast cells (Wareham *et al*, 2009) and multiple cardiac tissues (Berry *et al*, 1999). Additionally, in mice, P2X1 is similarly highly expressed in vas deferens (Mulryan *et al*, 2000), bladder and smooth muscle (Vial & Evans, 2000; Vial & Evans, 2001) and arteries (Vial & Evans 2002). P2X1 is also moderately expressed in multiple rodent immune cell types including neutrophils (Lecut *et al*, 2009) and macrophages (Sim *et al*, 2007).

The P2X1 subunit is 399 amino acids in length (~45kDA) and contains the P2XR superfamily characteristics including intracellular termini and a large extracellular loop between two transmembrane regions (Longhurst *et al*, 1996). When assembled as a homotrimeric LGIC, the resulting channel is cation selective and non-selectively permeable between Na<sup>+</sup> and K<sup>+</sup>, and highly permeable to Ca<sup>2+</sup> (Evans *et al*, 1996). Kinetically, P2X1 displays rapid desensitization within a timeframe of 10-100ms upon prolonged ATP stimulation (>1μM) as well as slow desensitization recovery (North, 2002; North & Jarvis, 2013). P2X1 is pharmacologically profiled by the equipotency of the full agonist αβ-methylene ATP (αβ-meATP) and ATP, both of which have an EC<sub>50</sub> of ~1μM (Valera *et al*, 1994; Evans *et al*, 1996). Additionally, both 2'(3')-O-(4-Benzoylbenzoyl)adenosine-5'-triphosphate (BzATP) and L-βγ-methylene ATP (βγ-meATP) are full agonists at P2X1, where βγmeATP is 30-fold more potent at P2X1 than P2X3 (Bianchi *et al*, 1999; Evans *et al*, 1995). Common P2XR pan blockers PPADS and suramin, as well suramin derived structural analogs such as NF449 and NF023 are antagonists at P2X1 (Evans *et al*, 1995; Jacobson *et al*, 2002; Hülsmann *et al*, 2003), however synthetic compounds have been

developed that are more selective to P2X1 including MRS2220 (Jacobson *et al*, 1998). Another class of P2X1 antagonists are Trinitrophenyl substituted nucleotides TNP-ATP, TNP-ADP and TNP-GTP however none are selective solely towards P2X1 and also act as antagonists at P2X2/3 (Virginio *et al*, 1998).

#### **1.5.4.2 P2X2**

As with P2X1, the cloning of P2X2 cDNA from rat origin nerve growth factor (NGF) differentiated PC12 neuronal cells (Brake *et al*, 1994) preceded the cloning of the human homologue, which was eventually isolated from the pituitary gland (Lynch *et al*, 1999). The human P2X2 gene (P2RX2) is located on chromosome 12 (Lynch *et al*, 1999). P2X2 is has widespread tissue distribution including extensive expression throughout the CNS as well as expression in various non-neuronal cell types (Burnstock & Knight 2004).

The human P2X2 subunit exists as six different splice variants and thus ranges in size from 379 amino acids (variant H) to 497 amino acids in length (variant D), where variant A is regarded as the canonical isoform which is 471 amino acids in length. Much of our current knowledge of the structure of P2XR subunits comes from data initial experiments on the P2X2 subtype. The ion channel pore formed by homotrimeric P2X2 subtype assembly is permeable to multiple monovalent cations, as well as  $\text{Ca}^{2+}$  (Evans *et al*, 1996). Stimulation by ATP of P2X2 produces relatively sustained currents (Brake *et al*, 1994), and shows resistance to desensitisation compared with P2X1 (North, 2002; North & Jarvis, 2013).

There are no known additional agonists for P2X2 other than the endogenous ligand ATP ( $\text{EC}_{50}$  1.5 $\mu\text{M}$ ) (Jacobson *et al*, 2009). However, P2X2 does have the unusual property of reversible potentiation by micromolar concentrations of extracellular zinc and copper ions

(Wildman *et al*, 1998), as well as protons (Stoop *et al*, 1997). Currently only the competitive antagonist PSB-10211 is selective for P2X2 (IC<sub>50</sub> 86nM) over other P2XRs (Baqi *et al*, 2011), but pan inhibitors such as PPADS also act as non-competitive antagonists at P2X2 albeit several magnitudes of potency lower than at P2X1 (Donnelly-Roberts *et al*, 2009).

#### **1.5.4.3 P2X3**

P2X3 subunits were first cloned from rat dorsal root ganglion cDNA libraries (Chen *et al*, 1995), with cloning of the human homologue from a heart cDNA library following soon after (Garcia-Guzman *et al*, 1997a). It is situated on chromosome 11, and early studies showed a limited distribution of hP2X3 to the spinal cord and heart (Garcia-Guzman *et al*, 1997a). Subsequent studies have demonstrated mP2X3 receptor expression throughout the sensory nervous system, including trigeminal, dorsal root and petrosal ganglia (Bradbury *et al*, 1998). P2X3 expression has also been shown in the rat retina, located at axon terminals of rod and cone cells, as well as in amacrine cells (Puthussery & Fletcher, 2007). Immune cells that express P2X3 include B cells (Przybyla *et al*, 2018) and mast cells (Cekic & Linden, 2016). The P2X3 subunit structure is a 397 amino acid protein for human, mouse and rat orthologs.

P2X3 has a similar pharmacological profile to that of P2X1, with approximate equipotency of ATP and  $\alpha\beta$ meATP (North, 2002). Additional agonists at P2X3 include BzATP and 2-MeSATP, which is more potent than ATP (Chen *et al*, 1995; Garcia-Guzman *et al*, 1997a). Some compounds with P2X3 selective antagonism with high potency have been developed, including A317491 (Jarvis *et al*, 2002), AF-906 and AF-219 (Jacobson & Müller, 2016). P2X3 is also inhibited by the pan blockers PPADS, TNP-ATP and suramin.

#### 1.5.4.4 P2X4

The rat P2X4 was cloned by 5 groups independently at around the same time (Buell *et al*, 1996; Séguéla *et al*, 1996; Soto *et al*, 1996a, Bo *et al*, 1996) from various brain regions and pancreatic islet cells (Wang *et al*, 1996). The human P2X4 was cloned shortly after the rat homologue from human brain (Garcia-Guzman *et al*, 1997b). P2X4 is one of the most widely expressed P2XR subtypes, being found on most glial cells and neurons (Buell *et al*, 1996 ; Amadio *et al*, 2007), including microglia (Tsuda *et al*, 2003; Vazquez-Villoldo *et al*, 2014). Immunohistochemical staining of the mammalian retina has revealed P2X4 localised to terminals post-synaptic to rod and bipolar cells, likely representing horizontal and amacrine cells (Ho *et al*, 2014), and separate studies have found P2X4 mRNA expression in bipolar cells (Wheeler-Schilling *et al*, 2000). P2X4 subunit structure forms a 388 amino acid protein subunit (Garcia-Guzman *et al*, 1997b).

The P2X4 receptor channel displays dual states of activation, where brief applications of agonist (such as ATP) cause a cation-selective channel, where Ca<sup>2+</sup> permeability is the highest amongst all P2XR subtypes (Egan & Khakh, 2004). Continual stimulation for several seconds causes the formation of an increasingly permeable channel to larger organic cations such as N-methyl D-glutamine (NMDG<sup>+</sup>) (Khakh *et al*, 1999a) and inorganic fluorescent dyes such as YOPRO-1 and ethidium bromide (Bernier *et al*, 2012). The pharmacological profile of P2X4 is interesting as it includes several positive allosteric modulators (PAMs), including ivermectin (Khakh *et al*, 1999b) and extracts of the *Panax ginseng* termed ginsenosides (Dhuna *et al*, 2019), although ginsenosides are less potent than their action at P2X7 receptors. The most potent agonist of P2X4 is ATP with a reported EC<sub>50</sub> of 7.4µM for the human ortholog (Garcia-Guzman *et al*, 1997b). 2-meSATP, CTP, αβ-meATP and dATP have also shown agonist activity at P2X4 (Soto *et al*, 1996b), with BzATP also acting as a partial agonist (Bowler *et al*, 2003; Stokes *et al*, 2011). Several synthetic P2X4 selective antagonist

have also been developed, including 5-BDBD, PSB12062 and BX430, which has no activity at mP2X4 (North & Jarvis, 2013).

#### **1.5.4.5 P2X5**

P2X5 was first isolated from rat heart and celiac ganglion cDNA libraries (Collo *et al*, 1996; Garcia-Guzman *et al*, 1996) followed by the human homologue a year later (Lê *et al*, 1997). P2X5 expression and tissue distribution has been less extensively explored, but it has been shown on both B cells and T cells (Przbyla *et al*, 2018; Cekic & Linden, 2016), and immunoreactivity has been shown in the soma of cholinergic amacrine cells in the ganglion cell layer (Shigematsu *et al*, 2007), as well as mRNA transcripts in Müller cells and retinal ganglion cells (Jabs *et al*, 2000; Wheeler-Schilling *et al*, 2001)

P2X5 currents are comparatively smaller than those of other P2XR subtypes, whilst they otherwise resemble channel dynamics of the P2X2 receptor, with little desensitization (North, 2002). Murine P2X5 subunits form a 455 amino acid protein, but is slightly truncated in human P2X5 at 422 amino acids (Lê *et al*, 1997).

A $\beta$ -meATP acts as an agonist at P2X5 with an approximate 10-fold lower potency than ATP (Ruppelt *et al*, 2001) and BzATP is a full agonist with similar potency to ATP at the human isoform (Bo *et al*, 2003). No synthetic P2X5 selective antagonist have been developed, however agonist action at P2X5 is inhibited by the purinergic pan-inhibitors PPADS, BBG, and suramin (Syed & Kennedy, 2012). TNP-ATP also acts as an antagonist at P2X5, albeit at several orders of magnitude less than P2X1 and P2X3 (North & Jarvis, 2013).

#### **1.5.4.6 P2X6**

The first P2X6 receptor ortholog to be cloned was from a rat superior cervical ganglion cDNA library and subsequently rat brain tissue (Collo *et al*, 1996; Soto *et al*, 1999), whilst the human ortholog was isolated from lymphocytes (Urano *et al*, 1997) and was originally designated

P2XM due to its widespread expression in human and mouse skeletal muscle (Nawa *et al*, 1998). P2X6 has also been shown to be expressed in B cells (Przbyla *et al*, 2018) and mRNA expression is extensive throughout the CNS, including in the brain and spinal cord (Collo *et al*, 1996). Homologous P2X6 expresses poorly and is usually unable to form functional homomers (Torres *et al*, 1999), and when it does express, no currents are evoked from ATP stimulation (Soto *et al*, 1999). P2X6 containing heterologs, including P2X2/6 and P2X4/6 are activated by 2-meSATP and antagonised by suramin and PPADS (King *et al*, 2000; Lê *et al*, 1997)

#### **1.5.4.7 P2X7**

Originally referred to as the P2Z receptor (Falzoni *et al*, 1995; Baricordi *et al*, 1996; Blanchard *et al*, 1996) before reclassification (Suprenant *et al*, 1996), the homomeric P2X7 receptor subtype is the most structurally and functionally unique of the P2X family. Full length cDNA sequences were first cloned from rat brain (Suprenant *et al*, 1996), followed by the human (Rassendren *et al*, 1997; Buell *et al*, 1998) and then mouse microglial cells (Chessel *et al*, 1998). The human P2X7 gene (P2RX7) contains 13 exons and is located on chromosome 12, within 130kb of P2RX4's location (Buell *et al*, 1996). With different combinations of exons, there exist several splice variants of P2X7, including seven of hP2X7 (Cheewatrakoolpong *et al*, 2005; Sluyter & Stokes, 2011), which can affect the binding properties of agonists and protein interactions (Xu *et al*, 2012). These splice variants were designated P2X7B-P2X7H, where the original full length variant was designated P2X7A (Figure 1.9). A further 3 splice variants, including one in rodent P2X7 (P2X7K), have since been discovered (Feng *et al*, 2006; Nicke *et al*, 2009). P2X7B is a biologically relevant splice variant, which contains a truncated c terminus caused by the transcription of the intron between exons 10 and 11, resulting in the introduction of a new stop codon (Cheewatrakoolpong *et al*, 2005; Adinolfi *et al*, 2010).

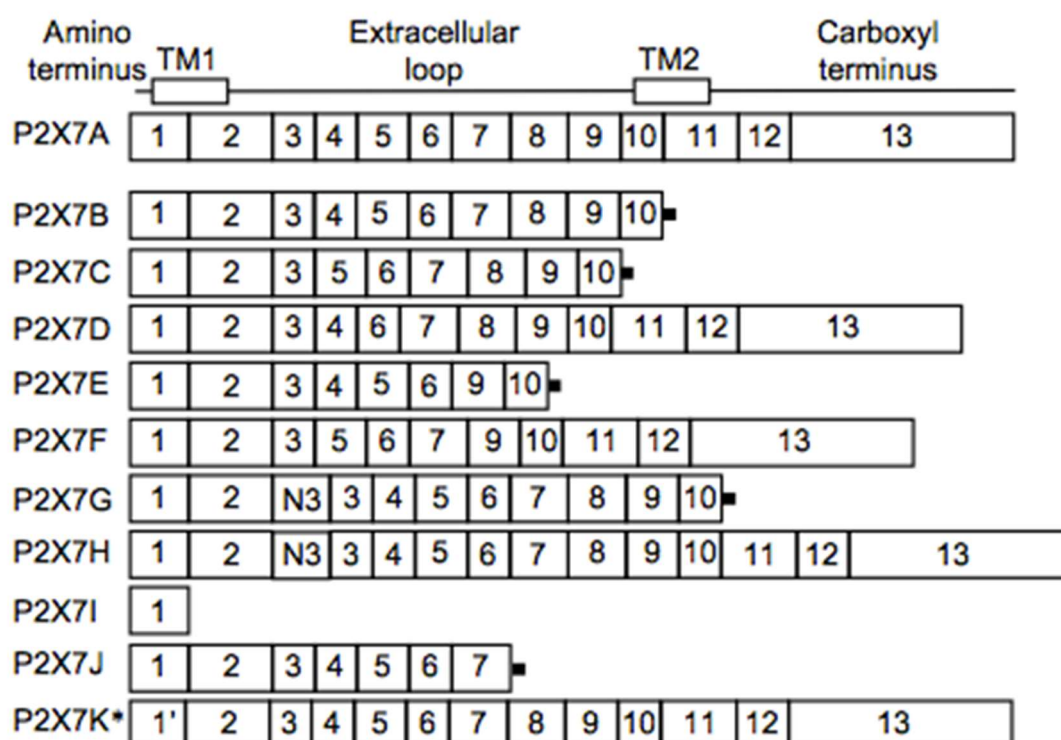


**Figure 1.9:** Schematic view of exons expressed (1-13) in known P2X7 splice variants. From Sluyter & Stokes, 2011

The hP2X7 gene also displays a large number (>686) of single nucleotide polymorphisms (SNPs), including 16 non-synonymous that have been well characterised (Sun *et al*, 2010; Sluyter & Stokes, 2011). Of those 16 characterised, multiple instances have shown evidence of a loss of function (Gu *et al*, 2001; Fernando *et al*, 2005; Sheman *et al*, 2006; Lees *et al*, 2010), with gain of function SNPs also evident (Stokes *et al*, 2010). One SNP has the unique property of loss of function for pore formation, but not for P2X7 channel function (Boldt *et al*, 2003). Expression of P2X7 is predominately on cells of the immune system (Collo *et al*, 1997; Burnstock & Lavin, 2004), including macrophages/monocytes (Collo *et al*, 1997), mast cells (Bulanova *et al*, 2005), lymphocytes (Gu, 2000), and microglia (Ferrari *et al*, 1997a; Xiang & Burnstock, 2005), where it is located primarily at the cell surface Boumechache *et al*, 2009). Additionally in the CNS, P2X7R is expressed on neurons (Anderson & Nedergaard, 2006), including RGCs

(Mitchell *et al*, 2009) and also Müller cells (Franke *et al*, 2001). P2X7 is also expressed outside of the CNS in a variety of tissues, including osteoblasts (Gartland *et al*, 2001), fibroblasts (Solini *et al*, 1999) and epithelial cells (Groschl-Stewart *et al*, 1999).

Translation of the original full-length P2X7 subunit gene produces a subunit 595 amino acids in length (Nicke, 2008), by far the largest of any P2XR subtype. It contains a characteristically large C-terminus, which contains an additional hydrophobic sequence that may be involved in the formation of another TM domain (North, 2002).

Repeated P2X7 stimulation does not display desensitisation kinetics for the ion channel (North, 2002), however the onset of inward current has been shown to become slower after successive agonist applications (Suprenant *et al*, 1996). When in a *Xenopus oocyte* expression system, P2X7 demonstrates two-component onset/offset kinetics, suggesting ATP binds at two different ligand binding domains (Klapperstuck *et al*, 2000; Klapperstuck *et al*, 2001). Similarly to P2X4, prolonged agonist stimulation of P2X7 recruits the formation of a large diameter cytolitic pore (Smart *et al*, 2003), which is commonly measurable by the use of DNA intercalating fluorescent dyes such as ethidium and YO-PRO-1. Whilst the identity of the large cytolitic pore remains elusive, connexin knockout and hemichannel antagonist studies (Pelegriin & Suprenant, 2006) suggest that the connexin and pannexin family of hemichannels, such as pannexin-1 may be responsible (Locovei *et al*, 2007; Qu *et al*, 2011), although other studies contradict this (Alberto *et al*, 2013).

Whilst it is an endogenous agonist, compared to other P2XR subtypes P2X7 requires much higher concentrations of ATP (>100 $\mu$ M, typically millimolar) to activate its central ion channel pore (North, 2002; Anderson & Nerdergaard, 2006), compared to other P2XRs.

Endogenous ADP and AMP are also very weak agonists for P2X7, however their efficacy increases if following a brief stimulation with ATP (Chakfe *et al*, 2002). Conversely the synthetic agonist BzATP is

more 10-30 times more potent than ATP at P2X7, but despite common conception, it is not P2X7 selective. BzATP also displays a progressive increase in agonist potency upon repeated stimulation (Hibell *et al*, 2000). There are numerous modulators for P2X7 activity. Extracellular ion concentration plays a role in modulating agonist potency, whereby lowering Mg<sup>2+</sup> and Ca<sup>2+</sup> increases ATP and BzATP potency (Suprenant *et al*, 1996). In similar fashion to its action at P2X4, ivermectin acts as a human-selective positive modulator of P2X7 (Nörenberg *et al*, 2012). Positive allosteric modulation has also been demonstrated with compounds from the *Panax ginseng* extract, termed ginsenosides (Helliwell *et al*, 2015). GW791343 has species dependent allosteric modulation, acting as a positive modulator at rat, and a negative modulator at human P2X7 (Michel *et al*, 2008). Oxidised ATP (oATP), an irreversible P2X7 antagonist, is also commonly used in experimental models (Murgia *et al*, 1993). Several P2X7 selective, highly potent synthetic antagonists have been developed and used experimentally, including AZ10606120 (Michel *et al*, 2008), JNJ-47965567 (Bhattacharya *et al*, 2013) and A839977 (Donnelly-Roberts & Jarvis, 2007; Donnelly-Roberts *et al*, 2009).

#### **1.4.5 Purinergic receptors in microglia**

Expression of P2 receptor mRNA in primary microglia has been extensively reported. Although it is likely that microglia express all P2Y subtypes, expression predominantly consists of subtypes P2Y2, 6, 12, 13 and 14 (Visentin *et al*, 2006; Inoue *et al*, 2006; Light *et al*, 2006; Koizumi *et al*, 2007; Crain *et al*, 2009). The most prominently expressed P2XRs appear to be P2X4 and P2X7 (Sperlagh & Illes, 2007; He *et al*, 2017). The function of many of these receptors has been linked to key microglial processes.

Under stimulation by pathological stimuli, microglial cells undergo directional migration toward areas of damage/injury by following a chemical gradient of a specific danger signal in a process known as

chemotaxis. Early studies demonstrated that microglia undergo chemotaxis in response to extracellular ATP and ADP (Honda *et al*, 2001). Microglial chemotaxis has been shown to be mediated by multiple purinergic receptors. Firstly, P2Y<sub>12</sub> was elucidated as the receptor responsible for ADP mediated chemotaxis (Haynes *et al*, 2006) and required downstream Akt activation and a phospholipase-C (PLC) mediated increase in intracellular Ca<sup>2+</sup> (Irimo *et al*, 2008). It was followed shortly by the discovery that ATP mediated microglial chemotaxis was via P2X<sub>4</sub> receptors (Ohsawa *et al*, 2007), in a phosphoinositol-3 kinase (PI3K) dependent mechanism of actin polymerisation at the leading edge membrane. The purinergic system also plays a key role in the signalling between microglia and neurons as neuronal derived ATP (and additionally glutamate) have been shown to attract microglial processes (Kato *et al*, 2016), which is thought to demonstrate the ability of microglia to detect changes in neuronal activity.

Phagocytosis is the process by which a cell ingests/engulfs relatively large particles (>1µm) from the extracellular milieu into an internal phagosome compartment. Phagocytosis is required for immune cells such as microglia in the clearing of bacteria, pathogens and cellular debris/apoptotic bodies. Microglia are able to phagocytose appropriate targets by their recognition by a number of receptors, including Fc receptors, complement receptors, scavenger receptors and endotoxin receptors (Ulvestad *et al*, 1994). P2Y<sub>6</sub> stimulation by its endogenous agonist UDP has been shown to stimulate microglial phagocytosis (Koizumi *et al*, 2007; Inoue, 2007). This experimental evidence suggests a role for UDP released from damaged/dying cells to act as a phagocytosis signal for neighbouring microglia in a mechanism that is separate from ATP/ADP mediated chemotaxis. P2X<sub>4</sub> mediated phagocytosis has also been demonstrated in alveolar macrophages (Stokes & Suprenant, 2009), however it is currently unknown if this is reproducible in microglia.

Recent evidence has emerged that demonstrates a role for microglial P2X4 in mediating neuropathic and chronic pain. Whilst the majority of microglial P2X4 receptor is located in intracellular lysosomal compartments (Quershi *et al*, 2007), P2X4 expression is upregulated in activated spinal microglia (Ulmann *et al*, 2008). Microglial P2X4 stimulation induces the release of brain derived neurotrophic factor (BDNF), which in turn signals to spinal interneurons to alter GABAergic signalling resulting in pain hypersensitivity (Coull *et al*, 2005). This is demonstrated by the lack of mechanical hyperalgesia development in P2X4<sup>-/-</sup> knockout mice following peripheral nerve injury (Ulmann *et al*, 2008).

Another important function of microglia is their ability to produce and process a number of inflammatory cytokines and interleukins in response to pathological stimuli. The processing of some interleukins such as interleukin-1 $\beta$  and interleukin-18 require proteolytic conversion from an inactive precursor, by a pattern recognition receptor (PRR) caspase complex known as an inflammasome (see 1.61).

#### **1.4.6 Purinergic signalling in glaucoma**

Due to the ubiquity of purinergic ligands/neurotransmitters, the role purinergic signalling in the eye is complex governing multiple ocular functions (Sanderson *et al*, 2014), with abundant evidence for purinergic signalling and specifically ATP involvement in glaucoma pathogenesis. Isolated rat retinas that have been mechanically stimulated have been shown to release ATP from Müller cells (Newman, 2003), and similarly stimulated optic nerve head astrocytes show a similar effect (Beckel *et al*, 2014). More specifically, several studies utilising elevated pressure to simulate glaucoma pathology have shown increases in vitreous/extracellular ATP concentrations (Reigada *et al*, 2008). However, this phenomenon of mechanical stress on the release of ATP is common throughout the body, as demonstrated in a number

of tissues including those found in the bladder (Ferguson *et al*, 1997) and blood vessels (Bodin, *et al*, 1991).

The effects of extracellular ATP on retinal tissue/cell types has been investigated in a number of studies. Key to glaucoma pathogenesis, are the effects of ATP on retinal ganglion cells. Healthy retinal ganglion cells contain an abundance of P2X7 receptors (Sperlagh *et al*, 2006), which appear to be the prime receptor for mediating ATP induced cell death (Zhang *et al*, 2005; Xue *et al*, 2016). A number of studies have been shown to support that ATP, and potent agonist BzATP, stimulation of P2X7 on retinal ganglion cells causes cell death via increase of intracellular Ca<sup>2+</sup> and caspase activation (Zhang *et al*, 2005; Hu *et al*, 2008; Hu *et al*, 2010). Pharmacological antagonism of the receptor with BBG have shown a reduction in the level of RGC death following BzATP stimulation (Hu *et al*, 2010). In support of this evidence, recent findings using a human retinal explant model have found that P2X7 activation resulting in RGCs death either by direct stimulation with BzATP; or when modelling retina ischaemia by oxygen glucose deprivation (OGD) (Niyadurupola, 2013).

In contrast to ATP, extracellular adenosine has shown a neuroprotective effect on RGCs. Methods to degrade extracellular ATP have shown increased RGC cell survival after elevated pressure stimulation (Zhang *et al*, 2006). Furthermore, adenosine, a purine signalling molecule produced by the degradation of ATP, provides general neuroprotective effects by stimulation of A<sub>1</sub> receptors (Newman, 2004), and adenosine stimulation of A<sub>3</sub> receptors on RGCs prevents P2X7 mediated cell death (Zhang *et al*, 2006). However, in direct contrast, there is also evidence that adenosine may play a deleterious role, as antagonism of the A<sub>2A</sub> Receptor with SCH 58261 caused a decrease in pro-inflammatory mediator secretion and also reduced RGC cell loss in an elevated IOP model (Madeira *et al*, 2015). This

evidence suggests that the homeostatic balance of extracellular ATP and adenosine could play a crucial role in the conditions that give rise to the pathogenesis of glaucoma, mediating both neuroprotection and cell death, exacerbating the latter when an imbalance of this natural homeostasis emerges.

## **1.5 Calcium Signalling**

Calcium ( $\text{Ca}^{2+}$ ) is a ubiquitous ionic second-messenger signalling molecule that regulates a diverse number of intrinsic and extrinsic cellular functions. All P2 receptors signal, at least in part, via  $\text{Ca}^{2+}$ .

### **1.5.1 Intracellular calcium homeostasis**

Under resting conditions, the cytoplasmic  $\text{Ca}^{2+}$  concentration of a mammalian cell is  $\sim 100\text{nM}$ , which is a large contrast to the typical millimolar (mM) concentration of extracellular  $\text{Ca}^{2+}$  (Breitwieser *et al*, 2008). Cells have several mechanisms in order to maintain such a low cytoplasmic  $\text{Ca}^{2+}$  including the constant extrusion of  $\text{Ca}^{2+}$  into the extracellular milieu by plasma membrane  $\text{Ca}^{2+}$  ATPase (PMCA) transporters, and by sequestration into intracellular organelles, such as the endoplasmic reticulum by smooth endoplasmic reticular  $\text{Ca}^{2+}$  ATPase (SERCA), both of which are active transporters and require ATP hydrolysis as an energy source (Bootman, 2012). Another mechanism utilised is the  $\text{Na}^+/\text{Ca}^{2+}$  (NCX) and  $\text{Na}^+/\text{Ca}^{2+}/\text{K}^+$  (NCXK) exchange transporters, which utilise the energy from inward  $\text{Na}^+$  movement to power  $\text{Ca}^{2+}$  extrusion from the cytosol.  $\text{Ca}^{2+}$  is also stored in the mitochondria, which is mediated by both mitochondrial calcium uniporters and NCXs

### **1.5.2 Calcium second messenger signalling**

$\text{Ca}^{2+}$  has excellent biochemical properties that allow it to act as an effective second messenger, such as its ubiquitous nature and the large concentration gradient between intra- and extracellular

compartments. For  $\text{Ca}^{2+}$  to act as a second messenger, it requires stimulus-based access to cytosolic components, such as enzymes and signalling proteins on which to exert its effects. Mechanisms for periodically increasing cytosolic  $\text{Ca}^{2+}$  can be broadly divided into two categories, extracellular  $\text{Ca}^{2+}$  entry through plasma membrane  $\text{Ca}^{2+}$  channels, and mobilisation of intracellular  $\text{Ca}^{2+}$  stores via intermediary signalling pathways.

Calcium channels are ion channels permeable to  $\text{Ca}^{2+}$ . When activated, a conformational change occurs leading to the opening of the channel and the rapid transmission of  $\text{Ca}^{2+}$  into the cytosol. The enormous ~20,000 fold concentration gradient across the plasma membrane means that  $\text{Ca}^{2+}$  channels allows rapid  $\text{Ca}^{2+}$  influx. Calcium permeable channels can be divided in two categories based on their activation stimulus, voltage-gated calcium channels (VGCC or VDCC) and ligand-gated ion channels (LGIC), which may or may not be selective for  $\text{Ca}^{2+}$ .

VGCCs are located in the membrane of excitable cells, such as muscle cells, and neurons. They are closed under resting physiological membrane potential and are activated upon depolarization of the cell membrane. All VGCCs share structural similarities, consisting of a complex of multiple protein subunits, which form around a central conductive pore that  $\text{Ca}^{2+}$  is transmitted through. VGCCs are categorized as L-, N-, P-, Q-, R- and T-type based on a number of factors, namely their  $\text{Ca}^{2+}$  conductance kinetics, activation and inactivation kinetics and their sensitivity to antagonists, which are all governed by the subunits that contribute to the assembled receptor (Catterall & Swanson, 2015).

LGICs are a diverse family of calcium channels that require stimulation via the binding of a specific ligand. Unlike VGCCs, LGICs can be found both in the plasma membrane and in the membranes of intracellular organelles where calcium is sequestered, and as such can

be responsible for both extracellular  $\text{Ca}^{2+}$  entry and internal store mobilisation. Ryanodine receptors (RyRs) are a class ER/SR bound  $\text{Ca}^{2+}$  permeable receptor channels found in various excitable tissue types such as cardiac and skeletal muscle. Three mammalian isoforms of RyRs have been discovered (RyR1-3) with differing tissue distributions (Lanner *et al*, 2010). RyRs are principally activated by elevated levels of cytosolic  $\text{Ca}^{2+}$  from events such as activation of VGCCs, and thus play a key role in the positive feedback process of  $\text{Ca}^{2+}$  induced  $\text{Ca}^{2+}$  release (Berridge *et al*, 2000). Inositol 1,4,5-trisphosphate ( $\text{IP}_3$ ) receptors ( $\text{IP}_3\text{R}$ ) are  $\text{Ca}^{2+}$  selective LGICs (Furuichi *et al*, 1989), expressed ubiquitously in almost all cell types (Taylor *et al*, 1999), and play an integral role in  $\text{Ca}^{2+}$  release from intracellular stores (Berridge, 1993) and is localised on the membrane of the ER (Otsu *et al*, 1990). Three isoforms of the  $\text{IP}_3\text{R}$  have been discovered ( $\text{IP}_3\text{R}1-3$ ), each with different  $\text{IP}_3$  binding affinities, as a result of structural differences. Upon activation of  $\text{IP}_3\text{Rs}$ , sequestered  $\text{Ca}^{2+}$  from the ER freely diffuses down the electrochemical gradient into the cytosol, where it is able to propagate further intracellular signalling pathways. Upon depletion of endoplasmic reticulum  $\text{Ca}^{2+}$ , the store-operated calcium channel (SOC) STIM accumulates at the endoplasmic reticulum plasma membrane and interacts with Orai channels in the cell plasma membrane to allow extracellular  $\text{Ca}^{2+}$  influx and restoration of endoplasmic reticular  $\text{Ca}^{2+}$  stores (Prakriya & Lewis 2015).

The principal agonist of  $\text{IP}_3\text{R}$  is the lipid second messenger molecule  $\text{IP}_3$ . A wide array of extracellular signalling molecules instigate the production of intracellular  $\text{IP}_3$ , principally via two classes of cell surface receptor, GPCRs and tyrosine kinase receptors (TRKs) (Berridge, 2016). The stimulation of both receptor classes results in the activation of one of multiple subclasses of the phospholipase C (PLC) class of enzymes. In the case of GPCRs, the PLC- $\beta$  isoform is activated, whereas TRK activation induces the PLC- $\gamma$  isoform (Cocco *et al*, 2015).

Once activated, PLC catalyses the cleavage of membrane bound phospholipid phosphatidylinositol 4,5-bisphosphate (PIP<sub>2</sub>), generating IP<sub>3</sub> and concurrently producing the secondary messenger molecule diacylglycerol (DAG) (Figure 1.10). IP<sub>3</sub> is then able to freely diffuse into the cytosol where it interacts with IP<sub>3</sub>Rs.

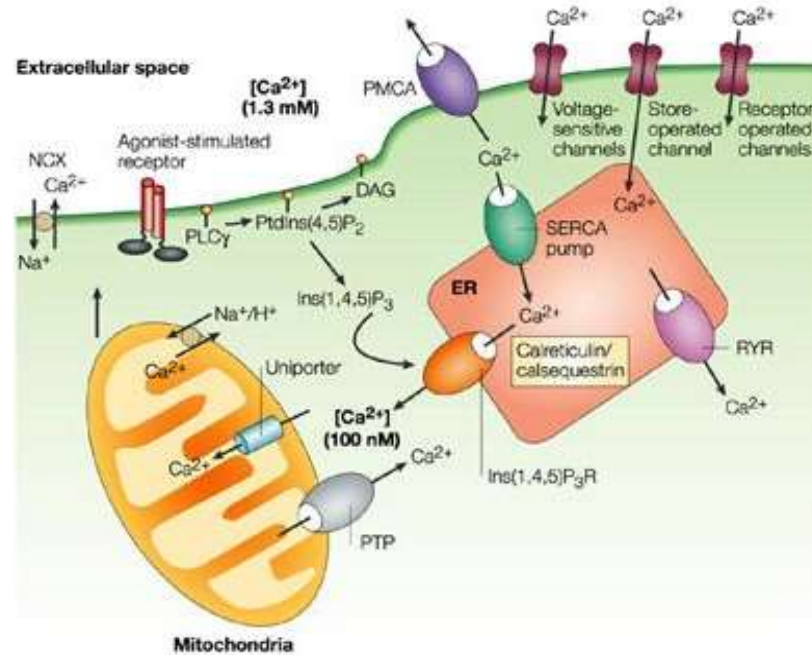


**Figure 1.10:** Diagram of cellular Ca<sup>2+</sup> homeostasis and mobilisation mechanisms. Adapted from Orrenius *et al*, 2004.

The mitochondrial permeability transition pore (MPTP) which is formed during the apoptotic signalling cascade of events and releases mitochondrial stored Ca<sup>2+</sup> into the cytoplasm.

LGICs, in the plasma membrane, also termed ionotropic receptors, constitute a primary mechanism of cytosolic Ca<sup>2+</sup> entry from the extracellular milieu, although most examples are not Ca<sup>2+</sup> selective, and conduct additional cations. A wide number of ionotropic receptors including the N-methyl D-aspartate (NMDA) subtype of glutamate (Glu) receptors, nicotinic acetylcholine (ACh) receptors and the P2X family of purinergic receptors have all been shown to have higher Ca<sup>2+</sup>

permeability than for monovalent cations (Punkratov & Lalo, 2014) and are widely expressed throughout the central nervous system.

### **1.5.3 Purinergic mediated Ca<sup>2+</sup> signalling**

Both P2Y and P2X receptor families play a role in Ca<sup>2+</sup> signalling. Intracellular Ca<sup>2+</sup> increase via store mobilisation, in response to P2YR agonists, has been demonstrated in a number of different cell types. Of the GPCR coupled P2Y family, receptor subtypes 1,2,4,6 & 11 all couple directly to Gq or G<sub>11</sub>, and thus their stimulation causes PLC-β activation, generation of IP<sub>3</sub> and subsequent mobilisation of intracellular calcium stores (Dubyak & El-Moatassim, 1993; Burnstock 1997). Furthermore, P2YR subtypes 12, 13 & 14 are also able to indirectly regulate intracellular Ca<sup>2+</sup> levels, including via modulation of N-type Ca<sup>2+</sup> channels (Burnstock, 2007). Despite being coupled to Gα<sub>o</sub>, P2Y14 has been shown to mediate Ca<sup>2+</sup> influx in endothelial cells via the β/γ subunits (Fumagalli *et al*, 2003). Additionally, UDP-glucose stimulation of glial cells causes Ca<sup>2+</sup> signalling, further highlighting a potential role for P2Y14 in cell specific Ca<sup>2+</sup> signalling.

In contrast to P2YRs, all P2XRs are ionotropic, and all subtypes have demonstrated Ca<sup>2+</sup> conductance (in addition to other cations) in isolated systems (Egan & Khakh, 2004). The subunit composition and ligand sensitivity of each P2XR subtype determines the magnitude and duration of the subsequent Ca<sup>2+</sup> response, thus there is a wide range of possible Ca<sup>2+</sup> responses following purinergic stimulation.

## **1.6 Cytokines**

Cytokines are a group of small molecular weight proteins consisting of chemokines, interleukins, tumour necrosis factor and several other groups. They are responsible for autocrine, paracrine and endocrine signalling and are intimately linked with many processes in the immune system. Interleukins are a group of 15 cytokines (1-13, 15 & 17). Of particular importance is the Interleukin-1 family of cytokines,

which play a key role in immune/inflammatory responses. Interleukin 1 $\beta$  (IL-1 $\beta$ ), alongside interleukin-1 $\alpha$  (IL-1 $\alpha$ ) are pro-inflammatory cytokines which belong to the interleukin-1 family. Both interleukins have a similar 3 dimensional profile despite only sharing roughly 20-30% amino acid sequence homology (Ferrari *et al*, 2006). IL-1ra, which is able to bind but not stimulate IL-1 receptors, is also part of the IL-1 family.

### **1.6.1 Interleukin-1 $\beta$**

Interleukin 1 $\beta$  (IL-1 $\beta$ ) is a pro-inflammatory cytokine produced by immune cells, including macrophages and microglia. IL-1 $\beta$  is initially formed from its inactive 31kDa precursor protein, pro-interleukin 1 $\beta$  (pro IL-1 $\beta$ ), which requires proteolytic cleavage from the enzyme caspase-1, previously known as interleukin converting enzyme (ICE), to produce the active and mature 17.5kD protein (Thornberry *et al*, 1992). Cytosolic pro- IL-1 $\beta$  is the product of gene induction and transcription, stemming primarily from NF $\kappa$ B signalling which can be initiated by the activation of a range of pattern recognition receptors (PRRs), which includes soluble, membrane bound and cytosolic receptors that are able to sense a variety of pathological stimuli. This results in NF $\kappa$ B activation is its translocation to the nucleus where it initiates the transcription of a range of proteins. A key example of one IL-1 $\beta$  gene inducer, utilised heavily in experimental studies for the production of intracellular pro-IL-1 $\beta$ , is the activation of Toll like receptor 4 (TLR4) by the pathogen associated molecular pattern (PAMP) bacterial Lipopolysaccharide (LPS) (Grahames *et al*, 1999), although IL-1 $\beta$  is also upregulated in the absence of PAMPs by damage associated molecular patterns (DAMPs) in a process known as sterile inflammation (Chen *et al*, 2010). The pro-inflammatory Caspase-1 enzyme is a member of the cysteine protease family called caspases, and is produced from the 45kDa precursor zymogen, pro caspase-1. The conversion of pro-caspase-1 to the active caspase-1 requires proteolytic cleavage at an aspartate residue, a process that requires

the assembly of previously described protein complexes termed inflammasomes (Martinon *et al*, 2002). Of particular importance in IL-1 $\beta$  processing is the NLRP3 inflammasome.

The NLRP3 oligomer functions as a pattern recognition receptor (PRR) of the NOD-like receptor (NLR) subfamily. The NLRP3 PRR is characterised by the containing of several key domains, including a central nucleotide-binding and oligomerization (NACHT) domain, which is conserved in all NLRs, a C-terminal leucine rich repeat (LRR) structural motif, and a pyrin (PYD) domain (Figure 1.11). Whilst the LRR motif is believed to function in ligand recognition, the PYD is essential for and mediates homotypic protein interactions with PYD on ASC (Vajjhala *et al*, 2012) leading to ASC recruitment. ASC subsequently recruits pro-caspase-1 via a caspase recruitment domain (CARD), leading to its proteolytic conversion and separation of the p10 and p20 catalytic domain fragments, to form of active caspase-1.

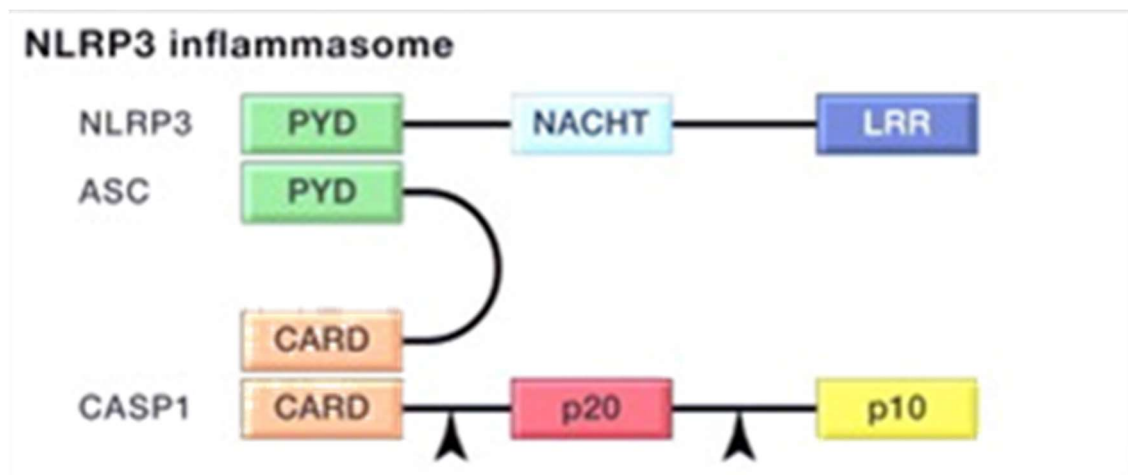


**Figure 1.11:** Schematic diagram of NLRP3 inflammasome assembly, highlighting key monomers PRR, ASC and caspase-1 (CASP1) as well as interaction domains. Arrowheads indicate positions of proteolytic cleavage. Adapted from Schroder & Tschopp, 2010.

Several stimuli for NLRP3 inflammasome assembly have been elucidated, including viruses (Kanneganti *et al*, 2006; Allen *et al*, 2009), bacteria (Gross *et al*, 2009; Mariathasan *et al*, 2006) and

various DAMPS, such as amyloid- $\beta$  plaques (Halle *et al*, 2008), sphingosine (Luheshi *et al*, 2012), silica and asbestos (Cassel *et al*, 2008), and extracellular ATP (Mariathasan *et al*, 2006). Additionally, cell swelling mediated by extracellular osmolarity (Compan *et al*, 2012), and prolonged  $Zn^{2+}$  depletion (Summersgill *et al*, 2014) have been shown to have important roles in NLRP3 activation.

One mechanism that is of particular importance is the stimulation of P2X7R by extracellular ATP (Kahlenburg & Dubyak, 2004), leading to  $K^+$  efflux and pannexin-1 recruitment (Kanneganti *et al*, 2007), which is thought to allow direct cytosolic access to NLRP3 agonists. In addition to NLRP3, microglia have a number of other PRRs are able to form functional caspase-1 inflammasomes, including NLRP1, IPAF and AIM (Schroder & Tschopp, 2010), each with variations in which domains they contain. ATP stimulation of cell surface P2X7 has been shown to activate the caspase-1 NLRP3 inflammasome, leading to the processing of pro-interleukin-1 $\beta$  (Mariathasan *et al*, 2006; Ferrari *et al*, 2006).

As IL-1 $\beta$  lacks a signal sequence peptide (Auron *et al*, 1984) and is absent from both the endoplasmic reticulum and golgi apparatus in LPS primed monocytes (Singer *et al*, 1988), its cellular release mechanism is not via the conventional ER/Golgi apparatus protein export mechanism (Rubartelli *et al*, 1990). Instead multiple potential mechanisms of IL-1 $\beta$  have been suggested based on experimental data, of which one or multiple may be responsible based on several factors. Early studies hypothesised release was by cellular lysis, and while this is true under certain conditions (Hogquist *et al*, 1991a), more regulated mechanisms have since been elucidated. Protected IL-1 $\beta$  release has been shown by microvesicle shedding (MacKenzie *et al*, 2001; Bianco *et al*, 2005; Pizzirani *et al*, 2007; Bianco *et al*, 2009), lysosomal exocytosis (Andrei *et al*, 1999) or similarly exosome release (Qu *et al*, 2007; Record *et al*, 2011), which may be important for distant IL-1 $\beta$

signalling. Alternatively, IL-1 $\beta$  release can occur with pyroptotic cell death (discussed in 1.7.3).

Once released, IL-1 $\beta$  exerts its effects through its corresponding membrane bound receptor, IL-1RI, which upon ligand binding, recruits IL-1 receptor accessory protein (IL-1RAcP), which stabilises the receptor complex and initiates several intracellular protein signalling cascades. IL-1 $\beta$  is also able to bind the type II receptor (IL-RII), although this receptor is unable to stimulate intracellular signalling, and sequesters IL-1RAcP, preventing it from interacting with IL-1RI (Lang *et al*, 1998), thus acting as a decoy receptor to decrease IL-1 $\beta$  activity. Additionally, the same stimuli that produce release of IL-1 $\beta$ , also produce the delayed release of the competitive IL-RI antagonist IL-1ra. Upon binding, IL-1ra cannot initiate IL-RI recruitment of IL-1RAcP, and thus does not propagate intracellular signalling (Greenfeder *et al*, 1995).

### **1.6.2 IL-1 $\beta$ in microglia**

As a cell of myeloid lineage, alongside macrophages, and as the immune regulatory cells of the CNS, microglia possess an array of components that are essential for the generation of IL-1 $\beta$  and its processing and release in response to various stimuli. Microglia produce IL-1 $\beta$  mRNA and pro-IL-1 $\beta$  precursor protein in response to a number of stimuli, such as LPS (Yao *et al*, 1992) and thus is often used as a marker for M1 phenotype microglial activation. This process is often termed “priming” in microglia and macrophages. LPS priming of microglia occurs via TLR4, which is expressed in microglia (Laflamme & Rivest, 2001; Kielian, 2006). Following priming, microglia are required to process and release IL-1 $\beta$  in its mature form (as previously described). Microglia have been shown to express multiple necessary components of the inflammasome, including scaffold PRRs (predominately NLRP3), ASC and caspase-1 (Gustin *et al*, 2015;). High levels of P2X7 expression have also been shown on microglia (Ferrari *et*

al, 1997a; Xiang & Burnstock, 2005) and there are numerous reports that P2X7 is required for the release of IL-1 $\beta$  from microglia (Ferrari *et al*, 1996; Ferrari *et al*, 1997b; Sanz *et al*, 2009).

### **1.6.3 IL-1 $\beta$ in glaucoma**

There is much evidence to support the role of IL-1 $\beta$  in the pathogenesis of glaucoma. Primary evidence from studies have shown that aqueous humor from glaucomatous patients contain elevated levels of pro-inflammatory cytokines, including  $\alpha$ - and  $\gamma$ -interferons, and interleukins (Chua *et al*, 2012; Takai *et al*, 2012). This has been supported by a number of experiments using glaucoma models. Levels of IL-1 $\beta$  mRNA in rat retinal astrocytes and possibly microglia, have been shown to increase after simulating retinal ischaemia by optic nerve ligation, to simulate glaucomatous optic neuropathy (Hangai *et al*, 1995). The optic nerve ligation model has also more recently shown an increase in extracellular levels of IL-1 $\beta$  protein in retinal tissue extracts (Zhang & Chintala, 2004).

Similarly, experimentally induced ischaemia by use of elevated pressure in rat retinas was shown to cause a pattern of damage that appeared similar to that of glaucomatous optic neuropathy, including reduced cell density in the ganglion cell layer (Peng *et al*, 2008; Russo *et al*, 2008). It was also shown to increase levels of IL-1 $\beta$  protein up to 12 hours after reperfusion (Yoneda *et al*, 2001) and elevated IL-1 mRNA expression (Sugiyama *et al*, 2013). The cellular damage observed has been demonstrably reduced upon administration of antagonists of IL-1  $\beta$  activity, including IL-1Ra and anti-IL-1 $\beta$  antibody (Yoneda *et al*, 2001).

IL-1 $\beta$  may also be linked to the mediation of excitotoxic cell death in the retina. Immunohistochemical studies have shown that intravitreal NMDA injections causes cell death in rat retinas caused by stimulation with excitotoxic agent NMDA caused increase levels of IL-1 $\beta$  mRNA in

several retinal cell types, including glial cells and retinal ganglion cells (Kitaoka *et al*, 2007), utilising the NF- $\kappa$ B pathway. As with the optic nerve ligation method, injection of IL-1 $\beta$  antagonist molecules including IL-1Ra and anti-IL-1 $\beta$  antibody prevented cell death in retinal tissues after NMDA induced IL-1 $\beta$  up regulation. Whether IL-1 $\beta$  plays a neuroprotective or deleterious role in excitotoxicity damage may be a depend on homeostatic control over the cytokine, where low endogenous levels play a neuroprotective role against damage, but elevated and/or sustained levels are mediators of cell death and long-term tissue damage.

Genetic variation may provide partial evidence to a link between IL-1 $\beta$  and some forms of glaucoma. A genetic polymorphism of the IL-1 $\beta$  gene, along with another polymorphism of the IL-1 $\alpha$  was found to be statistically more frequent in POAG patients than controls (Lin *et al*, 2003). The nature of this polymorphism is to increase the levels of secretion of IL-1 $\beta$  (Pociot *et al*, 1992), hinting that increased levels of IL-1 $\beta$  release may be involved in POAG pathogenesis. However, it is unclear that this polymorphism may lead to POAG, as similar studies have found no increased frequency of the genotype in POAG compared to controls (Li *et al*, 2017).

### **1.7 Cell death**

Cell death is an inevitable outcome for all cells and describes the process by which cells cease their biological function. Cells can undergo a variety of different types of cell death based on the type of stimulus received. Cell death can occur to fulfil a number of purposes, such as the maintenance of cell populations, or as the result of disease, infection or injury. Cell death is a broad term that can be further defined based on the specific mechanisms and outcome involved.

### 1.7.1 Apoptosis

Apoptosis, as a term was coined after observations of programmed cell death across multiple cell types and tissues (Kerr *et al*, 1972), and is a form of regulated cell death (RCD). Apoptosis is an essential regulation mechanism for both development and cellular homeostasis in maintaining appropriate cell numbers, millions of which are removed daily. Apoptosis occurs as result of a wide range of possible stimulus, including the withdrawal of required growth factors/essential survival factors, or stimulation of cell surface death receptors by their corresponding ligands. Once a cell receives adequate stimulus to undergo apoptosis, it undergoes a number of characteristic morphological and biochemical changes.

Mechanistically, apoptosis can be broadly divided into two pathways, the intrinsic mitochondrial and extrinsic receptor mediated pathways, although there is evidence of cross talk between signalling molecules of the two pathways. Extrinsic apoptosis is mediated by a series of cell surface death receptors, such as the tumor necrosis factor (TNF) family of receptors (TNFR, also known as Fas receptors) (Locksley *et al*, 2001), which contain a characteristic ~80 amino acid cytoplasmic death domain (Ashkenazi & Dixit, 1998). Upon stimulation by a suitable ligand (such as TNF $\alpha$ ), death receptors trimerise and recruit receptor specific intracellular adaptor proteins at corresponding death domains to initiate an intracellular signalling cascade. Once recruited, the adaptor proteins then bind procaspase-8 to form a death-inducing signalling complex (DISC), which results in the auto-catalytic activation to caspase-8 (Kischkel *et al*, 1995). Alternatively, dependence receptors such as DCC and Unc5H1–3 are also able to induce extrinsic apoptosis via the withdrawal of their respective ligand below a threshold level (Gibert *et al*, 2015).

The intrinsic pathway is initiated from within the cell by a range of diverse mediators that, unlike the extrinsic pathway, are not directly

receptor mediated. Examples of these stimuli include withdrawal of growth factors (Nunez *et al*, 1990; Brumatti *et al*, 2010), DNA damage (Roos *et al*, 2016), excessive reactive oxygen species (ROS) and endoplasmic reticulum damage (Pihan *et al*, 2017). All of these stimuli act to cause alteration of the mitochondrial membrane, resulting loss of mitochondrial membrane potential and opening of the mitochondrial permeability transition pore (MPTP). The permeabilization of the mitochondrial membrane is the critical step in intrinsic apoptosis, as the process becomes irreversible after this stage (Tait & Green, 2010). Subsequently, there is the release of mitochondrial proteins into the cytosol (Saelens *et al*, 2004), including the electron transport shuttle protein cytochrome c, which further initiates an apoptotic signalling cascade. The key regulators of mitochondrial release of cytochrome-c into the cytosol belong to the B-cell lymphoma-2 (BCL-2) protein family, which includes both pro-apoptotic (such as Bax and Bad) and anti-apoptotic protein mediators, which bind to and sequester the pro-apoptotic mediators (Czabotar *et al*, 2014). Cytochrome-c release from the mitochondria binds to pro-caspase apoptotic protease activating factor-1 (Apaf1) and procaspase-9, to form a multiprotein complex known as an apoptosome (Riedl & Salvesen, 2007). Apoptosome monomer units dimerise via their CARD domains, which causes the autolytic conversion of procaspase-9 to its active form (Hu *et al*, 2014).

After the activation of the initiator caspases 8 and 9 in their respective pathways, it is at this point that both pathways converge in the activation of the executioner caspase, caspase-3. Activated caspase-3 is responsible for the characteristic morphological and biochemical changes observed with apoptosis, primarily by the cleavage of various cellular components. One key feature of apoptosis is the fragmentation of cellular DNA by caspase activated endonucleases also known as karyorrhexis, which produces 180-200 base pair DNA fragments (Bortner *et al*, 1995) and a characteristic ladder-like pattern when separated by gel electrophoresis. These fragments can be detected

experimentally by the use of the fluorescent-based dye terminal deoxynucleotidyl transferase dUTP nick endlabelling (TUNEL). Several morphological and biochemical changes are also seen at the plasma membrane, including membrane blebbing (Sebbagh *et al*, 2001) and rounding up of the cell into apoptotic bodies, which is a result of degradation of the cytoskeleton. Apoptosis also induces the translocation of phosphatidyl serine residues to the extracellular surface of the plasma membrane surface (Bratton *et al*, 1997), which is due to caspase-3 mediated activation of scramblase enzyme. In turn this inactivates the flippase enzyme that homeostatically maintains phosphatidyl serine residues at the inner leaflet of the plasma membrane (Marino & Kroemer, 2013). The combination of degradation of cellular components and clearance of apoptotic bodies without the release of their cytoplasmic contents into the extracellular milieu, means that apoptosis does not induce an inflammatory response (Maderna & Godson, 2003).

### **1.7.2 Necrosis**

Necrosis is a term for a rapid and uncontrolled form of cell death. Unlike apoptosis, necrosis is passive and not usually a form of RCD. Necrotic cell death is defined by several characteristic morphological features, including swelling of organelles, increase in cell volume (oncosis), and eventual cell membrane rupture and uncontrolled release of cytoplasmic contents into the extracellular milieu. Several other characteristic events can occur alongside necrotic cell death, including mitochondrial ROS production and increases in cytosolic  $\text{Ca}^{2+}$  and subsequent activation of calpains and cathepsins (Yuan, *et al*, 2016), although it is not known if these are causative or resultant of necrosis.

The nature of necrotic cell death means it initiates an inflammatory response in surrounding environment and usually affects large regions of cells/tissues due to propagative outcome. Whereas apoptotic cell

death can be beneficial and even necessary for homeostatic function, necrotic cell death is almost always detrimental. Classification of necrotic cell death usually occurs in the absence of markers for alternative mechanisms of cell death.

### **1.7.3 Pyroptosis**

Pyroptosis is a form of RCD that has a key role in innate immunity, particularly against intracellular pathogens (Jorgensen & Miao, 2015), which depends on the formation of plasma membrane pores of the gasdermin family of proteins. Pyroptosis was initially defined as a form of cell death similar to apoptosis, but intimately linked to the activity of specific caspases, namely caspase 1, but also 4 & 5 in humans and the murine homologue caspase 11, and under certain circumstances caspase 3 (Rogers *et al* 2017). The initiation of pyroptosis requires activation of these caspases, which is mediated by a range of PRRs that are able to recognise a wide array of ligands. Cells that undergo pyroptotic cell death are mainly of myeloid lineage, such as macrophages (Fink & Cookson, 2006), neutrophils, dendritic cells, CD4+ T cells and microglia (Lee *et al*, 2019). However pyroptosis has been documented in other cell types including neurons (Adamczak *et al*, 2014).

The first elucidated pathway for pyroptosis was termed the canonical pathway and is reliant on caspase 1 activity (figure 1.12). As previously described, caspase 1 is activated from its precursor via an assembled inflammasome (also known as the pyroptosome), and is responsible for the processing of IL-1 $\beta$  and IL-18 from their immature forms.

Pyroptosis is therefore associated with the release of these mature cytokines, and thus induces an inflammatory response (Man *et al*, 2017). The non-canonical pathway is mediated by intracellular LPS from invading bacteria, which interacts directly with the CARD domain of caspases 11, 4 & 5 to cause their oligomerization and activation (Shi

*et al*, 2014), thus these caspases act as PRRs for LPS directly (Figure 1.12).

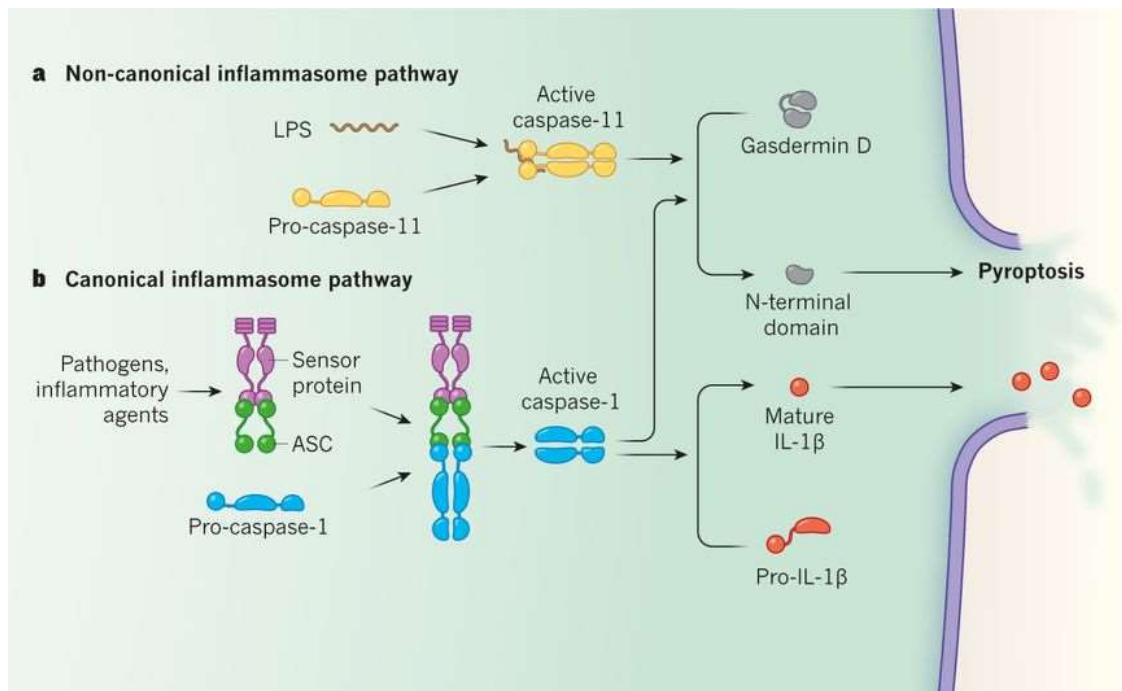


**Figure 1.12:** Diagram of the canonical (b) and non-canonical (a) inflammasome pathways involved in pyroptosis. From Broz, 2015

Activated pyroptosis-associated caspases propagate pyroptosis by cleaving the protein gasdermin D (GSDMD). GSDMD is one of six members of the gasdermin protein family, which is held inactive in its full-length form by the c-terminal domain (GSDMD-CT) auto-inhibiting the active pore forming terminus (GSDMD-NT). Activated caspases cleave GSDMD at the interdomain loop after Asp275 (Asp276 in mouse homologue) (Kayagaki *et al*, 2015), whereby the active GSDMD-NT translocates to the inner leaflet of the plasma membrane via and oligomerises to form a pore and permeabilization of the plasma membrane (Aglietti *et al*, 2016). This allows release of generated inflammatory cytokines IL-1 $\beta$  and IL-18, as well as other cytosolic DAMPs.

After gasdermin pore formation, key characteristic cell death associated morphological and biological changes are initiated. Pore formation causes influx of water via the osmotic gradient, which leads

to cell swelling and lysis (Fink & Cookson, 2006), in a manner similar to necrotic cell death.

#### **1.7.4 Necroptosis**

Necroptosis is a form of RCD with necrotic like phenotype. Although it shares many similarities with both necrosis and apoptosis, necroptosis is a distinct process, as it is not a passive (Linkermann & Green; 2014), and is highly regulated like apoptosis, however, unlike apoptosis, necroptosis elicits an inflammatory response via the release of cytosolic contents into the extracellular milieu (Kaczmarek *et al*, 2013). Necroptosis is initiated by activation of one of multiple death receptors, such as Fas (Vercammen *et al*, 1998) and TNFR1 (Vercammen *et al*, 1997), or PRRs such as TLR4 (Dhuriy & Sharma, 2018).

Unlike other RCD mechanisms, necroptosis does not involve the activity of caspases, and is instead executed on a molecular level by receptor-interacting kinase3 (RIPK3) (Cho *et al*, 2009) and the subsequent phosphorylation and activation of mixed lineage kinase domain like pseudokinase (MLKL) (Murphy *et al*, 2013). In some cases, such as in TNFR1 mediated necroptosis, RIPK3 activation is preceded by activation of the related receptor-interacting kinase1 (RIPK1), which interacts with RIPK3 via their shared RIP homotypic interaction motif domains (RHIM) (Vandenabeele *et al*, 2010), causing the formation of a complex known as a necrosome (Grootjans *et al*, 2017).

Phosphorylated MLKL forms oligomers, which translocate to the plasma membrane via binding to phosphatidylinositol phosphate molecules and cause permeabilization of the plasma membrane (Chen *et al*, 2014). MLKL phosphorylation also induces other cellular cascades, including the increase of  $[Ca^{2+}]_i$  thought to be mediated by the transient receptor potential cation channel subfamily M member 7 (TRPM7) (Cai *et al*, 2014).

Characteristically, necroptotic cell death presents with many features similar to those of pyroptotic cell death, including osmotic cell swelling/bursting following membrane permeabilization, as well as the release of cytosolic components that act as DAMPs in the extracellular milieu.

### **1.7.5 P2X7R mediated cell death**

Almost since its initial discovery, the ability of the P2X7R to induce cell death has been well documented. P2X7R mediated cell death was originally described as necrotic in mechanism (Di Virgilio *et al*, 1989), and is still considered the primary cell death mechanism in cases of sterile inflammation where DAMPS are released into the extracellular environment (Di Virgilio *et al*, 1998), however it was soon shown that a number of factors influence P2X7R mediated cell death. One such factor is cell type, which was demonstrated in a subsequent study (Zanovello *et al*, 1990).

Although apoptotic cell death has been widely reported as a P2X7R mediated outcome after prolonged ATP stimulation (Franceschi *et al*, 1996), surprisingly little investigation into the mechanisms of P2X7R apoptosis have been undertaken. It has been demonstrated that prolonged ATP stimulation of cells with high concentrations of ATP causes P2X7 induced apoptosis (Franceschi *et al*, 1996), whereas brief applications of the same stimulus induce a reversible state of 'pseudoapoptosis' with agonist washout (Mackenzie *et al*, 2005). There is evidence that ATP stimulation, acting at what is suspected to be P2X7R, is responsible for mitochondrial cytochrome c release and subsequent caspase 3 activation (Ferrari *et al*, 1999). In contrast, due to its high expression on immune cells, the role of P2X7R in pyroptosis is well documented. P2X7R mediated K<sup>+</sup> efflux is widely regarded as a stimulating factor in NLRP3 inflammasome assembly in the canonical pathway (Mariathasan *et al*, 2006), and thus acts to induce pyroptosis in cells that are primed. In the non-canonical pathway, P2X7R has

been shown to be activated downstream of caspase 11 mediated pannexin-1 activation and ATP release, leading to pyroptotic cell death (Yang *et al*, 2015a)

### **1.7.6 Cell death in Glaucoma**

Regulated cell death is an essential mechanism in both the development and homeostasis of the retina (Vecino & Acera, 2015). However, the key characteristic of glaucomatous neurodegeneration is the pathogenic death of RGCs, resulting in an associated permanent loss of vision. There is evidence that P2X7 may play a role in glaucomatous RGC death, since RGCs express P2X7 (Wheeler-Schilling *et al*, 2000; Mitchell *et al*, 2009; Niyadurupola *et al*, 2013), and several experimental models of glaucoma have explored the role of P2X7 on RGC death. The glaucoma model of optic nerve crush showed a delay in increased numbers of phagocytic microglia and RGC loss after blocking P2X7 and with P2X7 K/O mice (Nadal-Nicholás *et al*, 2016). This is supported by evidence that ATP stimulation, or treatment with potent P2X7R agonist BzATP induces the apoptotic death of dissociated rat RGCs, both *in vitro* (Zhang *et al*, 2005), and *in vivo* rat retinas (Hu *et al*, 2010), which was shown to be dependent on Ca<sup>2+</sup> influx and caspase activation (Zhang *et al*, 2005). Additionally, RGC cell death is delayed in the P2X7 associated PRR NLRP3 knockout mouse following optic nerve crush (Puyang *et al*, 2016). There is also evidence the P2X7 associated channel pannexin-1 on RGCs has a role in purinergic mediated RGC death, as pannexin-1 knockout mice (*panx1*<sup>-/-</sup>) demonstrated reduced inflammasome activation, Ca<sup>2+</sup> and cell death following ischaemic injury (Dvorientchikova *et al*, 2012). Additionally, it was shown that the NMDA receptor antagonist MK801 prevented RGC loss after BzATP treatment of rat retina (Hu *et al*, 2008), suggesting the NMDA receptor may play a downstream role in P2X7 mediated RGC death.

Cell death has also been shown in human models, in particular with the human organotypic retinal culture (HORC) model. Niyadurupola and colleagues (2013) demonstrated that BzATP caused a loss of RGC specific markers, and was inhibited by the antagonist BBG.

Furthermore, ischaemic damage of isolated optic nerves was inhibited with the same P2X7 antagonist (Domercq *et al*, 2010).

As well as direct P2X7 mediated cell death of RGCs, the expression of purinergic receptors, in particular P2X7 on various retinal cell types, including microglia, suggests there may be additional indirect mechanisms contributing to glaucomatous RGC death.

### **1.7.7 Cell death in microglia**

Throughout life, the numbers of microglia in the CNS is kept in a careful balance between proliferation and apoptosis, in order to maintain a sufficient number of microglial cells. A number of stimuli have been discovered to induce microglial cell death. The cytokines IL-13 and IL-4, both anti-inflammatory cytokines and stimulators of the M2A phenotype of active microglia have been demonstrated to induce apoptosis of activated microglia (Yang *et al*, 2002; Shin *et al*, 2004; Yang *et al*, 2006). This adds further evidence to the notion that M2A polarization of microglia is utilised to bring the resolution of the inflammatory response. Furthermore, overstimulation of TLR4 has been shown to induce apoptotic cell death of microglia in a Fas-independent manner (Jung *et al*, 2005), which suggests there are regulatory mechanisms for preventing over stimulation/activation microglial cells and the immune response. TLR4 has also been demonstrated to be responsible for the necroptotic cell death of retinal microglia in both rd1 retinal degeneration mice and in an NMDA induced model of acute retinal degeneration (Huang *et al*, 2018), whereby several inflammatory cytokines including CCL2, TNF- $\alpha$  and IL-1 $\beta$  were upregulated, with increased levels and phosphorylation of the necroptosis associated proteins RIPK1, RIPK3 and MLKL. Additionally,

treatment with necrostatin-1, a specific inhibitor of RIPK1 necroptosis, significantly reduced both microglial necroptosis and retinal degeneration.

A host of other stimuli have also been shown to induce cell death of microglia, including corticotrophin releasing hormone (CRH) (Ock *et al*, 2006), mitochondrial toxin 1-methyl-4-phenylpyridinium (Jin *et al*, 2012), and activation of the E prostanoid receptor 2 (EP2 receptor) (Fu *et al*, 2015).

In addition to its role in cell death in other cells and tissues, P2X7R has been shown to play an instrumental role in the regulation of microglial cell death in response to purinergic stimulus. Primary microglia stimulated with BzATP demonstrated a significant decrease in microglial cell number, which was not reproduced with antagonism from A-804598 or in P2X7<sup>-/-</sup> microglia (He *et al*, 2017). In this same study, P2X7 stimulation with BzATP was also sufficient to produce cell death in LPS primed microglia.

## **1.8 Aims and Objectives**

Numerous studies have highlighted the potential involvement of purinergic signalling and inflammatory cytokines, in particular IL-1 $\beta$  in the pathogenesis of glaucoma. As immune privileged cells of the CNS and the retina, and in addition to being endowed with a variety of purinergic receptors, microglia represent a potential modulator of glaucomatous events and as such are of key interest in the study of glaucomatous pathogenesis. The aim of this thesis is to investigate the role of microglial P2X7 activity in relation to glaucoma.

The specific aims of this research were:

- to generate a P2X7R-deficient microglial (BV-2) cell line as a tool for investigating the role of P2X7 in these cells.
- The use of pharmacological agonists and antagonists were then utilised to characterise Ca<sup>2+</sup> via purinergic receptors in BV-2 microglia, in particular the contribution of P2X7 to ATP-mediated Ca<sup>2+</sup> responses.
- Utilising similar methods to investigate purinergic-mediated proliferation and cell death mechanisms in microglia
- Investigate the role of ATP, and in particular the P2X7 receptor, in relation to both priming and release mechanisms of IL-1 $\beta$ .
- Briefly explore the link between simulated glaucomatous ischaemic conditions with OGD, and purinergic signalling.

The evidence generated by these experiments would help give new insight into the role of neuroinflammation and microglial cells into the pathogenesis.

## Chapter 2

### Materials and methods

#### 2.1 Cell culture

BV2 mouse microglial cells (Blasi *et al*, 1990), and P2X7 knockout BV2 cells were cultured in Dulbecco's Medium: Nutrient mixture F-12 (DMEM/F-12), containing 10% heat-inactivated foetal bovine serum (FBS) (Life Technologies), 1% 200mM L-Glutamine (Life Technologies, Paisley, UK) and 1% 10,000units Penicillin-Streptomycin antibiotic (Life technologies, Paisley, UK). Cultures were stored in 75cm<sup>3</sup> flasks (Nunc™ EasYFlask™, Thermo Scientific) and incubated at 37°C, 5% CO<sub>2</sub>.

When cells reached approximately 80-90% confluency, they were passaged. Culture medium was aspirated and washed in 5ml Dulbecco's phosphate buffered saline (DPBS) (Invitrogen, Paisley, UK). DPBS was then aspirated and 10mls of 5% Trypsin-EDTA solution (Life Technologies, Paisley, UK) was added and incubated for approximately 3 minutes, until cells were visibly detached from the culture flask under microscope. The trypsin was then neutralised with an equal volume of 10% FBS DMEM/F-12 and the cell suspension solution transferred to an aseptic 25ml centrifuge tube (Sterilin U.K). Cell suspensions were then centrifuged at 300 x G for 10 minutes until a visible pellet had formed. The supernatant was aspirated and the pellet re-suspended in 5ml 10% FBS DMEM/F-12. Re-suspended cells were then available for plating for use in experiments. Re-suspended cells were also seeded into a new 75cm<sup>3</sup> flask to maintain the cell cultures and the passage number recorded.

For seeding plates, the re-suspended cells were counted using a haemocytometer (Assistant, Sondheim-Rhön, Germany). For experiments, cells were seeded at a range of densities depending on the experimental assay (Table 2.1).

**Table 2.1** Seeding density of BV-2 microglial cells and P2X7 knockout BV-2 microglial cells for different experimental assays.

Assay	Assay environment	Seeding density	Volume of medium
Viability assays: MTS, LDH, Caspase 3/7	96 well Plate (Nunclon™ Delta Surface, Thermo Scientific)	6000 cells/well	200µl
Fura-2	Poly-D-Lysine coated 96 well Plate (Nunclon™ Delta Surface, Thermo Scientific)	10,000 cells/well	100µl
Transfection	6 well plate (Nunclon™ Delta Surface, Thermo Scientific)	100,000 cells/well	2ml
qRT-PCRs, Western blot	35mm cell culture dishes (Corning, USA)	120,000 cells/well	1.5ml
ELISA	24 well plate (Nunclon™ Delta Surface, Thermo Scientific)	500,000 cells/well	500µl

## 2.2 Transfection

For testing of transfection reagents, cells were initially seeded as stated previously (Table 2.1). After 24 hours, well medium contents were replaced with 900µl Opti-MEM™ reduced serum medium (Life Technologies, Paisley, UK) for 10 minutes at room temperature. In an Eppendorf, 1µg of endotoxin free rP2X7-GFP plasmid (Dr Stokes) was added to a transfection reagent solution according to manufacturer's instructions. The contents of each Eppendorf was then carefully added to a separate well of the 6 well plate. An additional well was exposed to 100µl fresh Opti-MEM™ as a mock transfection control. The plate was then gently shaken to ensure even distribution of plasmid containing transfection reagent throughout each well, and incubated at 37°C 5% CO<sub>2</sub>. After 24 hours exposure to transfection reagents, each plate was visually assessed for cell viability and successful transfection using brightfield and fluorescence imaging respectively.

For CRISPR transfection of BV-2 cells, well medium contents were replaced with 900µl fresh Opti-MEM™ reduced medium serum and allowed to sit for 10 minutes at room temperature.

In a separate Eppendorf, 1µg of endotoxin free pHCSVblast-Cas9 plasmid was combined with 25µl tracrRNA (10µM) and 25µl crRNA (10µM) was added to a transfection reagent solution according to manufacturer's instructions. The contents of each Eppendorf was then added to a separate well of the 6 well plate. An additional well was exposed to an additional 100µl fresh Opti-MEM™ as a mock transfection control. The plate was then gently swirled to ensure even distribution of plasmid containing transfection reagent throughout each well, and incubated at 37°C 5% CO<sub>2</sub>. To determine successful transfection/genomic modification of BV-2 microglia, 48 hours post transfections cells were incubated in 1µg/ml final concentration blasticidin antibiotic for 72 hours. Cells were visually assessed for viability and cell number following transfection and blasticidin selection.

### 2.3 Single cell clonal expansion

Single cell clonal expansion was performed using an array dilution method in a 96 well plate. 100 $\mu$ l of DMEM/F12 10% FBS media was added to all wells in the 96 well plate, except well A1, to which 200 $\mu$ l of a 2000 previously transfected cells/ml solution is seeded (Figure 2.1). 100 $\mu$ l of cell solution was then transferred from well A1 to B1 and mixed by pipetting up and down to produce a 1:2 dilution, which was then repeated down the first column of the plate until well H1. 100 $\mu$ l of DMEM/F12 10% FBS media was then added to wells A1-G1 so that all wells in column 1 had a total volume of 200 $\mu$ l. A second set of sequential 1:2 serial dilutions was then performed across the plate horizontally, followed by the addition 100 $\mu$ l of DMEM/F12 10% FBS media to all wells except column 12, to produce a cell density gradient across the plate, from most concentrated in well A1 to least concentrated in H12.

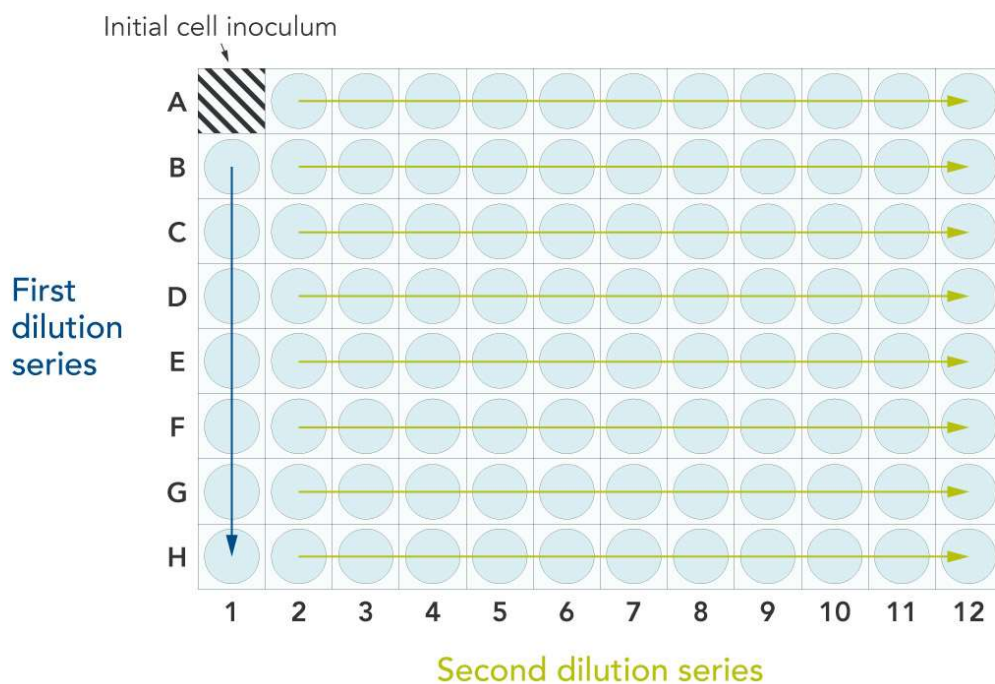


**Figure 2.1:** Diagram of dilution steps for 96 well plate clonal expansion. Available at <https://www.idtdna.com/pages/education/decoded/article/genome-editing-in-cell-culture-isolating-single-clones-for-genotypic-and-phenotypic-characterization>

Cells were then incubated at 37°C 5% CO<sub>2</sub>, for 72 hours to proliferate, after which the each well of the plate was assessed for the presence of colonies that had appeared to be generated from a single cell. In the event of singular cell colonies, cells were trypsinised and re-cultured in a larger well of a 6 well culture plate with fresh DMEM HAM/F12 10% FBS medium. Colonies were then cryogenically stored until further characterisation.

#### **2.4 Real time Ca<sup>2+</sup> response measurements**

A Fura-2 AM ratiometric, dual excitation/single emission wavelength calcium dye (Hello Bio, Bristol, UK) was used for measuring calcium responses to agonists/antagonists in cultured cells. Fura-2 AM is form of Fura-2 dye conjugated to a mildly hydrophilic acetoxymethyl (AM) group, which allows it to pass from the extracellular medium into cells across the phospholipid membrane. Once inside the cell, the AM group is cleaved by cellular esterases to trap Fura-2 intracellularly. Upon Ca<sup>2+</sup> binding Fura-2, it undergoes a shift in its optimum absorption wavelength intensity from 380nm (Ca<sup>2+</sup> free) to 340nm (Ca<sup>2+</sup> saturated) (Figure 2.2) with emission measured at 510nm. Expressing fluorescent excitation/emission data as a ratio (340nm/380nm) avoids problems associated with other calcium sensor dyes such as uneven dye loading, photobleaching and dye extrusion, as level of emission is independent of concentration

For Fura-2 AM calcium assay, cells were seeded on Poly-D-Lysine (PDL) (Sigma-Aldrich, Poole, UK) coated 96 well plate in 10% FBS supplemented DMEM/F-12 and incubated overnight at 37°C, 5% CO<sub>2</sub>. Medium was then removed and the cells incubated in 100µl loading buffer, consisting of Hank's Balanced Salt Solution (HBSS) (Life Technologies, Paisley, UK), containing 2µM Fura-2AM (Thermo Scientific, Surrey, UK) and 250µM Sulfinpyrazone (Sigma Aldrich) to prevent dye extrusion from cells. Cells were incubated in loading buffer at 37°C for 45 minutes.

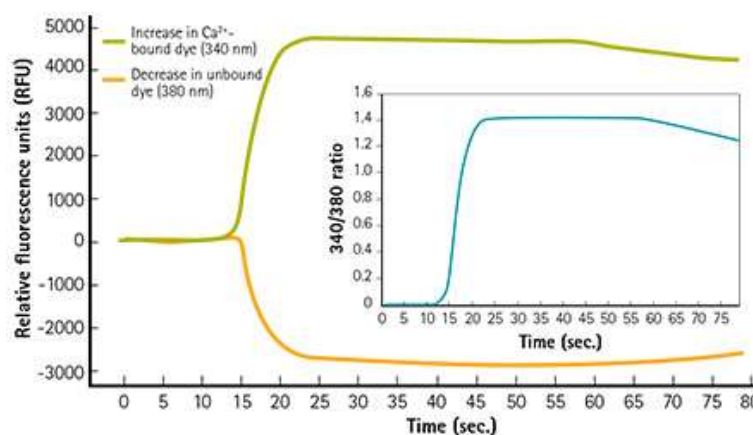


**Figure 2.2:** Representation of changes in fluorescent emission of Fura-2 ratiometric dye following  $\text{Ca}^{2+}$  binding at 15 seconds.

**Table 2.2:** Contents of ETotal physiological saline buffer. Buffer adjusted with 5mM NaOH (Sigma Aldrich, Poole, UK) to pH 7.4. Osmolarity measured with a Vapro 5520 vapor pressure osmometer (ELITechGroup, Berkhamsted, UK), to check on osmolarity of 300-310mOsm/kg.

	Concentration	Source
NaCl	147mM	Sigma Aldrich, Poole, UK
$\text{CaCl}_2$	2mM	Sigma Aldrich, Poole, UK
KCl	2mM	Sigma Aldrich, Poole, UK
$\text{MgCl}_2$	1mM	Sigma Aldrich, Poole, UK
D-(+)-Glucose	13mM	Sigma Aldrich, Poole, UK
Hepes	10mM	Sigma Aldrich, Poole, UK

Agonists were prepared in ETotal running buffer (Table 2.2) at 10x final concentration and distributed appropriately in a deep well drug plate with V-bottom (Greiner, UK). Loading buffer was then removed from the cell plate and replaced with 180 $\mu$ l of ETotal running buffer in combination with the desired concentration of any antagonists or allosteric modulators as appropriate. Cells were then incubated in the FlexStation 3 multi-mode microplate reader (Molecular Devices,

Wokingham, UK) at 37°C for ten minutes prior to the start of recordings. For the duration of the experiment (300seconds), fluorescence emission intensity at 510nm was measured following 340nm and 380nm excitation every 3.5 seconds for 300 seconds. Each reading was an average of 6 separate readings per well, on the medium PMT gain setting. 20µl of 10x agonist were injected into the cell plate after 30 seconds of baseline recording, to produce the final desired concentration.

Baseline fluorescent readings were recorded for 30 seconds prior to agonist application and subtracted from trace recordings for analysis. For peak analysis, maximum 340/380nm ratio values for each trace were determined using Softmax Pro 5.3 software (Molecular Devices) for the determined trace period. Area under the curve analysis was performed in Softmax Pro 5.3 software (Molecular Devices) for the determined trace period.

## **2.5 MTS**

CellTiter 96 AQueous One Solution Cell Proliferation Assay (MTS) (Promega, Southampton, UK), is a colorimetric assay used to determine cell viability and was utilised. The assay contains two active compounds, (3-(4,5dimethylthiazol-2-yl)-5-(3-carboxymethoxyphenyl)-2-(4-sulphophenyl)-2H-tetra-zolium) (MTS) and an electron coupling agent phenazine ethosulfate (PES). The mitochondria of metabolically active cells can indirectly reduce the MTS compound, which produces the soluble coloured formazan compound (Figure 2.3). This colour change can be quantified to assess cell viability.

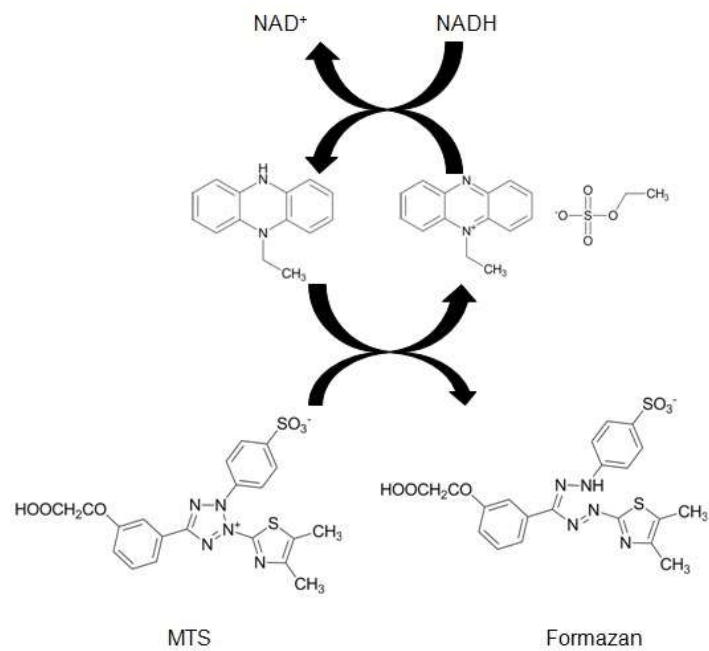


**Figure 2.3:** The oxidation of PES in the mitochondria allows the subsequent reduction of MTS to Formazan in the culture medium. From: <https://www.creative-bioarray.com/support/comparison-of-different-methods-to-measure-cell-viability.htm>

1:10 of the well volume of the MTS solution was added directly to cell culture medium and the plate was incubated for 1 hour at 37°C. Absorbance was then measured using a FlexStation 3 multi-mode microplate reader (Molecular Devices, Wokingham, UK) at 490nm. Average background readings from three samples of fresh Serum free DMEM/F-12 were subtracted from absorbance values. The processing of absorbance data was as follows:

$$\% \text{ Cell viability} = \frac{((\text{absorbance treated}) - (\text{absorbance background}))}{((\text{absorbance control}) - (\text{absorbance background}))} \times 100$$

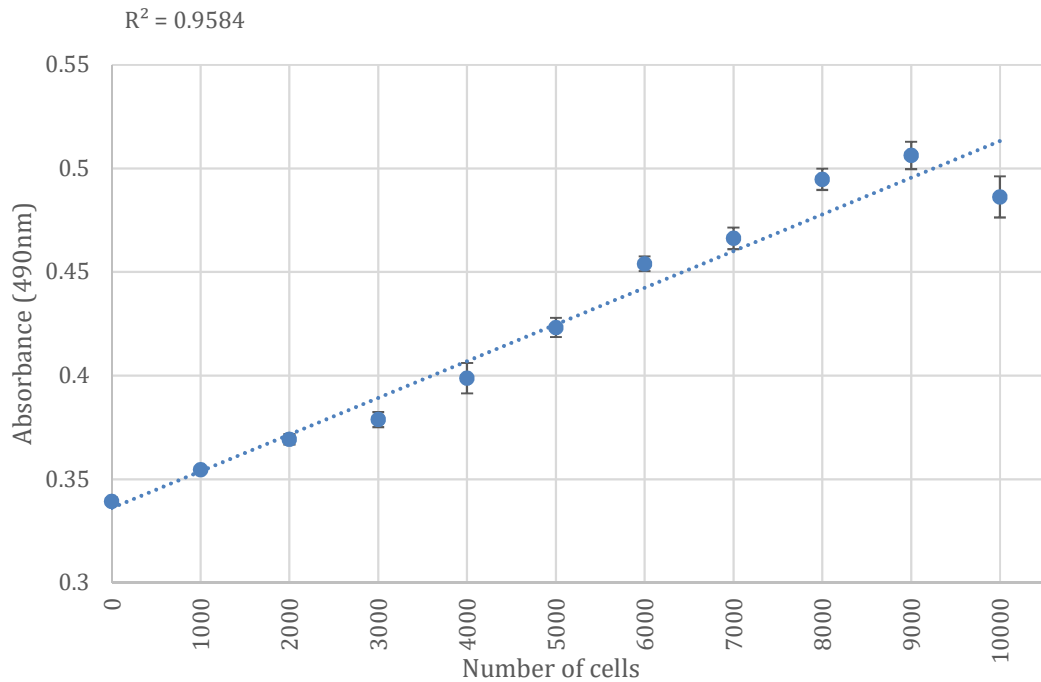


**Figure 2.4:** MTS absorbance values in relation to cell number. BV-2 cells at varying densities (0-10000 cells/well) were seeded in 96 well plates in serum-free medium containing 10% MTS solution. Absorbance at 490nm measured after 1hr. (n=4).

## 2.6 LDH

The cytotoxicity detection kit (LDH) (Roche, Indianapolis, USA) was used to assess lytic cell death in samples. The LDH assay measures the release of the enzyme Lactate Dehydrogenase into the culture medium through the disrupted cell membrane as a result of lytic cell death.  $NAD^+$  is reduced to  $NADH/H^+$  by the LDH catalysed conversion of lactate to pyruvate.  $NADH/H^+$  then reduces iodinitrotetrazolium (INT) to a coloured formazan product (Figure 2.5).

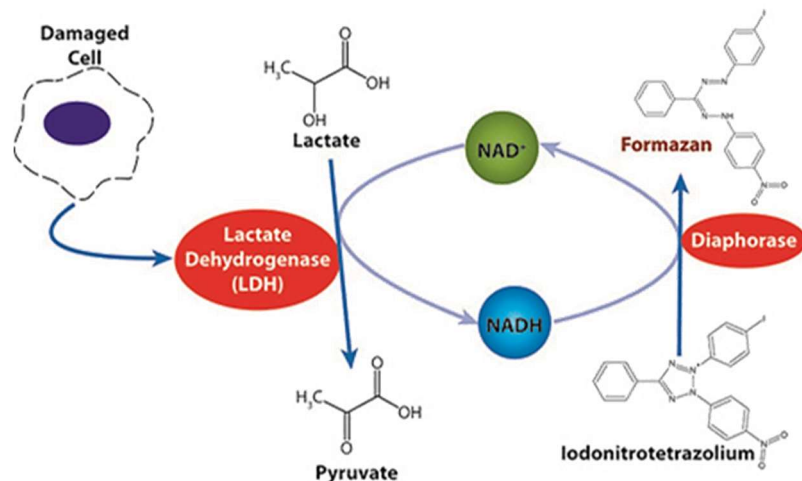


**Figure 2.5:** LDH release from damaged cells catalyses the production of NADH/H<sup>+</sup> by the conversion of lactate to pyruvate, which in turn catalyses the reduction of INT to formazan. Available from: <https://www.fishersci.com/shop/products/ldh-cytotoxicity-assay-200/501036376>

To perform the LDH assay, 100µl supernatant of each sample was transferred to a corresponding well position on a new 96 well plate. The reaction mixture was then prepared at a ratio of 1:45 of Diaphorase/NAD<sup>+</sup> catalyst solution to Sodium Lactate and INT dye solution. 100µl of the reaction mixture was then added to each sample and an additional three background wells, and the plate was incubated at 37°C and 5% CO<sub>2</sub>. The plate was read at 15 minutes using a FlexStation 3 multi-mode microplate reader (Molecular Devices, Wokingham, UK) at wavelengths 490nm assessing concentration of the formazan produced, and 660nm assessing background emission. The absorbance data values were wavelength adjusted and average background readings from three samples of fresh serum free DMEM/F-12 were subtracted. The processing of absorbance data was as follows:

$$LDH \text{ absorbance} = \left( \frac{\text{Sample absorbance}}{(490nm - 660nm)} \right) - \left( \frac{\text{Background absorbance}}{(490nm - 660nm)} \right)$$

LDH data was expressed as a fold change over control as follows:

$$\text{Fold change in LDH release (over control)} = \frac{\text{Sample LDH absorbance}}{\text{Control LDH absorbance}}$$

## 2.7 Caspase 3/7 activation live cell imaging

The Earlytox caspase-3/7 Nucview (Molecular Devices, Wokingham, UK) was used to assess caspase 3 activation. A 2X reaction mixture containing 6 $\mu$ M NucView 488 substrate reagent and 10 $\mu$ g/ml Hoechst 33342 nucleic acid stain (Thermo Scientific, Surrey, UK) was prepared in warmed (37°C) serum free, phenol red free DMEM HAM/F12 media (Life technologies, UK). 100 $\mu$ l supernatant of each sample was carefully removed avoiding disrupting the cultured cells and 100 $\mu$ l of the prepared reaction mixture was then added to each well for a final concentration of 3 $\mu$ M NucView 488 substrate reagent and 5 $\mu$ g/ml Hoechst 33342. Cells were then incubated, protected from light for 30 minutes at 37°C 5% CO<sub>2</sub>.

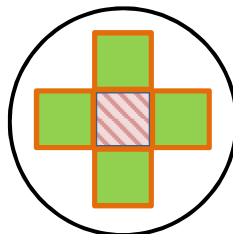


**Figure 2.6:** Diagrammatic representation of imaging pattern for each well. Hashed orange square represents field of vision over well centre. Green squares represent areas that were imaged. Diagram not to scale.

Earlytox caspase-3/7 treated cells were then imaged using a widefield Zeiss Axiovert 200M fluorescent microscope with a 100W mercury arc lamp. Cell morphology was detected with bright field light, whereas Hoechst 33342 stained nuclei were detected at 461nm and Caspase 3/7 activation staining was detected at 530nm. During imaging, Cells were incubated at 37°C, 5% CO<sub>2</sub>. Each well was imaged in random order to minimise time dependent effects on apoptosis. Four 10x

magnification images were taken per well, with six biological replicates per condition. Each image was taken from a region taken one full field of view width away from the centre of the well (Figure 2.6), in order to ensure an accurate representation of the entire well population.

## 2.8 Hoescht & Caspase 3/7 positive cell counting

Images were exported from Zeiss Axiovision 4.8 software (Carl Zeiss LTD, Cambridge, UK) as a tagged image file (.TIF) in order to avoid compression and loss of resolution, with separate images produced for each fluorescent channel. Hoescht and caspase 3/7 positive stained cells were counted in FIJI software (version 1.51a). Briefly, threshold images for each channel were generated and then analysed with the particle count function (figure 2.7). Watershed function was also performed in order to separate cells that had co-localized and gain a more accurate count. Percentage of Caspase 3/7 positive stained cells was calculated as follows:

$$\% \text{ of cells with active caspase 3/7} = \frac{\text{number of Hoechst positive cells}}{\text{number of Nucview positive cells}} \times 100$$

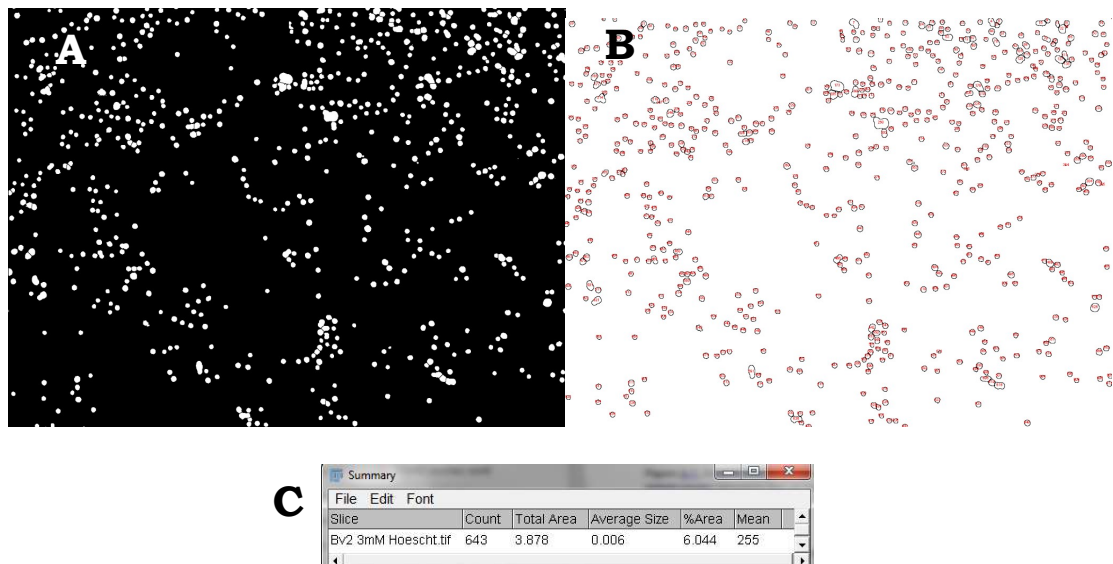


**Figure 2.7:** Fiji image software was used for counting the number of hoescht 33342 or caspase 3/7 positive stained cells. Representative images of **A** generated threshold image for 3mM ATP treated, Hoescht 33342 stained BV-2 cells, and **B & C** summary of FIJI particle count

function from corresponding threshold image **A**, displaying 643 individual, positively stained cells.

Multiple imaging per well in combination with 6 biological replicates per experiment resulted in a mean cell count for each field of view image of  $1167.53 \pm 49.08$  (S.E.M), with a mean total well cell count of  $4325.78 \pm 424.65$  (S.E.M) under control conditions. With cell death inducing stimuli, the average number of total cells/field of view decreased, likely due to removal of cells, however even with the highest level of reduction, the mean total cell count field of view image was  $642.25 \text{ cells} \pm 84.93$  (S.E.M), with a mean total well cell count of  $2848 \pm 268.32$  (S.E.M).

## **2.9 Genomic DNA extraction**

Genomic DNA of control BV-2 cells and BV-2 P2X7R knockout cell clone populations was extracted in order to determine the exact alterations in the genetic sequence of P2X7R. Genomic DNA was extracted using the Wizard SV genomic DNA purification system (Promega, Southampton, UK). Medium was removed from each well, and  $150\mu\text{l}$  Wizard<sup>®</sup> SV lysis buffer solution was added and mixed by pipetting. Cell lysate was then transferred to a Wizard<sup>®</sup> SV mini column contained in a collection tube, and centrifuged at 13,000rpm for 3 minutes and the flow through discarded. This was followed by four wash stages consisting of the addition of  $650\mu\text{l}$  of column wash solution to the minicolumn, centrifuging at 13,000rpm for 1 minute and discarding the flow through. The minicolumn binding matrix was then dried by centrifugation at 300xg for 2 minutes. Total gDNA was then eluted by adding  $250\mu\text{l}$  of nuclease free water (Qiagen) and centrifuging at 300xg for 1 minute, with the flow through gDNA being stored at  $-20^{\circ}\text{C}$ . Extracted gDNA was quantified using duplicate measurements using the NanoDrop ND-2000 spectrophotometer (NanoDrop Technologies, Wilmington, USA).

## **2.10 Non-quantitative gDNA PCR**

Extracted cell gDNA was then amplified at the region of Exon 2 in the P2X7 receptor, in order to be then sequenced. gDNA was first normalised to 200ng in 10µl nuclease free water (Qiagen) in a thin-walled Eppendorf and then mixed into a 25µl reaction mixture containing 1.25µl custom designed forward primer (Sigma Aldrich, Poole, UK), 1.25µl custom designed reverse primer (Sigma Aldrich, Poole, UK) and 12.5µl Hot Start *Taq* mastermix (New England Biolabs, Hitchin, UK). Each sample was then run on a LifeECO thermal cycler (BIOER, Hangzhou, China) for 35 cycles. Each cycle consisted of 10 seconds at 98°C for strand separation, 30 seconds at 66°C for annealing and 30 seconds at 72°C for strand extension.

## **2.11 RNA extraction**

The Qiagen RNeasy mini kit (Qiagen, Crawley, UK) was used for the total RNA extraction of treated cells. The supernatant was aspirated and 350µl of a 20% β-mercaptoethanol (Sigma Aldrich, Poole, UK) solution was added to the culture dish. The cells were then scraped using a sterile dish scraper per sample. The samples were then homogenised by passing through a 20 gauge needle ≥8 times and transferred to an individual sterile RNase free Eppendorf. At this point, the lysate was either frozen at -80°C for later extraction, or the protocol was continued. For each sample, an equal volume (350µl) of 70% ethanol was added to the extracted supernatant and the entire solution was mixed and transferred to an RNeasy mini spin column. The samples were then centrifuged at 13,000rpm for 15 seconds and the flow through was discarded. RW1 buffer was then added to the column and the samples were further centrifuged for 15 seconds and the flow through was discarded. A solution of DNase diluted in RDD buffer was made at a ratio of 1:7, and 80µl was added directly to the column for 15 minutes to digest any DNA in the samples. The samples were then washed with RW1 buffer and centrifuged twice at 13,000rpm followed by a further two washes with Buffer RPE and centrifugation at

13,000rpm for 15 seconds and then at 13,000rpm for 2 minutes. The column for each sample was then dried by centrifugation at 13,000rpm and then transferred into a new RNase free 1.5ml collection tube. To collect the RNA from the column, 50µl of RNase free water (Qiagen, Crawley, UK) was added directly to the spin column and centrifuged for 1 minute at 13,000rpm.

Concentrations of the extracted RNA for each sample were measured in duplicates using the NanoDrop ND-2000 spectrophotometer (NanoDrop Technologies, Wilmington, USA). 260/280 and 260/230 absorbance ratios were also measured to determine if the RNA samples were free from contaminating DNA and triazol reagents, (determined suitable if ratios were  $\geq 1.8$  for both samples)

## **2.12 cDNA synthesis**

As a template for qRT-PCR assays, RNA must be converted to the more stable complementary DNA (cDNA) by synthesis of a complementary DNA strand. RNA samples were first normalised to 100ng/µl with RNase free water to a volume of 10µl. A solution of dNTP (Invitrogen, Paisley, UK) and random primers (Promega, Southampton, UK) were added to the samples, which were then briefly centrifuged to vortex mix. The samples were then then loaded into a LifeECO thermal cycler (BIOER, Hangzhou, China) and heated at 65°C for 5 minutes. The samples were then chilled briefly on ice followed by the addition of a solution mixture containing 5×first strand buffer (Invitrogen, Paisley, UK), RNase inhibitor (Promega, Southampton, UK) and dithiothreitol (DTT) (Invitrogen, Paisley, UK). The samples were then heated using a LifeECO thermal cycler (BIOER, Hangzhou, China) to 25°C for 10 minutes, followed immediately by heating at 42°C for 2 minutes. Samples were then briefly chilled and 1µl Superscript II Reverse Transcriptase (Invitrogen, Paisley, UK) was added. Samples were then centrifuged briefly to mix before being heated in the thermal cycler to

42°C for 50 minutes, followed immediately by heating at 70°C for 15 minutes. cDNA samples were stored at -20°C until use.

### 2.13 Rotorgene qRT-PCR

For amplification, a 20µl reaction mixture was prepared, consisting of 1µl template cDNA, 1µl forward primer and 1µl reverse primer at a concentration of 5µM each (table 2.3), 2µl RNASE free water and 5µl SensiFAST™- SYBR® Lo-ROX master mix. In addition to each sample, a standard curve cDNA template was constructed to determine linear primer efficiency, by pooling 50µl of BV-2 cDNA and 50µl of clone-14 cDNA together to produce a top standard (100%) before performing a series of five 1:5 serial dilutions with RNase free water. Multiple reactions were run for each gene, with each sample run in triplicate, each standard curve sample run in duplicate and two non- template control samples with cDNA volume replaced with RNASE free water.

**Table 2.3:** Primer sequences for genes analysed with qPCR. Sequences pairs were selected from OriGene, available at:

<https://www.origene.com>

Gene	Direction	Primer Sequence
β-actin	F	5' – CAT TGC TGA CAG GAT GCA GAA GG
	R	5' – TGC TGG AAG GTG GAC AGT GAG G
P2rx1	F	5' – CTT TGG CTG GTG TCC TGT AGA G
	R	5' – CCT GTT GAC CTT GAA GCG TGG A
P2rx2	F	5' – ACT ACG AGA CGC CCA AGG TGA T
	R	5' – CCT GGT AGC TTT TCT GAC GAT G
P2rx3	F	5' – TCA TCA ACC GAG CCG TTC AGC T
	R	5' – ACT CTG TTG GCA TAG CGT CCG A
P2rx4	F	5' – GCT TTC AGG AGA TGG CAG TGG A
	R	5' – TGT AGC CAG GAG ACA CGT TGT G
P2rx5	F	5' – AGG ACG CAG AAG GCT TCA CCA T
	R	5' – GGC AGT AGA GAT TGG TGG AGC T
P2rx6	F	5' – TGC TAA CCA GGA ACT GTC GGT
	R	5' – AAG TCC CGT TCC TGG TAG CCT T
P2rx7	F	5' – GAA CAC GGA TGA GTC CTT CGT C
	R	5' – CAG TGC CGA AAA CCA GGA TGT C
P2ry1	F	5' – CCT GCT ATG ACA CCA CGT CCA A

	R	5' – AGC GGA GAG TTG TTC AGG TCA T
P2ry2	F	5' – TTC ACC TGG CAG TTT CGG ACT C
	R	5' – GTG TAG AAG AGG AAA CGC ACC AG
P2ry4	F	5' – CTG GAC AGT CAT CTT CTC GGC T
	R	5' – TTC GGC GTT CAA CAG TCT TGC C
P2ry6	F	5' – CAG TCT TTG CTG CCA CAG GCA T
	R	5' – AGC AAG AAG CCG ATG ACC GTG A
P2ry12	F	5' – CAA GGG GTG GCA TCT ACC TG
	R	5' – AGC CTT GAG TGT TTC TGT AGG G
P2ry13	F	5' – TGG GTT GAG CTA GTA ACT GCC
	R	5' – TTG TCC CGA GCA TCA GCT TT
P2ry14	F	5' – ACC TCC GTC AAG AGG AAG TCC A
	R	5' – GCT GTA GTG ACC TTC CGT CTG A
Adora1	F	5' – GAT CGG TAC CTC GAG TCA AGA
	R	5' – CAC TCA GGT TGT TCC AGC CAA AC
Adora2a	F	5' – CAC GCA GAG TTC CAT CTT CAG C
	R	5' – CCC AGC AAA TCG CAA TGA TGC C
Adora2b	F	5' – TTC GTG CTG GTG CTC ACA CAG A
	R	5' – AAG GAC CCA GAG GAC AGC AAT G
Adora3	F	5' – GCC ATT GCT GTA GAC CGA TAC A
	R	5' – CCC ACC AGA AAG GAA ACT AGC C

Each primer pair was assessed for linear amplification of target cDNA by running the standard curve samples (as described previously). Primer specificity was also assessed by running a melt curve following PCR amplification consisting of an increase of 1°C every 5 seconds to a target temperature of 95°C (Figure 2.8).

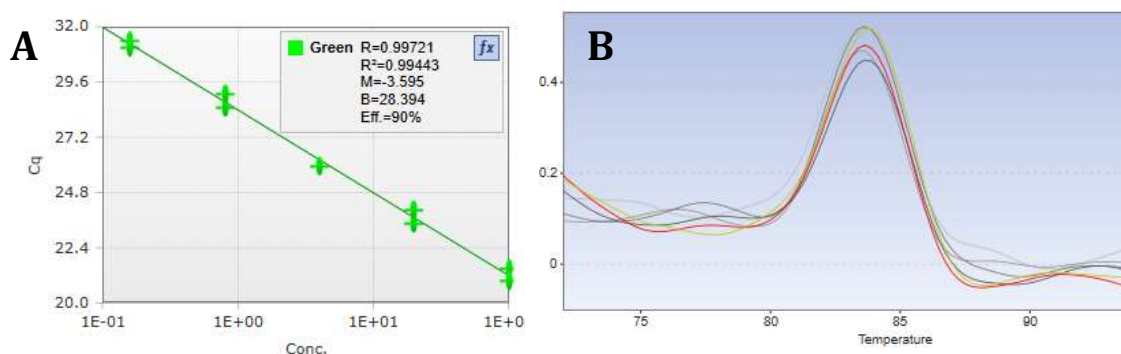


**Figure 2.8:** **A** representative plot of linear amplification for a primer pair and **B** representative trace of melt curve demonstrating a singular peak, indicating primer specificity for a single product (p2rx1 primer pair).

Data was analysed using Q-rex software (Qiagen Crawley, UK) with the  $\Delta$ CT method:

$$\Delta Ct = Ct (\text{Target gene}) - Ct (\beta\text{-actin housekeeping gene})$$

Data was presented as mean values  $\pm$  S.E.M from cells of three independent passages.

#### 2.14 Taqman® qRT-PCR

Taqman® quantitative real-time polymerase chain reaction (qRT-PCR) was conducted using the Applied Biosystems 7500 fast real-time PCR System (Applied Biosystems, Warrington, UK) to quantify changes in RNA expression levels. cDNA produced from RNA samples was diluted to 0.5ng/ $\mu$ l using RNase free water. 5ng total cDNA for the gene of interest samples and 1ng total cDNA for the housekeeping gene (due to 18s gene abundance) were loaded in duplicates into wells of a microAmp Optical 96 well reaction plate (Applied Biosystems, Warrington, UK). A solution mixture containing Master Mix (PCR Biosystems LTD, London, UK), Primers/probes (Applied Biosystems, Warrington, UK) (Table 2.5) and RNase free water was produced for each gene being investigated, to a produce a total well volume of 25 $\mu$ l (see table 2.4)

**Table 2.4:** Quantities of reagents mixed and added to genetic material for qRT-PCR.

Gene	Sample vol $\mu$ l	Master mix vol $\mu$ l	Prime/ Probe vol $\mu$ l	RNase free water $\mu$ l	Total vol $\mu$ l
mIL-1 $\beta$ mm00434228_m1	10	8.33	1.25	5.42	25
18s mm03928990_g1	2	8.33	0.5 F 0.5 R 0.5 P	13.17	25

**Table 2.5:** Taqman qRT-PCR probe/primer sources

Gene	Sequence	Reporter	Supplier
mIL-1 $\beta$	mm00434228_m1	FAM	Applied Biosystems, Warrington, UK
18s	mm03928990_g1	FAM	

The plate was then sealed with a PCR film cover (Thermo Scientific, Surrey, UK). The qRT-PCR procedure began with heating the plate at 50°C for 2 minutes, followed by heating at 90°C for 10 minutes to reduce non-specific amplification. The plate then underwent 40 cycles of heating to 95°C for 15 seconds to denature the double stranded cDNA/DNA, then cooling to 60°C for 60 seconds to allow primer annealing to the single strands.

Analysis of the data was conducted utilising the Ct value set in the exponential phase of amplification, then normalised using housekeeping probe values. The delta Ct method was adopted to assess changes in expression. This method calculates a fold change in expression by using the following equation:

$$\Delta Ct1 = Ct (\text{Target A-treated}) - Ct (\text{Ref B-treated})$$

$$\Delta Ct2 = Ct (\text{Target A-control}) - Ct (\text{Ref B-control})$$

$$\Delta \Delta Ct = \Delta Ct1 (\text{treated}) - \Delta Ct2 (\text{control})$$

$$\text{Normalised target gene expression level} = 2^{-\Delta \Delta Ct}$$

### 2.15 ELISA

An Enzyme-Linked Immunosorbent Assay, specific for the detection of IL-1 $\beta$  was used to quantify IL-1 $\beta$  protein. 500 $\mu$ l of medium from the experimental plate well sampled to determine secreted IL-1 $\beta$  and stored at -80°C. The cells were then lysed and total protein content extracted with 200 $\mu$ l RIPA extraction buffer (Thermo Scientific, Surrey, UK), mixed briefly and stored as two 100 $\mu$ l aliquots at -80°C.

Preparation of the plate (Corning Costar 9018) began with diluting the Anti-mouse IL-1 $\beta$  capture antibody (BD Biosciences, California, USA) in a NaHCO<sub>3</sub>/Na<sub>2</sub>CO<sub>2</sub> coating buffer solution. 100 $\mu$ l the diluted antibody solution was then applied to each well and the plate was sealed and incubated overnight at 4°C. The plate contents were then aspirated and the plate washed with 300 $\mu$ l of a 0.05% Tween 20 PBS wash buffer solution  $\geq$ 3 times. The plate wells were then blocked with 200 $\mu$ l of a 10% FBS-Phosphate buffer saline (PBS) assay diluent solution for 1 hour at room temperature, followed by aspiration and a further  $\geq$ 3 washes with wash buffer solution. For quantifying IL-1 $\beta$ , recombinant mouse IL-1 $\beta$  (BD Biosciences, California, USA) was reconstituted in deionised water and used to produce a standard curve by dilution in varying amounts of assay diluent solution. 100 $\mu$ l of each standard, a negative control (100 $\mu$ l assay diluent) and 100 $\mu$ l of each medium sample or extracted protein sample were transferred to an appropriate well on the plate, which was then incubated at room temperature for 2 hours. This was then followed by washing the plate in wash buffer solution  $\geq$ 5 times. The Biotinylated Anti-mouse IL-1 $\beta$  detection antibody (BD Biosciences, California, USA) was then diluted in assay diluent and transferred to each well on the plate, followed by incubation of the plate at room temperature for 1 hour. This was then followed by washing the plate  $\geq$ 5 times. The enzyme reagent Streptavidin-horseradish peroxidase conjugate (BD Biosciences, California, USA) was then diluted in assay diluent solution, and 100 $\mu$ l was added to each well on the plate, which was then incubated at room temperature for 30 minutes. The plate was then aspirated washed in wash buffer solution  $\geq$ 7 times. 100 $\mu$ l of 3,3',5,5'-Tetramethylbenzidine (TMB Substrate Solution) (Thermo Scientific, Surrey, UK) was then added to each well and the plate incubated in the dark at room temperature for 30 minutes. 50 $\mu$ l of 2N H<sub>2</sub>SO<sub>4</sub> stop solution was then added to each well and the absorbance of was then measured using a FlexStation 3 multi-mode microplate reader

(Molecular Devices, Wokingham, UK) at 450nm and 570nm. The absorbance data was then processed to find the amount of IL-1 $\beta$  using from the standard curve.

## 2.16 Flow cytometry

For each sample, cells were trypsinised and 500,000 cells extracted for flow cytometry analysis. Selected cells were washed once with cold phosphate buffered saline (PBS) containing 0.5% bovine serum albumin (BSA) buffer, then either stained with primary antibody (rat-anti mouse P2X7 antibody (Hano43; Enzo Life Sciences UK Ltd, Exeter, UK)) at 1:10 dilution in PBS/BSA 0.5% buffer, or re-suspended in PBS/BSA 0.5% buffer alone for negative controls, for one hour on ice. Following primary staining, cells were further washed with PBS/BSA 0.5% buffer followed by staining with secondary antibody (goat anti-rat IgG Alexa488 secondary antibody (Fisher Scientific, Loughborough, UK)) for one hour on ice. Cells were then washed with PBS/BSA 0.5% buffer followed by resuspension in 300 $\mu$ l with PBS/BSA 0.5% buffer for acquisition.

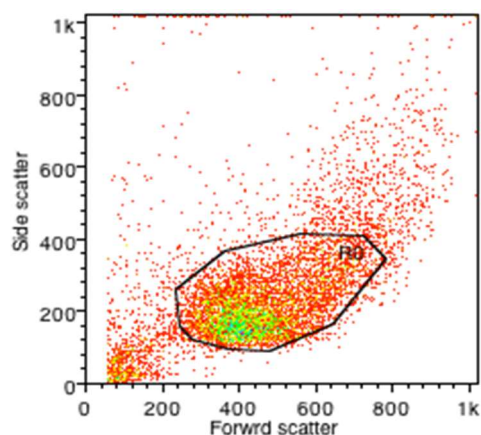


**Figure 2.9:** Example of manual gating method of cells, in order to avoid cellular debris in data acquisition.

Acquisition was performed with either a FACSCalibur (Becton Dickinson, Swindon, UK) or CytoFLEX flow cytometers (Beckman Coulter, High Wycombe, UK), using CellQuest and CytExpert software respectively. Sample populations were manually gated to select only viable cells and eliminate cellular debris (Figure 2.9), with each run

capturing a total of 5000 gated events using FL1 channel with medium PMT voltage gain setting. Each clonal population was assessed for the presence of surface P2X7R against its corresponding negative control sample.

### **2.17 BCA**

A biconchic assay (BCA) was used to determine protein quantities from cell lysates. Protein standards were prepared by diluting bovine serum albumin (BSA) in radio-immunoprecipitation assay (RIPA) lysis buffer at a range of 0-1000 $\mu$ g/ml. Protein standards and samples were separately applied to a 96 well plate in duplicate. Each well then received ddwater and BCA reagents A and B (Thermo Scientific) mixed at a ratio of 10:50:1. The plate was then covered and placed on a shaker for 1 minute before being incubated at 37°C for 1 hour. A FlexStation 3 multi-mode microplate reader (Molecular Devices, Wokingham, UK) was used to measure the absorbance at 550nm. The protein concentrations of the unknown samples were calculated from the standard curve.

### **2.18 Western Blot**

Whole cell lysates were prepared RIPA lysis buffer (Fisher Scientific, Loughborough, UK) containing protease inhibitors (Fisher Scientific, Loughborough, UK). Cell pellets were disrupted by briefly pipetting and lysed on ice for 30 minutes. Cell pellets were then centrifuged at 10,000rpm for ten minutes to separate cellular debris, with the supernatant transferred to a new Eppendorf tube. A BCA assay was performed to determine the quantity of extracted protein in each sample. For each sample, a loading mixture was prepared containing 10 $\mu$ l LDS sample buffer, 4 $\mu$ l reducing agent, 25 $\mu$ g of sample total protein and adjusted to 40  $\mu$ l total volume with deionised water. Sample loading mixtures were then briefly heated to 70°C for ten minutes using a LifeECO thermal cycler (BIOER, Hangzhou, China). Each sample loading mixture was loaded into separate lanes of a

precast Bolt™ 4-12% Bis-Tris Plus gradient gel (Fisher Scientific, Loughborough, UK), and electrophoresis was performed in 2-(*N*-morpholino)ethanesulfonic acid (MES) buffer (Sigma Sigma Aldrich, Poole, UK) at 200V for 22 minutes.

Protein was then transferred to a polyvinylidene fluoride (PVDF) membrane (Immobilon P, Fisher Scientific, Loughborough, UK) with a semi-dry transfer method using Fisherbrand™ semi-dry blotter (Fisher Scientific, Loughborough, UK) at 320mA constant current for 30 minutes. The membrane was subsequently blocked overnight at 4°C in blocking solution, consisting of TBST solution (Thermo Scientific, Surrey, UK) containing 5% non-fat milk to prevent non-specific antibody binding.

PVDF blots were then incubated with anti-P2X7 C-terminal antibody APR-002 (Alomone Laboratories, Jerusalem, Israel) or anti-P2X4 antibody APR-004 (Alomone Laboratories, Jerusalem, Israel) at 1:2000 dilution in blocking solution. After primary incubation, blots were washed in PBST ≥3 times. Blots were then incubated with a horseradish peroxidase conjugated goat anti-rabbit IgG secondary antibody (Sigma Aldrich, Poole, UK) at a 1:2000 dilution, in blocking solution for two hours at room temperature. Following secondary antibody incubation, blots were washed in PBST ≥3 times. Blots were then developed by applying Luminata Crescendo chemiluminescent substrate (Merck Millipore, Watford, UK) and imaged with an Image Quant LAS 4000 imager (GE Healthcare Life Sciences, Amersham, UK). Following primary staining and imaging, blots were stripped with a 200nM NaOH solution for fifteen minutes, washed ≥3 times, re-blocked and re-probed for β-actin with a mouse monoclonal anti-β-actin antibody A5316 (Sigma Aldrich, Poole, UK) at a 1:2000 dilution, followed by staining with horseradish peroxidase conjugated goat anti-rabbit IgG secondary antibody (Sigma Aldrich, Poole, UK) at a 1:10,000 dilution, in blocking solution for 1 hour at room temperature.

### **2.19 Oxygen glucose deprivation**

For experiments modelling ischaemia in cultured cells, an oxygen glucose deprivation model previously described (Niyadurupola *et al*, 2013) was used. Glucose-free media was bubbled with 95% N<sub>2</sub>, 5% CO<sub>2</sub> for 10 minutes prior to use and sealed to eliminate residual O<sub>2</sub>. Cell culture medium was replaced with either glucose-free serum-free DMEM or serum-free DMEM (Life Technologies, Paisley, UK) supplemented with 1% Penicillin-Streptomycin antibiotic (Life technologies). Cells were then placed in a sealed modular incubator container (Billups-Rothenburg, Del March, CA) with gas inlet and outlet valves and a moisture reservoir. Gas in the chamber was then replaced by passing 95% N<sub>2</sub> 5% CO<sub>2</sub> through the modular incubator for ten minutes. The inlet and outlet valves were then sealed to create an oxygen free environment, and the container was incubated at 37°C for the duration required for the experiment.

### **2.20 Data Analysis**

Data is represented as the mean ± standard error of the mean (S.E.M) of at least 4 independent experiments, unless otherwise stated. All statistical analysis was performed using GraphPad Prism software (versions 6.00 or 7.03). Data consisting of only two groups was analysed for significance using the Student's T-test. Data of more than two variables were analysed with a one-way analysis of variance, in combination with a Dunnett's post hoc test for testing significance against a control group, or a Tukey's post hoc test for testing significance against all groups. For the presentation of dose response curves, data was transformed using non-linear regression. Statistical significance between groups was described when a null hypothesis could be rejected with at least 95% confidence ( $P \leq 0.05$ ).

## Chapter 3

### Generation and characterisation of a P2X7 receptor knockout microglial cell line

#### 3.1 Introduction

Clustered regularly interspaced short palindromic repeats (CRISPR) refers to sequences of DNA from prokaryotes, which along with associated RNA molecules and enzymes, plays a role in acquired immune defence in these organisms. One such CRISPR system that has been extensively studied and is commonly used for genome editing was developed from *Streptococcus pyogenes*, the type II CRISPR/Cas9 system (le Rhun *et al*, 2019). This form of acquired immunity is a bacterial defence system that can defend against viruses and other foreign DNA such as bacteriophages. The bacteria is able to recognise foreign nucleic acids with the nuclease enzyme Cas1. Cas1 cleaves the foreign DNA it into small sections, thus inactivating it and incorporates it into the host cells DNA, resulting in the accumulation of small segments of acquired DNA which are separated by palindromic spacer regions. These palindromic regions produce hairpin bends when transcribed into RNA.

The host cell produces complimentary RNA (crRNA), using the acquired DNA as a template, which is then able to bind specifically to the foreign nucleic acid upon subsequent infection. The host cell also produces trans-activating crRNA (tracrRNA), a hairpin RNA molecule derived from the translation of a palindromic region of the host CRISPR DNA, which is able to bind to crRNA. The combination of crRNA and tracrRNA is able to form a stable complex with the Cas9 helicase/nuclease enzyme, effectively guiding the enzyme to the DNA

and activating it to produce specifically targeted double stranded DNA breaks.

The ability of this system to cause specific and precise targeted DNA strand breaks has highlighted its potential use in genomic engineering. The transfection of a eukaryotic cell with elements of the type II CRISPR/Cas9 system can be utilised to induce permanent, stable genetic alterations in the cell genome, including gene knock ins and knock outs. Essential to this process are the Cas9 helicase/nuclease and an RNA molecule to guide Cas9 and activate/stabilise the complex (Cong *et al*, 2013). Transfection of a cell with plasmid DNA containing Cas9, along with a transfection marker for selection such as antibiotic resistance or green fluorescent protein (GFP), allows expression of the Cas9 enzyme. Co-transfection of single guide RNA (sgRNA), a synthetic combination of crRNA and tracrRNA, allows the guiding and activation of Cas9 to a user determined site based on the sequence of the sgRNA, causing a site-specific double strand break in the cell genome (Figure 3.1). Alternatively, sgRNA and Cas9 can be incorporated into the Cas9 plasmid as an all-in-one construct.

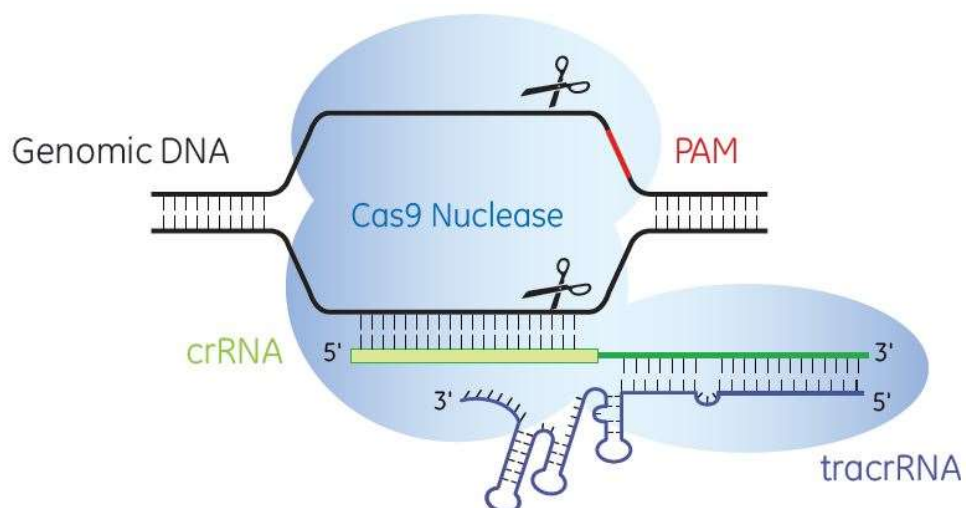


**Figure 3.1:** Representative diagram of the Cas9 crRNA tracrRNA protein-RNA assembly around a strand of gDNA, indicating double stranded cut sites upstream of the protospacer adjacent motif (PAM).

Available from: <https://dharmacon.horizondiscovery.com/gene-editing/crispr-cas9/crispr-guide-rna/>

The cut site of Cas9 requires the recognition of a specific sequence that is known as the protospacer, as well as a the protospacer adjacent motif (PAM) situated next to the protospacer (Anders *et al*, 2014)

With a double strand break in the host cell DNA, the cell will attempt to repair the damage utilising one of two methods, the rapid but error prone non-homologous end joining repair (NHEJ) method, or with the more precise homology directed repair (HDR). When the cell attempts NHEJ repair, the process is often prone to errors resulting in genetic mutation (Lieber, 2010). For example the introduction of an extra nucleotide base during NHEJ, resulting in a shift for the reading frame for any RNA transcription and potentially a non-functional protein, or a premature stop codon resulting in a truncated protein product. Due to the random nature of mutation in this method, the end result can be a variety of different genetic mutations in a transfected population. It is therefore desirable to isolate a single genetic knockout from the population in order to minimise any variation for use in experiments. This can be achieved with the use of single cell clonal expansion.

In comparison with earlier gene disruption techniques, such as siRNA, CRISPR/Cas9 technology offers a stable and permanent alteration of target cells, whereby a single cell containing the desired gene modification can be used to generate a new cell line. As the P2X7 receptor is of key interest in both microglial functions and glaucomatous pathophysiology, the generation of a P2X7 receptor knockout microglial cell line would provide an extremely valuable tool in microglial function, as well as glaucoma research. This chapter describes the optimization of transfection conditions for BV-2 microglia, and the subsequent production of a CRISPR/Cas9 mediated P2X7 knockout microglial cell line.

## 3.2 Results

### 3.2.1 Optimisation of transfection conditions for BV-2 microglia

It is known that immune cells, particularly microglial cells, are difficult to transfect. However, despite low reported transfection efficiencies, various transfection reagents have been used to successfully transfect microglial cells (Zhang *et al*, 2012; Smolders *et al*, 2018; Raas *et al*, 2019). Based on reported past successes, as well as advantageous features such as loading of multiple components, several commercially available transfection reagents (Table 3.1) were assessed for cytotoxicity and transfection efficiency of a reporter plasmid, in order to optimise a transfection protocol for use with the BV-2 cell line. A rat P2X7 GFP reporter plasmid was chosen due to requirement for quick and easy screening by visual assessment with fluorescent microscopy, as well as mimicking a larger transfection load that is required for subsequent CRISPR transfection.

**Table 3.1:** List of commercially available transfection reagents tested with BV-2 microglia in initial transfection efficiency experiment.

<i>Transfection Reagent</i>	<i>Manufacturer</i>	<i>Location</i>
JetPEI®	PolyPlus	Illkirch, France
DharmaFECT Duo®	Dharmacon	Lafayette, CO, US
Lipofectamine 2000®	Invitrogen	Paisley, UK
Fugene®	Promega	Southampton, UK

Preliminary experiments were carried out where BV-2 cells were visually assessed for viability after 24 hour incubation with the selected transfection reagents in the presence and absence of rat P2X7 GFP reporter plasmid.

In the absence of rat P2X7 GFP reporter plasmid, BV-2 cells displayed no substantial morphological changes with any of the transfection reagents tested. The additional presence of rat P2X7 GFP reporter plasmid caused both loss in cell number, and morphological changes (Figure 3.3). Of the plasmid transfected cells, the DharmaFECT Duo reagent was the best tolerated, producing limited cell number and morphological changes.

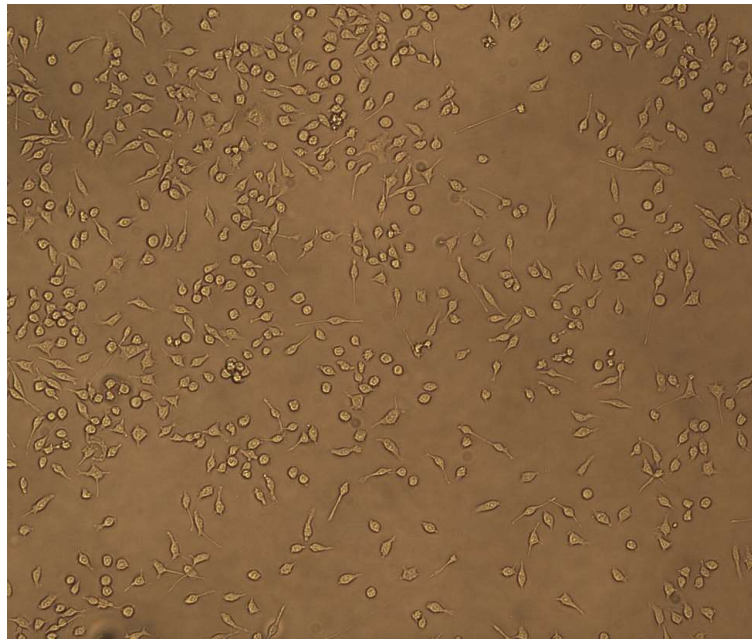


**Figure 3.2:** Representative images of BV-2 microglia morphology

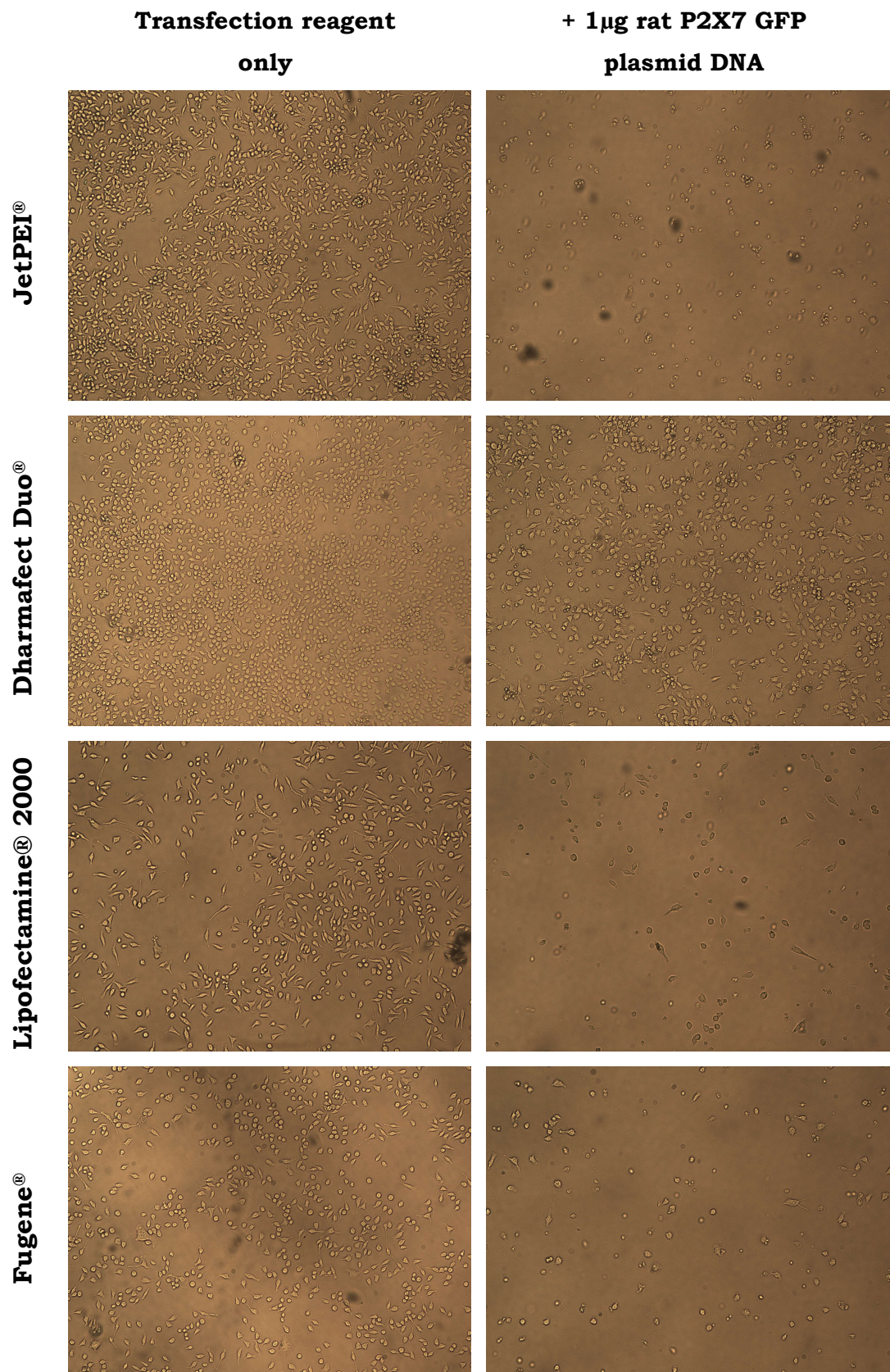


**Figure 3.3:** Representative images of BV-2 microglia morphology after 24-hour incubation with various transfection reagents, in isolation (left) or in combination with 1 $\mu$ g rat P2X7R GFP reporter plasmid (right).

BV-2 cells were then assessed for successful transfection when using Dharmafect Duo. Following transfection with 1 $\mu$ g rat P2X7 GFP with DharmaFECT duo, BV-2 cells demonstrated moderate levels of fluorescently labelled cells after 24-hour treatment (Figure 3.3).

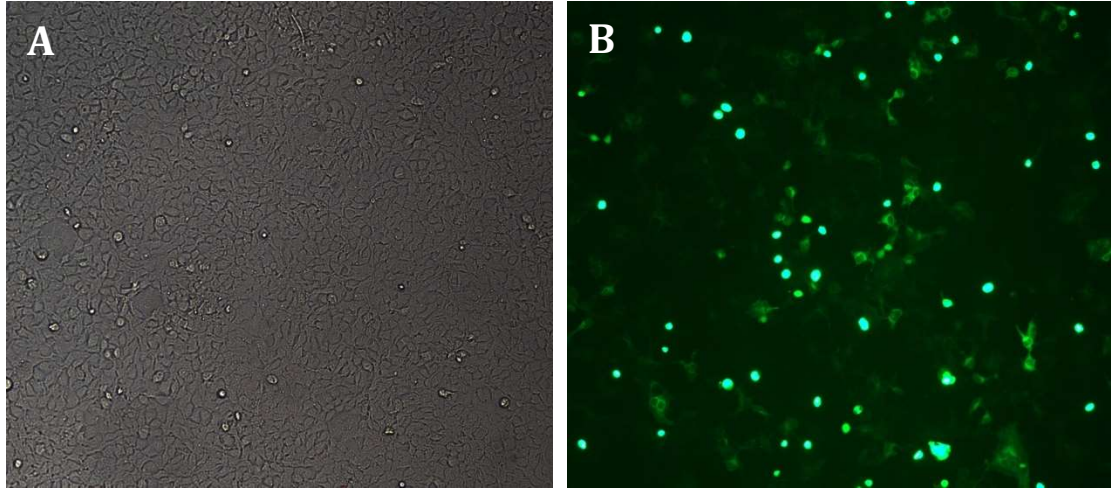


**Figure 3.4:** Representative (A) brightfield and (B) immunofluorescent images of rat P2X7 GFP transfected BV-2 cells, utilising Dharmafect Duo transfection reagent, Images were taken 24 hours after transfection. Fluorescent cells indicate successful transfection of BV-2 microglia with rat P2X7R GFP plasmid.

Dharmafect duo reagent was selected to carry out CRISPR/Cas9 transfection, based on several factors, including lowest cytotoxic effect on the cells compared with alternative reagents (Figure 3.3), and the successful expression of rP2X7-GFP reporter plasmid in a proportion of the cell population (Figure 3.4 B). A further advantage of this system is the use of a single transfection step for multiple CRISPR components.

In order to initiate Cas9 protein expression for use with CRISPR gene editing, BV-2 cells have to be transfected with a plasmid containing expression vectors for Cas9 nuclease enzyme and a selectable marker/reporter gene for population enrichment, such as a fluorescent tagged protein or antibiotic resistance, and appropriate promoter regions for both. The pHCSVblast-Cas9 plasmid (GE Healthcare Dharmacon, Lafayette, CO, US) contains the essential Cas9 nuclease vector controlled by a human cytomegalovirus (hCMV) promoter, in

addition to a blasticidin resistance (Blast<sup>R</sup>) gene for transfection enrichment, which is controlled by a simian virus 40 (SV40) promoter (Figure 3.5). The pHCSVblast-Cas9 plasmid also contains an additional ampicillin resistance (Amp<sup>R</sup>) gene for plasmid propagation in *Escherichia coli* cultures, which simplifies the procedures required to produce knockout cells.

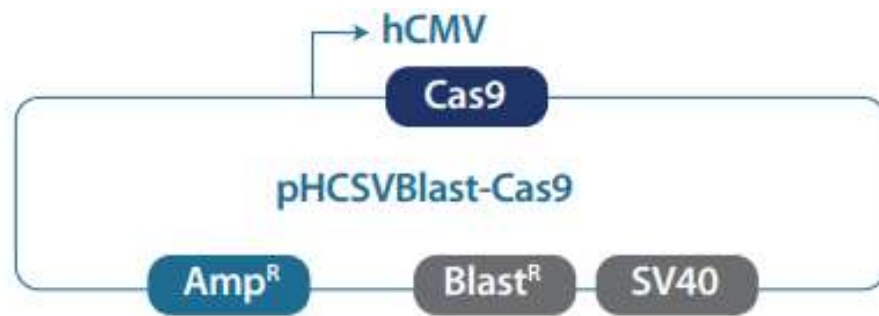


**Figure 3.5:** Plasmid map containing vector elements of the Dharmacon<sup>®</sup> Edit-R plasmid. (**Cas9**) Cas9 nuclease enzyme gene vector. (**hCMV**) human cytomegalovirus promoter. (**Blast<sup>R</sup>**) blasticidin antibiotic resistance. (**SV40**) Simian virus 40 promoter. (**Amp<sup>R</sup>**) ampicillin resistance gene vector. Available from: <https://dharmacon.horizondiscovery.com/uploadedFiles/Resources/edit-r-cas9-nuclea-express-plasmid-synth-rnas-manual.pdf>

### 3.2.2 Design of mP2X7 exon2 targeting crRNA sequences

The P2X7 receptor exists in several splice variant forms, in both human and mouse homologues (Sluyter & Stokes, 2011; Nicke *et al.* 2009), due to different combinatorial assembly of exon regions. As such, previous attempts at producing a P2X7 knockout model, specifically the Glaxo P2X7<sup>-/-</sup> knockout mouse, resulted in one isoform of the P2X7 (P2X7(k)) with an alternative N-terminus and TMD 1, escaping gene deletion (Nicke *et al.* 2009). To ensure a complete P2X7 knockout is generated that covers all known mouse splice variants, crRNA was designed to target exon2, which is shared by all isoforms of the mP2X7 receptor. P2X7 exon2 potential complimentary crRNA sequences are shown in table 3.2

**Table 3.2:** Predicted crRNA sequences generated with Millipore/sigma CRISPR design tool (now available online: [https://www.milliporesigmabioinfo/bioinfo\\_tols/faces/secured/crispr/crispr.xhtml](https://www.milliporesigmabioinfo/bioinfo_tols/faces/secured/crispr/crispr.xhtml)).

Name	Sequence	PAM	Target strand	No. of sites in genome 1, 2 or 3 nucleotides different from target sequence		
				1	2	3
MM0000047168	5' - TGTGCACGGAGCTGATAAC	AGG	†	0	0	4
MM0000047167	5' - GATAACAGGCTCTTTCCGC	TGG	†	0	0	1
MM0000047169	5' - ATCAGCTCCGTGCACACCA	AGG	*	0	0	3
MM0000047166	5' - GAGCGATAAGCTGTACCAG	CGG	*	0	0	0

Since BV-2 cells are of mouse origin, the generated crRNA sequences were subsequently BLAST searched against the *Mus musculus* (mm10) genomic DNA library in order to identify potential instances liable to off target genetic modification. All of the generated crRNA transcripts demonstrated high specificity to the exon2 mP2X7 sequence, with potential off site targets only emerging when allowing for a nucleotide mismatch of  $\geq 3$ .

Based on the predicted likelihood of off target effects, of the 4 sequences generated, sequences MM0000047167 and MM0000047169 were selected for use in the CRISPR/cas9 treatment of BV-2 microglia (Figure 3.6).

5' CTTTGCTTTGGTGAGCGATAAGCTGTA **CCAGCGGAAAGAGCCTGTTA**  
**TCAGCTCCGTGCACACCAAGG**TCAAAGGCATAGCAGAGGTGACGGAGAA  
TGTCACAGAGGGTGGGGTGACGAAGTTAGGACACAGCATCTTTGACACT  
GCAGACTACACCTTCCCTTTGCAG

**Figure 3.6:** Base sequence of mP2X7 exon2. Green/cyan highlighted region represents MM0000047167 crRNA sequence and cyan/pink highlighted region represents MM0000047169 crRNA sequence.

Identification of cells expressing the pHCSVblast-Cas9 plasmid would increase the chances of isolating cells with successful CRISPR-mediated modification of P2X7. Following transfection, cell cultures were treated with blasticidin antibiotic in order to select only cells expressing Blast<sup>R</sup> gene, a component of the pHCSVblast-Cas9 plasmid (Figure 3.5).

Following blasticidin treatment, wells demonstrated a moderate reduction in cell number, indicating the removal of cells that were not expressing the Blast<sup>R</sup> gene. In order to determine disruption to P2X7R expression in CRISPR treated/blasticidin selected cell cultures, flow cytometry was subsequently performed.

### 3.2.3 P2X7R flow cytometry screening of blasticidin resistant CRISPR treated BV-2 cells

Wells that displayed cells with antibiotic resistance, along with untreated BV-2 cells as a positive control were screened for surface P2X7 protein expression by indirect flow cytometry.

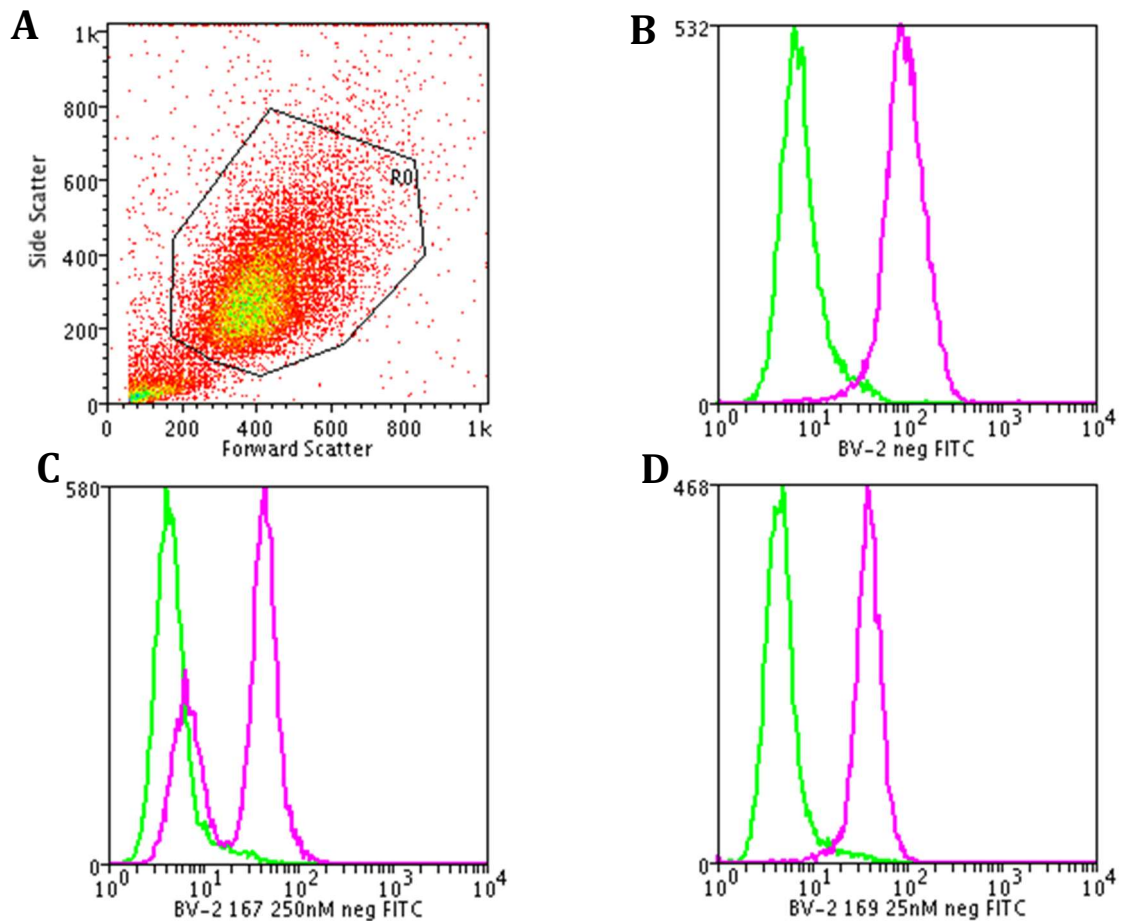


**Figure 3.7:** **A** Forward side scatter plot demonstrating manual gating of viable cells to avoid cell debris, cell plot density represented as colour change from red (low density) to green (high density) **B-D** Representative flow cytometry plots of P2X7 screened CRISPR treated BV-2 cells, pink trace is P2X7 positive population, green is corresponding non-primary antibody stained negative control. **B** control BV-2 microglia, **C** MM0000047167 cRNA treated BV-2 cells **D** MM0000047169 cRNA treated BV-2 cells. Data acquired with FACSCalibur flow cytometer and CellQuest software.

Untreated BV-2 cells demonstrated clear rightward shift in fluorescence, with little population overlap with the corresponding negative control population (Figure 3.7 B), indicating presence of P2X7. Screening of CRISPR treated BV-2 populations produced varied results, with some populations producing identical plots to that of untreated BV-2 cells, indicating that, despite inheritance of antibiotic resistance, these populations had not altered the presence of cell surface P2X7 protein. In contrast, several CRISPR treated populations exhibited dual distinct peaks in fluorescence, where one peak overlapped with the negative control (Figure 3.7 C). The overlap of one peak with the population's corresponding negative control indicates the loss of cell surface P2X7 protein in a proportion of the cell population.

#### **3.2.4 Single cell clonal expansion of P2X7 deficient BV-2 populations**

In order to generate a complete P2X7R knockout population, CRISPR/cas9 MM0000047167 crRNA treated BV-2 cells that demonstrated a P2X7 deficient sub-population were subjected to single cell clonal expansion using serial array dilution method (see 2.3). Array dilution single cell clonal expansion produced, 27 colonies of cells of single cell origin. Following single cell clonal expansion, cells were subsequently cultured and expanded for further characterisation.

### 3.2.5 P2X7 flow cytometry screening of single cell clones

Following clonal expansion, 27 generated single cell colonies, in addition to parental BV-2 cells as a positive control, were screened for the surface expression of P2X7 protein by indirect flow cytometry (as described in 3.2.3).

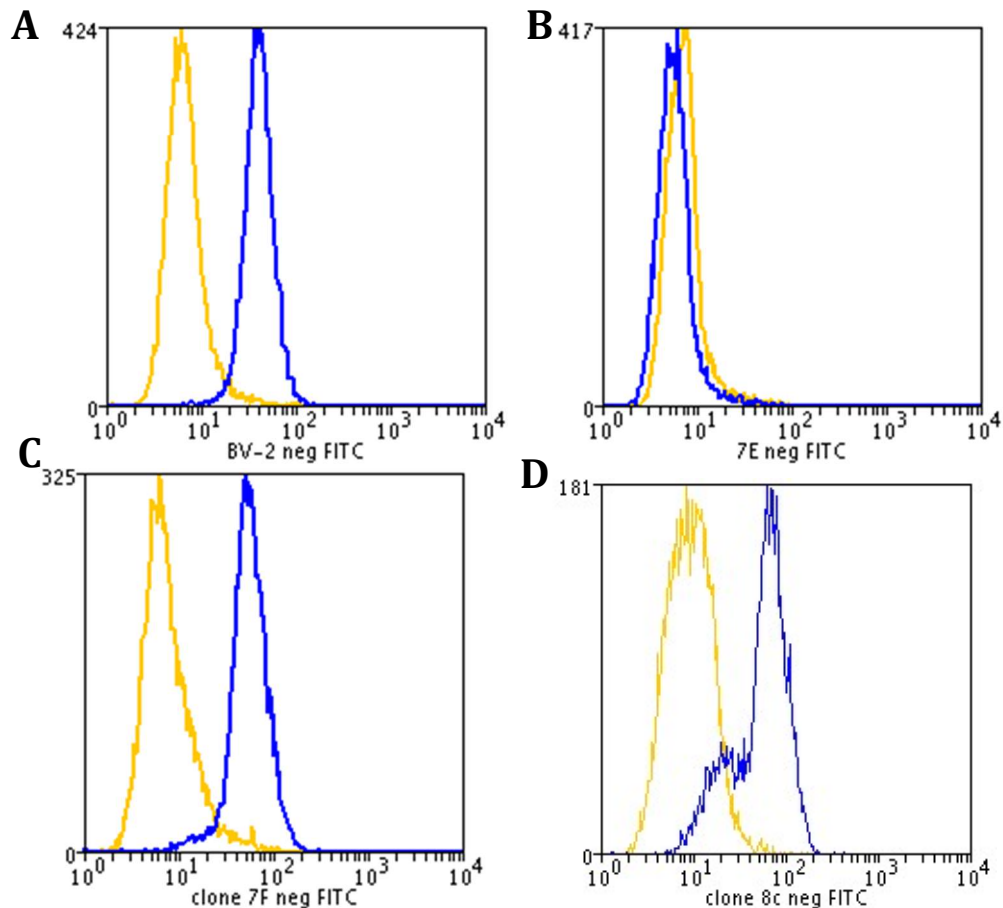


**Figure 3.8: A-D** Representative flow cytometry plots of P2X7 screened cells colonies, blue trace is P2X7 stained population, yellow is corresponding non-primary stained negative control. **A** parental BV-2 microglia, **B** Clone 7E, **C** Clone 7F, **D** Clone 8C. Data acquired with FACSCalibur flow cytometer and CellQuest software.

Parental BV-2 cells acting as a positive control demonstrated clear rightward shift in fluorescence, with little population overlap with the corresponding negative control population (Figure 3.8 A). In a similar manner to the BV-2 positive control, many of the colonies tested demonstrated no overlap with corresponding negative control

population (Figure 3.8 C), indicating single cell clonal expansion had failed to isolate a P2X7 deficient cell from the mixed population. In contrast many of the colonies displayed a singular defined fluorescent peak that overlapped entirely with their corresponding negative control population (Figure 3.8 B), indicating an entirely P2X7 surface deficient population had been successfully generated.

In addition, there were several instances of colonies producing two distinct fluorescent peaks, of which one produced a clear rightward shift, in a similar manner demonstrated by mixed populations observed in the initial indirect flow screening of CRISPR transfected BV-2 cells (Figure 3.8 D). Colonies demonstrating dual fluorescent peaks indicates that following single cell clonal expansion, a well was mistakenly observed to have produced a colony from a single cell, where two or more cells were initially seeded. A detailed assessment of the surface expression of P2X7 for each single cell clonal expansion generated colony is presented in table 3.3.

**Table 3.3:** Table of colonies screened for surface expression of P2X7 with indirect flow cytometry. The expression of surface P2X7 is designated based on the number of fluorescent peaks observed and the overlap of peaks with each clone's corresponding negative control population.

<i>Single cell generated colony</i>	<i>Overlap with negative control (P2X7 stain)</i>	<i>Selected for storage</i>
7E	Full	*
9D	Full	*
6D	Full	*
29B	None	
F12	Full	*
F6	Full	*
7D	None	
7F	None	
8C	Mixed	
7C	None	
39B	Mixed	
9C	None	
Clone 1	Full	*
Clone 2	None	
Clone 4	Full	*
Clone 5	Full	*
Clone 6	Mixed	
Clone 8	Full	*
Clone 10	Mixed	
Clone 11	None	
Clone 13	Mixed	
Clone 14	Full	*
Clone 15	Full	*

### 3.2.6 P2X7 mediated Fura-2 Ca<sup>2+</sup> screening of generated clone populations

In order to further explore potential abolition of surface P2X7 receptor activity on CRISPR generated knockout clones, Intracellular Ca<sup>2+</sup> measurements were recorded for 200 seconds using Fura-2 AM fluorescent indicator dye, following stimulation with 500µM ATP at 30 seconds. Each individual knockout clone area under the curve response was compared to that of unedited BV-2 and BV-2 cells incubated with the P2X7 antagonist AZ10606120 (10µM) as negative and positive controls of P2X7 activity respectively (Figure 3.9).

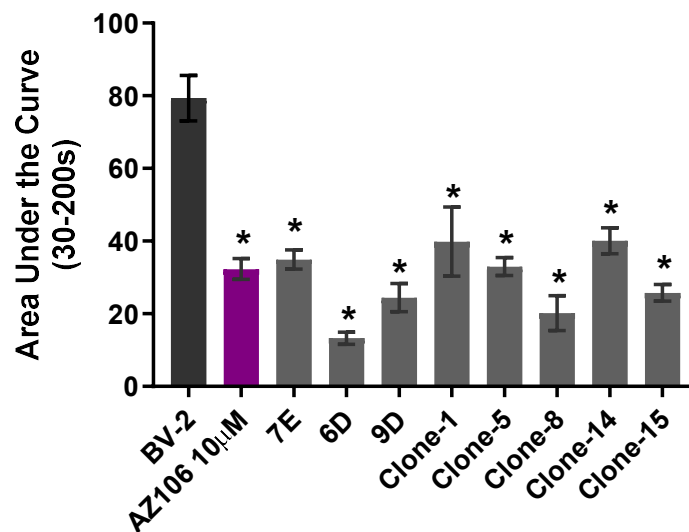


**Figure 3.9:** Average area under the curve Fura-2 ratio Ca<sup>2+</sup> responses (30-200s) in BV-2 and single cell generated P2X7 K/O clones, following 500µM ATP stimulation, represented as Mean ± S.E.M (minimum of n=3 traces). For P2X7 inhibition in BV-2 cells, AZ10606120 (10µM) was used as a positive control. \* indicates significance against BV-2 control group using one-way ANOVA with Dunnett's post hoc test (P<0.05).

Pre-incubation of BV-2 cells with 10µM AZ10606120 demonstrated significant reduction in the ATP mediated area under the curve Fura-2 Ca<sup>2+</sup> response (Figure 3.9). Similarly, each individual knockout clone tested here demonstrated either similar or greater reduction in the ATP mediated area under the curve Fura-2 Ca<sup>2+</sup> response compared to AZ106 preincubated BV-2 microglia, demonstrating a loss of P2X7 receptor functionality.

### 3.2.7 P2X7R Genomic DNA region sequencing

Due to the appearance of successful P2X7 knockout in several clone populations, one such population, Clone-14 was selected at random for further characterisation. Clone-14 total genomic DNA was extracted, and exon 2 genomic region amplified by standard PCR. Primers were designed against P2X7 exon2 region sequence (Table 3.4).

**Table 3.4:** Sequences of primers designed against exon2 of mP2X7

Primer	Primer sequence
MF_mP2X7-ex2_For	5'-CCCAAAGTGTGCTGTCCTCTGT
MF_mP2X7-ex2_Rev	5'-CCCTAGACCCCTAAGGATGG

PCR was performed with the designed primers on extracted gDNA from parental BV-2 cells and Clone-14 cells, followed by separation of the PCR products on an agarose gel (Figure 3.10). Amplified PCR products from both cell sources demonstrated similar sized bands of an expected 289bp size.

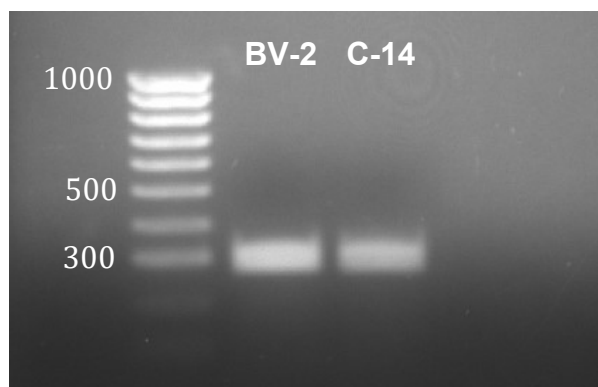


**Figure 3.10:** Gel of non-quantitative PCR products from BV-2 and clone-14 gDNA

Sanger sequencing was subsequently performed on PCR amplified gDNA samples from each BV-2 knockout clone, as well as untreated BV2 gDNA (performed by Eurofins Genomics), in order to validate

genetic modification as a result of CRISPR treatment. Each sequence file was analysed in Chromas software (version 2.6) and the base sequence data exported as a txt file. The base sequence of untreated BV-2 cells was searched against chromosome 5 of the *Mus musculus* genome (Figure 3.12) using the Basic Local Alignment Search Tool (BLAST), to determine whether the region-specific PCR had amplified exon2 of P2X7 correctly, as well as any potential deviations from the parental BV-2 sequence in the clones tested.

The chromatogram of P2X7 exon2 gDNA from BV-2 cells demonstrated clearly distinct peaks for each base position above minimal background noise with no unclear base designations (Figure 3.11) from base position 20 onwards. When aligned with the *Mus musculus* (mm10) mp2rx7 sequence the result was a sequence that encompassed exon2 of P2X7 and demonstrated a homology of 99%, highlighting a single missing cysteine base residue at position 15 in the BV-2 cell line (Figure 3.12). Due to the unclear designation of bases at the beginning of the chromatogram, it is unclear whether there is truly a missing base

The chromatogram sequence of clone-14 gDNA, like that of BV-2 gDNA demonstrated a clearly defined beginning sequence from base 20 onward (Figure 3.13). In contrast to the BV-2 sequence however, from base 44 onward the clone-14 chromatogram demonstrated multiple instances of unclearly defined double peaks (Figure 3.13), indicative of mutations or variation in the sequence between the two diploid alleles. When aligned with the *Mus musculus* (mm10) mp2rx7 sequence the result was a sequence that demonstrated extensive base sequence deviation (Figure 3.14), including multiple base deletions, additions and nucleotide mis-matches, resulting in a sequence homology of only 74%. This indicated that CRISPR treatment had caused significant alteration in the exon2 region of mp2rx7 in clone-14 cells.



```

BV-2 sequence  TTTTTCTCTGTCCCTCAGCTTTTGGTGGTGAGCGATAAAGCTGTACCAGCGGAAAGAGCC
                |||||
mP2X7 sequence TTTTTCTCTGTCCCTCAGCTTTGGTGGTGAGCGATAAAGCTGTACCAGCGGAAAGAGCC
                |||||
BV-2 sequence  TGTTATCAGCTCCGTGCACACCAAGGTCAAAGGCATAGCAGAGGTGACGGAGAAATGTCAC
                |||||
mP2X7 sequence TGTTATCAGCTCCGTGCACACCAAGGTCAAAGGCATAGCAGAGGTGACGGAGAAATGTCAC
                |||||
BV-2 sequence  AGAGGGTGGGGTGACGAAAGTTAGGACACAGCATCTTTGACACTGCAGACTACACCTTCCC
                |||||
mP2X7 sequence AGAGGGTGGGGTGACGAAAGTTAGGACACAGCATCTTTGACACTGCAGACTACACCTTCCC
                |||||
BV-2 sequence  TTTGCAGGTGAGTGCCCGTGGAATTCAGGTCACGTTTCTGTCCCCATCCCCATCCTTAGG
                |||||
mP2X7 sequence TTTGCAGGTGAGTGCCCGTGGAATTCAGGTCACGTTTCTGTCCCCATCCCCATCCTTAGG
                |||||
BV-2 sequence  GGTCTAGGG
                |||||
mP2X7 sequence GGTCTAGGG
                |||||

```

**Figure 3.12:** mP2X7 exon 2 sequence of BV-2 gDNA, as determined by sanger sequencing, aligned to *mus musculus* (mm10) mP2X7 exon 2 sequence. Green highlight indicates nucleotide base omission. Yellow highlight indicates start of exon 2

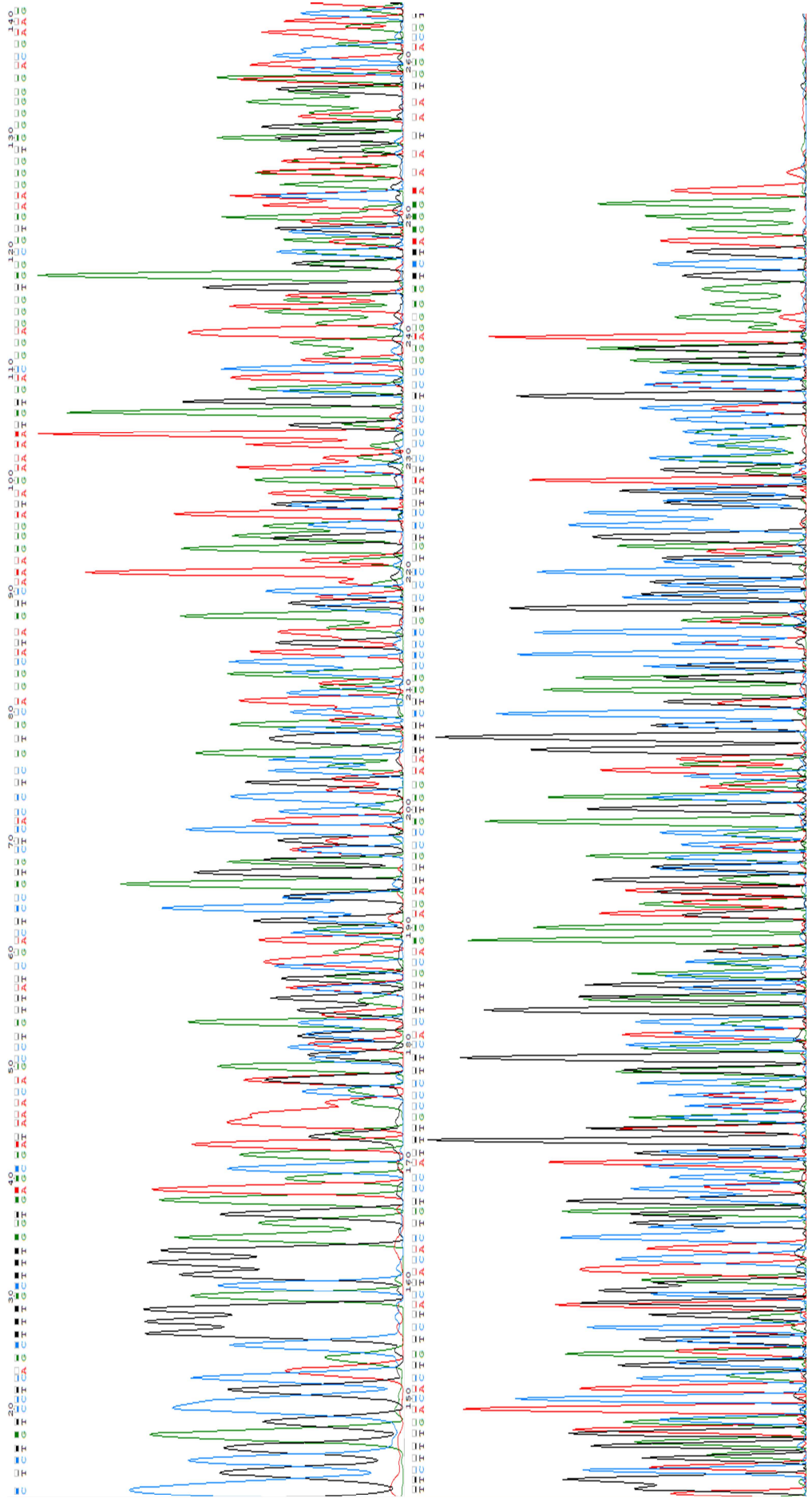


**Figure 3.13:** Chromatogram of exon 2 P2X7 gDNA derived from Clone-14 P2X7 K/O, as viewed in Chromas software. Red: Adenine, Blue: Cytosine, Green: Guanine, Black: Thymine



### **3.2.8 qRT-PCR analysis of purinergic receptor expression in BV-2 and BV-2 P2X7 K/O cells**

Following Sanger sequencing of gDNA, the mRNA expression levels of all purinergic receptor subtypes present in the mouse genome were screened from cDNA generated from parental BV-2 and clone-14 cells, to investigate P2X7 receptor knockout in clone-14 cells, as well as determine any effects on other purinergic receptors following CRISPR gene editing. cDNA was generated from total RNA and expression levels were assessed by qRT-PCR (Table 3.5).

qRT-PCR analysis of BV-2 and clone-14 cell purinergic and adenosine receptor family mRNA expression demonstrated the presence of mRNA transcripts for all tested receptors in both cell types (Table 3.5), except for the Adenosine A3 receptor (Adora3), which was not detected in either cell type within 40 amplification cycles. Relative expression levels (based upon mean CT above  $\beta$ -actin housekeeping gene), demonstrated wide variation amongst the different subtypes of receptor. High expression levels, designated as  $<10 \Delta CT$ , was detected for multiple purinergic receptors mRNA transcripts in parental BV-2 cells (Table 3.5), for P2X4, P2X5 and P2Y1. A similar pattern of high expression was seen in clone-14 cells. Clone-14 cells also demonstrated high expression P2Y2 and the adenosine A2A receptor. For most receptors, there was no significant difference in expression between BV-2 and clone-14 cells. The only significant difference in expression was a 7.8 fold downregulation of P2Y12 in clone-14 cells.

For most receptors there was no significant difference in expression between BV-2 and clone-14 cells. However, there was a significant mRNA down regulation of P2Y12 in Clone-14 cells. Intriguingly, mRNA transcript expression was detected in clone-14 cells, with no significant alteration in relative expression compared to parental BV-2 cells.

**Table 3.5:** Purinergic and adenosine receptor family mRNA expression in BV-2 and clone-14 cells, expressed as mean  $\Delta ct \pm S.E.M.$  +++ indicates high expression, ++ indicates moderate expression, + indicates low expression, - not detected. N=3 on cells from 3 independent passages. \* indicates significant difference between expression in BV-2 and clone-14 cells ( $p < 0.05$ ) using students T-test.

Gene	$\Delta CT$ (BV-2)	Relative expression (BV-2)	$\Delta CT$ (Clone-14)	Relative expression (Clone-14)	Significant change in expression
P2rx1	11.20 $\pm$ 0.15	++	11.11 $\pm$ 0.34	++	
P2rx2	13.96 $\pm$ 1.42	++	14.32 $\pm$ 1.31	++	
P2rx3	13.19 $\pm$ 2.24	++	12.67 $\pm$ 2.87	++	
P2rx4	7.42 $\pm$ 0.61	+++	8.09 $\pm$ 0.77	+++	
P2rx5	7.86 $\pm$ 0.68	+++	7.68 $\pm$ 0.98	+++	
P2rx6	16.78 $\pm$ 1.41	+	16.09 $\pm$ 1.52	+	
P2rx7	12.18 $\pm$ 1.66	++	12.23 $\pm$ 1.71	++	
P2ry1	8.68 $\pm$ 0.78	+++	9.15 $\pm$ 1.57	+++	
P2ry2	10.23 $\pm$ 0.94	++	9.27 $\pm$ 0.73	+++	
P2ry4	14.79 $\pm$ 0.72	++	15.76 $\pm$ 1.21	+	
P2ry6	12.79 $\pm$ 3.71	++	13.92 $\pm$ 2.10	++	
P2ry12	14.03 $\pm$ 0.25	++	17.00 $\pm$ 0.77	+	*
P2ry13	14.70 $\pm$ 2.00	++	13.67 $\pm$ 1.13	++	
P2ry14	17.80 $\pm$ 1.09	+	17.22 $\pm$ 1.58	+	
Adora1	13.50 $\pm$ 4.81	++	15.29 $\pm$ 4.46	+	
Adora2a	14.40 $\pm$ 0.87	++	14.10 $\pm$ 1.30	++	
Adora2b	10.54 $\pm$ 0.92	++	9.28 $\pm$ 0.61	+++	
Adora3	ND	-	ND	-	

### 3.2.9 Western Blot analysis of total cell P2X7 protein

The previously utilised methods for P2X7 phenotypic assessment, flow cytometry screening and live cell imaging assays, were only selective for only surface protein expression. In order to assess total cellular P2X7 protein content of BV-2 and BV-2 P2X7 K/O cells, Western blotting of cell lysates was performed, alongside J774 macrophage cell lysate as a positive control (Figure 3.15). Blots were then stripped and re-stained for  $\beta$ -actin as a protein loading control.

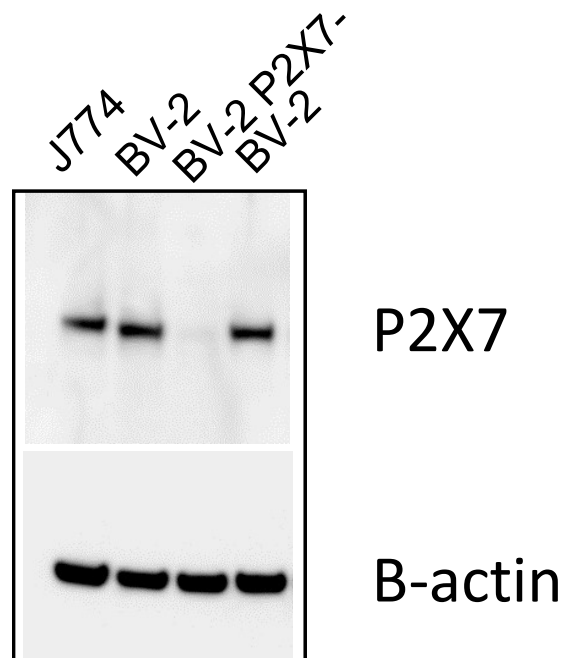


**Figure 3.15:** Western blot images demonstrate no anti-P2X7 reactive band in clone-14 cells (BV-2 P2X7-), compared to anti-P2X7 reactive bands in untreated BV-2 cells and J774 macrophages.  $\beta$ -actin bands indicate equal protein loading/well (25 $\mu$ g).

A P2X7 band was seen in both native BV-2 and J774 macrophage sample lanes, however there was no reactive band in clone-14 lane (Figure 3.15). Stripped and re-probed plots exhibited anti- $\beta$ -actin immune reactivity in all sample lanes, with even band widths indicative of even sample loading.

### 3.3 Discussion

The P2X7R has several established roles in microglial functions as well as a reported role in glaucomatous neurodegeneration (Niyadurupola *et al*, 2013). The primary aim of this chapter was to generate a P2X7 knockout microglial cell line, for study of the P2X7R in various microglial functions in relation to glaucoma. Alongside this, was the aim to optimise a set of conditions for the successful transfection of microglial cells, for use in potential future studies. Nuclease based tools for targeted genomic engineering including CRISPR/Cas9 are advantageous over other knockdown tools such as siRNA, due to the permanent and non-reversible outcome, allowing long term analysis of the modified target. The CRISPR/Cas9 system utilises gRNAs to target a nuclease to the site of modification, which represents a significant advantage in the ease of design and low cost associated with developing gRNAs compared to other nuclease based tools. For these reasons, CRISPR/cas9 mediated gene editing was selected as the technique of choice to generate the P2X7 knockout microglia cell line described in this chapter.

Immortalized BV-2 cells are a widely used model for *in vitro* research of microglial function and have been used as a model for retinal microglia (Langmann, 2007). In terms of suitability, BV-2 cells have a high level of resemblance to isolated primary microglia (Henn *et al*, 2009; Stansley *et al*, 2012), although caution must be exercised in the extrapolation of results as considerable differences have been demonstrated between BV-2 cells and *in vivo* microglia (Butovsky *et al*, 2014). Despite their ease of manipulation for use with a variety of experimental techniques, phagocytic cells such as macrophages and microglia have limitations that make them difficult to transfect. The primary transfection obstacle is likely due to expression of enzymes, which are responsible for the degradation of foreign nucleic acids (Zhang *et al*, 2012), due to their role of protection against bacterial pathogens in inflammatory responses. Additionally, transfection,

particularly with liposomal based reagents, has been associated with reduced cell viability in BV-2 cells (Rao *et al*, 2015), as well as the transient release of IL-6 into culture medium (Smolders *et al*, 2018). For these reasons, microglial transfection has been associated with low overall transfection efficiencies when using chemical/liposomal based transfection reagents such as Lipofectamine® 2000 (Zhang *et al*, 2012). Despite this, there is evidence of successful transfection of BV-2 cells (Raas *et al*, 2019).

Initially, a series of experiments were developed to optimize the transfection of BV-2 microglia. All of the transfection reagents tested in the absence of reporter plasmid (mock transfections) exhibited minimal instances of morphological characteristics associated with cell death (Figure 3.3). However, the addition of plasmid material to the transfection conditions caused some reduction in cell number and (Figure 3.3), compared to corresponding mock transfection controls although DharmaFECT duo reagent showed less cell damage than other reagents. Additionally, due to the potentially narrow window of Cas9 protein expression after transfection, and the potential compounding effect of multiple transfections on cell viability, a reagent that delivered both the required plasmid and CRISPR associated RNA molecules in one step was deemed advantageous over separate transfections of each component. Dharmafect® Duo is optimised for co-transfection of plasmids and small RNA templates, and for these reasons, was selected as the plasmid delivery vehicle of choice.

Based on the submitted sequence template (Table 3.2), 4 unique crRNA sequences were and checked for off-target effects. Two of these were selected and used in transfections, with transfected cells then analysed for P2X7 protein expression using flow cytometry. Populations were found in which the P2X7R was absent at the cell surface; single cell clonal expansion was used to grow clonal colonies which were further characterised by flow cytometry to find cells where

the P2X7R was successfully eliminated. Flow cytometry of colonies generated by single cell clonal expansion demonstrated several populations with complete knockout of P2X7R surface expression. These colonies were then cryogenically stored, with one colony, clone-14 selected for further characterisation.

For additional characterisation, Sanger sequencing of clone-14 PCR amplified gDNA was performed. Sequencing of the parental BV-2 cells as a positive control was aligned to the *Mus musculus* (mm10) reported genome sequence and demonstrated a 99% homology match. High homology matching of the BV-2 sequence acts as validation for the study of P2X7 receptor function in BV-2 cells with other studies in similar immortalised cell lines and in vivo studies. Conversely, P2X7 exon2 sequence of Clone-14 cells displayed a significant base sequence alteration, in comparison/alignment to parental BV-2 sequence, indicating that significant alteration of exon 2 sequence in Clone-14 cells had occurred as a result of CRISPR/Cas9 mediated modification had occurred. Since protein translation from mRNA transcripts occurs in triplet codons, single base deletions or insertions cause mutations in the reading frame, resulting in altered amino acid sequence and subsequently alterations in the construction of the mature protein such as differences in tertiary interactions. Although indels typically manifest in alterations of less than 20 base pairs (van Overbeek *et al*, 2016), rare occurrences of indels hundreds of base pairs in length and resulting significant disruption of the target gene have also been observed (Kosicki *et al*, 2018).

In order to further characterise P2X7 knockout of clone-14 cells, as well as associated receptor expression levels, total isolated RNA was surveyed for expression of purinergic receptor transcripts in parental BV-2 and Clone-14 cells (Table 3.5).  $\beta$ -actin was used as a loading control housekeeping gene for comparison between BV-2 and lone-14 cDNA, and demonstrated high stability between technical repeats and

between cell types. Transcripts of all surveyed purinergic receptors were detected within 40 amplification cycles for both cell types (Table 3.5), with the sole exception of the A3 adenosine receptor subtype. Relative expression, based on average cycle appearance above  $\beta$ -actin ( $\Delta$ CT) housekeeping expression, demonstrated high expression of transcripts for the receptor subtypes P2X4, P2X5 and P2Y1 in parental BV-2 cells. In contrast, several receptor subtypes demonstrated relatively low transcript expression including P2X2, P2Y4, P2Y14 and the Adenosine A1 receptor.

The detection of transcripts for nearly all purinergic receptors in BV-2 cells is unsurprising given the multitude of studies demonstrating expression of functional purinergic receptors in microglia. For primary microglia, P2Y and P2X expression has been shown (Visentin *et al*, 2006; Inoue, 2006; Koizumi *et al*, 2007; Light *et al*, 2006; Crain *et al*, 2007), although it has been identified that P2Y mRNA expression is predominantly of subtypes P2Y2, P2Y6, P2Y12, P2Y13 and P2Y14 (Hidetoshi *et al*, 2012), and following development, P2X subtype expression is predominately of the P2X4 and P2X7 subtypes in primary rat microglia (Xiang & Burnstock, 2005), plus P2X1 in isolated human brain stem microglia (Smith *et al*, 2013). Likewise, immortalised microglia (N9 cell line) have previously been shown via RT-PCR and Western blotting to express six P2X and seven P2Y receptor subtypes (Bianco *et al*, 2006). The presence of mRNA transcripts of all four adenosine receptor subtypes have previously been demonstrated in isolated primary rat microglia (Bianco *et al*, 2005), although the absence of the A3 receptor subtype in our BV-2 cells could be explained by the species difference. Additionally, detection of the mRNA transcript for the adenosine receptor A3 subtype was previously detected by RT-PCR of N13 and BV-2 immortalised microglia cDNA (Hammarberg *et al*, 2003), although transcript for the A1 subtype was not detected in this study, which is in contradiction with these findings as A1 mRNA transcript was detected. Furthermore, it was not stated

how many PCR amplification cycles were performed in this study, raising the possibility that it was fewer than the required for detection.

In comparison to parental BV-2 cells, the expression levels of purinergic receptor transcripts in clone-14 microglia demonstrated mild variation, albeit with one instances of significant downregulation for P2Y12 (Table 3.5). Expression of purinergic receptors in microglia is highly plastic (Crain *et al*, 2009). It is perhaps therefore unsurprising that small changes in receptor expression were detected between BV-2 and clone-14 cells. It is also important to note, that mRNA analysis doesn't provide information on expression of receptors at the protein level, as exemplified by P2X7. mRNA transcript levels for P2X7 were not significantly different between BV-2 and clone-14 cells (Table 3.5), despite significant alterations to the genomic DNA sequence (Figure 3.13) and a corresponding absence of cell surface receptor protein expression (Figure 3.14). Furthermore, previous studies have also demonstrated no change in target mRNA transcript expression, despite the absence of functioning target protein (Dabrowska *et al*, 2018), which helps validate the lack of reduction in expression of P2X7R transcript in clone-14 cells.

In microglia, the trafficking and expression of purinergic receptors at the cell surface, specifically P2X4 and P2X7, is a highly dynamic process (Boumechache *et al*, 2009). Additionally, evidence exists that some purinergic receptors, such as P2X4 are stored within intracellular lysosomes under resting conditions (Qureshi *et al*, 2007; Boumechache *et al*, 2009). In order to determine whether CRISPR/Cas9 mediated gene editing had altered trafficking of the P2X7 receptor and cell surface expression, instead of producing a knockout, total cellular P2X7 protein content of BV-2 and Clone-14 cells, was assessed by Western blot analysis. Alongside BV-2 and Clone-14 lysates, J774 macrophage cell lysate was utilised as a positive control (Coutinho-Silva *et al*, 2005). Western blot analysis

demonstrated an immunoreactive band for P2X7 protein in parental BV-2 cells and the positive control J774 macrophage cell line (Figure 3.14). In contrast, no immunoreactive band was detected in Clone-14 cells. Stripped and re-probed blots for loading control protein  $\beta$ -actin displayed equally sized immunoreactive bands in all cell types tested (Figure 3.14), demonstrating even protein loading in all wells. The lack of anti-P2X7 immunoreactivity in total cellular lysate contents of Clone-14 cells suggests either a complete abrogation of P2X7 protein synthesis, or the production of a severely modified P2X7 protein structure as the result of a P2X7 mRNA transcript that escapes NMD. This modified protein structure disrupted antibody binding epitope, which is subsequently no longer recognised by the Hano43 antibody.

The combination of data presented in this chapter has shown the successful knockout of P2X7 protein expression in clone-14 microglia following CRISPR/Cas9 mediated gene editing. The generation of a P2X7 knockout cell line can be now in further experiments to investigate the role of P2X7R in BV-2 microglia.

## Chapter 4

P2X7, along with P2X4 and P2Y2 receptors mediate ATP stimulated intracellular  $\text{Ca}^{2+}$  responses in resting microglia

### 4.1 Introduction

Due to its ubiquitous nature, ATP release can be invoked from nearly all mammalian cells, which can occur as a response to a wide variety of stimuli. ATP and similarly related purinergic/nucleotide signalling molecules have been demonstrated to be released under a variety of different conditions, including mechanical stimulation (Patel *et al*, 2005), hydrostatic pressure (Ferguson *et al*, 1997) and inflammatory conditions (La-Sala *et al*, 2003). Key findings have also implicated ATP release in the pathogenesis of glaucoma. For example, levels of ATP are elevated in the anterior chamber of patients with PCAG, which were correlated to the levels of increased pressure (Zhang *et al*, 2007; Li *et al*, 2011). Experimental models of glaucoma have also reproduced similar results, with increased hydrostatic pressure of bovine eye cups causing an increase in ATP concentration in the vitreal compartment adjacent to the retina (Reigada *et al*, 2008), as well as a coinciding upregulation of the nucleotide transporter VNUT in the glaucomatous DBA/2J mouse model (Perez de Lara *et al*, 2015).

As resident immune cells of the retina, microglia are sensitive to modulation by purinergic signalling molecules and are endowed with various purinergic receptors (Table 3.5) for the detection of such molecules. The subsequent modulation of intracellular calcium ( $[\text{Ca}^{2+}]_i$ ) as a secondary signalling system following purinergic receptor stimulation occurs as direct plasmalemmal entry following P2X receptor activation or as mobilisation of intracellular stores from  $\text{G}_q$

coupled P2Y receptor mediated activation (James & Butt, 2002). Changes in  $[Ca^{2+}]_i$  are important to various microglial functions, including chemotaxis (Ohsawa *et al*, 2007), process extension, de-ramification, cytokine release and phagocytosis (Mizoguchi & Monji, 2017). As such, measuring  $[Ca^{2+}]_i$  as a marker for purinergic receptor activation in microglia and similar cell types has been utilised historically (Walz *et al*, 1993), and extensively since.

The aims of this chapter are to characterise  $[Ca^{2+}]_i$  responses in BV-2 microglia, following stimulation with various endogenous purinergic signalling ligands, in particular with regards to the P2X7R. Furthermore, stimulation of P2X7 K/O Clone-14 cells generated in the previous chapter can provide both functional evidence for the successful knockout of the P2X7 receptor, as well as characterisation of this receptor's contributions to purinergic  $Ca^{2+}$  signalling.

## 4.2 Results

### 4.2.1 ATP mediated Ca<sup>2+</sup> responses in BV-2 microglia

In order to explore the activation of BV-2 microglia in response to the endogenous purinergic agonist ATP, intracellular Ca<sup>2+</sup> secondary messenger responses were explored. Fura-2 acetoxymethyl loaded BV-2 cells were stimulated with a wide range of ATP concentrations (100nM-3mM) and Ca<sup>2+</sup> responses were measured for 300 seconds (Figure 4.1).

ATP stimulation caused a dose dependant increase in intracellular Ca<sup>2+</sup> in BV-2 microglia, and manifested as a biphasic response (Figure 4.1 **A**). The initial phase response consisted of a rapid increase in Ca<sup>2+</sup> reaching a peak within 30 seconds of agonist application, then returning towards baseline levels. This initial peak phase was observed at ATP concentrations above 300nM and was concentration dependent, reaching a maximum response by 100μM (Figure 4.1 **B**). The calculated EC<sub>50</sub> was 1.9μM ATP. At higher ATP concentrations (≥300μM), an additional sustained Ca<sup>2+</sup> response was observed (Figure 4.1 **A**), characterised as a dose dependant increase in Ca<sup>2+</sup> concentration, following the initial peak. Sustained phase elevated Ca<sup>2+</sup> did not return to baseline levels over the course of the experiment (300s). Additionally, higher ATP concentrations led to a quicker onset of the sustained phase, with the two phases merging at 1mM ATP.

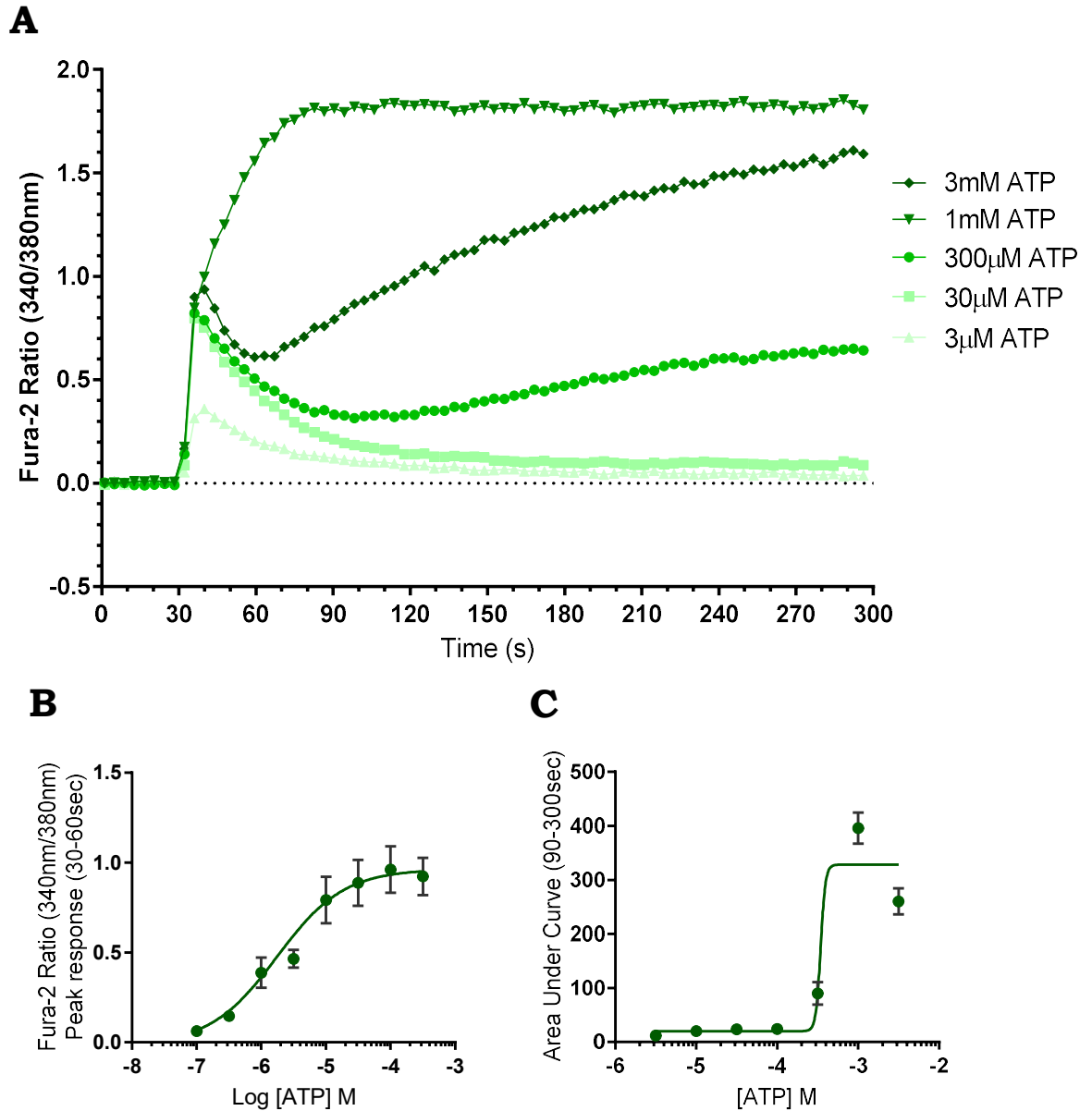


**Figure 4.1:** **A** Average intracellular  $\text{Ca}^{2+}$  concentration (340/380nm Fura-2 ratio) in BV-2 microglia following ATP stimulation (3 $\mu\text{M}$ -3mM) (n=3). Baseline fluorescence was recorded for 30 seconds prior to ATP stimulation and was subtracted from the measurements. **B & C** Concentration response relationship for ATP mediated  $\text{Ca}^{2+}$  increase in BV-2 microglia, measured as **B** Peak response (30-60s) and **C** Area under the curve (90-300s), represented as mean values  $\pm$  S.E.M (n=3). Data was fitted using non-linear regression in GraphPad Prism, with  $\text{EC}_{50}$  values determined as 1.9 $\mu\text{M}$  (**B**) and 344 $\mu\text{M}$  (**C**) respectively

The EC<sub>50</sub> of the sustained phase (determined as the area under the curve between 90-300 seconds) was determined as 344 $\mu$ M (Figure 4.1 C). The two phase Ca<sup>2+</sup> response to ATP could indicate either the contribution of two or more purinergic receptors, or multiple states of receptor activation. Interestingly, the maximal response of the sustained phase was not observed at the highest concentration tested (3mM), but at the second highest concentration (1mM), which could suggest a mechanism of fairly rapid receptor desensitization occurs to prevent excessive receptor stimulation.

#### **4.2.2 ATP mediated Ca<sup>2+</sup> responses in P2X7 K/O Clone-14 microglia**

In order to determine the functional characteristics of the P2X7 receptor in ATP mediated intracellular Ca<sup>2+</sup> responses, intracellular Ca<sup>2+</sup> levels were also measured in P2X7 K/O Clone-14 microglia. Clone-14 microglia were Fura-2 loaded and stimulated with an identical range of ATP concentrations (100nM-3mM), with resulting Ca<sup>2+</sup> responses measured for 300 seconds (Figure 4.2).

In contrast to BV-2 microglia, Clone-14 cells displayed only a monophasic Ca<sup>2+</sup> response following ATP stimulation (Figure 4.2 **A**), consisting of the rapid initial peak only. The calculated EC<sub>50</sub> peak response (30-60 seconds) in clone 14 microglia was 4.1 $\mu$ M ATP (Figure 4.2 **B**), closely resembling the calculated EC<sub>50</sub> peak response in BV-2 microglia, suggesting the absence of P2X7R does not alter the initial peak phase response to ATP. The sustained phase of Ca<sup>2+</sup> increase observed in BV-2 cells (Figure 4.1 **A**) was completely absent in Clone-14 cells at all ATP concentrations tested, representing a significant reduction the in AUC (90-300 seconds) response (Figure 4.2.**C**).

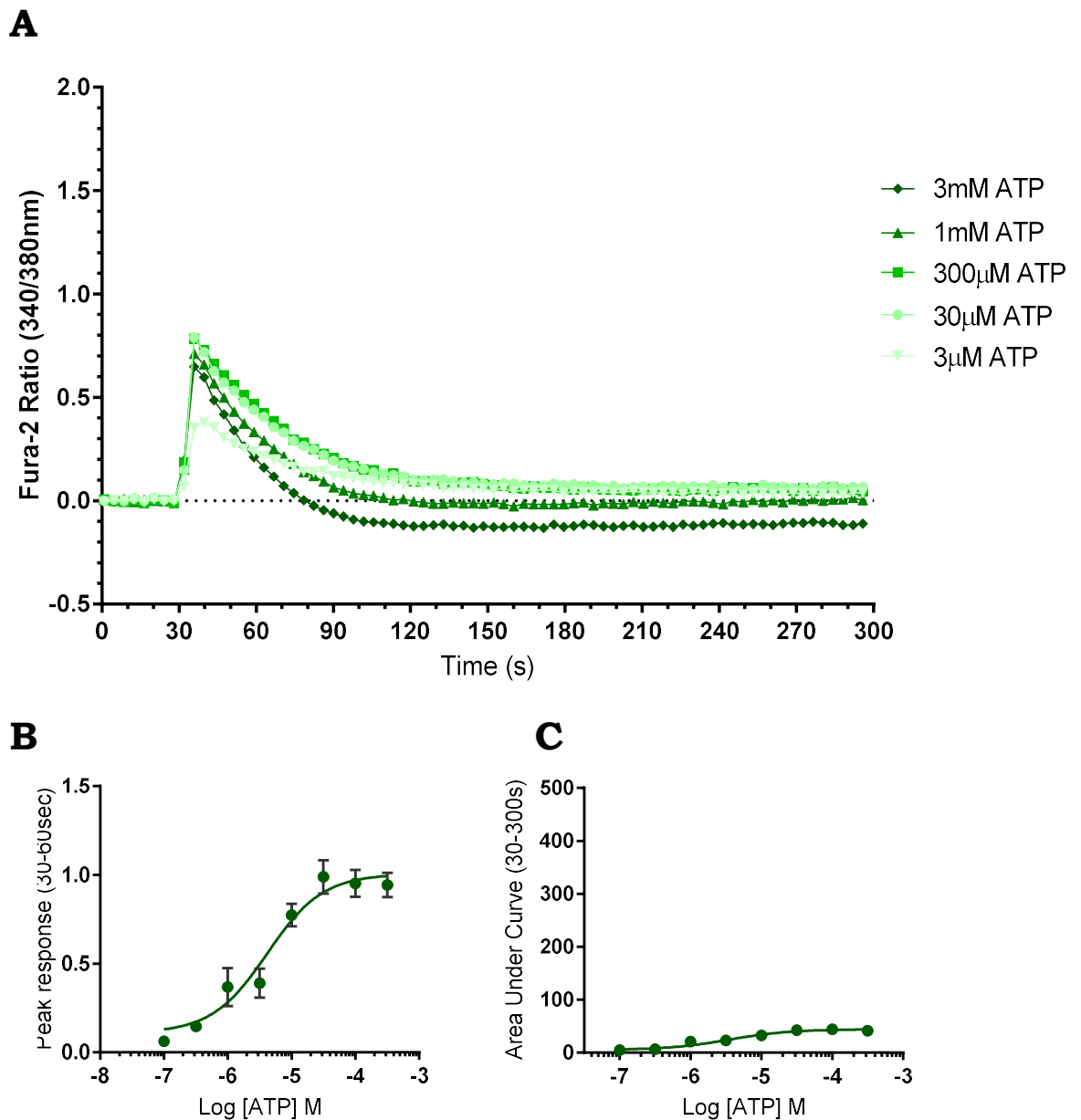


**Figure 4.2: A** Average intracellular  $\text{Ca}^{2+}$  concentration (340/380nm Fura-2 ratio) in P2X7 K/O clone-14 microglia following ATP stimulation (3µM-3mM) (n=3). Baseline fluorescence was recorded for 30 seconds prior to ATP stimulation and was subtracted from the measurements. **B & C** Concentration response relationship for ATP mediated  $\text{Ca}^{2+}$  increase in P2X7 K/O clone-14 microglia, measured as **B** Peak response (30-60s) and **C** Area under the curve (90-300s), represented as mean values  $\pm$  S.E.M (n=3). Data was fitted using non-linear regression in GraphPad Prism, with  $\text{EC}_{50}$  values determined as 4.1µM (**B**) 3.5µM (**C**) respectively

### **4.2.3 AZ10606120 antagonism of ATP mediated Ca<sup>2+</sup> responses in BV-2 microglia**

As further evidence for the role of P2X7 in the sustained phase Ca<sup>2+</sup> response to high dose ATP stimulation, BV-2 microglia pre-treated with the potent P2X7 receptor antagonist AZ10606120 (0-10 $\mu$ M) for 30 minutes before being stimulated with a wide range of ATP concentrations (3 $\mu$ M-3mM), and resulting Ca<sup>2+</sup> responses measured for 300 seconds (Figure 4.3).

Each concentration of AZ10606120 (1, 3 & 10 $\mu$ M) demonstrated significant inhibition in the sustained phase Ca<sup>2+</sup> response to ATP stimulation of BV-2 cells (Figure 4.3). AZ10606120 had no significant effect on the initial peak Ca<sup>2+</sup> response at any concentration tested. The inhibition demonstrated with AZ10606120 further indicates a role for P2X7 in the sustained phase response, but not the initial phase.

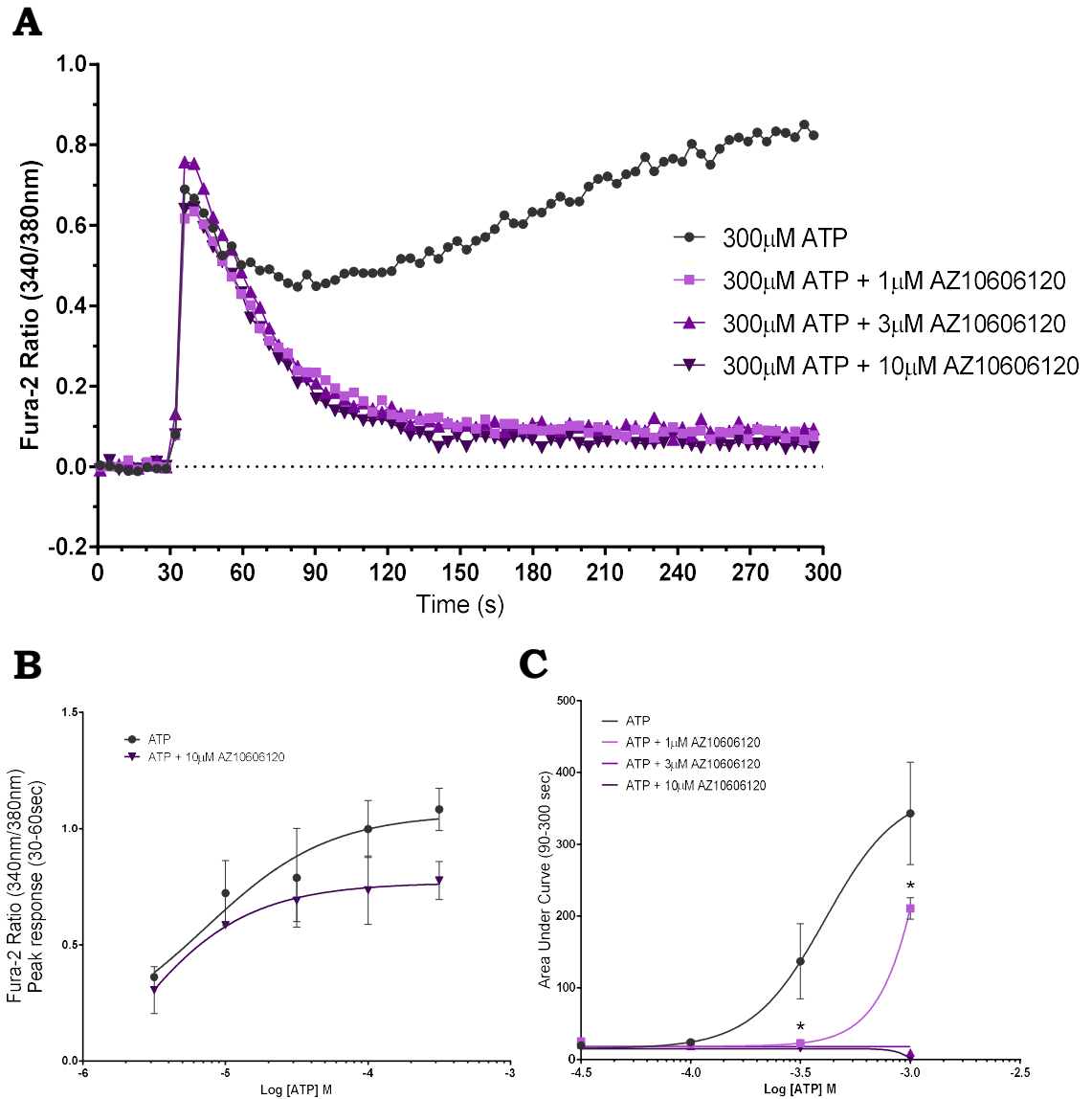


**Figure 4.3: A** Average intracellular  $\text{Ca}^{2+}$  concentration (340/380nm Fura-2 ratio) in BV-2 microglia following ATP stimulation (300µM) at 30 seconds in the presence of various concentrations (0-10µM) of P2X7 receptor antagonist AZ10606120. Mean values displayed (n=3). Baseline fluorescence was recorded for 30 seconds prior to ATP stimulation and was subtracted from the measurements. **B** Concentration response relationship for ATP mediated  $\text{Ca}^{2+}$  increase in BV-2 microglia, measured as area under the curve (90-300s) represented as mean values  $\pm$  S.E.M (n=3). **C** Concentration response relationship for ATP mediated  $\text{Ca}^{2+}$  increase in BV-2 microglia, measured as peak Fura-2 ratio (30-60s) represented as mean values  $\pm$  S.E.M (n=3). \* Indicates significance compared to the ATP control group using two-way ANOVA with Dunnett's post hoc test. Data was fitted using non-linear regression in GraphPad Prism

#### **4.2.4 BzATP mediated Ca<sup>2+</sup> responses in BV-2 microglia**

To further delineate the contribution of P2X7 receptor activation in BV-2 microglia [Ca<sup>2+</sup>]<sub>i</sub> responses, BV-2 cells were stimulated with the potent synthetic P2X7 agonist BzATP at a range of concentrations (300nM-300μM). The responses measured for 300 seconds (Figure 4.4).

Like ATP, BzATP stimulation of BV-2 cells demonstrated a dose dependent increase in intracellular Ca<sup>2+</sup> in BV-2 microglia (Figure 4.4 **A**). However, in contrast to ATP, BzATP stimulation lacked an initial rapid peak phase and produced only a sustained phase response, which manifested similarly to the sustained phase with ATP stimulation. Non-linear regression of AUC was performed, which determined the EC<sub>50</sub> for BzATP to be 64μM.

#### **4.2.5 BzATP mediated Ca<sup>2+</sup> responses in P2X7 K/O Clone-14 microglia**

The role of P2X7s role was further explored with BzATP in P2X7 K/O Clone-14 microglial cells. Clone-14 cells were stimulated with BzATP at a range of concentrations (300nM-300μM). The responses were measured for 300 seconds (Figure 4.5).

Unlike with BV-2 cells, BzATP stimulation of Clone-14 microglia failed to elicit a strong sustained phase of elevate [Ca<sup>2+</sup>]<sub>i</sub>, with only a minor increase observed at the highest concentration tested 300μM (Figure 4.5). The absence of P2X7 demonstrating a lack of BzATP efficacy in eliciting a sustained phase [Ca<sup>2+</sup>]<sub>i</sub> response indicates that P2X7 mediates the majority of this phase response.

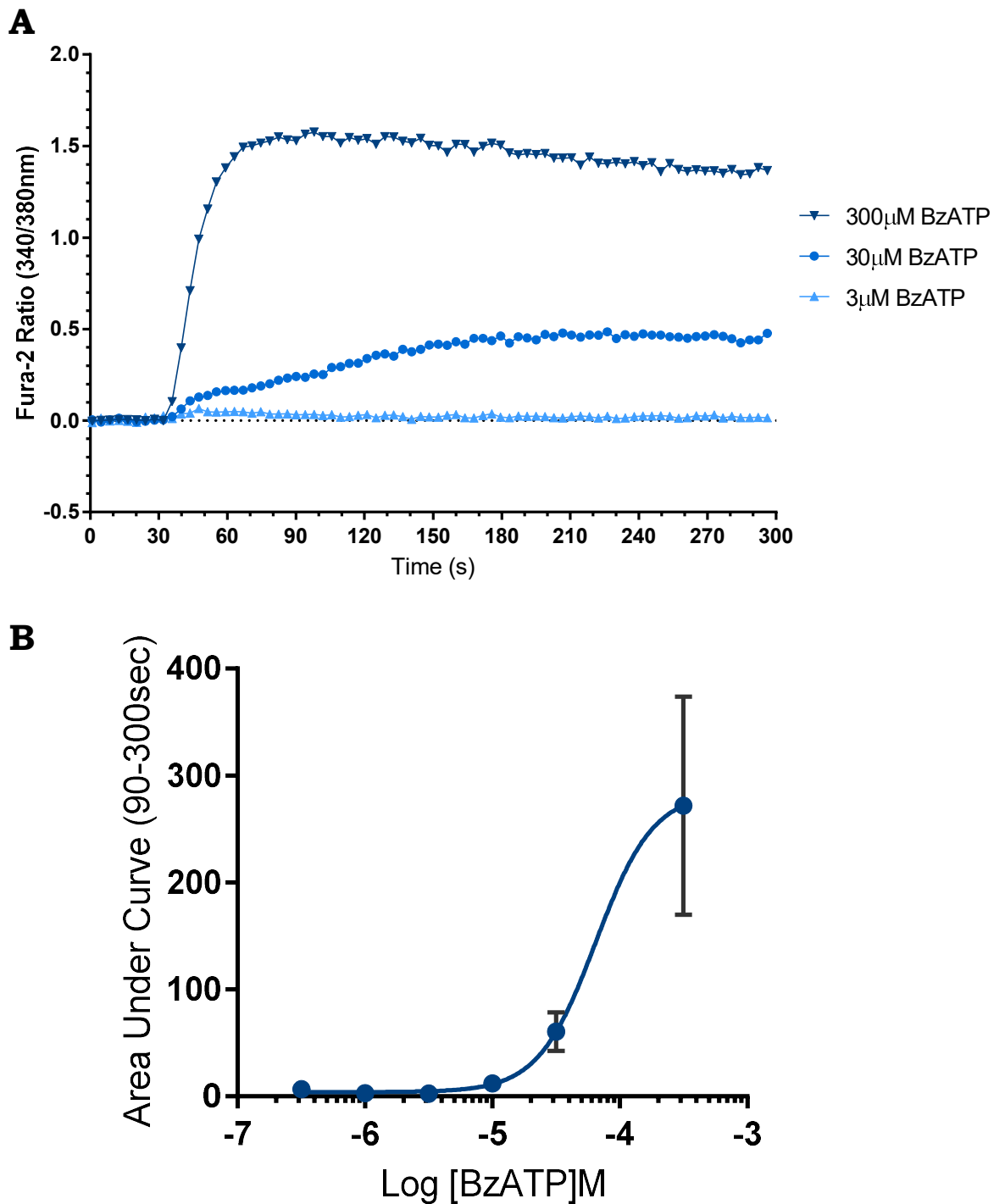


**Figure 4.4: A** Average intracellular  $\text{Ca}^{2+}$  concentration (340/380nm Fura-2 ratio) in BV-2 microglia following BzATP stimulation (300nM-300 $\mu$ M) (n=3). Baseline fluorescence was recorded for 30 seconds prior to agonist stimulation. **B** Concentration response relationship for BzATP mediated  $\text{Ca}^{2+}$  increase in BV-2 microglia, measured as area under the curve (30-300s), represented as mean values  $\pm$  S.E.M (n=3).

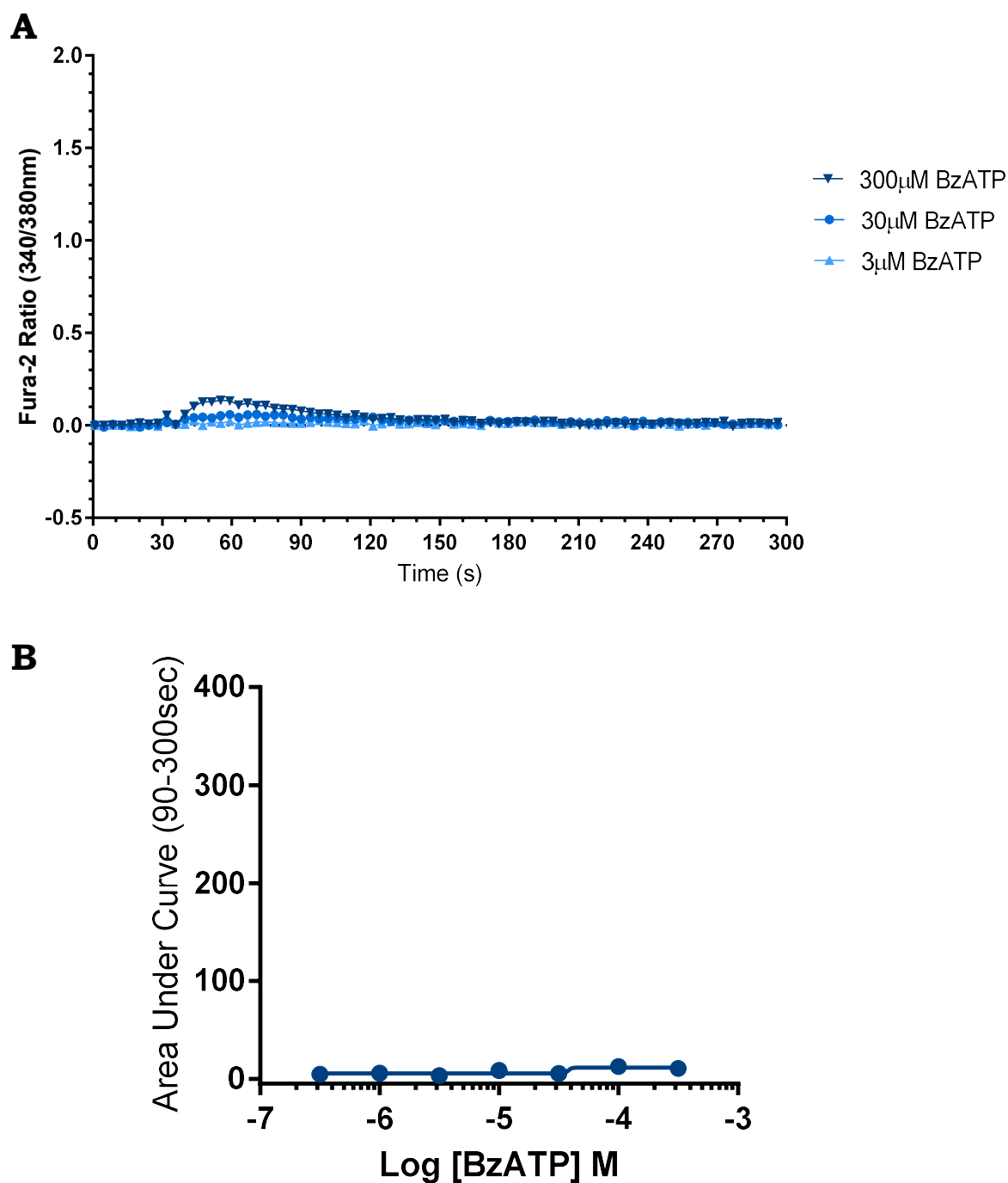


**Figure 4.5: A** Average intracellular  $\text{Ca}^{2+}$  concentration (340/380nm Fura-2 ratio) in P2X7 K/O clone-14 microglia following BzATP stimulation (300nM-300 $\mu$ M) (n=3). Baseline fluorescence was recorded for 30 seconds prior to agonist stimulation. **B** Concentration response relationship for BzATP mediated  $\text{Ca}^{2+}$  increase in P2X7 K/O clone-14 microglia, measured as area under the curve (30-300s), represented as mean values  $\pm$  S.E.M (n=3).

#### **4.2.6 AZ10606120 antagonism of BzATP mediated Ca<sup>2+</sup> responses in BV-2 microglia**

In a similar manner to the antagonism of ATP responses (Figure 4.3), AZ10606120 was utilised to investigate the role of the P2X7 receptor in BzATP mediated [Ca<sup>2+</sup>]<sub>i</sub> responses. BV-2 cells were stimulated as previously described (Figure 4.4) in the absence or presence of AZ10606120 (1-10µM) (Figure 4.6).

AZ10606120 demonstrated significant inhibition of 300µM BzATP mediated sustained phase responses at all concentrations tested (1, 3 & 10µM), although it did not produce any significant effect at any other BzATP concentrations explored. Responses in the presence of high concentration AZ10606120 were similar to BzATP mediated responses in P2X7 K/O Clone-14 cells (Figure 4.6).

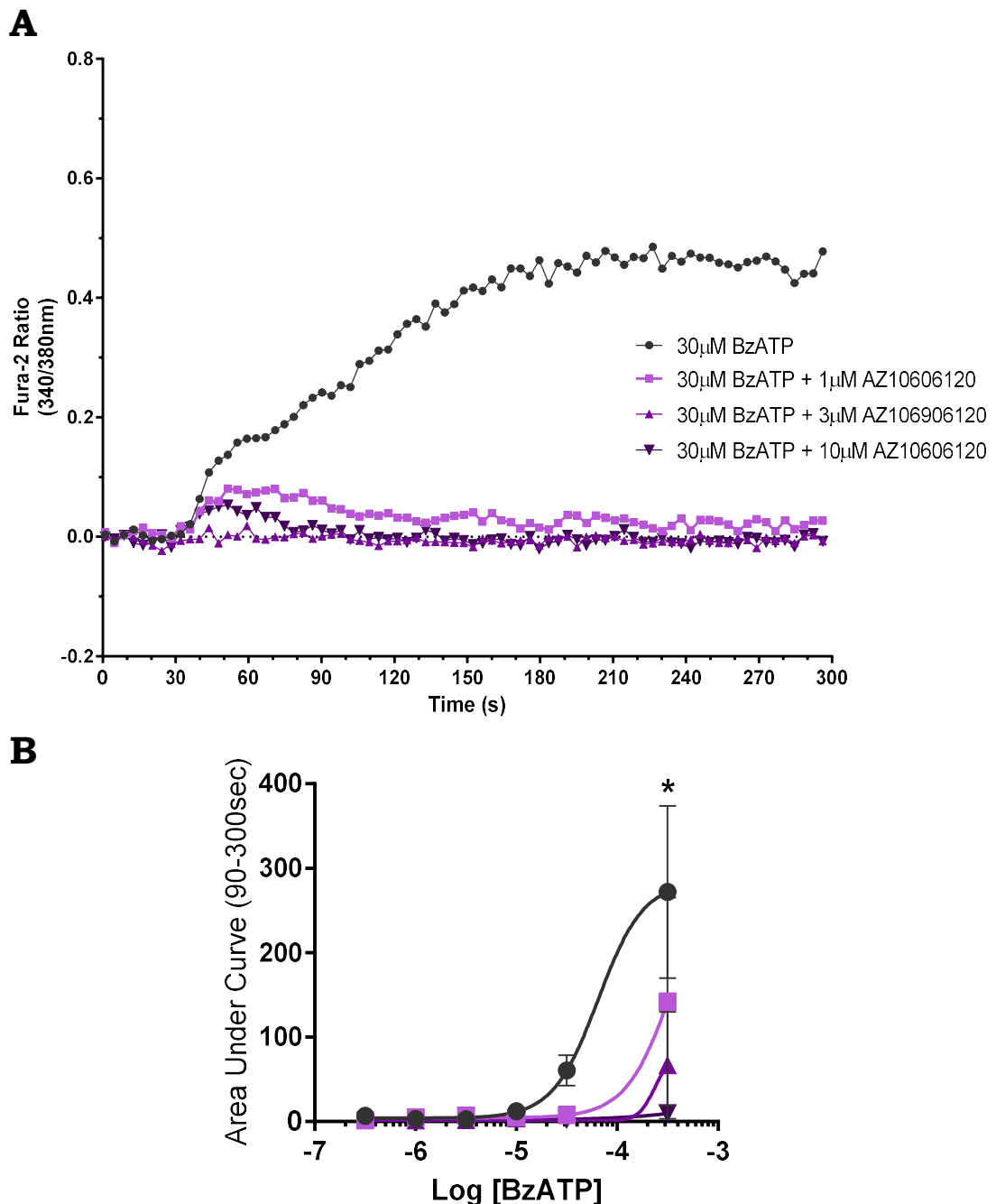


**Figure 4.6: A** Average intracellular  $\text{Ca}^{2+}$  concentration (340/380nm Fura-2 ratio) in BV-2 microglia following BzATP stimulation (30 $\mu$ M in the presence of various concentrations (0-10 $\mu$ M) of the P2X7 antagonist AZ10606120 (n=3). Baseline fluorescence was recorded for 30 seconds prior to ATP stimulation and was subtracted from the measurements. **B** Concentration response relationship for ATP mediated  $\text{Ca}^{2+}$  increase in BV-2 microglia, measured as area under the curve (90-300s), represented as mean values  $\pm$  S.E.M (n=3). \* Indicates significance compared to BzATP control group using two-way ANOVA with Dunnett's post hoc test. Data was fitted using non-linear regression in GraphPad Prism

#### **4.2.7 PSB12062 antagonism of ATP mediated Ca<sup>2+</sup> responses in P2X7 K/O Clone-14 microglia**

In order to explore the involvement of purinergic receptors in the initial ATP mediated Ca<sup>2+</sup> response in BV-2 cells, the potent P2X4 antagonist PSB12062 was utilised, in combination with P2X7<sup>-/-</sup> Clone-14 cells in order to negate the effects of P2X7 mediated contribution to the ATP response. Clone-14 cells were stimulated with a wide range of ATP concentrations (3μM-3mM) in the presence of PSB12062 (0-10μM) and Ca<sup>2+</sup> responses were measured for 300 seconds (Figure 4.7).

Antagonism with PSB12062 (1-10μM) demonstrated a significant inhibition of the initial phase (peak intracellular Ca<sup>2+</sup>) response compared to ATP stimulation alone (Figure 4.7), indicating that P2X4 activation plays a significant role in the initial peak phase response to ATP stimulation BV-2 microglia cells.

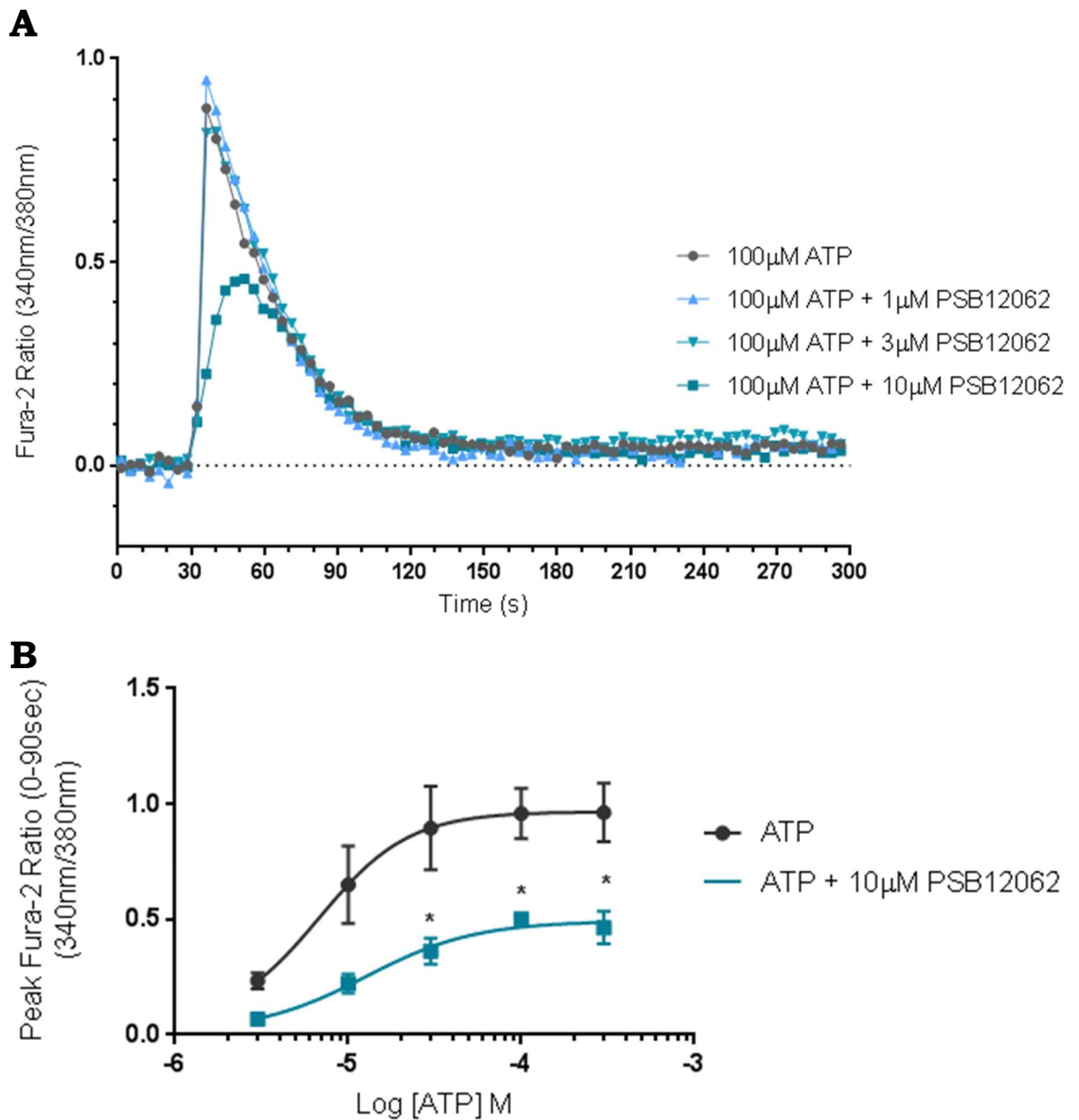


**Figure 4.7:** Average intracellular  $\text{Ca}^{2+}$  concentration (340/380nm Fura-2 ratio) in P2X7 K/O Clone-14 microglia following 300µM ATP, in the presence of varying concentrations of P2X4 antagonist PSB12062 (0-10µM). Mean values displayed (n=3). Baseline fluorescence was recorded for 30 seconds prior to ATP stimulation and was subtracted from the measurements. **B** Peak  $\text{Ca}^{2+}$  response in P2X7 K/O Clone-14 responses following ATP stimulation in the absence and presence of PSB12062 (10µM). Data represented as mean values  $\pm$  S.E.M (n=3). \* indicates significance compared to control ATP response using one-way ANOVA with Dunnett's post hoc test ( $P < 0.05$ ). Data was fitted using non-linear regression.

#### **4.2.8 5-BDBD antagonism of ATP mediated Ca<sup>2+</sup> responses in P2X7 K/O Clone-14 microglia**

As further evidence for the role of P2X4 in the ATP-mediated Ca<sup>2+</sup> response of BV-2 cells, the competitive P2X4 antagonist 5-BDBD was utilised, once again using P2X7 K/O Clone-14 cells in order to negate the P2X7 mediated component of the ATP response. Clone-14 cells were stimulated with a wide range of ATP concentrations (3µM-3mM) in the presence 5-BDBD (0-10µM) and Ca<sup>2+</sup> responses were measured for 300 seconds (Figure 4.8).

As with PSB12062, antagonism with 5-BDBD (10µM) demonstrated a significant inhibition (P<0.05) of the initial peak [Ca<sup>2+</sup>]<sub>i</sub> response compared to ATP stimulation alone (Figure 4.8). Significant inhibition with 5-BDBD (10µM) was observed at all ATP concentrations tested, in comparison to just the higher ATP concentrations observed with PSB12062. This suggests that P2X4 activation plays a significant role in the initial peak phase response to ATP stimulation of P2X7 K/O Clone-14 microglia.

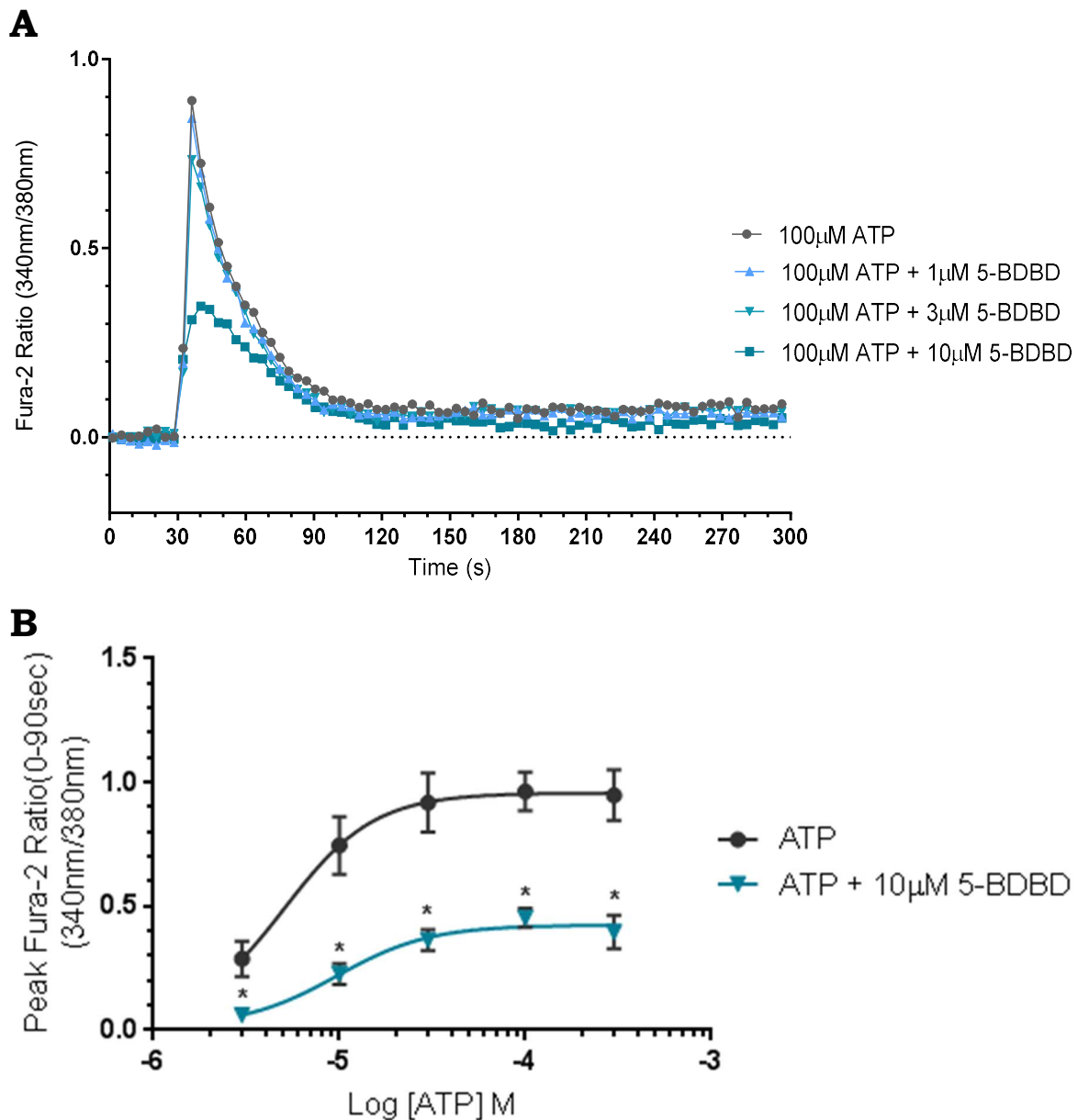


**Figure 4.8: A** Average intracellular  $\text{Ca}^{2+}$  concentration (340/380nm Fura-2 ratio) in P2X7 K/O Clone-14 microglia following 300µM ATP, in the presence of varying concentrations of P2X4 antagonist 5-BDBD (0-10µM). Mean values displayed (n=3). Baseline fluorescence was recorded for 30 seconds prior to ATP stimulation and was subtracted from the measurements. **B** Peak  $\text{Ca}^{2+}$  response in P2X7 K/O Clone-14 responses following ATP stimulation in the absence and presence of 5-BDBD (10µM). Data represented as mean values  $\pm$  S.E.M (n=3). \* indicates significance compared to control ATP response using one-way ANOVA with Dunnett's post hoc test ( $P < 0.05$ ). Data was fitted using non-linear regression.

#### 4.2.9 AR-C 118925XX antagonism of UTP mediated $\text{Ca}^{2+}$ responses in BV-2 microglia

To explore the potential contribution of the P2Y2 receptor to ATP mediated  $[\text{Ca}^{2+}]_i$  responses, stimulation with the more potent P2Y2 receptor endogenous agonist UTP was utilised, in combination with the competitive potent P2Y2 receptor antagonist AR-C118925XX. Fura-2 BV-2 cells were stimulated with a wide range of UTP concentrations ( $1\mu\text{M}$ - $1\text{mM}$ ) in the presence or absence of AR-C118925XX ( $1$ - $10\mu\text{M}$ ), or in isolation (Figure 4.9 & 4.10).

Stimulation with UTP produced a dose dependent single phase  $[\text{Ca}^{2+}]_i$  response (Figure 4.9), similar in shape to that observed with ATP stimulation. Antagonism with AR-C118925XX demonstrated a robust significant inhibition of the UTP-induced increase in  $[\text{Ca}^{2+}]_i$  (Figure 4.10).

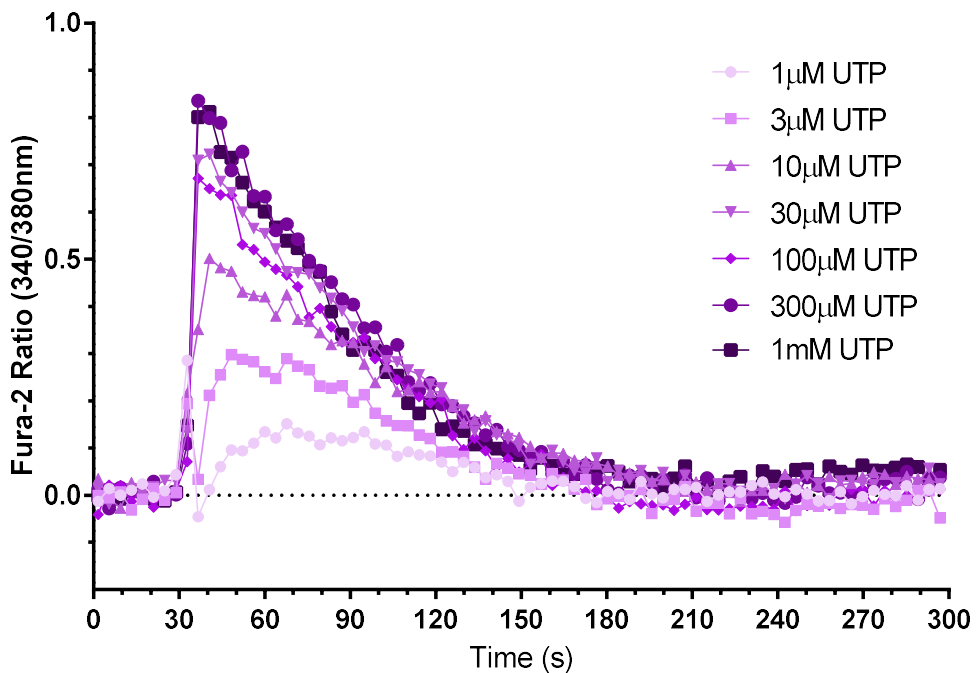


**Figure 4.9:** Average intracellular  $\text{Ca}^{2+}$  concentration (340/380nm Fura-2 ratio) in BV-2 microglia following UTP stimulation ( $1\mu\text{M}$ - $1\text{mM}$ ) ( $n=3$ ). Baseline fluorescence was recorded for 30 seconds prior to ATP stimulation and was subtracted from the measurements.

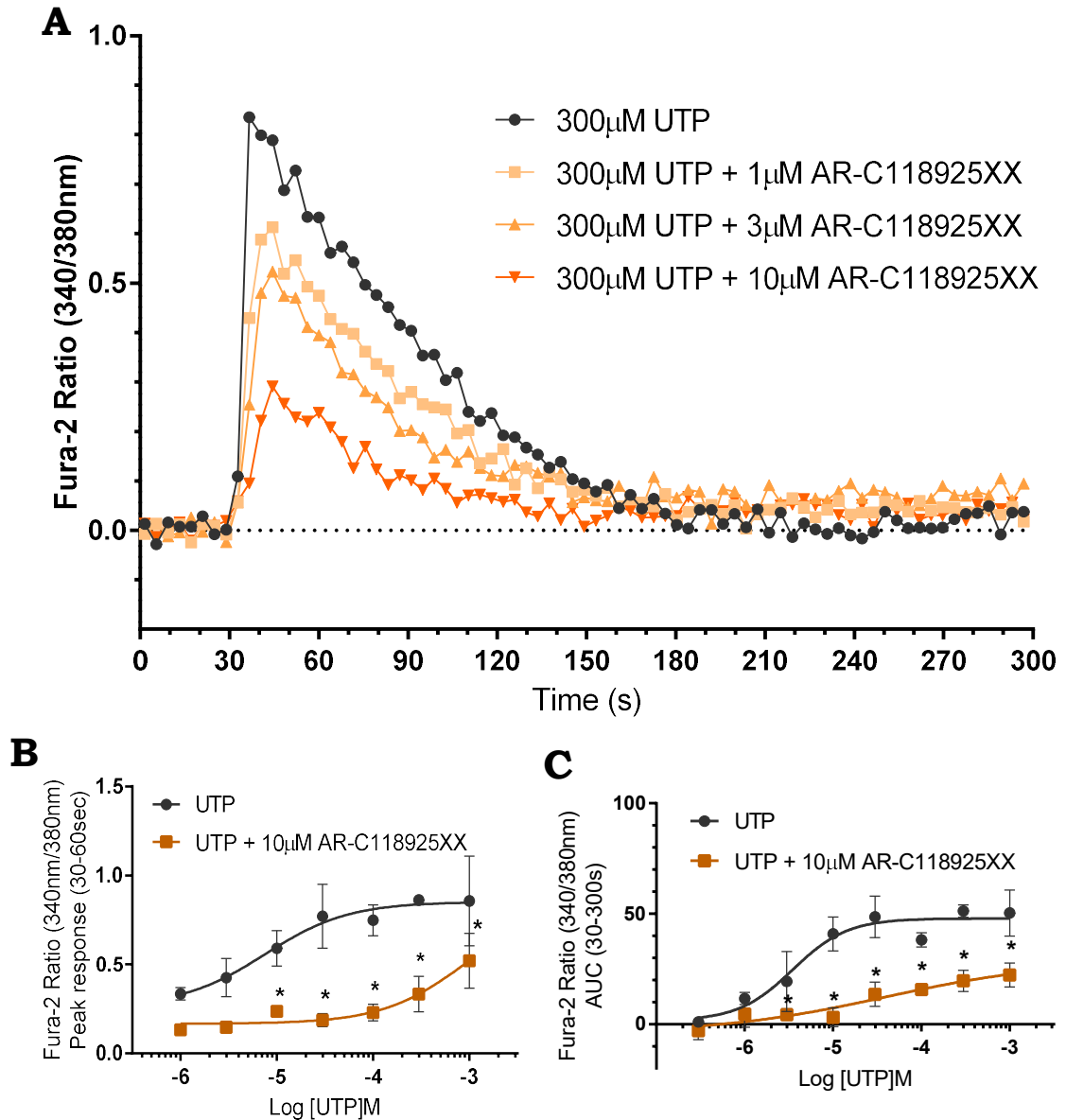


**Figure 4.10: A** Average intracellular  $\text{Ca}^{2+}$  concentration (340/380nm Fura-2 ratio) in BV-2 microglia following UTP stimulation (300 $\mu\text{M}$ ) at 30 seconds in the presence of various concentrations (0-10 $\mu\text{M}$ ) of P2Y<sub>2</sub> receptor antagonist AR-C118925XX. Mean values displayed (n=3). Baseline fluorescence was recorded for 30 seconds prior to ATP stimulation and was subtracted from the measurements. **B** Concentration response relationship for UTP mediated  $\text{Ca}^{2+}$  increase in BV-2 microglia, measured as area under the curve (90-300s) represented as mean values  $\pm$  S.E.M (n=3). **C** Concentration response relationship for ATP mediated  $\text{Ca}^{2+}$  increase in BV-2 microglia, measured as peak Fura-2 ratio (30-60s) represented as mean values  $\pm$  S.E.M (n=3). \* Indicates significance compared to the UTP control group using two-way ANOVA with Dunnett's post hoc test. Data was fitted using non-linear regression in GraphPad Prism

#### **4.2.10 ADP mediated Ca<sup>2+</sup> responses in BV-2 microglia**

To explore contribution of other purinergic agonists to [Ca<sup>2+</sup>]<sub>i</sub> signalling, ADP stimulation of BV-2 Cells was investigated by stimulating with a wide range of ADP concentrations (100nM-3mM) (Figure 4.11).

ADP mediated [Ca<sup>2+</sup>]<sub>i</sub> responses demonstrated a dose dependent increase in peak response, similar to the observed initial phase response with ATP stimulation (Figure 4.11). An additional sustained phase response was also observed, however in contrast to ATP, stimulation, this phase was only observed at the highest concentration tested (3mM).

#### **4.2.11 ADP mediated Ca<sup>2+</sup> responses in P2X7 K/O Clone-14 microglia**

Due to the presence of a characteristic P2X7 like sustained phase [Ca<sup>2+</sup>]<sub>i</sub> response following 3mM ADP stimulation, ADP stimulation was explored the in P2X7 K/O Clone-14 cells.

ADP responses in P2X7 K/O Clone-14 cells (Figure 4.12) mimicked those observed in parental BV-2 cells (Figure 4.11), with the exception of the absence of the sustained phase response observed at 3mM. The absence of the sustained phase response has subsequently highlighted the involvement of P2X7 in the mediation of this phase response.

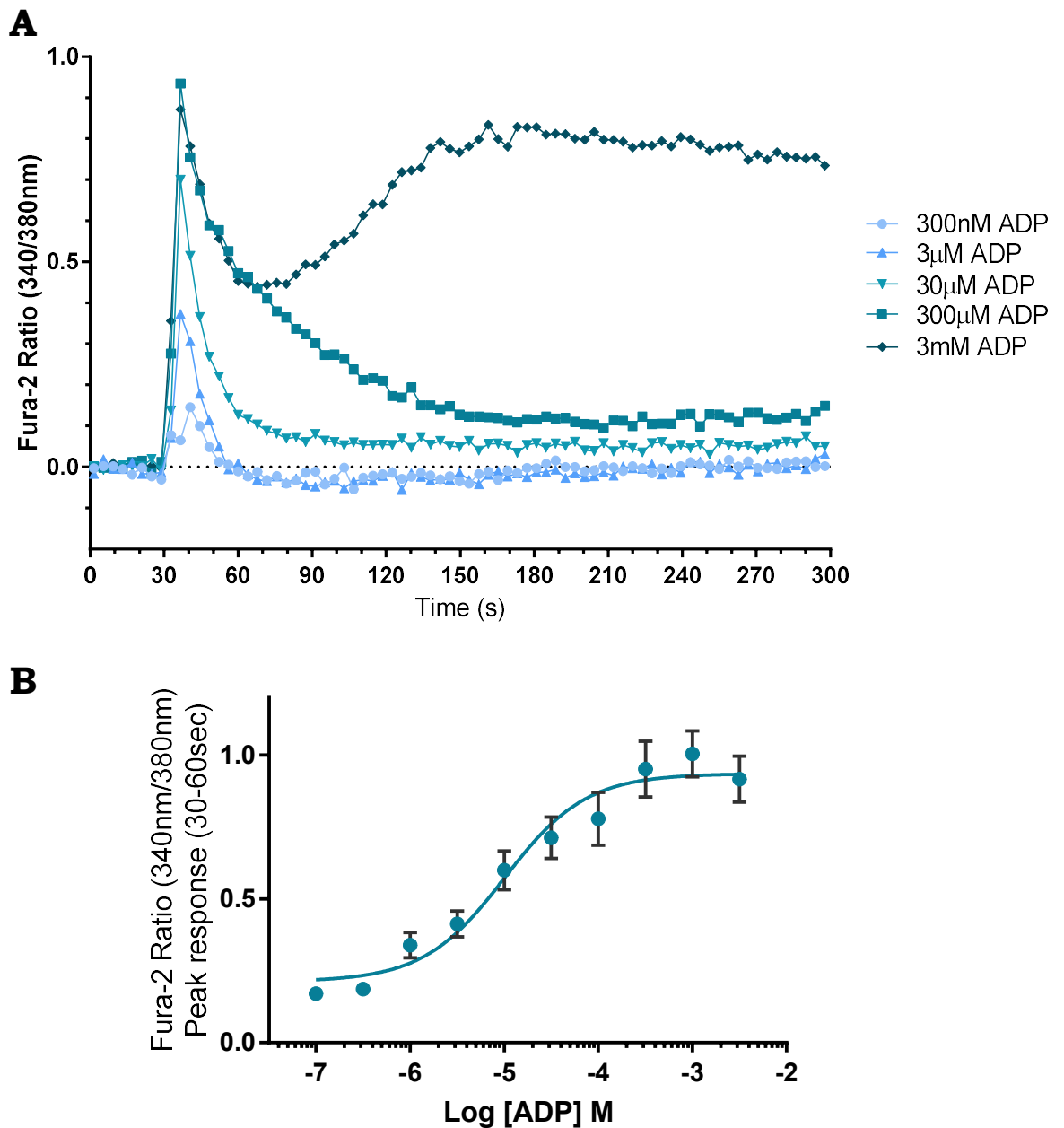


**Figure 4.11: A** Average intracellular  $\text{Ca}^{2+}$  concentration (340/380nm Fura-2 ratio) in BV-2 microglia following ADP stimulation (300nM-3mM) ( $n=3$ ). Baseline fluorescence was recorded for 30 seconds prior to agonist stimulation. **B** Concentration response relationship for ADP mediated  $\text{Ca}^{2+}$  increase in BV-2 microglia, measured as peak Fura-2 ratio (30-60s), represented as mean values  $\pm$  S.E.M ( $n=3$ ). Data was fitted using non-linear regression, with  $\text{EC}_{50}$  values determined as  $10.1\mu\text{M}$ .

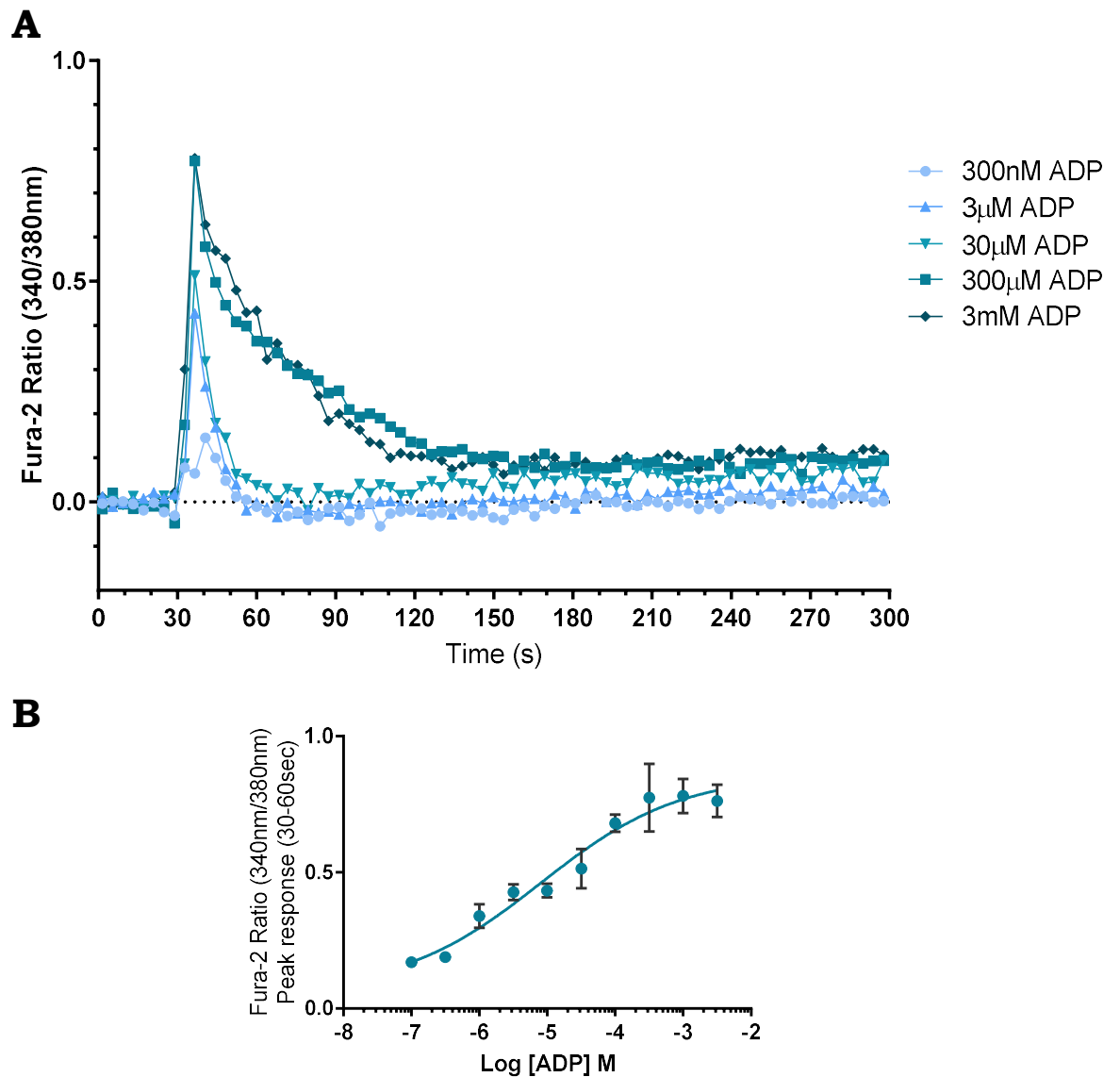


**Figure 4.12: A** Average intracellular  $\text{Ca}^{2+}$  concentration (340/380nm Fura-2 ratio) in BV-2 microglia following ADP stimulation (300nM-3mM) ( $n=3$ ). Baseline fluorescence was recorded for 30 seconds prior to agonist stimulation. **B** Concentration response relationship for ADP mediated  $\text{Ca}^{2+}$  increase in BV-2 microglia, measured as peak Fura-2 ratio (30-60s), represented as mean values  $\pm$  S.E.M ( $n=3$ ). Data was curve fit using non-linear regression, with  $\text{EC}_{50}$  values determined as  $10.1\mu\text{M}$ . Data was fitted using non-linear regression, with  $\text{EC}_{50}$  values determined as  $8.02\mu\text{M}$ .

#### **4.2.12 MRS2179 antagonism of ADP mediated Ca<sup>2+</sup> responses in BV-2 microglia**

Like ATP, ADP is a promiscuous ligand with affinity for multiple P2 receptor subtypes. The P2Y1 receptor antagonist MRS2179 was used to probe P2Y1 receptor contribution (Figure 4.13).

Antagonism, with MRS2179 (10 $\mu$ M) did not produce significant inhibition of ADP mediated [Ca<sup>2+</sup>]<sub>i</sub> responses at any concentration explored, suggesting P2Y1 is not involved in ADP mediated [Ca<sup>2+</sup>]<sub>i</sub> of BV-2 microglia.

#### **4.2.13 MRS2578 antagonism of ADP mediated Ca<sup>2+</sup> responses in BV-2 microglia**

To further probe the role of purinergic receptor contribution to the ADP mediated [Ca<sup>2+</sup>]<sub>i</sub> response, the potent P2Y6 receptor antagonist MRS2578 was utilised. (Figure 4.14).

Antagonism with MRS2578 (10 $\mu$ M) demonstrated a robust and significant inhibitive effect on ADP mediated [Ca<sup>2+</sup>]<sub>i</sub> responses, with a dose dependent antagonist effect observed. Reduction in peak fluorescent responses was observed at concentrations of 10 $\mu$ M ADP and above, suggesting mediation from P2Y6.

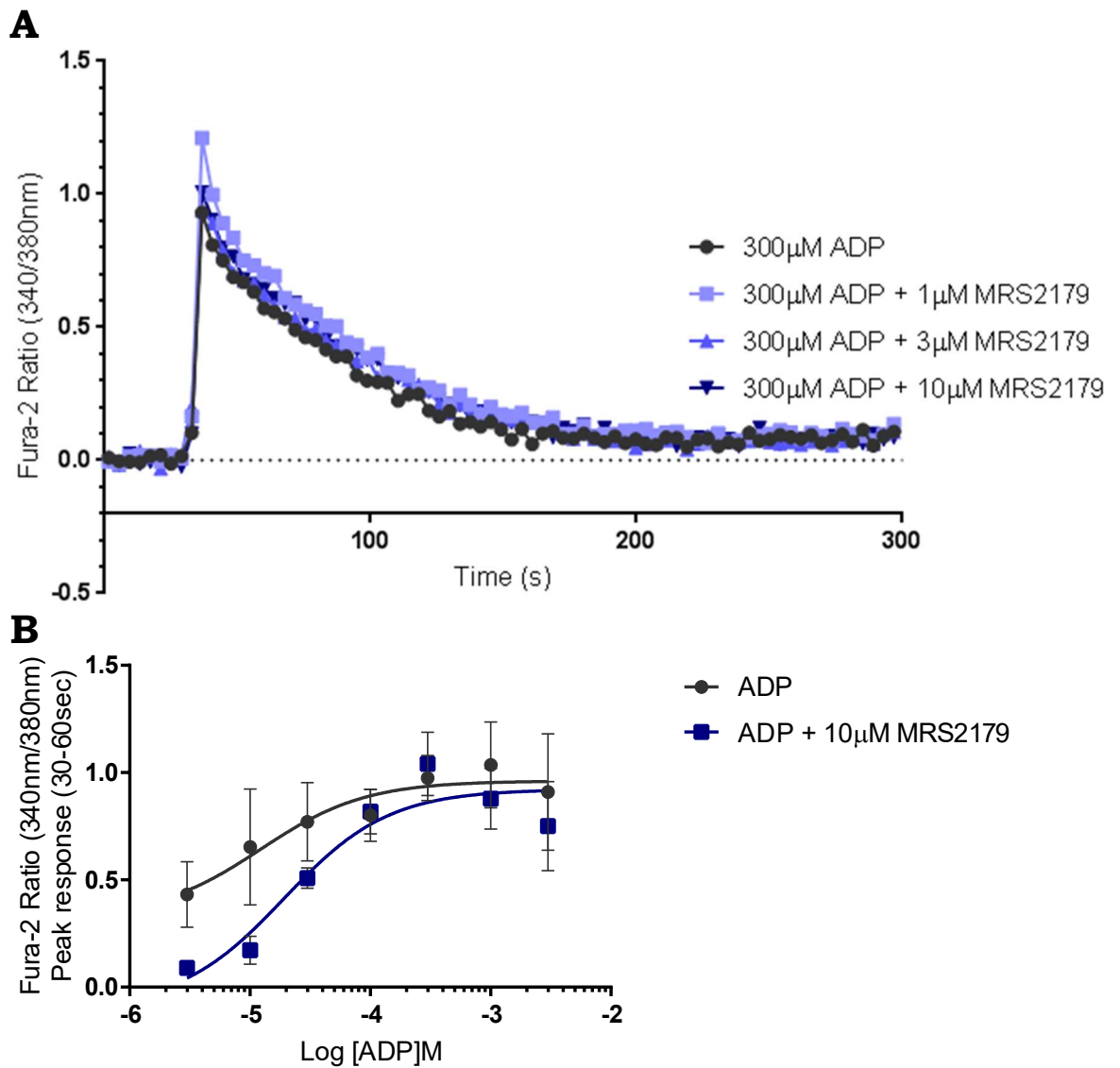


**Figure 4.13: A** Average intracellular  $\text{Ca}^{2+}$  concentration (340/380nm Fura-2 ratio) in BV-2 microglia following 300µM ADP, in the presence of varying concentrations of P2Y1 antagonist MRS2179 (0-10µM). Mean values displayed (n=3). Baseline fluorescence was recorded for 30 seconds prior to ATP stimulation and was subtracted from the measurements. **B** Peak fura-2 ratio quantification of Fura-2AM  $\text{Ca}^{2+}$  BV-2 responses following ADP stimulation in the absence and presence of MRS2179 (10µM). Data represented as mean values  $\pm$  S.E.M (n=3). \* indicates significance compared to control ADP response using one-way ANOVA with Dunnett's post hoc test ( $P < 0.05$ ). Data was fitted using non-linear regression.

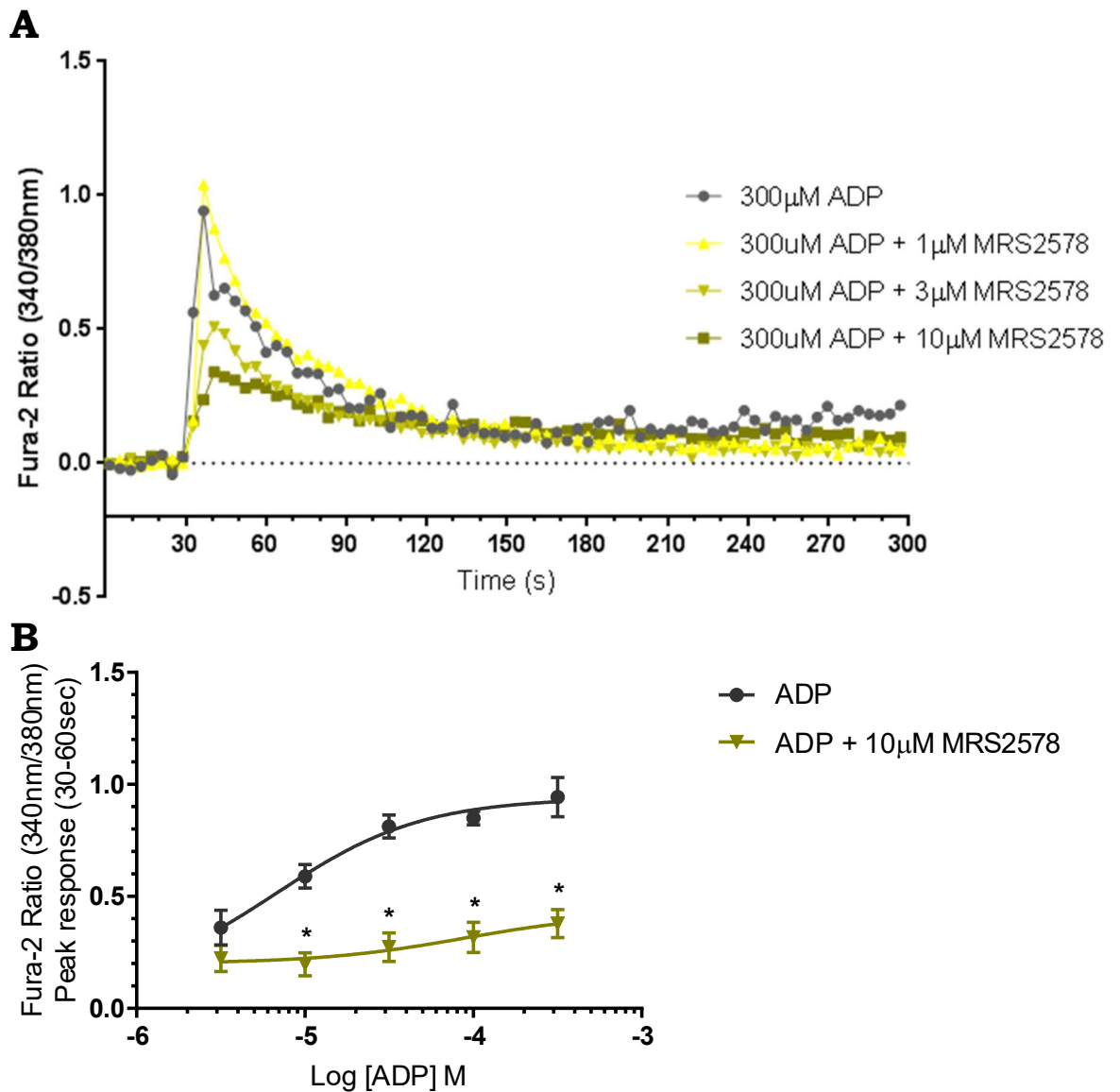


**Figure 4.14: A** Average intracellular  $\text{Ca}^{2+}$  concentration (340/380nm Fura-2 ratio) in BV-2 microglia following 300µM ADP, in the presence of varying concentrations of P2Y6 antagonist MRS2578 (0-10µM). Mean values displayed (n=3). Baseline fluorescence was recorded for 30 seconds prior to ATP stimulation and was subtracted from the measurements. **B** Peak fura-2 ratio quantification of Fura-2AM  $\text{Ca}^{2+}$  BV-2 responses following ADP stimulation in the absence and presence of MRS2578 (10µM). Data represented as mean values  $\pm$  S.E.M (n=3). \* indicates significance compared to control ADP response using one-way ANOVA with Dunnett's post hoc test ( $P < 0.05$ ). Data was fitted using non-linear regression.

#### **4.2.14 PSB0739 antagonism of ADP mediated Ca<sup>2+</sup> responses in BV-2 microglia**

As residual ADP mediated [Ca<sup>2+</sup>]<sub>i</sub> signalling was present with the highest concentration of P2Y<sub>6</sub> antagonism, further delineation of other purinergic receptor contributions was explored with the potent P2Y<sub>12</sub> receptor antagonist PSB0739. PSB0739 was selected over other commercially available P2Y<sub>12</sub> receptor antagonists, as it is bioactive without enzymatic conversion in contrast to other commonly used antagonists such as tricagrelor. Fura-2 acetoxymethyl loaded BV-2 microglial cells were stimulated with a wide range of ADP concentrations (3μM-3mM) in the presence PSB0739 (0-10μM) and [Ca<sup>2+</sup>]<sub>i</sub> responses were measured for 300 seconds (Figure 4.15).

Antagonism with PSB0739 (10μM) a moderately significant inhibition in AUC [Ca<sup>2+</sup>]<sub>i</sub> responses at the ADP stimulations concentrations (3-10μM), and unusually at 300μM (Figure 4.15). This significant difference was observed mainly in the decay phase of the peak, whereby return to baseline fluorescent levels occurred quicker in the presence of PSB0739 (10μM)

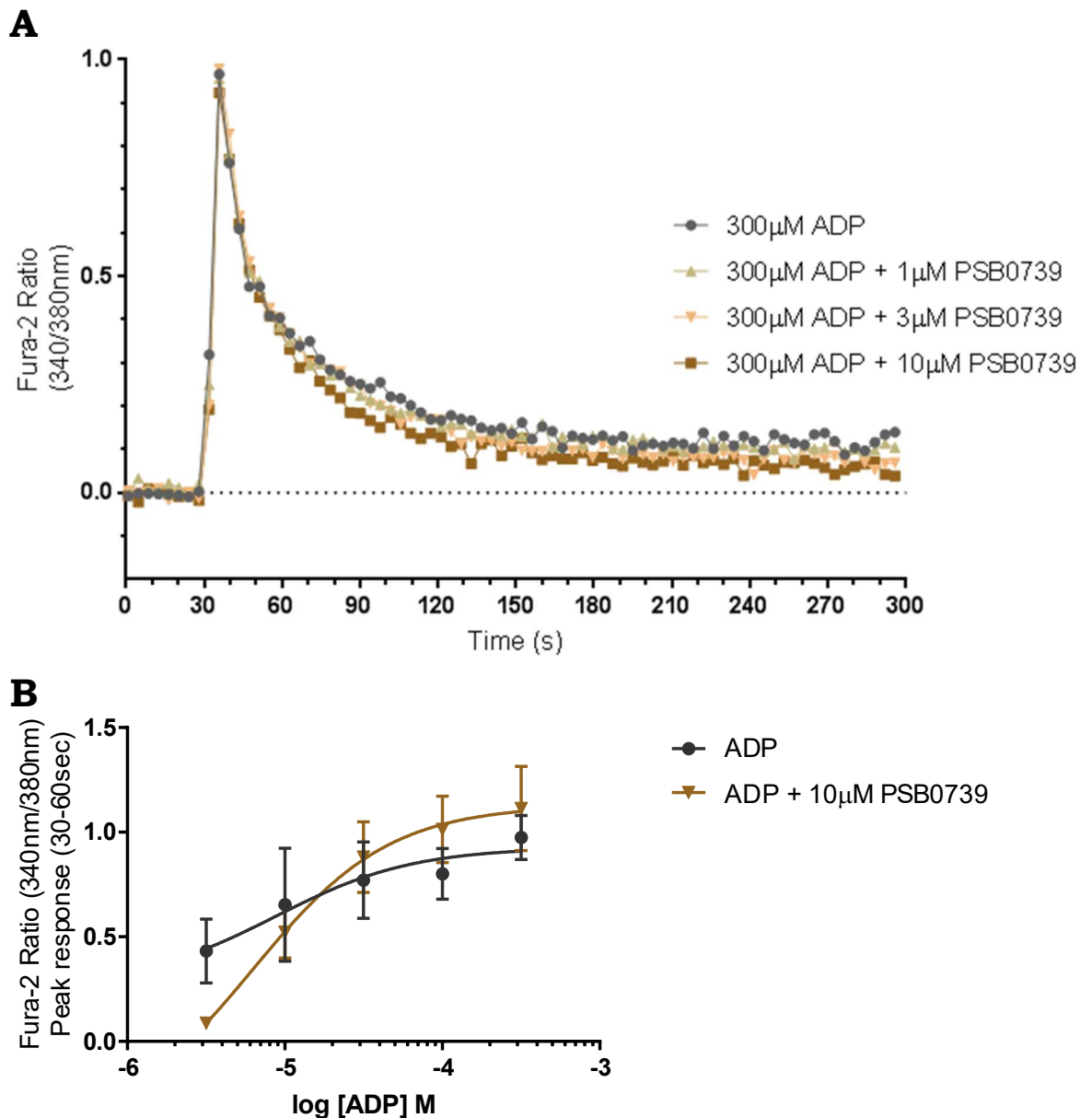


**Figure 4.15: A** Average intracellular  $\text{Ca}^{2+}$  concentration (340/380nm Fura-2 ratio) in BV-2 microglia following 300µM ADP, in the presence of varying concentrations of P2Y12 antagonist PSB0739 (0-10µM). Mean values displayed (n=3). Baseline fluorescence was recorded for 30 seconds prior to ATP stimulation and was subtracted from the measurements. **B** Peak fura-2 ratio quantification of Fura-2AM  $\text{Ca}^{2+}$  BV-2 responses following ADP stimulation in the absence and presence of PSB0739 (10µM). Data represented as mean values  $\pm$  S.E.M (n=3). \* indicates significance compared to control ADP response using one-way ANOVA with Dunnett's post hoc test ( $P < 0.05$ ). Data was fitted using non-linear regression.

### 4.3 Discussion

Initial experiments were conducted to establish a dose response relationship for the ubiquitous purinergic agonist ATP in BV-2 microglia. ATP (100nm-3mM) stimulation of BV-2 microglia displayed a complex and dynamic  $[Ca^{2+}]_i$  response (Figure 4.2.1 A), consisting of a dose dependent initial rapid transient rise at low and moderate ATP concentrations ( $\leq 300\mu M$ ), followed by a subsequent and distinct period of elevated  $[Ca^{2+}]_i$  at higher ATP concentrations ( $\geq 300\mu M$  ATP). The exhibited biphasic  $[Ca^{2+}]_i$  response following stimulation with high concentrations of ATP is in agreement with multiple previous fluorimetric  $Ca^{2+}$  studies, and has been demonstrated in multiple different cell types including primary rat astrocytes (Nobile *et al*, 2003; Balerini *et al*, 2005), and primary mouse microglia (Visentin *et al*, 1999; Shieh *et al*, 2014). Isolation of the initial peak phase response, by quantification of peak fluorescent responses within 30 seconds of agonist stimulation (Figure 4.1 B) determined an  $EC_{50}$  value of  $1.9\mu M$ . Of important note, with increasingly higher concentrations of ATP, the sustained phase  $[Ca^{2+}]_i$  response onset is shortened following stimulation, and it became difficult to separate from the peak phase response, which is exemplified by the 1mM ATP response. Additionally, the maximal sustained phase response elicited by ATP was at 1mM and not the highest concentrations (3mM) tested (Figure 4.2.1 A), which may suggest the rapid occurrence of receptor desensitization/internalization following overstimulation, an effect which has been shown to occur with purinergic receptors (Brinson & Harden, 2001).

Quantifying the sustained phase response to ATP (Figure 4.2.1 C) determined an  $EC_{50}$  value of  $344\mu M$  for ATP. This is substantially higher than reported  $EC_{50}$  values for all purinergic receptors, with the exception of P2X7, which is several orders of magnitude less sensitive to ATP than related P2X subtypes with a reported  $EC_{50}$  of 0.3-1mM at

physiological concentrations of  $Mg^{2+}$  and  $Ca^{2+}$  (Gever *et al*, 2006; Kaczmarek-Hajek *et al*, 2012).

In order to differentiate the contribution of different purinergic receptors in the ATP mediated  $[Ca^{2+}]_i$  response in BV-2 microglia, several pharmacological tools were subsequently used, in combination with the P2X7 deficient clone-14 cells described in the previous chapter. In contrast to BV-2 cells, ATP stimulation of Clone-14 cells demonstrated only an initial transient  $[Ca^{2+}]_i$  peak (Figure 4.2), with a complete absence of the characteristic sustained phase, even at the highest concentrations tested (3mM), confirming the role of P2X7 in the sustained phase of the response. Quantification of the initial phase of the  $[Ca^{2+}]_i$  response in Clone-14 cells demonstrated similarity with that of BV-2 cells, indicating P2X7 does not have a role on the initial response. It also further indicates that the use of CRISPR to knockout P2X7 didn't affect the functional expression of the purinergic receptors involved in mediation of the initial phase  $[Ca^{2+}]_i$  response.

To further clarify P2X7's role in  $[Ca^{2+}]_i$  signalling, stimulation with the potent P2X7 receptor synthetic agonist BzATP was performed in BV-2 (Figure 4.4) and Clone-14 cells (Figure 4.5). Due to its selective profile for P2X7 over related P2X subtypes, BzATP is widely used in experimental studies to investigate P2X7 responses. BzATP stimulation of BV-2 cells exhibited a dose dependent calcium response, manifested as an isolated sustained phase of elevated  $[Ca^{2+}]_i$  and an absence of the initial transient phase response observed with ATP. These findings mimic the BzATP induced  $[Ca^{2+}]_i$  response pattern demonstrated in previous calcium fluoroscopy studies, shown in primary rat (Parvathenani *et al*, 2003) and cultured mouse (Shieh *et al*, 2014) microglia, as well as rat brain astrocytes (Ballerini *et al*, 2005). In contrast to BV-2 cells, BzATP exhibited only a minimal residual sustained phase response in Clone-14 cells, indicating it is a good

pharmacological tool for P2X7 responses in these cells, with a minimal contribution for other purinergic receptors.

Confirmation of the role of P2X7 in the sustained phase  $[Ca^{2+}]_i$  response utilised the potent P2X7 antagonist AZ10606120, which has been validated in previous studies, specifically in blocking BzATP induced  $Ca^{2+}$  responses (Tozzi *et al*, 2018). Pre-treatment with AZ1060610 (1-10 $\mu$ M) caused significant inhibition of the sustained phase responses to both BzATP and elevated ATP stimulation (Figures 4.3 & 4.6), with no significant alteration to the ATP-mediated peak phase response. This demonstrates both further evidence for the role of P2X7 in the sustained phase response, and that AZ10606120 is a good pharmacological tool for investigating P2X7 receptor activity.

Following confirmation of P2X7 receptor mediation of the sustained phase  $[Ca^{2+}]_i$  response by ATP, a series of experiments were conducted in order to identify the involvement of additional purinergic receptor subtypes in the peak phase of the response. Due to its high expression in BV-2 cells (Raouf *et al*, 2007), and higher reported affinity for ATP (100 $\mu$ M range), the role of P2X4 on the initial phase  $[Ca^{2+}]_i$  response was subsequently explored. These experiments utilised selective P2X4 antagonists, in combination with P2X7 deficient Clone-14 cells in order to eliminate the potential effects of P2X7 activation. Both P2X4 antagonists tested, PSB12062 (10 $\mu$ M) and 5-BDBD (10 $\mu$ M) demonstrated significant reduction in the peak  $[Ca^{2+}]_i$  response (Figure 4.7 & 4.8), following ATP stimulation, indicating a role for P2X4 in mediation of the transient peak  $[Ca^{2+}]_i$  response. The presented P2X4 antagonist data corroborates previous findings in microglial cells. For example potentiation of ATP  $[Ca^{2+}]_i$  responses were demonstrated with the P2X4 positive allosteric modulator ivermectin, and were subsequently blocked with PSB12062 or 5-BDBD pre-treatment (Dhuna *et al*, 2018). P2X4 involvement in ATP mediated peak  $[Ca^{2+}]_i$  responses has also been demonstrated in cell models other than

microglia, for example, in THP-1 macrophages, antagonism with either 10 $\mu$ M PSB12062 or 5-BDBD was sufficient to significantly inhibit a 100 $\mu$ M ATP mediated transient  $[Ca^{2+}]_i$  response (Layhadi & Fountain, 2017).

UTP is a full agonist at mP2Y2, and equipotent with ATP (Tovell & Sanderson, 2008). UTP was therefore utilised in BV-2 microglia to explore the contributions of the P2Y2 receptor to  $[Ca^{2+}]_i$  responses, without contribution from P2X7 and P2X4 activation. UTP stimulation of BV-2 cells demonstrated a dose dependent increase in  $[Ca^{2+}]_i$  response (Figure 4.9), in a manner similar to that observed to the initial (peak) phase seen with ATP stimulation. Further exploration with the use of the competitive P2Y2 receptor antagonist demonstrated a significant inhibition of UTP-induced increase in  $[Ca^{2+}]_i$  (Figure 4.10). In previous studies, UTP stimulation has demonstrated a rapid rise in microglial  $[Ca^{2+}]_i$ , similar to that observed in this experiment, despite low mRNA expression of P2Y2 (Light *et al*, 2006). However, the receptor identity was not probed further with antagonism or receptor knockout cells. Although not in a microglial model, other systems expressing P2Y2, for example in human adipose derived mesenchymal stromal cells have been previously shown to signal via  $Ca^{2+}$  following UTP stimulation, with significant inhibition by AR-C118925XX (Ali *et al*, 2018). This UTP and AR-C118925XX data, in combination with antagonism of P2X4 mediated ATP responses suggests that a combination of both P2Y2 and P2X4 contribute to the initial  $[Ca^{2+}]_i$  response. Future investigations combining the use of P2Y2 and P2X4 receptor antagonists would help determine if additional purinergic receptors also contribute to the initial ATP-mediated  $[Ca^{2+}]_i$  response.

Although ATP is considered the primary endogenous signalling molecule of the purinergic system, a number of additional related endogenous agonists also have activity in control of physiological processes. In addition to ATP, a range of nucleotide signalling

molecules can be released into the extracellular milieu, including UDP, UTP and ADP. ADP is itself a product of the degradation of ATP, which is mediated by a family of ecto-nucleotidase enzymes, which are expressed by BV-2 microglia (Braun *et al*, 2000), as well as numerous other cells. The combination of these factors makes ADP a potential key signalling molecule in mediation of Ca<sup>2+</sup> responses.

ADP (100nM-3mM), demonstrated a dose dependent increase in [Ca<sup>2+</sup>]<sub>i</sub> manifesting as rapid peak followed by a decrease back to baseline, similar to that observed with low to moderate ATP stimulation. At low concentrations of ADP, elevated [Ca<sup>2+</sup>]<sub>i</sub> levels returned to baseline rapidly, however at higher concentrations (≥300μM), return to baseline was more gradual. 3mM ADP induced the sustained phase response that was similar to that seen with high concentrations of ATP, although ATP induced a sustained phase response at lower concentrations (≤300μM) (figure 4.11). The sustained phase response was absent in Clone-14 cells, suggesting a P2X7-mediated component, which could be through direct ADP stimulation of the receptor, ADP mediated ATP release, or possibly ATP contamination of ADP stocks. There has been no previous reports of activity of ADP at P2X7 receptors, suggesting ADP stimulation of BV-2 cells may induce ATP release as an autocrine signalling system, a mechanism which has been demonstrated previously in urothelial cells (Mansfield & Hughes, 2014). Most studies utilising ADP stimulation use far lower concentrations than 3mM. Unfortunately, without further investigation no definitive conclusion can be made about the mechanism responsible.

In order to determine the receptors which contribute to the ADP mediated [Ca<sup>2+</sup>]<sub>i</sub> response, a series of pharmacological antagonists with selectivity for specific receptors were utilised. Due to the detection of relatively high mRNA receptor transcript levels for P2Y1, in addition to its reported coupling to G<sub>q</sub>/G<sub>11</sub> and phospholipase C mediated [Ca<sup>2+</sup>]<sub>i</sub>

signalling, the role of P2Y1 contribution to ADP mediated  $[Ca^{2+}]_i$  responses was explored. The P2Y1 receptor selective antagonist MRS2179 was used, but did not demonstrate any significant inhibition of the ADP mediated  $[Ca^{2+}]_i$  responses in BV-2 microglia (Figure 4.13). This is in agreement with previous studies in microglia, whereby MRS2179 did not block  $[Ca^{2+}]_i$  responses (Light *et al*, 2006). In contrast, other cell systems have demonstrated a robust P2Y1 mediated ADP response, such as in astrocytes (Fumagalli *et al*, 2003) and *Vas vasorum* endothelial cells (Lyubchenko *et al*, 2010). In combination with these reported findings, these results suggest P2Y1 mediated  $[Ca^{2+}]_i$  responses are cell type specific. It is interesting that despite relatively high levels of mRNA expression (Table 3.5), no evidence of pharmacological activity was found in BV-2 cells.

As well as activating P2Y1, the role of P2Y6 was subsequently explored due to its moderate mRNA expression (Table 3.5), in addition to its reported role in phagocytosis (Koizumi *et al*, 2007), where ADP has been reported as a partial agonist. In contrast to MRS2179, the P2Y6 antagonist MRS2578 demonstrated a strong, significant inhibition of the ADP-mediated  $[Ca^{2+}]_i$  responses, at moderate and high concentrations ( $\geq 10\mu\text{M}$ ). The role of P2Y6 in microglial phagocytosis was first demonstrated following UDP stimulation, where it was shown that subsequent  $Ca^{2+}$  responses were blocked by MRS2578 in a manner similar to results found here. Later studies demonstrated similar MRS2578 antagonism of ADP responses in THP-1 monocytes (Micklewright *et al*, 2018) and human adipose derived mesenchymal stromal cells ( $10\mu\text{M}$  MRS2578) (Ali *et al*, 2018). The significant inhibition demonstrated with MRS2578 occurred generally at higher stimulation concentrations, which suggests that P2Y6 receptor activation may play a more significant role in microglial function in closer proximity to sites of cellular damage/purine nucleotide release, where concentrations are likely to be significantly higher.

The role of P2Y12 receptor in ADP mediated  $\text{Ca}^{2+}$  responses was also explored with the selective antagonist PSB0739. Although P2Y12 does couple predominately to via adenylate cyclase inhibition, and not PLC mediated  $\text{Ca}^{2+}$  signalling, P2Y12 mediated  $\text{Ca}^{2+}$  responses have previously been demonstrated in various cell types. Inhibition of ADP mediated  $[\text{Ca}^{2+}]_i$  responses with an alternative P2Y12 antagonist tricagrelor and siRNA P2Y12 knockdown has also been shown in THP-1 monocytes (Micklewright *et al*, 2018), and similarly the P2Y12 antagonist AR-C69931MX significantly blocked  $[\text{Ca}^{2+}]_i$  responses following P2Y12 agonist (2MESADP) stimulation in C6 transformed glial cells (Suplat *et al*, 2007). When challenged with the P2Y12 antagonist PSB0739, no significant inhibition of the ADP induced  $[\text{Ca}^{2+}]_i$  response was demonstrated. It should be noted that the major intracellular signalling pathway coupled with P2Y12 is via adenylate cyclase inhibition, and not  $\text{Ca}^{2+}$ . This does not however mean that P2Y12 doesn't have a role in purinergic  $\text{Ca}^{2+}$  signalling responses. PSB0739 antagonism strongly inhibited ADP-mediated  $\text{Ca}^{2+}$  signalling in polarized (M2) primary microglia, compared to non-polarized microglia (Moore *et al*, 2015). M2 polarization also significantly up-regulated P2Y12 expression, suggesting polarization may enhance the role of the receptor in  $[\text{Ca}^{2+}]_i$ .

The combination of the data presented in this chapter has highlighted the dynamic and complex role different purinergic nucleotide receptor agonists play in microglia and the subsequent changes in  $[\text{Ca}^{2+}]_i$  signalling, and has highlighted that various receptors including P2Y2, P2Y6, P2X4 and P2X7 have potential in mediating microglial function. It is possible that additional purinergic receptors also contribute to  $\text{Ca}^{2+}$  signalling in microglia, however several challenges still remain in investigating them further. For example, PCR analysis demonstrated high expression of P2X5 in BV-2 microglia, however there is a lack of selective pharmacological agonists and antagonists for investigating P2X5 receptor activity in a cell culture system. The potential for

alternate receptor subtype knockout BV-2 clones to be generated with the use of CRISPR described in the previous chapter also exists, as well as the use of other techniques such as siRNA receptor knockdown. Experiments exploring functional activity of highlighted purinergic receptors will be presented in the following chapter.

## Chapter 5

P2X7 receptor mediates viability and cell death of resting microglia

### 5.1 Introduction

As microglia are the resident immune cells of the retina, they represent the first line of immune defence against pathological disturbances and subsequent retinal damage. Although much research has been conducted on the response of primed/polarised microglial responses following purinergic stimulation, the role of resting state microglia is often overlooked with regards to the initial pathogenic response stages. Additionally, due to their phagocytic role, particular focus is often prioritised to microglial induction of cell death in neighbouring, particularly in regards to developing or damaged neurons, which may have particular implications for RGCs in glaucoma (Thanos *et al*, 1991; Schuetz & Thanos, 2004). There is however a relative lack of understanding regarding the processes of cell death in microglial cells themselves, which is particularly important due to their established homeostatic roles throughout the body (Yin *et al*, 2017).

The contribution of microglial cells to glaucomatous RGC degeneration is currently unclear, whether the overall balance is beneficial with the clearance of damaged RGCs contributing to a return to homeostasis within the retina (Sierra *et al*, 2013), or whether microglial clearance of RGCs is inappropriate and accelerates the process due to the clearance of neurons that are not beyond recovery (Brown & Neher, 2014). Gaining understanding of the delicate balance between proliferation and cell death in a resting state microglial cell population, in response to purinergic signalling molecules from damaged tissue, could provide valuable insight into the mechanisms underlying the early stages of conditions involving retinal damage, such as glaucoma. This chapter

aims to investigate the effects of purinergic stimulation on the cell death mechanisms in resting microglia in response to endogenous purinergic signalling molecules, in order to gain better understanding of the response these cells during early stage pathophysiological conditions in the retina.

## 5.2 Results

### 5.2.1 Cell viability/death in response to ATP in BV-2 microglia

In order to determine the effects of purinergic stimulation on microglial viability and the induction of possible cell death pathways, BV-2 microglia were initially stimulated with varying concentrations of ATP for 24hrs in serum free media, with measurements of cell viability and cell death recorded with the MTS (Figure 5.1) and LDH (Figure 5.2) assays respectively.

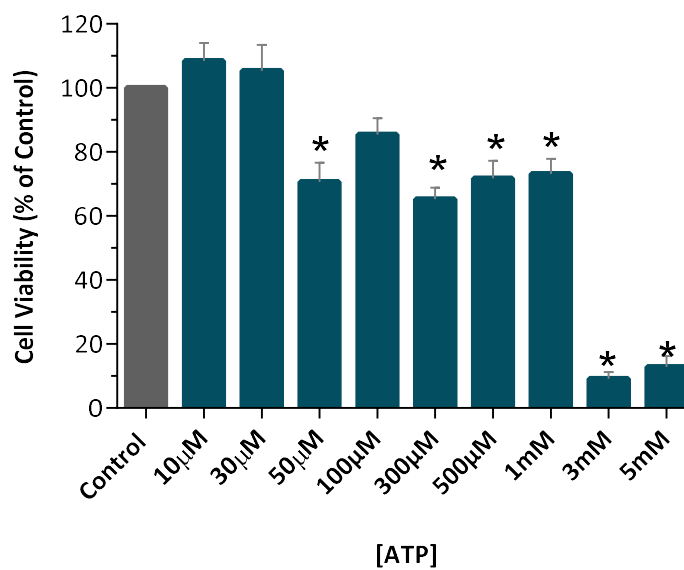


**Figure 5.1:** BV-2 cell viability measured using MTS assay in response to varying concentrations of ATP (10µM-5mM) for 24 hours (n=4). Data presented as Mean  $\pm$  S.E.M. \* indicates significance compared to control ( $P > 0.05$ ) using one-way ANOVA with Dunnett's post-hoc test.

ATP stimulation of BV-2 microglia demonstrated a biphasic reduction in cell viability, where concentrations of 50µM-1mM elicited an approximate 30% reduction in viability compared to control, whereas concentrations  $\geq 3$ mM produced a near total abolishment of viability (figure 5.1).

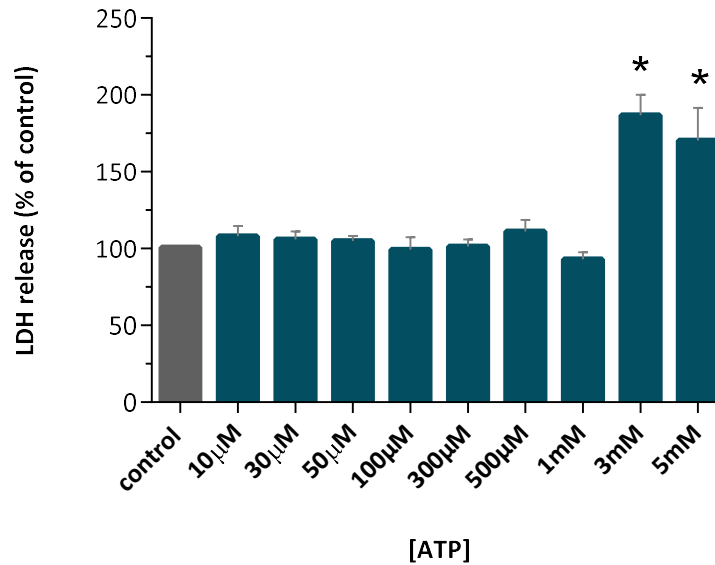


**Figure 5.2:** BV-2 cell death measured using LDH assay in response to varying concentrations of ATP (10µM-5mM) for 24 hours (n=4). Data presented as Mean ±S.E.M. \* indicates significance compared to control ( $P>0.05$ ) using one-way ANOVA with Dunnett's post-hoc test.

In contrast to results from the MTS assay, LDH release following ATP stimulation for 24 hours did not produce a biphasic response in BV-2 cells, with a significant increase in release of LDH only occurring at concentrations of  $\geq 3\text{mM}$ , mirroring the large reduction in viability observed at these concentrations.

### 5.2.2 Caspase 3/7 activation in response to ATP in BV-2 microglia

In order to validate the use of MTS assay as a means of detecting cell death, a live cell (non-fixed) fluorescence microscopy assay for detection of active caspase 3/7 was utilised. MTS assay conditions were reproduced with fluorescence images recorded following 24 hour treatment of BV-2 cells with varying concentrations (10µM-5mM) of ATP (Figure 5.3).

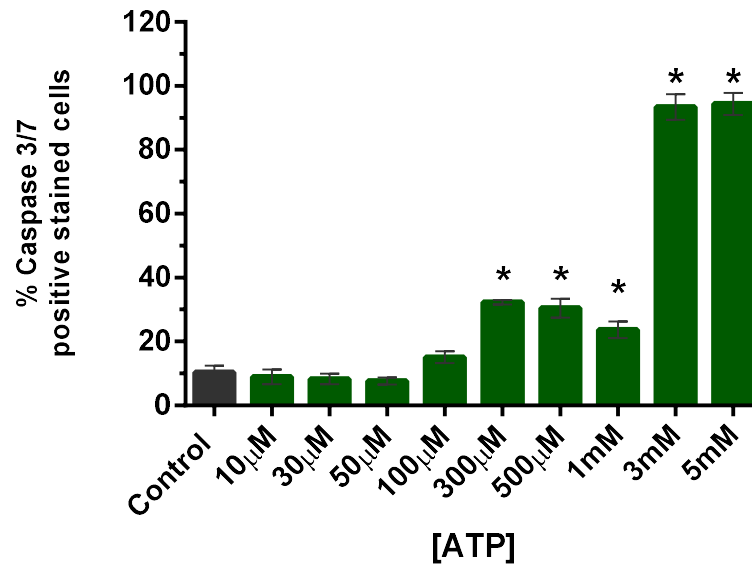


**Figure 5.3:** BV-2 cell death measured as percentage of caspase 3/7 active cells (Nucview 488) of total cell number (Hoescht 33342) following stimulation with various concentrations of ATP (10µM-5mM) for 24 hours (n=4). Data presented as Mean ±S.E.M. \* indicates significance compared to control (P>0.05) using one-way ANOVA with Dunnett's post-hoc test.

Similar to observations with the MTS assay, ATP stimulation demonstrated a biphasic increase in the percentage of treated cells with active caspase 3/7 (Figure 5.3). An initial significant increase in the percentage of cells with active caspase 3/7 of approximately 25% was demonstrated at ATP concentrations from 300µM-1mM, whereas concentrations of ≥3mM produced activation of caspases 3/7 in the near totality of cells. These observed increases in the percentage of cells with active forms of caspase 3/7 with this assay mirrors the reduction in cell viability demonstrated in the MTS assay (Figure 5.1).

### 5.2.3 Cell viability/death in response to ATP P2X7 K/O Clone-14 microglia

Due to the promiscuity of ATP as a ligand at purinergic receptors and the expression of multiple subtypes in BV-2 cells (Table 3.5), the role of different purinergic receptors on ATP-mediated viability reduction/increase in cell death was explored. With the use of P2X7 K/O clone-14 microglia, the role of P2X7 was initially explored using MTS (Figure 5.4) and active caspase 3/7 fluorescent live cell imaging (figure 5.4) assays were utilised.

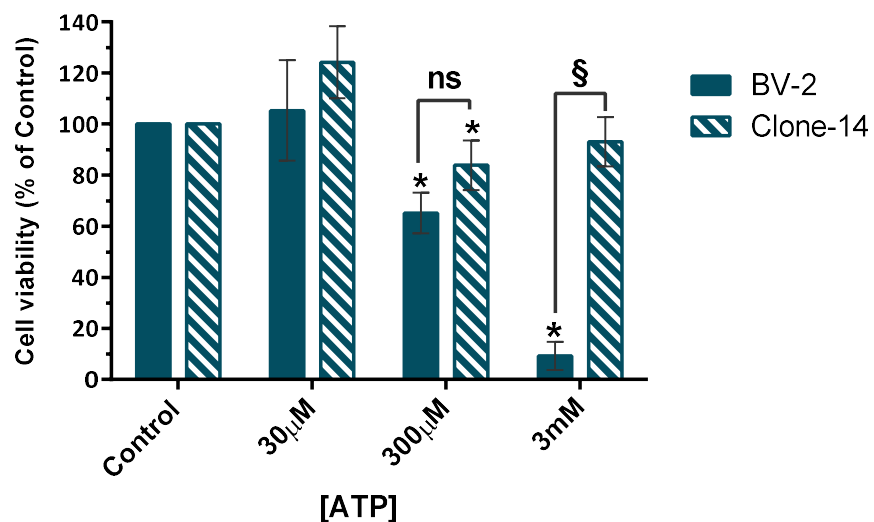


**Figure 5.4:** Cell viability measured using MTS assay in BV-2 (solid) and Clone-14 (hashed) microglial cells, in response to varying concentrations (30µM-3mM) of ATP for 24 hours (n=4). Data presented as mean  $\pm$  S.E.M. \* indicates significance (P<0.05) compared to control using one-way ANOVA with Dunnett's post hoc test. § indicates significance (P<0.05) between cell types at given ATP concentrations using two-way ANOVA with Sidak's post hoc test.

Similarly to with wild type BV-2 cells, 300µM ATP stimulation produced a significant reduction in cell viability in clone-14 cells, of approximately 20% (Figure 5.5). Although less severe than the approximate 30% reduction in viability demonstrated at equal concentration in wild type BV-2 microglia, this difference in viability was not significant between the two cell types. However 3mM ATP

treated clone-14 cells demonstrated an inhibition of loss of cell viability, which is in contrast to and significantly different from the results demonstrated with wild type BV-2 microglia. Additionally, live cell fluorescent imaging demonstrated a significant increase in the percentage of total cells with active caspase 3/7 in clone-14 microglia following ATP stimulation at concentrations of  $\geq 100\mu\text{M}$  (Figure 5.5). The significant increase in percentage of cells with active caspase 3/7 began with an approximate 15% increase over control at  $100\mu\text{M}$ , before peaking and plateauing at approximately 35% with concentrations of  $\geq 300\mu\text{M}$ . Where a near total activation of caspase 3/7 was demonstrated in wild type BV-2 microglia following stimulation with elevated concentrations of 3-5mM ATP (Figure 5.3), this effect was not replicated in clone-14 microglia, with no increase over the approximate 45% caspase 3/7 activation observed at  $300\mu\text{M}$ .

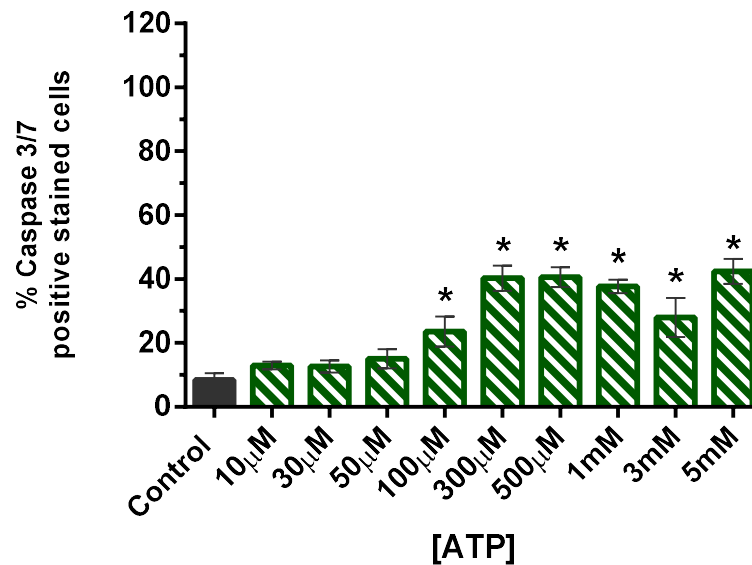


**Figure 5.5:** P2X7 K/O clone-14 cell death measured as percentage of caspase 3/7 active cells (Nucview 488) of total cell number (Hoescht 33342) following stimulation with various concentrations of ATP (10  $\mu\text{M}$ -5mM) for 24 hours (n=3). Data presented as Mean  $\pm$  S.E.M. \* indicates significance compared to control ( $P > 0.05$ ) using one-way ANOVA with Dunnett's post-hoc test.

#### 5.2.4 BzATP dose response in BV-2 microglia

In order to further probe the role of P2X7 receptor in purinergic mediated microglial cell death, the potent P2X7 receptor agonist was utilised. BV-2 microglia were stimulated with a range of concentrations (1-500 $\mu$ M) to produce a dose response comparable to those previously demonstrated with ATP, where cell viability and cell death were assessed by MTS (Figure 5.6) and LDH (Figure 5.7) assays respectively.

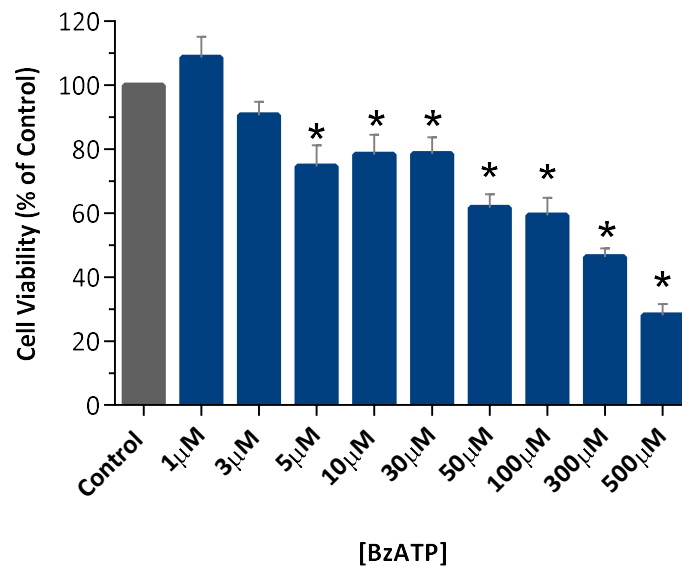


**Figure 5.6:** BV-2 cell viability measured using MTS assay, in response to varying concentrations of BzATP stimulation (1-500 $\mu$ M) for 24 hours (n=4). Data presented as Mean  $\pm$  S.E.M. \* indicates significance compared to control ( $P > 0.05$ ) using one-way ANOVA with Dunnett's post-hoc test.

Unlike the clearly biphasic response to following ATP stimulation, BzATP demonstrated a significant dose-dependent reduction in cell viability from concentrations  $\geq 5\mu$ M (Figure 5.6), reaching a maximum reduction in viability of 70% with the highest concentration of 500 $\mu$ M. Whilst the results of MTS assays demonstrated different patterns of cell viability reduction by ATP and BzATP stimulation, BzATP stimulation produced a similar LDH release profile to that of ATP stimulated BV-2 cells (Figure 5.2), whereby no significant LDH release was detected until the two highest BzATP tested concentrations (Figure

5.7). However, this BzATP LDH release profile mirroring occurred at concentrations ten-fold less concentrated than those demonstrated with ATP. Both assays highlight BzATP as more efficacious/potent than ATP in reducing cell viability and increasing cell death mediated LDH release.

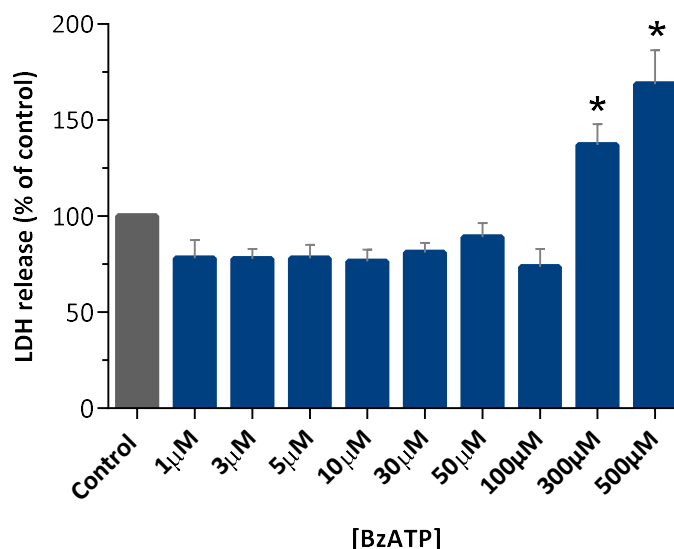


**Figure 5.7:** BV-2 cell death measured using LDH assay, in response to varying concentrations of BzATP (1-500 μM) for 24 hours (n=4). Data presented as Mean ±S.E.M. \* indicates significance compared to control (P>0.05) using one-way ANOVA with Dunnett’s post-hoc test.

### 5.2.5 P2X7 receptor antagonism with ATP stimulation in BV-2 microglia

In a similar manner to previous experiments utilising BzATP, the role of P2X7 receptor in purinergic mediate microglial cell death was explored using the highly potent P2X7 receptor antagonist AZ10606120. BV-2 cells were first incubated in varying concentrations of AZ10606120 (1-10 μM) to assess the cytotoxicity of the antagonist itself in the absence of additional purinergic receptor stimulation. Despite minor variation, AZ10606120 demonstrated no significant change in cell viability of BV-2 cells at any concentration tested (Figure 5.8). Following incubation of BV-2 microglia AZ10606120, viability was subsequently assessed with MTS assay following stimulation with

3mM ATP in the presence of varying concentrations of AZ10606120 (1-10 $\mu$ M) for 24 hours (Figure 5.9).

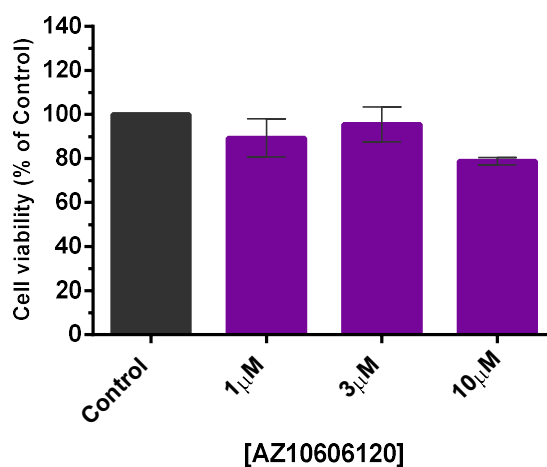


**Figure 5.8:** BV-2 cell viability measured using MTS assay, in response to varying concentrations of AZ10606120 (0-10 $\mu$ M) for 24 hours (n=3). Data presented as Mean  $\pm$ S.E.M. \* indicates significance compared to control (P>0.05) using one-way ANOVA with Dunnett's post-hoc test.

As with previous results, BV-2 microglia treated with 3mM ATP in the absence of AZ10606120 demonstrated a dramatic and significant reduction in cell viability to approximately 15% of control (Figure 5.9). The pre-incubation and presence of 1 $\mu$ M AZ10606120 was insufficient to block this. However, increased concentrations of AZ10606120 ( $\geq$ 3 $\mu$ M) demonstrated a significant protection from 3mM ATP mediated cell viability decrease, rescuing cell viability to between 60-70% of control, values which are consistent with the decrease of cell viability observed with 300 $\mu$ M ATP stimulation. Increasing concentrations of AZ10606120 above 3 $\mu$ M did not provide further protection from 3mM ATP mediated reduction in cell viability.

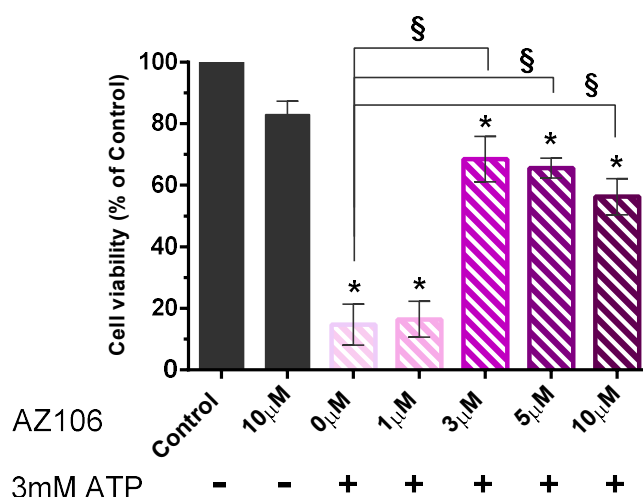


**Figure 5.9:** BV-2 cell viability measured using MTS assay, in response to ATP (3mM) in the presence of varying concentrations of AZ10606120 (0-10 $\mu$ M) for 24 hours (n=3). Data presented as Mean  $\pm$  S.E.M. \* indicates significance compared to control (P>0.05) using one-way ANOVA with Dunnett's post-hoc test.

### 5.2.6 P2X4 receptor antagonism with ATP stimulation in BV-2 microglia

Following exploration of P2X7 receptor involvement in purinergic mediated reduction in microglial cell viability, the initial phase of reduced cell viability observed with ATP concentrations between 300 $\mu$ M-1mM (Figure 5.1), which was not prevented in P2X7 K/O clone-14 cells, was subsequently investigated. Due to the involvement of the P2X4 receptor in the initial phase of the ATP-induced Ca<sup>2+</sup> responses, as well as the high expression of the P2X4 receptor subtype in BV-2 microglia (Table 3.5), the highly potent P2X4 antagonist PSB12062 (Figure 5.10) was utilised in isolation and combination with 300 $\mu$ M ATP stimulation. As with previous antagonist experiments, cell viability was measured with MTS assays.

Unlike previous experiments with AZ10606120, incubation of BV2 microglia with PSB12062 was not well tolerated at any concentration tested, demonstrating significant levels of reduction in cell viability to

between 40-60% of control (Figure 5.10 A). The addition of 300 $\mu$ M ATP to experimental conditions demonstrated the significant and predictable approximate 35% reduction in cell viability compared to control in absence of PSB12062 (Figure 5.10 B). 300 $\mu$ M ATP stimulation in the presence of PSB12062 failed to prevent the reduction in cell viability, and instead provided further significant reductions in cell viability to around 40% of control, at every concentration of antagonist tested.

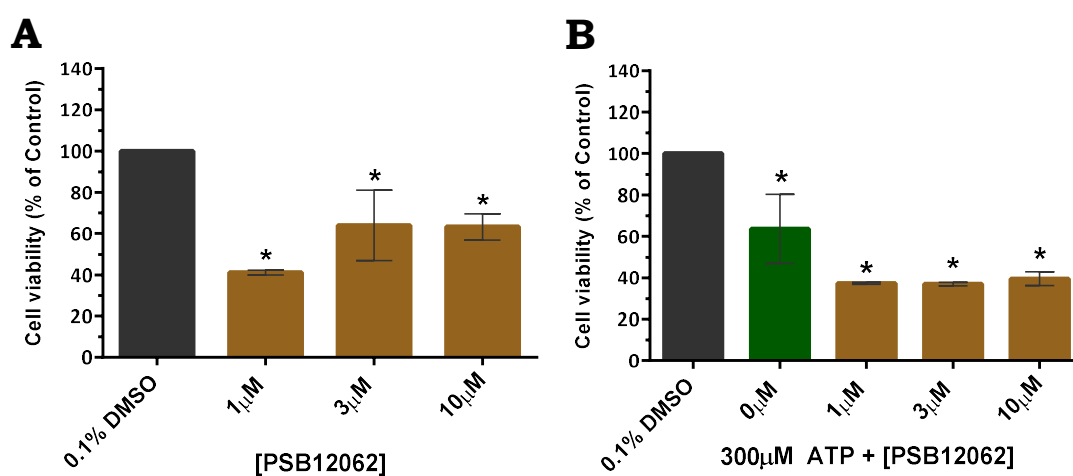


**Figure 5.10:** BV-2 cell viability measured using MTS assay, in response to **A** varying concentrations of PSB12062 (0-10 $\mu$ M), or **B** ATP stimulation (300 $\mu$ M) in the presence of varying concentrations of PSB12062 (0-10 $\mu$ M) for 24 hours (n=3). Data presented as Mean  $\pm$  S.E.M. \* indicates significance compared to control (P>0.05) using one-way ANOVA with Dunnett's post-hoc test.

It was not possible to determine whether P2X4 was involved due to the toxic effects of this antagonist. An alternative potent P2X4 antagonist 5-BDBD was therefore explored, in order to further probe the role of this receptor in purinergic mediated reduction in cell viability. In a similar manner to previous antagonist experiments, BV-2 microglia were pre-incubated with varying concentrations of 5-BDBD (1-10 $\mu$ M) in isolation (Figure 5.11 A) or in the presence of 300 $\mu$ M ATP (Figure 5.11 B). MTS assay was used for cell viability measurements.

Unlike PSB12062, 5-BDBD was not cytotoxic to BV-2 microglia at all concentrations tested in the absence of ATP stimulation, however a dose dependent reduction in microglial viability was observed (Figure 5.11A), with significant viability reductions at 3-10 $\mu$ M. Microglial viability reduction with 1 $\mu$ M 5-BDBD produced a minor approximate 10% reduction in cell viability which was not significant. 5-BDBD in combination with 300 $\mu$ M ATP was unable to provide any recovery of cell viability at any concentration tested.

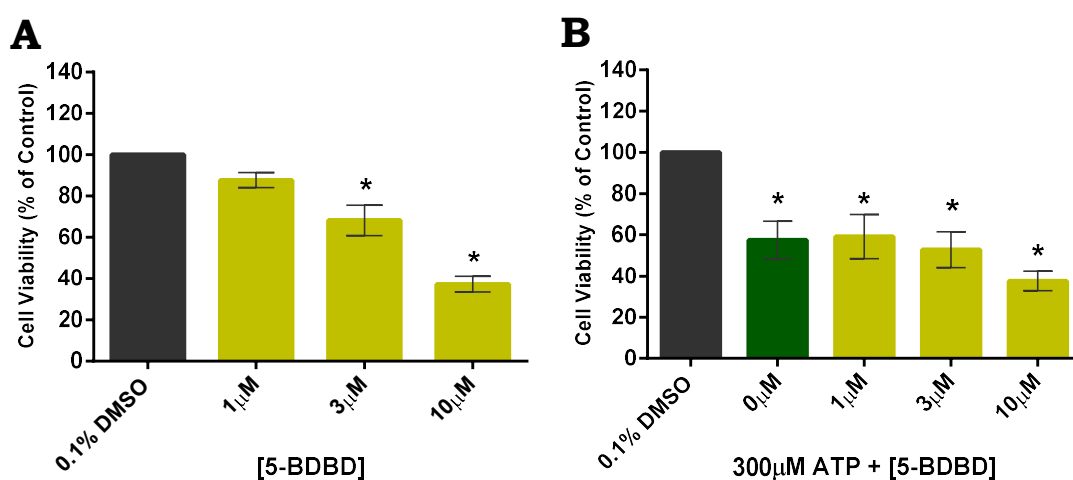


**Figure 5.11:** BV-2 cell viability measured using MTS assay, in response to **A** varying concentrations of 5-BDBD (0-10 $\mu$ M), or **B** ATP (300 $\mu$ M) in the presence of varying concentrations of 5-BDBD (0-10 $\mu$ M) for 24 hours (n=3). Data presented as Mean  $\pm$ S.E.M. \* indicates significance compared to control (P>0.05) using one-way ANOVA with Dunnett's post-hoc test.

### 5.2.7 P2Y2 receptor antagonism with ATP stimulation in BV-2 microglia

The role of P2Y2 was also probed with the antagonist AR-C118925XX (Figure 5.14).

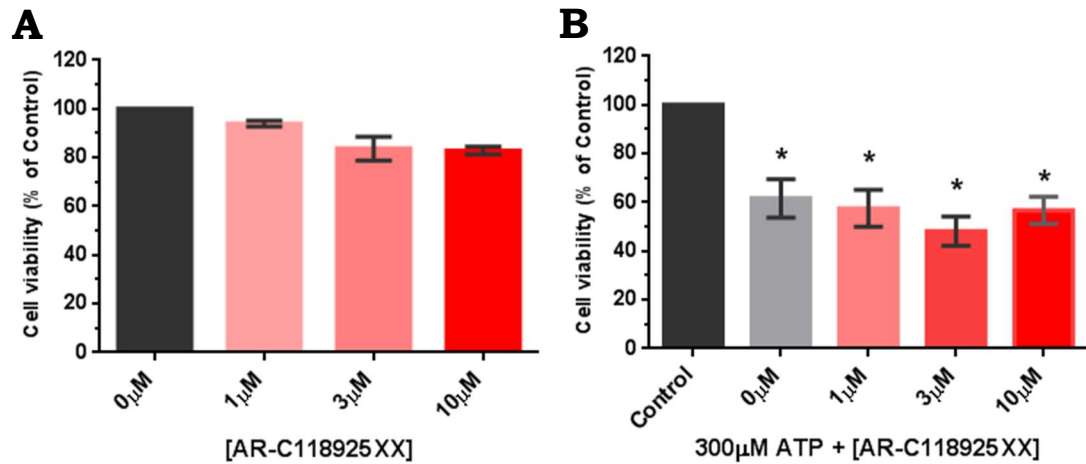


**Figure 5.12:** BV-2 cell viability measured using MTS assay, in response to **A** varying concentrations of AR-C118925XX (0-10 μM), or **B** ATP stimulation (300 μM) in the presence of varying concentrations of AR-C118925XX (0-10 μM) for 24 hours (n=3). Data presented as Mean ± S.E.M. \* indicates significance compared to control (P>0.05) using one-way ANOVA with Dunnett's post-hoc test.

In isolation, incubation with AR-C118925XX was well tolerated and demonstrated no significant reduction in viability (Figure 5.12 A). However, in combination with 300 μM ATP stimulus, no significant protective effect was observed (Figure 5.12 B).

### 5.2.8 ATP $\gamma$ S dose response in BV-2 microglia

In order to investigate potential P2Y receptor involvement following the breakdown of ATP, the non-hydrolysable synthetic purinergic agonist ATP $\gamma$ S was investigated. BV-2 microglia were stimulated with an ATP $\gamma$ S concentration range (1-500 $\mu$ M) for 24 hours and viability measured with an MTS assay (Figure 5.12). An additional condition of 300 $\mu$ M was included as a positive control.

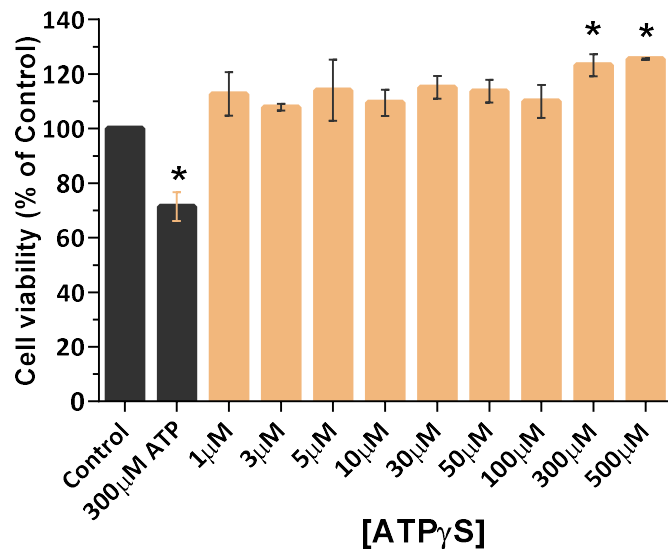


**Figure 5.13:** BV-2 cell viability measured using MTS assay, in response to varying concentrations of ATP $\gamma$ S stimulation (1-500 $\mu$ M) for 24 hours (n=3). Data presented as Mean  $\pm$  S.E.M. \* indicates significance compared to control (P>0.05) using one-way ANOVA with Dunnett's post-hoc test.

In contrast to the effects of ATP, non-hydrolysable ATP $\gamma$ S stimulation produced a mild increase in cell viability above control at all concentrations tested, which only significant over control at the highest concentration of 300-500 $\mu$ M tested. This indicates that ATP breakdown products are involved in the loss of viability seen with ATP.

### 5.2.9 ATP metabolite dose responses in BV-2 microglia

Due to the lack of reduced cell viability/cytotoxicity following ATPyS stimulation, the effects ADP, a metabolite product from the breakdown of ATP, on cell viability was investigated in BV-2 cells (Figure 5.13).

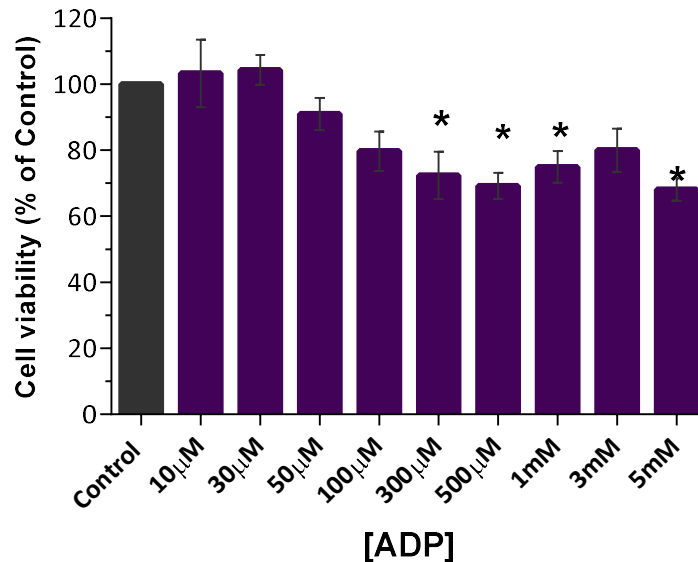


**Figure 5.14:** BV-2 cell viability measured using MTS assay, in response to varying concentrations of ADP stimulation (10µM-5mM) for 24 hours (n=4). Data presented as Mean ±S.E.M. \* indicates significance compared to control ( $P>0.05$ ) using one-way ANOVA with Dunnett's post-hoc test.

ADP stimulation produced a dose dependent reduction in cell viability of BV-2 microglia (Figure 5.13). Similarly to 300µM ATP stimulation, a significant cell viability reduction of approximately 30% was demonstrated with 300µM ADP stimulation, as well as all concentrations above this excluding 3mM. However, in contrast to ATP, ADP concentrations of 3-5mM did not produce any further reductions in cell viability.

Following stimulation with ADP, the related purinergic ligand and ADP metabolite adenosine was subsequently explored. Cell viability of BV-2 microglial cells stimulated with a range of concentrations (10µM-5mM) of adenosine was assessed with MTS assay (Figure 5.14). Unlike related purinergic ligands ATP and ADP, adenosine stimulation of BV-2

cells produced no significant alterations in cell viability compared to control at any concentration tested.

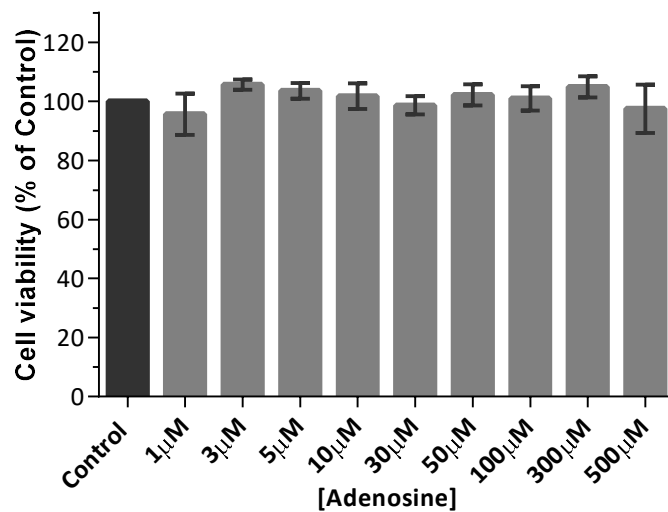


**Figure 5.15:** BV-2 cell viability measured using MTS assay, in response to varying concentrations of adenosine stimulation (1µM-500µM) for 24 hours (n=3). Data presented as Mean ±S.E.M. \* indicates significance compared to control (P>0.05) using one-way ANOVA with Dunnett's post-hoc test.

#### **5.2.10 P2Y1 receptor antagonism with ADP stimulation in BV-2 microglia**

As ADP ( $\geq 300\mu\text{M}$ ) demonstrated a similar 30% reduction in cell viability, the contribution of various P2Y receptor subtypes was probed for their contribution to this effect. The role of P2Y1 was assessed using the P2Y1 selective antagonist MRS2179 (Figure 5.15).

A mild significant reduction in cell viability was observed with MRS2179 in isolation at the highest concentrations tested (10µM). With the addition of 300µM ADP, no significant protective effect was observed.

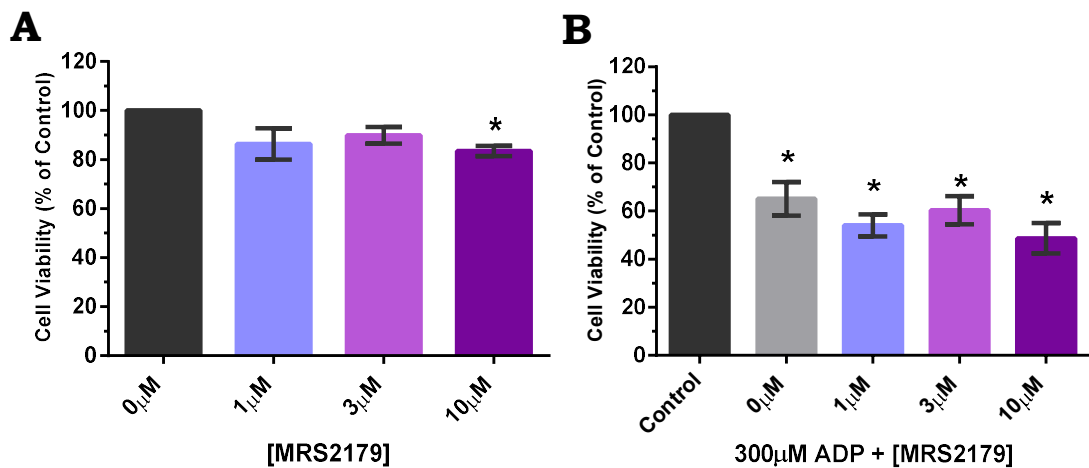


**Figure 5.16:** BV-2 cell viability measured using MTS assay, in response to **A** varying concentrations of MRS2179 (0-10 $\mu$ M), or **B** ADP stimulation (300 $\mu$ M) in the presence of varying concentrations of MRS2179 (0-10 $\mu$ M) for 24 hours (n=3). Data presented as Mean  $\pm$ S.E.M. \* indicates significance compared to control (P>0.05) using one-way ANOVA with Dunnett's post-hoc test.

### 5.2.11 P2Y12 receptor antagonism with ADP stimulation in BV-2 microglia

The P2Y12 receptor was subsequently explored with the use of pharmacological antagonist PSB0739 (Figure 5.17).

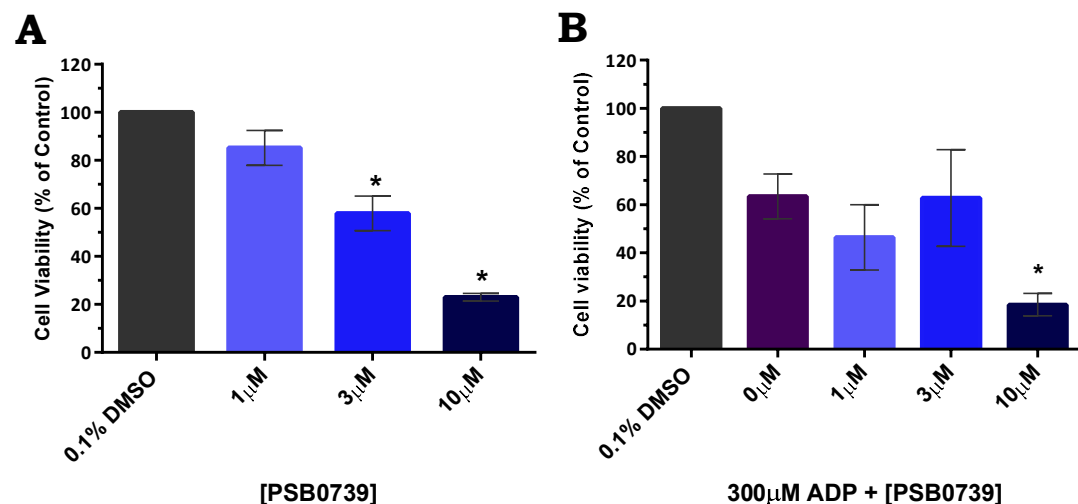


**Figure 5.17:** BV-2 cell viability measured using MTS assay, in response to **A** varying concentrations of PSB0739 (0-10 $\mu$ M), or **B** ADP stimulation (300 $\mu$ M) in the presence of varying concentrations of PSB0739 (0-10 $\mu$ M) for 24 hours (n=3). Data presented as Mean  $\pm$ S.E.M. \* indicates significance compared to control (P>0.05) using one-way ANOVA with Dunnett's post-hoc test.

As with select previous antagonists, incubation of BV-2 microglia with PSB0739 in isolation was not well tolerated, and provided a dose dependent decrease in cell viability, with significant reductions observed at both 3 $\mu$ M and 10 $\mu$ M (Figure 5.17 A). PSB0739 was unable to provide any significant protection from 300 $\mu$ M ADP stimulation (Figure 5.17 B).

### 5.2.12 Uracil-nucleotide dose responses in BV-2 microglia

Due to the cytotoxicity associated with multiple selective P2Y receptors probed under experimental conditions, further experiments exploring the contribution of purinergic receptors to the ADP mediated cytotoxicity utilised selective purinergic agonists UTP (Figure 5.18) and UDP (Figure 5.19). Ca<sup>2+</sup> responses had indicated that the P2Y6 receptor was functional in these cells and UDP is an agonist for these receptors.

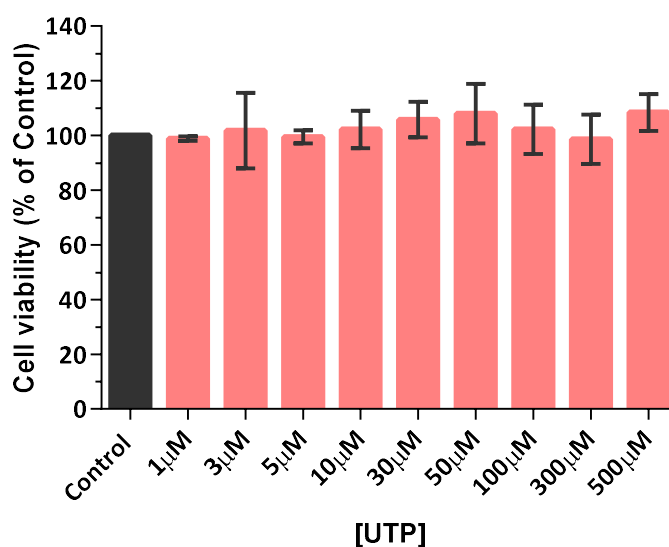


**Figure 5.18:** BV-2 cell viability measured using MTS assay, in response to varying concentrations of UTP (1-500 $\mu$ M) for 24 hours (n=4). Data presented as Mean  $\pm$  S.E.M. \* indicates significance compared to control (P>0.05) using one-way ANOVA with Dunnett's post-hoc test.

Stimulation with either uracil-nucleotide agonist (Figures 5.18 & 5.19) did not demonstrate reduction in cell viability of BV-2 microglia at any concentration tested.

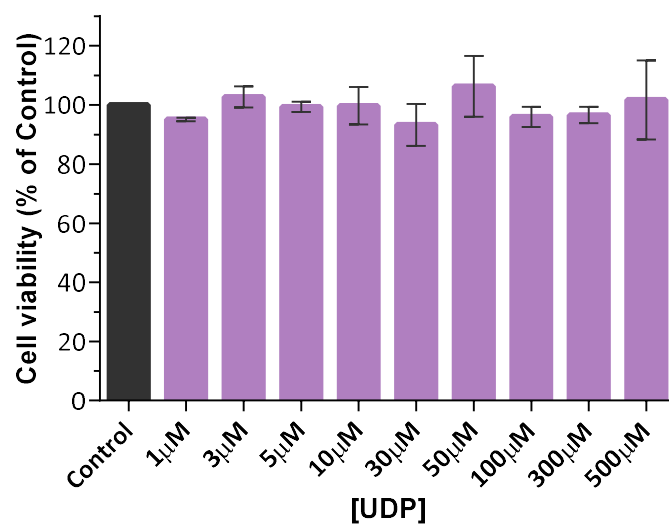


**Figure 5.19:** BV-2 cell viability measured using MTS assay, in response to varying concentrations of UDP (1-500 $\mu$ M) for 24 hours (n=4). Data presented as Mean  $\pm$ S.E.M. \* indicates significance compared to control (P>0.05) using one-way ANOVA with Dunnett's post-hoc test.

### 5.3 Discussion

Stimulation of resting BV-2 microglia with an ATP dose range produced a biphasic reduction in viability (MTS), with a significant reduction of approximately 30% at concentrations of 300 $\mu$ M or greater, followed by an almost complete abolition of viability with 3-5mM ATP. (Figure 5.1). In contrast to MTS assay results, significant release of LDH over control only occurred at highest 3-5mM concentrations tested (Figure 5.2) which parallels the with the near complete loss of viability in MTS assay at these concentrations. Both assays utilised initially are indirect measurements of cell death. In the MTS assay, viability is measured as mitochondrial metabolism and thus can be susceptible to changes in mitochondrial metabolism independent of cell death. For example, both P2X7 mediated Ca<sup>2+</sup> influx and K<sup>+</sup> efflux have been shown to negatively modulate mitochondrial respiration and concurrently positively modulate the autophagy mediated process of mitochondrial degradation, mitophagy (Sekar *et al*, 2018). The LDH assay is measures release of cellular contents into the extracellular medium, which only occurs under certain cell death pathways/conditions such as necrosis. Due to the discrepancies observed in the MTS and LDH assay results at concentrations between 300 $\mu$ M-1mM, a further assay was utilised to corroborate MTS and LDH data and provide insight into potential cell death mechanisms.

Caspase 3 and 7 isoforms are members of the executioner caspase family, with sequential activation of 3 followed by 7 shown to play a key role in the execution phase of apoptotic cell death (Porter & Jänicke, 1999). Outcome of caspase 3/7 fluorescent imaging assay mirrored the results of MTS assay, seeing a moderate rise in the percentage of cells with active forms of caspase 3/7 at moderate concentrations (300 $\mu$ M-1mM), and a near total activation at 3-5mM ATP (Figure 5.3). The caspase 3/7 assay also provided further information over MTS assay, in that the intermediate rise in caspase activation was shown to occur in a sub-population of approximately

30% of cells, rather than a 30% reduction in mitochondrial metabolism for the entire population. Although assay conditions were conducted in serum free medium to minimise the impact of different cell cycle stages on receptor expression profiles and minimise potential serum protein interactions, it is unclear from these results why a sub-population of the homogenous cell culture is susceptible to stimulation with intermediate ATP concentrations.

The activation of caspases 3/7 also provides additional information about the potential mechanisms of cell death occurring. Despite there being a role for active caspases in pyroptotic cell death, most commonly caspase 1/11 in the canonical pathway (Miao *et al*, 2011), but additionally caspase 4 in the non canonical pathway (Chen *et al*, 2019). A further isoform, caspase 8 has also been shown to cleave gasdermin-D in pyroptosis (Scanlon, 2018). As pro-caspase-8 is activated by caspase 3, the activation of caspase 3 in the fluorescent imaging assay alone cannot exclude pyroptotic cell death as a possibility in ATP treated microglia. However, due to the lytic mechanism of pyroptotic cell death, LDH release quantification is a commonly used technique for detection of pyroptosis (Rayamajhi *et al*, 2013). LDH assay results of BV-2 microglia showed no significant increase in LDH release over control at intermediate ATP concentrations (300µM-1mM), release of which would be highly likely under pyroptotic or necrotic conditions. Additionally, BV-2 microglia were under resting conditions and not primed prior to ATP stimulation, thus lacking the necessary inflammasome assembly and further reducing the likelihood of pyroptotic cell death. Therefore, the evidence presented here suggests apoptosis is the most likely mechanism of cell death.

The activation of caspase 3/7 in nearly the entire population of BV-2 microglia at elevated concentrations (3-5mM) of ATP stimulation seems contradictory to the significant increase of LDH release as this implies

necrotic cell death in which caspase activation does not occur. However this LDH release could be explained as secondary necrosis, a process of autolytic degradation of apoptotic bodies in the absence of phagocytic uptake by surrounding cells (Silva, 2010). Microglia are phagocytic cells responsible for the uptake of dead cells and debris, thus apoptotic bodies formed when a proportion of the cells undergo apoptosis would likely be phagocytosed by remaining ~70% of the, preventing secondary necrosis and LDH release. However with elevated ATP concentrations (3-5mM) affecting essentially the entire cell culture population, there would be no capacity for surrounding microglia to phagocytose the apoptotic bodies, leading to substantial LDH release by secondary necrosis of the apoptotic bodies. The biphasic pattern of cell death observed can therefore be explained by one mechanism, which is induced by different receptors.

As an endogenous signalling ligand, ATP acts promiscuously at multiple purinergic receptors. This combined biphasic cell death response to ATP and additional data demonstrated from the combination of MTS, LDH and caspase assays suggests the cell death is occurring either as a result of the contribution of multiple different receptor subtypes, or from a single receptor that is exhibiting multiple states of activation. Due to P2X7Rs historical role in cell death (Adinolfi *et al*, 2005), as well as its reported multiple states of activation (Smart *et al*, 2003), and the high concentrations of ATP required, a series of further experiments were designed to determine the contribution of P2X7 receptor subtypes involvement in ATP mediated microglia cell death, involving the use of selective pharmacological agonists, antagonists and the P2X7R K/O clone-14 microglial cell line.

Unlike with ATP stimulation, the potent synthetic agonist P2X7R agonist BzATP induced a dose dependent significant decrease in cell viability (Figure 5.6), characteristic of activity of an isolated receptor. The BzATP dose response was also an order of magnitude more potent

than with ATP, which supports the reported potency of BzATP over ATP at P2X7R in the literature (Suprenant *et al*, 1996; Baraldi *et al*, 2004). Unlike the contrasting MTS results between ATP and BzATP stimulation, the LDH release profile of BzATP stimulated BV-2 (Figure 5.7) cells bore a striking resemblance to that of ATP stimulated BV-2 microglia, with significant release over control only occurring at the two highest concentrations tested (300-500 $\mu$ M). These results again validate the increased efficacy of BzATP over ATP at the P2X7, as well as supporting the hypothesis that the LDH release demonstrated is occurring as secondary necrosis of apoptotic bodies once the cell culture environment reaches a critical threshold of cell death and loses its ability of phagocytic clearance. Similarly, BzATP has been shown to induce P2X7 mediated cell death in primary microglia, where a concentration of 380 $\mu$ M induced a similar approximate 40% reduction in cell viability after 4.5 hours, which was absent in microglia from P2X7 K/O mice and significantly inhibited with A-804598 pre-incubation (He *et al*, 2017). Despite BzATPs potency at the P2X7R subtype, it also acts as an agonist at other purinergic receptor subtypes such as P2X1, P2X3 and even P2Y11 (only relevant in humans) (Jarvis & Khakh, 2009), meaning the contribution of these receptors to BzATP mediated cell death of BV-2 microglia cannot be excluded. However, the Ca<sup>2+</sup> described in the previous chapter indicates that BzATP is not acting at the receptors that would cause Ca<sup>2+</sup> increase.

In order to support BzATP experimental data and further explore the role of P2X7, an ATP dose response was repeated in P2X7 K/O clone-14 microglial cells (Figures 5.4 & 5.5), whereby ATP induced a near identical reduction in cell viability and increase in percentage of active caspase 3/7 positive cells at intermediate concentrations of ATP (300-500 $\mu$ M), to wild type BV-2 cells (Figures 5.1 & 5.3). However, in contrast to wild type BV-2 cells, elevated concentrations of ATP of 3-5mM were unable to induce the further near total abolition of cell

viability and activation of caspases-3/7 in clone-14 cells. Additionally, 3 $\mu$ M AZ1060120 incubation was unable to provide full recovery of cell viability in 3mM ATP stimulated BV-2 cells (Figure 5.9), instead reducing cell viability loss to approximately 70% of control, similar to levels observed with 300 $\mu$ M ATP stimulation in the absence of antagonist. As 3 $\mu$ M AZ10606120 significantly inhibited P2X7R mediated intracellular Ca<sup>2+</sup> elevation (Figures 4.3 & 4.6), and incubation with AZ1060120 was well tolerated in BV-2 microglia up to concentrations of 3 $\mu$ M in the absence of ATP stimulation (Figure 5.8), the combination of these results suggest that P2X7R plays a critical role in the response to elevated (3mM) ATP stimulation, but not substantially with the intermediate reduction of cell viability with ATP concentrations below 3mM.

As mentioned previously, it is unsurprising that P2X7 plays a key role in purinergic mediated cytotoxicity in BV-2 microglia, due to its early discovery in immune cells including microglia (Ferrari *et al*, 1996), and also its historically significant role as a cell death receptor in a variety of cell types (Adinolfi *et al*, 2005). Reported mechanisms of P2X7 mediated cell death vary from apoptosis (Humphrys *et al*, 2000), necrosis (Ferrari *et al*, 1999) to pyroptosis (Yang *et al*, 2018), with each mechanism dependent on a seemingly multitude of factors including cell type, duration of receptor stimulation (Di Virgilio *et al*, 1998), and for immune cells, the activation state/polarization phenotype. With particular focus on P2X7 in microglial cells, Ferrari and colleagues (1997a) demonstrated with early studies in both primary mouse microglia and N9 and N13 human microglial cell lines that ATP stimulation of P2X7 induced cell death, was occurring via an apoptotic pathway due primarily to morphological changes characteristic of apoptosis, such as membrane blebbing. This study also demonstrated significant LDH release following stimulation with ATP, BzATP and ATP $\gamma$ S, which could be interpreted as secondary necrosis of apoptotic bodies. Both these effects were prevented with the irreversible P2X7

antagonist oATP. Subsequent investigation by the same group demonstrated activation of effector family caspases 3, 7 and 8, chromatin condensation and fragmentation of DNA (detected by gel electrophoresis), all hallmark features of apoptosis in response to 3mM ATP stimulation of N13 microglia (Ferrari *et al*, 1999). Since these initial reported results, further studies have demonstrated supporting evidence for the apoptotic mechanism of cell death following P2X7R activation in microglia, including phosphatidyl-serine residue exposure (Bianco *et al*, 2005) and AKT/ERK pathway activation (He *et al*, 2017).

In order to determine the receptor(s) responsible for the initial phase of ATP-mediated cytotoxicity, a range of further experiments were conducted. Although this stage of cytotoxicity is reliant on ATP concentrations <3mM, this range of concentrations (300µM -1mM) is still supramaximal for the remaining purinergic receptor subtypes. Due to extensive microglial expression (Ulmann *et al*, 2008; Table 3.5), as well as reported functional roles of the in microglia and related macrophages (Stokes *et al*, 2017), plus the availability of more potent pharmacological tools over other subtypes, that have successfully inhibited the initial phase of the ATP-induced Ca<sup>2+</sup> responses (Chapter 4), P2X4R function in relation to ATP/purinergic mediated cytotoxicity in BV-2 microglia was subsequently explored. Two potent P2X4 antagonists utilised in the prior chapter, PSB12062 (Figure 4.7) and 5-BDBD (Figure 4.8) were used in the MTS assay in both isolation and in combination with 300µM ATP to assess long term antagonist cytotoxicity on BV-2 microglia and potential cytoprotective effects against ATP mediated intermediate cytotoxicity. Unlike AZ10606120, both P2X4 antagonists explored demonstrated cytotoxicity to microglial cells in the absence of additional purinergic receptor stimulation (Figures 5.10 A & 5.11 A), making the assessment of any cytoprotective effects difficult. In fact, combination of ATP stimulus and P2X4 antagonists, particularly PSB12062, produced further reductions in cell viability than ATP stimulus alone. It was therefore not possible to

determine whether the P2X4R was involved in this response with this set of antagonists. However, later experiments using ATP $\gamma$ S showed no cell death, which would have been expected if P2X4 was involved, as a modified radioligand form of ATP $\gamma$ S, [ $^{35}$ S]ATP $\gamma$ S has been shown to bind to P2X4 (Abdelrhaman *et al*, 2017) and act as an agonist (L Stokes, personal communication).

In addition, there is little evidence to support a role for P2X4 in microglial cell death. It has been shown that sustained stimulation of P2X4R in resting BV-2 cells lead to pore formation but not cytoskeletal rearrangement/membrane blebbing or detectable LDH release (Bernier *et al*, 2012). Furthermore, Dhuna and colleagues (2019) demonstrated that P2X7 deficient microglia were insensitive to cell death following ATP stimulation. However the concentration of ATP utilised for this study was 200 $\mu$ M. Correlating this information with the data presented in this chapter, 200 $\mu$ M may not be sufficient to elicit the intermediate cytotoxic effects on BV-2 microglia. In the same study, ATP stimulation of HEK cells over-expressing hP2X4 did not cause cell death, although the lack of cytotoxicity could be attributed to differences of cell type or the use of orthologous human P2X4 (Dhuna *et al*, 2019). P2X4R stimulation has been shown to exacerbate LPS induced microglial cell death (Vazquez-Villoldo *et al*, 2014), however the requirement of LPS priming in this study differs significantly from use of resting/non-polarized microglia. Overall, it seems unlikely that P2X4 is involved in the cell death seen in the current experiments, however it cannot be ruled out without further investigation.

Due to full agonist activity of ATP at the P2Y2 receptor, and the involvement of this receptor in the ATP-mediated initial phase Ca $^{2+}$  response, this receptor subtype was also explored. The P2Y2 antagonist AR-C118925XX (Figure 5.12 A) was well tolerated, but did not provide any inhibition of 300 $\mu$ M ATP-mediated cytotoxicity. AR-C118925XX is a competitive antagonist, which in combination with the

high concentration of ATP stimulation used may explain its lack of efficacy. Its involvement in the ATP-induced cell death can therefore not be ruled out from these experiments.

Microglia, including the BV-2 cell line, express the necessary enzymes to rapidly hydrolyse extracellular ATP (Rodrigues-Neves *et al*, 2018). The expression of such enzymes in combination with the long-term model of assays (24hrs) provides the potential for ATP breakdown, and concurrently the generation of large quantities of related purinergic signalling ligands, such as ADP and adenosine, leading to potential stimulation of additional families of purinergic receptors. In order to isolate the potential involvement of P2Y and P1Rs, a viability dose response of the ATP derivative ATP $\gamma$ S in BV-2 microglia was determined. In contrast to the intermediate cytotoxic effect caused by ATP stimulation, ATP $\gamma$ S was not cytotoxic at any concentration tested (up to 500 $\mu$ M) (Figure 5.12), instead producing a mildly significant proliferative effect at  $\geq 300\mu$ M. Much of the rationale for agonists and antagonists used in this chapter was derived from the results of the previous chapter assessing intracellular Ca<sup>2+</sup> mobilization, as Ca<sup>2+</sup> as a secondary messenger system has been linked to cell death pathways (Orrenius *et al*, 2003; Yuan, *et al*, 2016). It is entirely possible however, that the mobilisation of Ca<sup>2+</sup> and cell death pathways demonstrated in this chapter are occurring as independent parallel responses, thus explaining the discrepancy between the ATP and ATP $\gamma$ S responses at relative concentrations. Proliferation from purinergic stimulation is not unheard of, on the contrary tonic low-level stimulation of P2X7 provides proliferative effects in a range of cell types (Di Virgilio *et al*, 2009; Adinolfi *et al*, 2012). The lack of cytotoxicity of the non-hydrolysable ATP $\gamma$ S indicates that the intermediate cell death phase is as a result of one or more ATP degradation products stimulating receptors alternative to P2X subtypes. As such, ADP and adenosine viability dose responses were established in BV-2 microglia (Figures 5.13 & 5.14).

ADP stimulation produced a significant decrease in cell viability at concentrations  $\geq 300\mu\text{M}$ , at a level effectively identical to that seen with  $300\mu\text{M}$  ATP (Figure 5.13). In contrast to ATP however, no P2X7 mediated cytotoxicity component was observed with 3-5mM ADP stimulation. Despite functional roles for multiple P2Y receptor subtypes in microglia, ADP-mediated cytotoxicity in microglia or other comparable cell types has not previously been shown.

Both cytotoxicity and proliferation mediated from adenosine receptor stimulation has been previously reported in a multitude of cell types. A3 receptor stimulation has demonstrated apoptotic cell death of mesangial cells (Duann *et al*, 2005), as well as tumour cells (Bar-Yehuda *et al*, 2008), with activation of caspase 3 (Aghaei *et al*, 2011). Conversely, A3 receptor stimulation has also demonstrated cytoprotective effects against optic nerve transection induced apoptosis of RGCs (Galvao *et al*, 2012), suggesting that the role of A3 receptors in cytoprotection/cytotoxicity is cell type and situation dependant. Specific to microglia, adenosine stimulation has been shown to induce the characteristic apoptotic cell death marker of fragmented DNA after 12 hours, however individual adenosine receptor subtype blockade was ineffective in preventing this effect, suggesting a receptor independent pathway (Ogata & Schubert, 1996). BV-2 stimulation with adenosine demonstrated no significant change in either cytotoxicity or proliferation at any concentration tested (Figure 5.14), indicating that breakdown of ATP to adenosine was not responsible for ATP-induced cell death in BV-2 microglia.

In order to explore the responsible P2Y receptor subtype, a combination of pharmacological receptor inhibition and selective purinergic agonists were utilised. Despite microglial tolerance to the P2Y1 antagonist MRS2179 (Figure 5.16 A), it did not demonstrated significant reduction in  $300\mu\text{M}$  ADP mediated cytotoxicity Figures 5.16

B). This is not surprising since functional expression of this receptor was not detected in the  $\text{Ca}^{2+}$  signalling experiments. With regard to P2Y12 receptor antagonism, PSB0739 was not well tolerated in BV-2 cells and induced a significant dose dependent cytotoxic effect (Figure 5.17). As such, whether P2Y12 antagonism was effective in blocking ADP mediated cytotoxicity was undetermined (Figure 5.17B). In order to avoid the seemingly sensitive nature of BV-2 microglia to long term antagonist exposure, P2Y subtype selective purinergic agonists UTP (P2Y4) and UDP (P2Y6, P2Y14), that are also endogenous, were explored in inducing apoptosis. Neither UDP or UTP demonstrated no significant change in cell viability at any concentration tested, indicating that these receptor subtypes are not involved in the ADP-mediated cell death observed. This is despite clear functional expression of P2Y6 as demonstrated in  $\text{Ca}^{2+}$  signalling experiments. Like with ADP, there is little literature evidence for uracil-nucleotide purinergic ligand based cytotoxicity in microglia or related cell types. UTP was unable to induce LDH release from microglial cells at concentrations up to 2mM (Ferrari *et al*, 1997a).

Due to lack of useful selective pharmacological tools, the identification of the receptors responsible for the first phase of cell death was not possible, although P2Y2 and P2Y12 remain potential candidates. The successful generation of the P2X7R K/O microglial cell line represents an avenue of investigation that could be explored in the future, by generation of similar P2YR K/O cell lines. This research however demonstrated a clear role for the P2X7 receptor in microglial cell death, demonstrating the central role for this receptor to microglial function.

## Chapter 6

Prole of P2X7 receptor in purinergic mediated IL-1 $\beta$  mRNA expression, protein processing and release in microglia

### 6.1 Introduction

The inflammatory cytokine interleukin-1 $\beta$  is a key regulator of the inflammatory response within the central nervous system, and as such has been shown to play a role in many neuroinflammatory diseases (Liu & Quan, 2018). To date there have been multiple reports of changes in IL-1 $\beta$  expression in experimental models of glaucoma, which are discussed further below.

An elevated IOP-induced retinal ischaemia model in rat retina has demonstrated a transient increase in expression of IL-1 $\beta$ , which correlated with reduced cell density in the inner plexiform layer, an effect that was abolished with IL-1ra or anti-IL-1 $\beta$  antibody pretreatment (Yoneda *et al*, 2001). Optic nerve ligation, a simulation of glaucomatous RGC damage, also demonstrated significant upregulation of IL-1 $\beta$  mRNA (Hangai *et al*, 1995) and corresponding increases in apoptotic BAX protein and RGC loss, which was similarly inhibited with IL-1ra treatment (Zhang & Chintala, 2004). Additionally, in an acute glaucoma elevated IOP model, retinal ischaemia/reperfusion demonstrated the production of the inflammasome component NLRP3, as well as IL-1 $\beta$ , which were shown to be reliant on caspase 8 and TLR4 (Chi *et al*, 2014). More recently, mechanical strain demonstrated an upregulation in IL-1 $\beta$  mRNA, alongside associated inflammasome genes NLRP3, ASC and CASP in optic nerve head derived astrocytes (Albalawi *et al*, 2017), in a process which was shown to be ATP and P2X7 dependent. Furthermore,

experiments utilising HOCR models demonstrated the application of BzATP to the retina induced a large upregulation of IL-1 $\beta$  mRNA and IL-1 $\beta$  secretion (Niyadurupola, 2009).

Microglial function has long been the focus in neuroinflammatory conditions, due to their role as immune response cells in the CNS, alongside their inflammasome related functions, including the processing and release of IL-1 $\beta$  (Liu & Quan, 2018). Having explored the effects of purinergic stimulation on intracellular Ca<sup>2+</sup> signalling and viability in resting microglia in previous chapters, this chapter aims to investigate the role of purinergic stimulation on the processing and release of IL-1 $\beta$  from resting microglia, in the hope of gaining better understanding of the relationship between purinergic signalling and IL-1 $\beta$  with regards to early stage glaucomatous pathophysiology.

## 6.2 Results

### 6.2.1 LPS priming of BV-2 microglia

The TLR-4 agonist and bacterial cell wall component lipopolysaccharide (LPS), is a known and widely used priming stimulus for IL-1 $\beta$  (Yao *et al*, 1992), and the P2X7 receptor is known to play a major role in its processing and release. Initial experiments therefore sought to replicate these findings and also use the clone-14 cells to confirm the role of P2X7 in IL-1 $\beta$  release in BV-2 cells. A series of experiments were first conducted to determine suitable conditions for using LPS as a positive priming control. To determine the suitability of time course conditions, BV-2 microglia were stimulated with LPS, and media was sampled at stimulation and after 3, 6, 12 and 24 hours for LDH assay to determine lytic cell death during the course of the experiment (Figure 6.1).

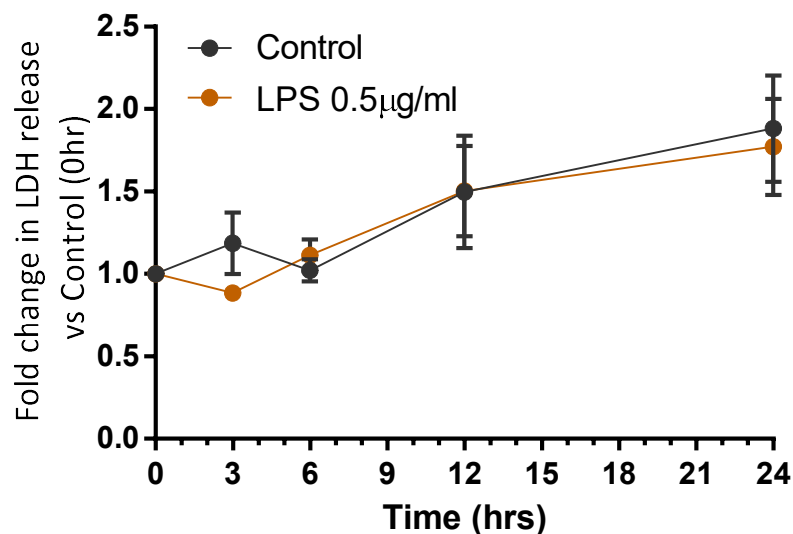


**Figure 6.1:** Fold change in LDH release from BV-2 microglia following stimulation 0.5 $\mu$ g/ml LPS, over 24 hours (n=4). Data presented as mean  $\pm$  S.E.M. \* Indicates significance (P<0.05) compared to control at equivalent time point using one-way ANOVA with Tukey's post-hoc test.

LDH release under experimental conditions demonstrated an increase in LDH release for both control and LPS stimulation, with an

approximate 2-fold increase at 24 hours. LPS stimulus did not produce any significant changes in LDH release compared to control.

As the LDH release profile demonstrated the suitability of experimental conditions, mRNA expression of IL-1 $\beta$  was assessed initially following stimulation with LPS at 3, 6, 12 and 24 hour time points using TaqMAN q-RT-PCR in BV-2 microglia (Figure 6.2 & 6.3).

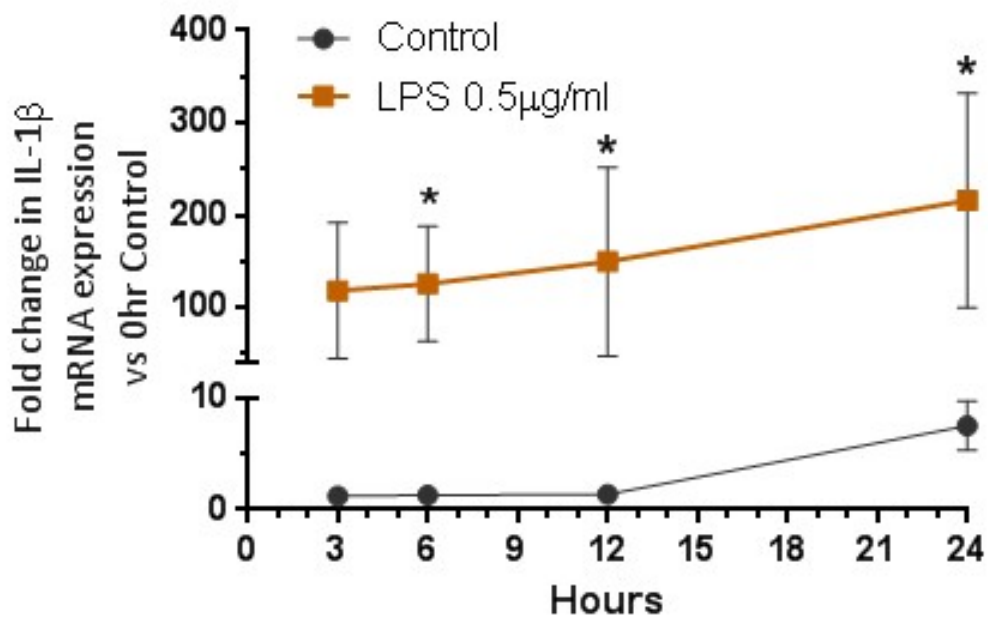


**Figure 6.2:** Fold change in IL-1 $\beta$  mRNA expression in BV-2 microglia following stimulation with 0.5 $\mu$ g/ml LPS, at various intervals over 24 hours (n=3). Data presented as mean  $\pm$  S.E.M. \* Indicates significance (P<0.05) compared to control at equivalent time point using one-way ANOVA with Dunnett's post-hoc test.

LPS treatment (0.5 $\mu$ g/ml) of BV-2 microglia induced a strong increase in IL-1 $\beta$  mRNA expression over control at every time point assessed over the 24 hour timecourse, with statistical significance at the 6-24 hour time points (Figure 6.2). The increase in expression peaked at an approximate ~200 fold increase at 24 hours, representing a significant 28-fold increase when compared to the equivalent 24 hour control sample (Figure 6.3).

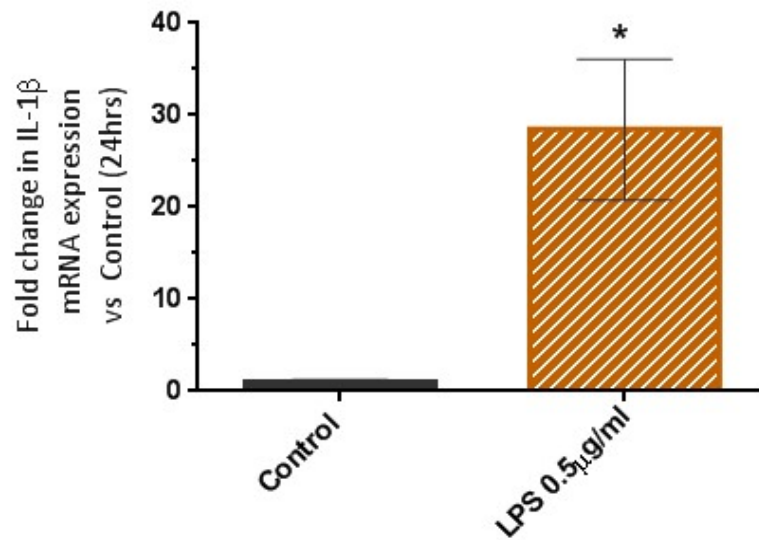


**Figure 6.3:** Fold change in IL-1 $\beta$  mRNA expression at 24 hours in BV-2 microglia following stimulation with 0.5 $\mu$ g/ml LPS (n=3). Data presented as Mean  $\pm$  S.E.M. \* Indicates significance (P<0.05) compared to control at equivalent time point using one-way ANOVA with Dunnett's post-hoc test.

Following significant upregulation of IL-1 $\beta$  mRNA with LPS treatment, the level of IL-1 $\beta$  protein was also assessed in BV-2 microglia (Figure 6.4 A) and P2X7 K/O clone-14 microglia (Figure 6.4 B). Cell lysates were collected following 4 hour LPS priming and assessed for IL-1 $\beta$  with an ELISA.

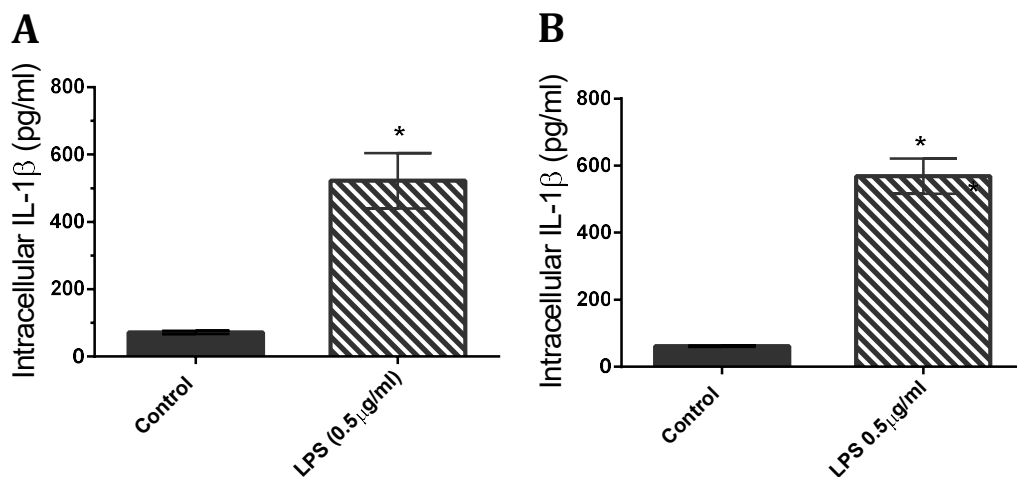


**Figure 6.4:** Intracellular IL-1 $\beta$  protein levels in (A) BV-2 microglia and (B) P2X7 K/O clone-14 microglia, following priming with 0.5 $\mu$ g/ml LPS for 4 hours (n=4). Data presented as mean  $\pm$  S.E.M. \* Indicates significance (P<0.05) compared to control using Student's T-test.

As with mRNA expression, LPS priming of BV-2 microglia induced a strong significant increase in intracellular IL-1 $\beta$  protein levels (Figure 6.4 A). This IL-1 $\beta$  protein upregulation was also demonstrated in P2X7 K/O clone-14 cells (Figure 6.4 B), indicating P2X7 is not involved in the LPS priming mechanism.

### 6.2.2 P2X7 in IL-1 $\beta$ release in BV-2 and clone-14 microglia

Due to the documented role of P2X7 in the maturation and release of IL-1 $\beta$  protein (Ferrari *et al*, 1997b; López-Castejón *et al*, 2007), P2X7-mediated IL-1 $\beta$  release was subsequently explored. IL-1 $\beta$  release from BV-2 microglia was determined by ELISA in media samples, following pretreatment/priming with LPS, followed by stimulation with ATP (3mM) to activate P2X7 (Figure 6.5).

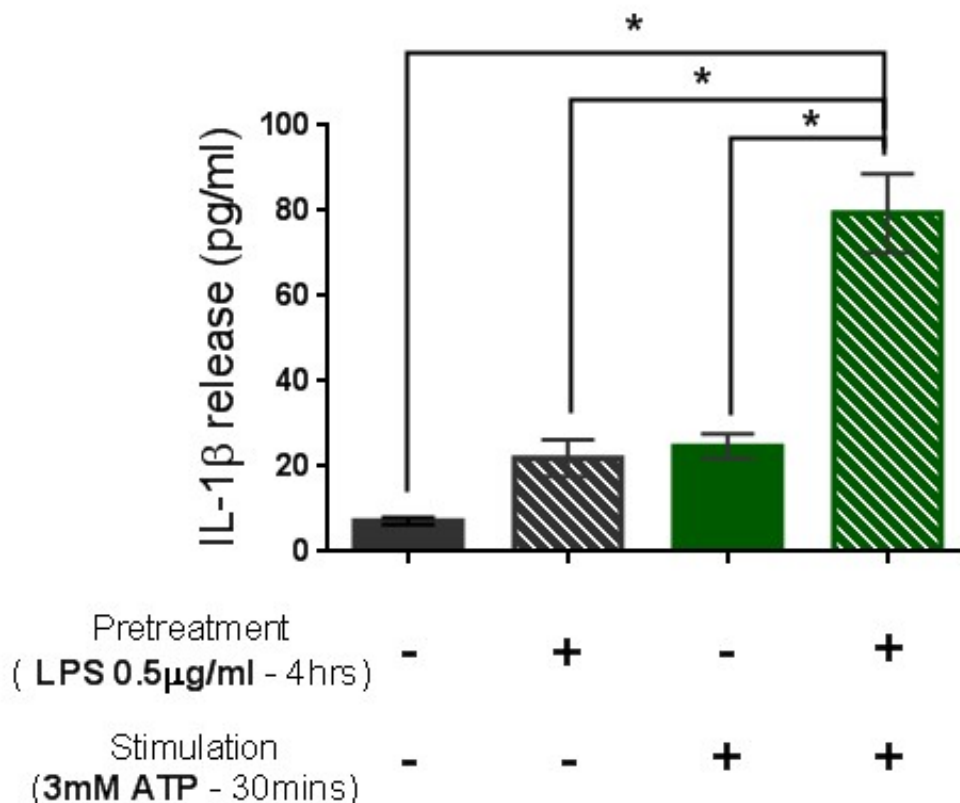


**Figure 6.5:** IL-1 $\beta$  release in BV-2 microglia following priming with 0.5 $\mu$ g/ml LPS for 4 hours, and stimulation with 3mM ATP for 30 minutes (n=4). Data presented as mean  $\pm$  S.E.M. \* Indicates significance (P<0.05) compared to control using one-way ANOVA with Tukey's post-hoc test.

Pretreatment with LPS alone or stimulation with 3mM ATP alone did not produce a significant increase in IL-1 $\beta$  protein release, whereas the combination of both conditions induced a significant increase in IL-1 $\beta$  release (Figure 6.5). To confirm the role of P2X7 in IL-1 $\beta$  release, conditions were replicated in P2X7 K/O clone-14 microglia (Figure 6.6).

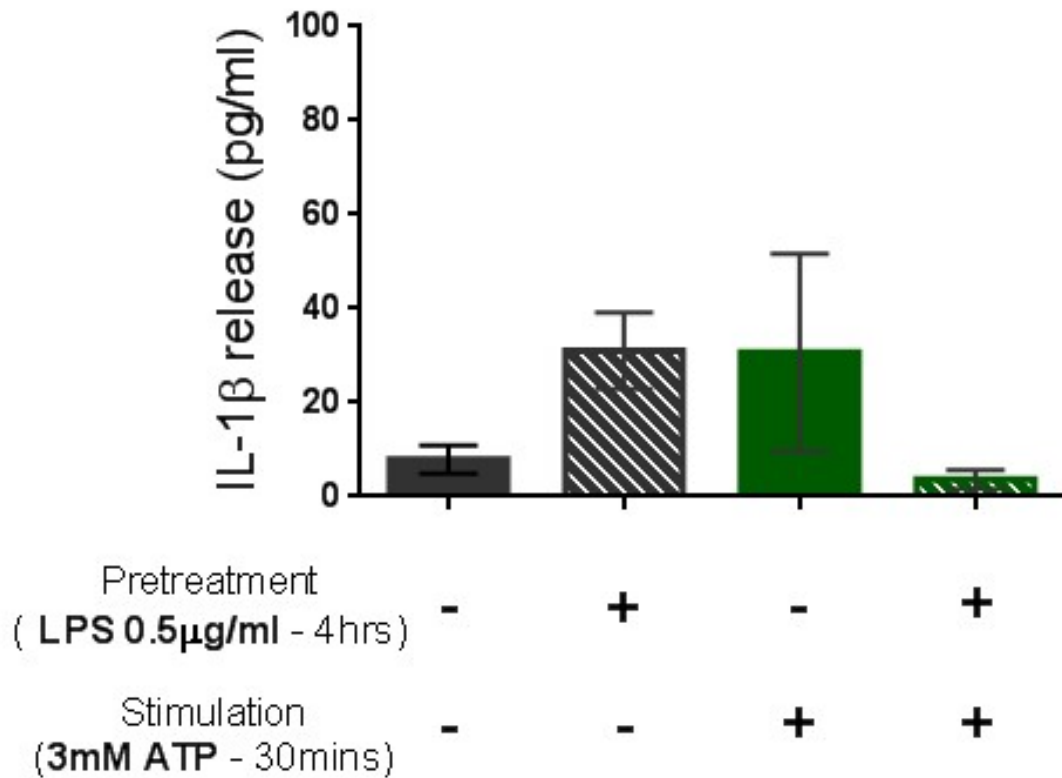
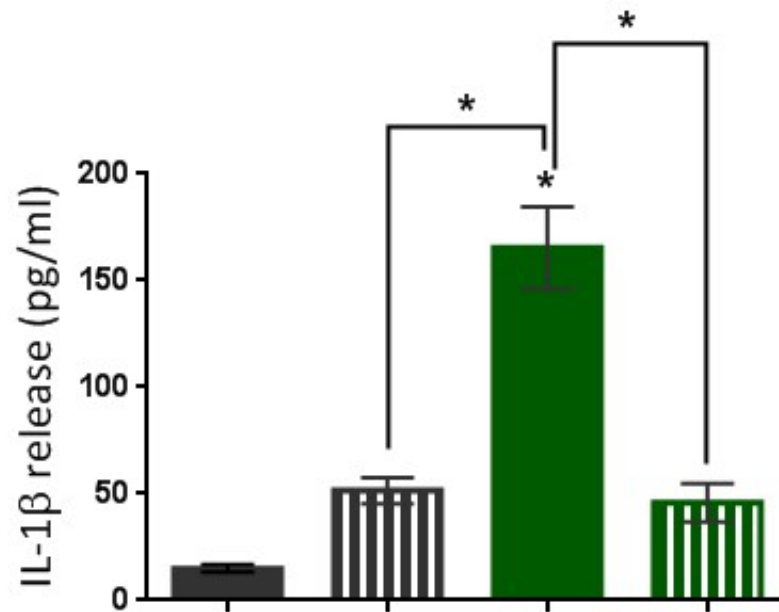


**Figure 6.6:** Intracellular IL-1 $\beta$  protein levels in P2X7 K/O clone-14 microglia following priming with 0.5 $\mu$ g/ml LPS for 4 hours, and stimulation with 3mM ATP for 30 minutes (n=4). Data presented as mean  $\pm$  S.E.M. \* Indicates significance (P<0.05) compared to control using one-way ANOVA with Tukey's post-hoc test.

In contrast to BV-2 microglia, IL-1 $\beta$  was completely abolished in P2X7 K/O clone-14 microglia (Figure 6.6), indicating ATP stimulation is acting at P2X7, which in turn mediates IL-1 $\beta$  release. Neither LPS nor ATP exhibited significant increase in IL-1 $\beta$  release in isolation.



Pretreatment ( LPS 0.5μg/ml - 4hrs)	-	+	+	+
Stimulation (3mM ATP - 30mins)	-	-	+	+
Antagonism (10μM AZ10606120)	-	-	-	+

**Figure 6.7:** Extracellular IL-1β release in BV-2 microglia following priming with 0.5μg/ml LPS for 4 hours, and stimulation with 3mM ATP for 30 minutes, in the presence or absence of 10μM AZ10606120 (n=4). Data presented as mean ± S.E.M. \* Indicates significance (P<0.05) compared to control using one-way ANOVA with Tukey's post-hoc

As further confirmation for the role of P2X7 in IL-1β release, The P2X7 antagonist AZ10606120 was used (Figure 6.7). AZ10606120 significantly inhibited release of IL-1β from LPS primed/ATP stimulated BV-2 cells.

### 6.2.3 Purinergic priming of BV-2 microglia

Despite LPS acting as a strong priming stimulus and positive control for IL-1 $\beta$  upregulation, LPS modelling glaucomatous pathophysiology cannot be considered appropriate as there is no evidence for such a pathogenic involvement. However, changes in extracellular ATP concentrations have been demonstrated with glaucoma (Zhang *et al*, 2007) and under experimental glaucoma conditions (Reigada *et al*, 2008). Furthermore, BzATP induces IL-1 $\beta$  expression and release in human retina in the absence of any other priming stimulus (Niyadurupola, 2009). Based on this, the role of purinergic agonists as priming stimulus for microglial IL-1 $\beta$  production and release were investigated. Expression of IL-1 $\beta$  mRNA was assessed following stimulation with ATP (300 $\mu$ M) and BzATP (30 $\mu$ M) at 3, 6, 12 and 24 hour time points using TaqMAN q-RTPCR in BV-2 microglia (Figure 6.8).

ATP and BzATP stimulation of BV-2 microglia demonstrated dissimilar patterns of IL-1 $\beta$  mRNA induction (Figure 6.8 A & B). BzATP stimulation demonstrated no significant changes in IL-1 $\beta$  expression compared to control at any time point. In contrast, ATP stimulation demonstrated a substantial increase in IL-1 $\beta$  expression compared to control, beginning with a small non-significant rise at 12 hours, before a more pronounced ~30 fold increase at 24 hours (Figure 6.8 A). When adjusted against the equivalent 24 hour time point control expression value, ATP demonstrated a significant 4.5 fold increase in IL-1 $\beta$  (Figure 6.8 B).

The difference in activity of ATP and BzATP in causing IL-1 $\beta$  upregulation suggests that the effect may not be mediated by the P2X7R. To confirm this, ATP and BzATP stimulation conditions were replicated in P2X7 K/O clone-14 cells, and IL-1 $\beta$  mRNA was assessed at 24 hours using TaqMAN q-RTPCR (Figure 6.9).

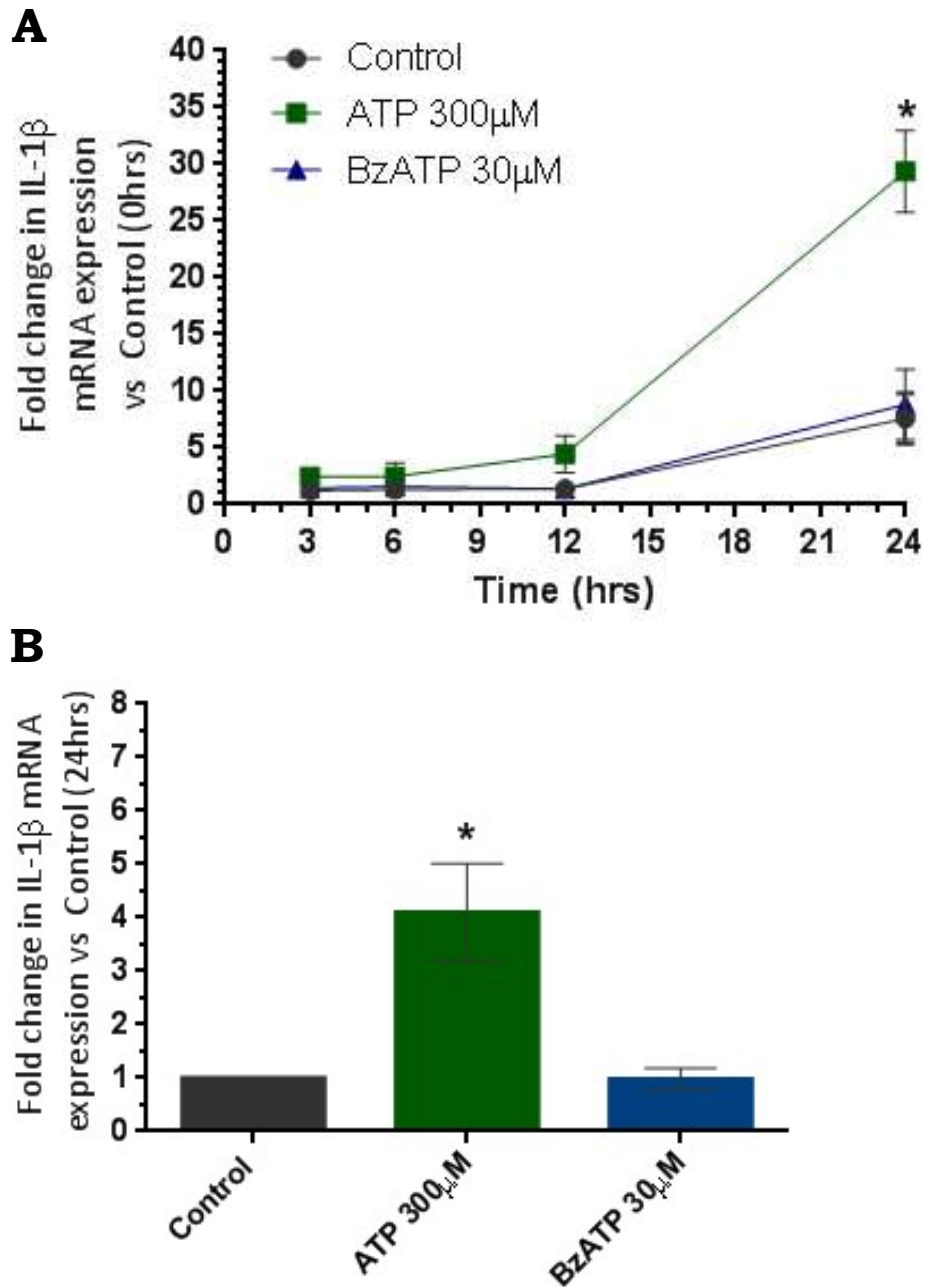


**Figure 6.8: A** Fold change in IL-1 $\beta$  mRNA expression in BV-2 microglia following stimulation with 300 $\mu$ M ATP or 30 $\mu$ M BzATP, over 24 hours (n=4). **B** Mean fold change in IL-1 $\beta$  mRNA expression in BV-2 microglia following stimulation with 300 $\mu$ M ATP or 30 $\mu$ M BzATP for 24 hours (n=4). Data presented as mean  $\pm$  S.E.M \* Indicates significance (P<0.05) compared to control at equivalent time point using one-way ANOVA with Dunnett's post-hoc test.

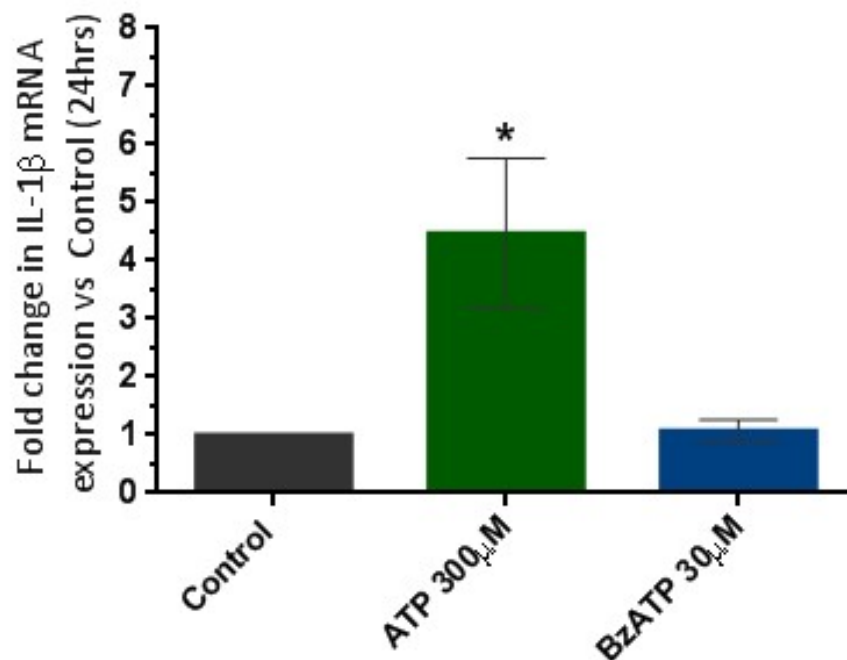


**Figure 6.9:** Fold change in IL-1 $\beta$  mRNA expression in clone-14 microglia following stimulation with 300 $\mu$ M ATP or 30 $\mu$ M BzATP for 24 hours (n=4). Data presented as mean  $\pm$  S.E.M. \* Indicates significance (P<0.05) compared to control at equivalent time point using one-way ANOVA with Dunnett's post-hoc test

Stimulation of P2X7 K/O clone-14 microglia with the purinergic agonists demonstrated a near identical outcome to that seen in BV-2 cells, whereby BzATP failed to elicit any significant changes in IL-1 $\beta$  mRNA expression, however ATP stimulation caused a significant ~4 fold upregulation of IL-1 $\beta$  (Figure 6.9).

Furthermore, AZ10606120 was unable to inhibit the upregulation seen with 300 $\mu$ M ATP (Figure 6.10). The lack of inhibition by AZ10606120, or in P2X7 K/O clone-14 microglia indicates P2X7 is not involved in the ATP mediated upregulation of IL-1 $\beta$  mRNA.

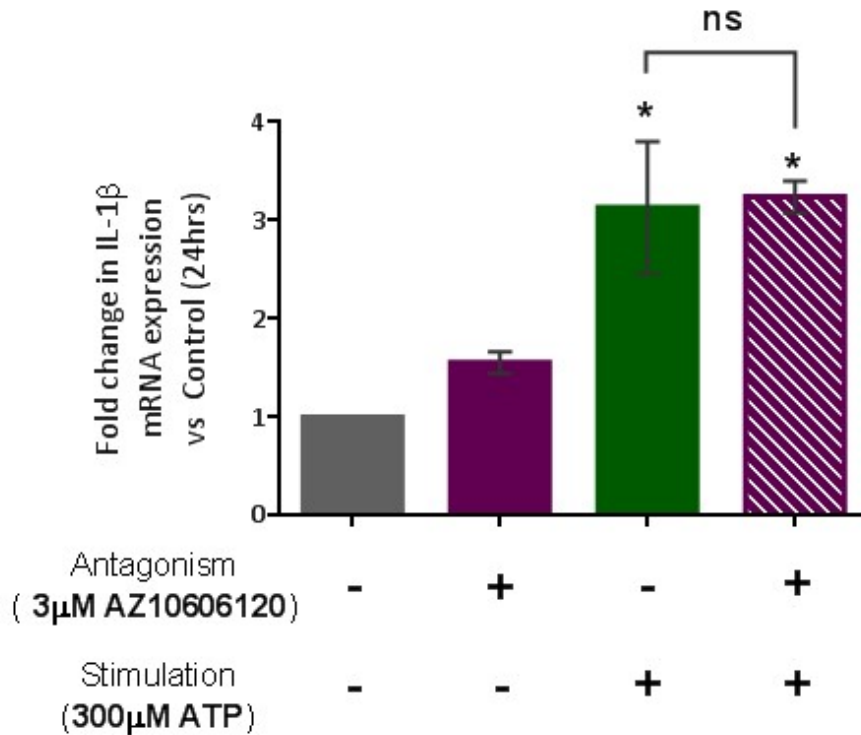


**Figure 6.10:** Fold change in IL-1 $\beta$  mRNA expression in BV-2 microglia following stimulation with 300 $\mu$ M ATP in the presence or absence of 3 $\mu$ M AZ10606120 after 24 hours (n=3). Data presented as mean  $\pm$  S.E.M. \* Indicates significance (P<0.05) compared to control using one-way ANOVA with Tukey's post-hoc test.

With the evidence that moderate ATP (300 $\mu$ M) stimulation can induce upregulation of IL-1 $\beta$  (Figure 6.4), the effect of long term ATP stimulation on IL-1 $\beta$  mature protein production and release in BV-2 microglia was assessed. Due to the longer incubation required for significant IL-1 $\beta$  upregulation with ATP compared to LPS priming, pre-treatment with ATP was extended to 24 hours, with intracellular (Figure 6.11) and release (Figure 6.12) measured from cell lysates and media samples respectively.

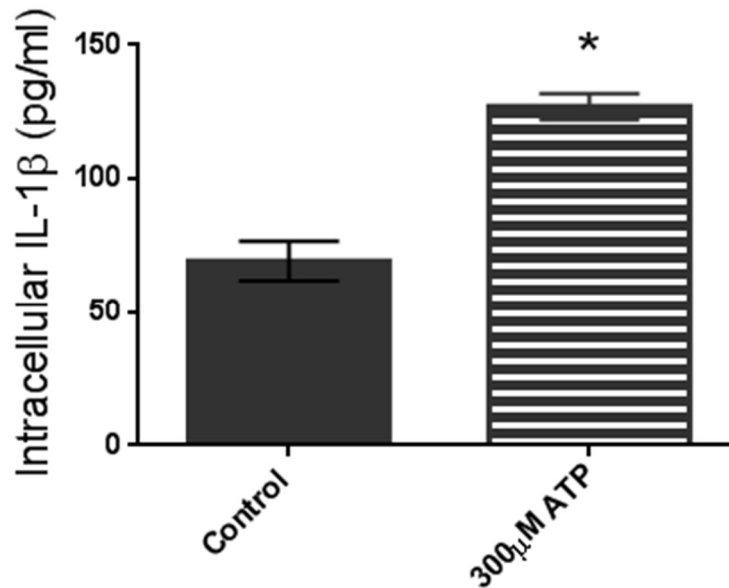


**Figure 6.11:** Intracellular IL-1 $\beta$  protein levels in BV-2 microglia following priming with 300 $\mu$ M ATP for 24 hours (n=3). Data presented as mean  $\pm$  S.E.M. \* Indicates significance (P<0.05) compared to control using one way ANOVA with Tukey's post hoc test.

Following 24 hour ATP priming, BV-2 microglia demonstrated a moderate significant increase in IL-1 $\beta$  protein levels (Figure 6.11), albeit at a lower magnitude compared to LPS priming. Stimulation of P2X7 with elevated ATP (3mM) induced a significant release of IL-1 $\beta$  from ATP primed BV-2 microglia (Figure 6.12), which like intracellular protein levels, was at a lower magnitude compared to LPS priming/P2X7 stimulation.

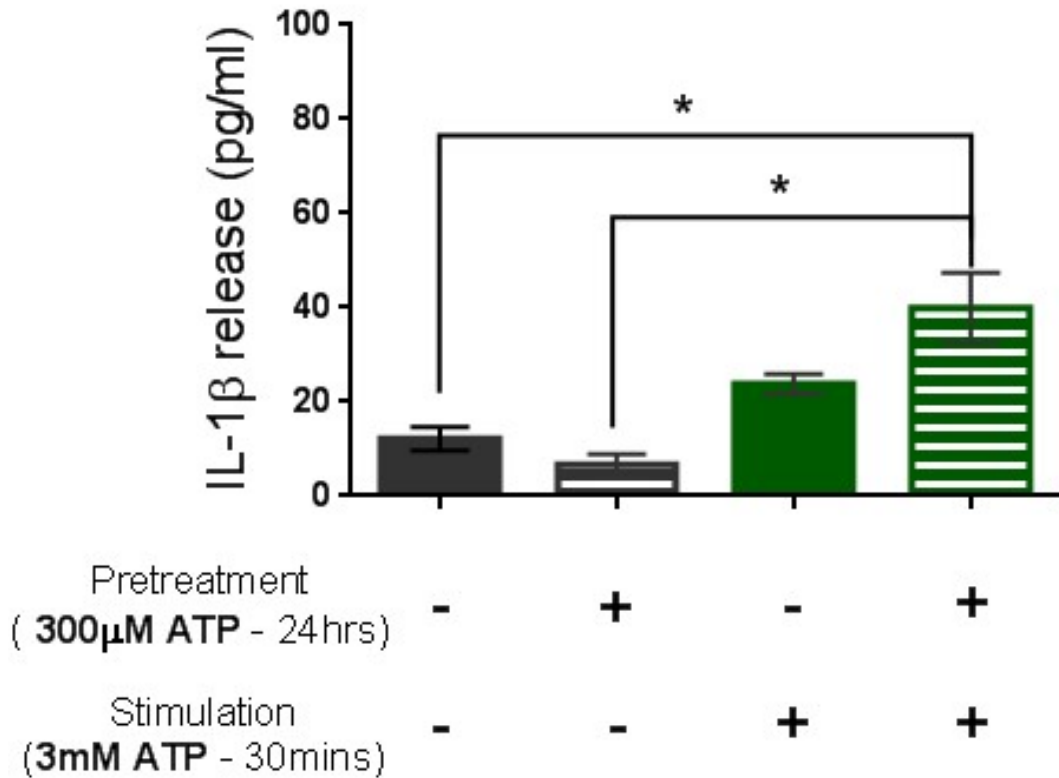


**Figure 6.12:** Extracellular IL-1 $\beta$  protein release in BV-2 microglia after priming with 300 $\mu$ M ATP for 24 hours, followed by 3mM ATP stimulation for 30 minutes (n=3). Data presented as S.E.M. \* Indicates significance (P<0.05) compared to control using one-way ANOVA with Tukey's post hoc test.

### 6.3 Discussion

Several studies have shown a potential link between the inflammatory cytokine IL-1 $\beta$  and glaucomatous pathophysiology (Hangai *et al*, 1995; Yoneda *et al*, 2001; Zhang & Chintala, 2004; Chi *et al*, 2014; Albalawi *et al*, 2017). As such, the role of microglial processing and release of IL-1 $\beta$  and a potential link with purinergic signalling was explored.

Initial experiments in this chapter monitored LDH release following LPS priming conditions over 24 hours, with the aim to determine suitable experimental conditions for the subsequent investigation of IL-1 $\beta$  i.e. conditions that did not induce cell death. This was confirmed, therefore, LPS-induced IL-1 $\beta$  expression and release could be investigated. LPS exhibited a robust upregulation of IL-1 $\beta$  mRNA in BV-2 cells at every time point sampled. The role of the bacterial cell wall component LPS as an inducer of microglial activation with corresponding IL-1 upregulation is well documented (Lund *et al*, 2006) and is subsequently widely employed as positive control (Hoogland *et al*, 2015). As a positive control, the LPS/TLR-4 pathway to IL-1 $\beta$  upregulation has been extensively studied, shown to be reliant on a cascade of intracellular adaptor proteins including MyD88, with the eventual translocation of active NF- $\kappa$ B to the nucleus (Lu *et al*, 2008). The strong response of BV-2 microglia to LPS stimulation in these experiments is therefore unsurprising, but helps to demonstrate the suitability of BV-2 microglia as a model for studying IL-1 $\beta$  processing further. Following investigations of IL-1 $\beta$  on an mRNA level, the subsequent mature protein production and processing functions in microglia were explored. LPS demonstrated significant increases in intracellular IL-1 $\beta$  protein levels (Figure 6.4 A) that were not dependent on the presence of P2X7 (Figure 6.4 B).

Before accumulated IL-1 $\beta$  protein is released, it requires enzymatic processing by an inflammasome complex, the formation of which is

dependent on additional factors. P2X7R stimulation has been well documented as a potent inducer of the oligomerization of the canonical NLRP3 inflammasome (Mariathasan *et al*, 2006; Di Virgilio, 2007; Lister *et al*, 2007), and direct stimulation of microglial P2X7 has demonstrated IL-1 $\beta$  release (Sanz & Di Virgilio, 2000; Brough *et al*, 2002), as well as in other mononuclear phagocytes (Hogquist *et al*, 1991b). To determine P2X7-mediated IL-1 $\beta$  release under our experimental conditions, experiments were replicated utilising antagonism with AZ10606120 and P2X7 K/O clone-14 microglia. ATP (3mM) caused significant release of IL-1 $\beta$  in LPS-primed BV-2 cells (Figure 6.5). Both P2X7R K/O (Figure 6.6) and pharmacological antagonism (Figure 6.7) significantly abrogated ATP-mediated IL-1 $\beta$  protein release in LPS primed cells, validating the role of P2X7 in microglial inflammasome oligomerization and the processing and release of IL-1 $\beta$ .

Despite LPS being a useful positive control for IL-1 $\beta$  upregulation, its use in models simulating glaucomatous conditions isn't particularly appropriate as it is not a pathogenic component of glaucoma. There are however increases in purinergic release demonstrated in glaucomatous eyes (Zhang *et al*, 2007) and under simulated glaucomatous conditions *in vivo* (Lu *et al*, 2015). Therefore, the role of purinergic agonists as DAMPs was explored, in their ability to act as priming and release stimuli in BV-2 microglia

Purinergic stimulation of BV-2 cells presented a vastly different pattern of IL-1 $\beta$  mRNA expression over the experimental timecourse compared to LPS (Figure 6.8). ATP stimulation was effective in upregulating IL-1 $\beta$  mRNA, however at a much lower magnitude than with LPS, and only after substantial delay, with significant upregulation over control only after 24 hours (Figure 6.8). Additionally, BzATP stimulation was insufficient in upregulating IL-1 $\beta$  mRNA expression at any time point sampled. The discrepancies in response magnitude and induction time

between LPS and ATP may suggest a different mechanistic pathway of induction is occurring with the two agonists.

Compared to the LPS/TLR-4 pathway, there are relatively few reported instances of purinergic stimulation inducing IL-1 $\beta$  upregulation. In fact studies have found that ATP is ineffective as a priming stimulus in glial cultures (Savage *et al*, 2012). Despite this, it has been shown that direct intravitreal injection of BzATP led to IL-1 $\beta$  upregulation in mouse retinas after 24 hours (Albalawi *et al*, 2017) in a mechanism that implicated the involvement of the P2X7R and NF- $\kappa$ B. Similarly, BzATP application to human retinal cultures also induced a significant mRNA upregulation as well as release of IL-1 $\beta$  protein (Niyadurupola, 2009). The magnitude of IL-1 $\beta$  upregulation in these studies was also much more comparable to the effects of ATP stimulation in BV-2 cells (Figure 6.8).

Under the experimental conditions for these experiments, BzATP was not sufficient to induce IL-1 $\beta$  upregulation. This is contradictory to the previously described studies (Niyadurupola, 2009; Albalawi *et al*, 2017), however a number of differences in experimental design may explain this discrepancy. Firstly, the concentration of BzATP used (30 $\mu$ M) is far below that utilised in the aforementioned studies (100 $\mu$ M and 250 $\mu$ M respectively), however this concentration was chosen as it was shown to be sufficient to activate P2X7 in both Ca<sup>2+</sup> (Figure 4.4) and viability assays (Figure 5.6). Furthermore, pharmacokinetic considerations of intravitreal injection would render much lower final concentrations at the intended site of action, than that administered due to the use of an intact organ system. Additionally, due to the use of an organ/tissue system, it is unclear which cell types are responsible for the IL-1 $\beta$  upregulation, with multiple contenders alongside microglia, such as astrocytes and Müller cells.

Following these experiments, the novel role of ATP as an inducer of IL-1 $\beta$  mRNA expression was further explored in relation to IL-1 $\beta$  at the protein level. Due to the longer timescale required for intermediate ATP to upregulate IL-1 $\beta$  mRNA, priming with intermediate ATP concentrations was extended to a 24 hour incubation, but the same ATP release stimulus conditions were retained (Figures 6.5 & 6.6). In a similar manner to mRNA expression, intermediate ATP priming of BV-2 cells demonstrated a significant upregulation of intracellular IL-1 $\beta$  protein levels (Figure 6.11), but at a level that was much less than seen with LPS priming. These results demonstrate for the first time that long term ATP stimulation can act as a sufficient, albeit relatively weak, priming agent in microglia, in comparison with traditional agents such as LPS, zymosan or polyinosinic:polycytidylic acid (Poly(I:C)) (Facci *et al*, 2014). Use of alternative sterile DAMPs as priming agents, such as TNF- $\alpha$  has also shown induction of IL-1 $\beta$  in macrophages, at a lower magnitude than with LPS induction (Bezbradica *et al*, 2017).

In order to clarify the potential role for P2X7R in the ATP mediated upregulation of IL-1 $\beta$ , a combination of P2X7R K/O clone-14 microglia and pharmacological antagonism with AZ10606120 were subsequently explored (Figures 6.9 & 6.10). Both methods explored failed to block the ATP mediated IL-1 $\beta$  upregulation, which in combination with the aforementioned BzATP data, indicates the P2X7 is not involved. Due to the concentration of ATP (300 $\mu$ M), as well as the ability for ligand degradation to produce related compounds such as ADP and adenosine, and the expression of various purinergic receptors on BV-2 microglia (Table 3.5), there could be multiple receptor candidates responsible for the observed IL-1 $\beta$  upregulation and determining the exact signalling pathway resulting from ATP priming remains difficult, however using results from this and previous chapters combined with data reported in the literature, it can be speculated upon.

Previously, 300 $\mu$ M concentrations of ATP and ADP were shown to cause partial population death of BV-2 microglia over a long-term 24-hour timecourse (Figure 5.1 & 5.14), which in combination with the requirement for similar length incubation for ATP mediated IL-1 $\beta$  priming suggests a link between the two outcomes. As the precise purinergic receptor subtype receptor dictating this intermediate cytotoxicity remains elusive, screening with the use of more potent and selective pharmacological agonists/antagonists would prove difficult due to the sensitivity of BV-2 microglia, however the use of ADP may provide further insight. Additionally, the presence of apoptotic bodies and cell debris resulting from intermediate ATP stimulation, may act as an inducer of IL-1 $\beta$  upregulation in surrounding microglia in an indirect paracrine manner. Regardless of the pathway responsible, the demonstration that ATP acts as a priming agent has potential implications for the pathophysiological progression of glaucoma.

## Chapter 7

P2X7 role in viability and IL-1 $\beta$  regulation in simulated oxygen glucose deprived (OGD) microglia

### 7.1 Introduction

Whilst elevated IOP is an established risk factor for glaucoma pathophysiology, the prevalence of normotensive glaucoma indicates the potential for additional pathogenic mechanisms in the development of glaucoma. Per weight, the retina is the most oxygen demanding tissue in the human body (Ames, 1992), and as such requires a constant supply of both oxygen and glucose via retinal vasculature to maintain functional homeostasis. Abnormalities in both retinal and optic nerve head blood flow in glaucoma have previously been reported (Kerr *et al*, 1998; Fuchsjager-Mayrl *et al*, 2004), including reduced ocular blood flow in both high and NTG patients (Hamard *et al*, 1994). Furthermore, vasospastic conditions have been found to predispose to glaucoma (Broadway & Drance, 1998). Oxygen glucose deprivation (OGD) resulting from reduced ocular blood flow is therefore established possible mechanism in glaucoma development (Mozaffarieh *et al*, 2008).

Links between OGD and altered purinergic signalling have previously been shown, including extracellular  $\gamma$  release following ischaemia in the brain (Cavaliere *et al*, 2004; Cavaliere *et al*, 2007; Arbeloa *et al*, 2012), from optic nerve oligodendrocytes via pannexin hemichannels (Domercq *et al*, 2010) and from RPE cells following chemically induced ischaemia (Reigada & Mitchell, 2005), suggesting multiple sources exist for retinal release under ischaemic conditions. In the retina, OGD/ischaemia and purinergic signalling have been explored with particular focus on RGC cell death. Simulated ischaemia has been

shown to induce death of RGCs in human organotypic retinal cultures (HORCs) (Niyadurupola *et al*, 2011). Furthermore, with HORCs, this loss in RGCs was prevented following P2X7R antagonism (Niyadurupola *et al*, 2013). Similarly, P2X7R mediation of hypoxia-induced retinal neuronal cell death has been demonstrated in rat tissue (Sugiyama *et al*, 2010).

Whilst there is evidence that retinal ATP may act directly on RGCs via P2X7 to induce cell death, fewer studies have explored the effects of simulated OGD on surrounding retinal support cells such as astrocytes, Müller cells and microglia, regarding their ability to respond and influence the overall outcome. Both cultured Müller cells (Aldarwesh, 2015) and primary astrocytes (Schmid-Brunclik *et al*, 2008) have exhibited both cytotoxicity and proliferation following OGD stimulation. Studies of microglia including cultured cells (Lyons & Kettenmann, 1998; Yenari & Giffard, 2001) and tissue preparations (Eyo & Dailey, 2012) have demonstrated cytotoxic susceptibility under ischaemic conditions, which in at least one case was mediated by P2X7R activity (Eyo *et al*, 2013). Furthermore, ischaemic stimulation of microglia has been shown to induce an M2 like phenotype and promote tissue and vascular remodelling (Perego *et al*, 2011; Hu *et al*, 2012). Despite this, there is still much information yet to be elucidated about the role of microglia in response to ischaemia, and due to the lack of clear understanding on the effects of OGD-mediated purinergic signalling on microglia, further exploration of these processes is required. This chapter aims to investigate the effects of OGD simulated ischaemia on BV-2 microglial viability and inflammatory/cytokine response to gain better understanding of the potential role for retinal microglia following ischaemic insult.

## 7.2 Results

### 7.2.1 OGD stimulated MTS viability and LDH release in BV-2 microglia

Preliminary investigations probed the effects of complete OGD treatment on cell viability (Figure 7.1A) and LDH release (Figure 7.1B) in BV-2 microglia at various time points over 24 hours.

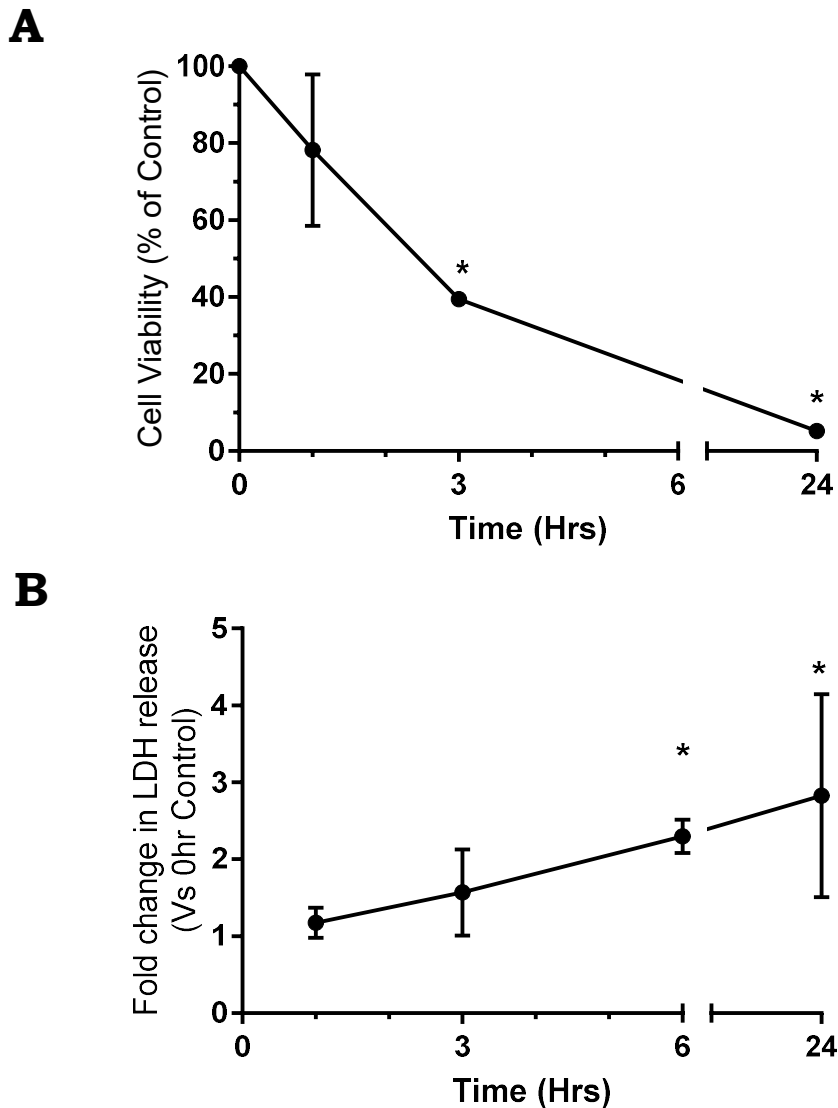


**Figure 7.1:** Cell viability as % percentage of control (**A**) and fold change in LDH release (**B**) from BV-2 microglia at various time points over 24 hours under complete OGD (n=3). Data presented as mean  $\pm$  S.E.M. \* indicates significance ( $P < 0.05$ ) over 0hr control using one-way ANOVA with Dunnett's post hoc test

BV-2 cells demonstrated both a time dependent decrease in cell viability and increase in LDH release under complete OGD conditions (Figure 7.1). At the earliest time point investigated of 1 hour, complete OGD was insufficient to induce a significant change in LDH release or cell viability, however a significant reduction in viability of approximate 60% was exhibited at 3 hours, and preceded the first instance of significant LDH release which was observed at 6 hours. By 24 hours there was a near total loss of cell viability alongside an approximate 2.5-fold increase in LDH release, which closely resembled the effects of 3-5mM ATP stimulation in BV-2 cells demonstrated in previous experiments (Figures 5.1 & 5.2).

### 7.2.2 MTS viability in BV-2 and Clone-14 microglia following 3hr OGD stimulation

The role of P2X7 in OGD mediated cytotoxicity was then investigated. Viability in P2X7 K/O clone-14 cells alongside BV-2 microglia was assessed by MTS assay following complete OGD conditions for 3 hours.

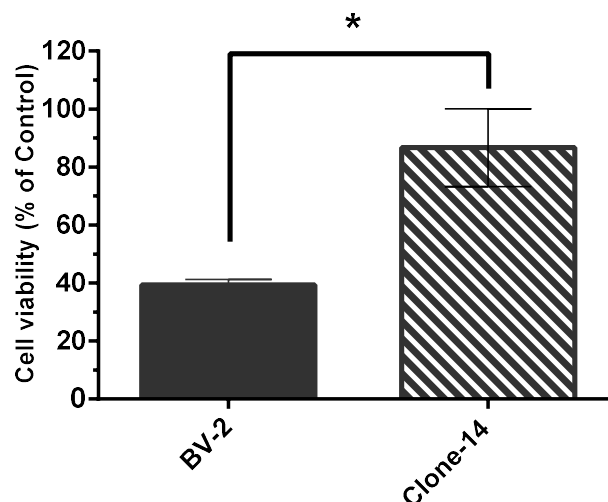


**Figure 7.2:** Cell viability of BV-2 microglia and P2X7 K/O clone-14 microglia following complete OGD for 3 hours (n=3). Data presented as mean  $\pm$  S.E.M. \* indicates significance ( $P < 0.05$ ) using Student's T-test.

In contrast to the significant reduction of cell viability in BV-2 microglia, P2X7 deficient clone-14 microglia showed no significant

decrease in viability in response to complete OGD. The results implicate P2X7 activity in OGD mediated cytotoxicity of microglia.

### 7.2.3 IL-1 $\beta$ mRNA expression in BV-2 microglia following 3 hours of complete OGD

Following the demonstrated effects of OGD on viability, expression of IL-1 $\beta$  following complete OGD was explored in BV-2 microglia (Figure 7.3).

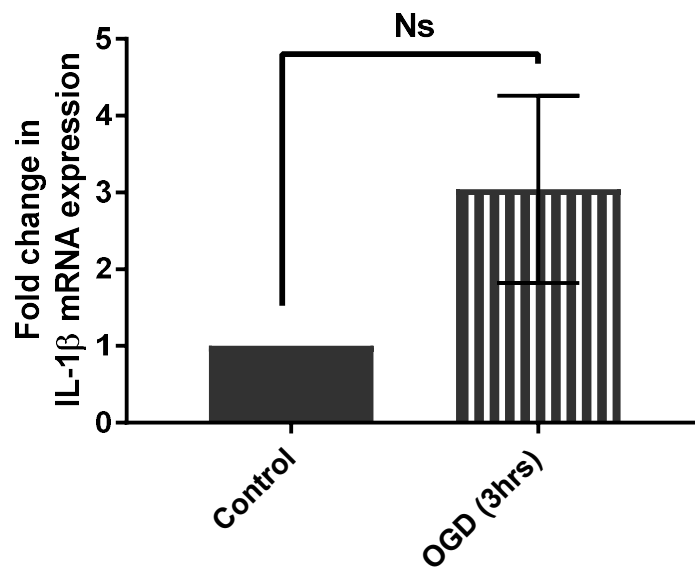


**Figure 7.3:** Fold change in IL-1 $\beta$  mRNA expression over control in microglia following complete OGD for 3 hours (n=3). Error bars represent S.E.M. \* indicates significance (P<0.05) using Student's T-test

Despite a moderate increase in IL-1 $\beta$  mRNA expression following OGD, due to high variability this observed effect was not found to be significant.

### 7.3 Discussion

The results presented in this chapter have demonstrated the cytotoxicity of BV-2 microglia to complete OGD conditions. This cytotoxicity was demonstrated primarily by a dramatic time-dependent decrease in MTS viability and increase in extracellular LDH release, detectable from as early as 3 and 6 hours respectively. Due to similarities in viability and LDH release profiles of BV-2 cells under complete OGD for 24 hours, to that with 3-5mM stimulated ATP, the role of P2X7 in OGD stimulated cytotoxicity of BV-2 microglia was explored. For this, P2X7 K/O clone-14 cells were subject to identical conditions for 3 hours, which in comparison to BV-2 cells demonstrated a significant protective effect. Despite these cytotoxic changes, 3hr OGD was insufficient to significantly up-regulate IL-1 $\beta$  mRNA.

OGD mediated viability/cytotoxicity has been explored in primary microglia, whereby total OGD induced a biphasic response consisting of a mildly proliferative effect from 15-30 minutes, followed by a cytotoxic effect with longer OGD stimulation (Kong *et al*, 2014). Similarly, hypoxic conditions have demonstrated the induction of autophagic cell death in primary microglia in a time dependent manner (Yang *et al*, 2015b). Cytotoxicity under OGD conditions has also been explored in BV-2 microglia (Eyo *et al*, 2013), whereby induction of cell death occurred with 4-6 hours of complete OGD treatment, which more closely resembles the data demonstrated in this chapter. This loss of cell viability was also shown to be dependent on both extracellular Ca<sup>2+</sup> and P2X7 receptor activity, as depletion of extracellular Ca<sup>2+</sup> or pharmacological blockade with BBG demonstrated significant protection. The combination of these findings suggests that one potential mechanism for microglial cytotoxicity under OGD conditions involves the release of high concentrations of eATP from microglial cells themselves. Release of ATP has been

previously shown under OGD conditions in hippocampal slices (Juranyi *et al*, 1999; Frenguelli *et al*, 2007), however as these preparations utilised whole tissue samples it is difficult to determine the source of extracellular ATP as other cell types such as Müller cells and astrocytes may also contribute. Released eATP could in turn act as an autocrine signalling mechanism to stimulate microglial P2X7 causing an influx of Ca<sup>2+</sup> ions, causing an intracellular signalling cascade resulting in cell death. However, more experimental data is needed to confirm this theory, which could include the use of luciferase assays to determine extracellular ATP release from BV-2 microglia, as well as the use of pharmacological antagonists of various intracellular signalling cascades to determine the cell death signalling pathway.

Another factor to consider is that only conditions of complete OGD were explored in this chapter, and it is unknown whether withdrawal of oxygen or glucose regulates the cytotoxic effect, or whether the combination withdrawal of both is required. It has been previously shown in Müller cells that glucose, but not O<sub>2</sub>, is necessary for survival (Aldarwesh, 2015). Glucose is a critical metabolic energy source for microglial cells, which express the glucose transporter Glut 5 (Payne *et al*, 1997), and primary cultured microglia have been shown to undergo drastic cell death from 30-48 hours in the absence of glucose (Yenari & Giffard, 2001), showing that glucose supply is essential for microglial survival.

However, a complete oxygen glucose deprivation event for any extended period of time would be highly unlikely and would not be expected in glaucoma. More likely would be partial or transient OGD resulting from retinal hypoperfusion following vasospastic events. Or a decrease in the perfusion pressure as a result of raised IOP Future investigation with partial, transient or repeated OGD deprivation insults may more accurately reflect predicted changes during glaucoma pathophysiology.

## Chapter 8

### General Discussion

Microglia express a multitude of purinergic family receptors, and as such, a number of key microglial functions are reported to be regulated by purinergic receptor activity (Sperlágh & Illes, 2007). Alterations in purinergic signalling homeostasis have also been reported in both patient studies and in vitro models of glaucomatous neurodegeneration (Zhang *et al*, 2007; Lu *et al*, 2015). The research presented in this thesis aimed to explore the effect of purinergic signalling on multiple functions in resting microglial cells, such as intracellular calcium signalling, proliferation and cytotoxicity, and the processing and release of the inflammatory cytokine IL-1 $\beta$ , in order to gain better insight into the role of microglial activation in the early pathophysiological stages of glaucoma.

In many ways, the P2X7 receptor is perhaps the most unique purinergic subtype and is therefore the focus of a great deal of research, including in relation to both microglia (Calovi *et al*, 2019) and neurodegenerative diseases such as glaucoma (Takenouchi *et al*, 2010; Sanderson *et al*, 2014). In anticipation of exploring the functional role of P2X7 in this thesis, initial experiments focused on the generation of a P2X7 receptor knockout microglial cell line, using CRISPR mediated gene editing on the well-established BV-2 immortalised cell line. The use of receptor knockout models when studying receptor function present various advantages over alternative methods, such as pharmacological antagonism, due to the elimination of non-selective action at similar receptor subtypes, and the more complete and longevity of alteration in comparison with interference based techniques such as siRNA.

Despite the documented difficulties of transfection in microglial cells (Carrillo-Jimenez *et al*, 2018), early experiments optimised a set of conditions that demonstrated successful transfection of BV-2 microglia. Transfection followed by selection processes generated a number of individual colonies with unique and theoretically homogenous genetic ablation of P2X7. Due to time constraints, only one of the generated colonies that demonstrated early signs of P2X7 K/O, clone-14, was carried forward for further analysis of P2X7R presence and function, however the alternate colonies were stored for potential future analysis and characterisation at a future date if needed.

Further characterisation assays probed the extent of P2X7 K/O in clone-14 cells whereby cell surface or intracellular P2X7 protein was not detected. Interestingly, despite the absence of P2X7R at the protein level, mRNA transcript signal was still present and recognised by the qRT-PCR primer pair. Although unusual, this is not unheard with reports of mRNA transcripts in CRISPR targeted knockout proteins still present in the literature (Dabrowska *et al*, 2018). Additional evidence for the knockout of functional P2X7 in clone-14 microglia was also established in following experiments, where absence of P2X7 abolished several characteristic functions, including the loss of sustained elevated intracellular calcium signalling, lack of extensive cytotoxicity following elevated ATP stimulation, and the loss of IL-1 $\beta$  release in primed microglia. The successful knockout of P2X7 from BV-2 microglia represents a powerful tool for the investigation of P2X7 mediated functions in microglia.

Although purinergic receptor mediated intracellular Ca<sup>2+</sup> signalling has been explored in multiple in vivo tissues and cell lines, microglial responses, particularly in the BV-2 model are less well reported. Fundamental differences in BV-2 microglia Ca<sup>2+</sup> signalling may exist in comparison with reported models such as macrophages and HEK over-

expression systems. Resting microglia demonstrated a dynamic intracellular  $\text{Ca}^{2+}$  signalling response following purinergic stimulation, which was shown to be dependent on the contribution of multiple P2 receptor subtypes.

ATP stimulation at elevated concentrations demonstrated a multi-component  $\text{Ca}^{2+}$  response, whereby P2X7 was shown to be responsible for a later sustained phase response, which was similar to previously reported P2X7  $\text{Ca}^{2+}$  responses in primary cultured microglia (Shieh *et al*, 2014). The remaining initial peak phase response at lower ATP concentrations was mediated predominantly by P2X4, although P2Y2 activation may also contribute, due to the efficacy of AR-C118925XX antagonism of UTP responses. In contrast, ADP mediated  $\text{Ca}^{2+}$  responses in resting microglia was similar to the peak phase response following ATP stimulation, and was found to be predominantly P2Y6 mediated. Additional purine nucleotide responses were not explored, so require further investigation. Extrapolating these results to glaucomatous pathophysiology suggests that retinal microglial purinergic-mediated  $\text{Ca}^{2+}$  responses and subsequent intracellular signalling, are heavily dependent on the availability of purinergic ligands in the extracellular milieu. Furthermore, proximity to regions of ATP release, may be crucial in terms of resting microglial response. Additionally, the presence of related purine nucleotide signalling molecules such as UTP and UDP, as well as the generation of ADP from ATP degradation may further shape microglial responses. The activation of intracellular  $\text{Ca}^{2+}$  signalling demonstrated also opens up various avenues of investigation in terms of subsequent activation of intracellular signalling pathways and resulting microglial functions.

One cellular mechanism linked to elevated intracellular  $\text{Ca}^{2+}$  is the induction of regulated cell death pathways. The P2X7 receptor, as previously reported (Franceschi *et al*, 1996; Ferrari *et al*, 1997a), was shown to mediate a drastic cytotoxic response following long term

stimulation with either BzATP or high concentrations of ATP. P2X7-mediated cytotoxicity demonstrated the activation of executioner phase caspases 3 and/or 7, strongly suggesting apoptotic mechanisms of cell death. Subsequent extracellular LDH release was also present, although this was likely the result of secondary necrosis of apoptotic bodies. Due to the requirement for elevated extracellular concentrations, as well as the rapid degradation of ATP in the extracellular space, P2X7 mediated cell death would only be important for resting microglia situated within close vicinity of cellular damage. Microglial activation can be beneficial in neuroinflammatory situations, by mediating the phagocytotic clearance of cellular debris. However, excessive stimulation of microglia may induce a neurotoxic phenotype (Langmann, 2007), which may be detrimental to RGCs and contribute to glaucomatous progression. Moreover, the prevention of microglial activation with minocycline (Bosco *et al*, 2008) has shown improved RGC survival following simulated glaucomatous events. Since the mechanism of P2X7-mediated cell death appears to be apoptotic, an outcome that does not propagate an inflammatory response, this might suggest a mechanism whereby microglia situated within close vicinity to the site of cellular damage/ATP release are prevented from excessive stimulation/activation and removed in order to prevent a detrimental response.

One of the most interesting results of this research came with investigations into alternate purine nucleotide mediated cytotoxicity in resting microglia. ADP was shown to have a cytotoxic effect in an approximate 30% proportion of the homogenous cell culture population, in mechanism that involved executioner caspases 3/7, but was independent of P2X7. ADP-mediated cytotoxicity in cells is so far unreported. Further investigation was unsuccessful in determining the receptor subtype responsible, due in part to a number of the antagonists tested causing toxicity in the BV-2 cells. However the use of alternate purine nucleotides and adenosine as agonists provided

evidence against the involvement of several possible candidates, including P2Y1, P2Y2, P2Y4, P2Y6, P2Y14 and the entire P1 family of receptors. The lack of a murine P2Y11 also precludes this subtype from the observed cytotoxicity. The remaining potential receptor subtypes were P2Y12 & P2Y13. The P2Y12 antagonist PSB0739 couldn't be used effectively due to toxicity, plus there is a lack of selective agonists between these receptor subtypes. Generation of receptor knockouts with CRISPR as demonstrated in chapter 3 may provide additional insight. Replication of experimental conditions in alternative microglia models, such as primary cells or N9 immortalised microglial cell line may also provide additional insight. The wider impact of this ADP-mediated cytotoxic effect in microglia in relation to glaucoma is unclear. It could, however, be speculated that, as with P2X7 mediated cell death, removal of a proportion of microglial cells may act as a mechanism to limit excessive stimulation and prevent a subsequent detrimental outcome.

P2X7 was also shown to be a sufficient release stimulus for accumulated intracellular IL-1 $\beta$ , albeit with no effect on the priming stage, which is in agreement with previous reports. Novel data, however, showed that long-term pre-incubation with ATP was a sufficient priming stimulus, independent of P2X7 activity, although ATP priming is less efficacious than the well-established LPS/TLR4 pathway. ATP as a priming stimulus has only previously been shown in astrocytes (Albalawi *et al*, 2017), however in this case was shown to be P2X7 mediated. ATP acting as an IL-1 $\beta$  priming stimulus at moderate concentrations has implications for the glaucomatous pathophysiology. The increase in extracellular concentrations of purine nucleotides under glaucomatous pathophysiological conditions, by a lytic form of cell death such as pyroptosis, from pannexin hemichannels following periods of elevated IOP (Reigada *et al*, 2008) or from RPE cells following hypoxia/ischaemia stimulation (Reigada & Mitchell, 2005) may act as priming stimulus for resting microglia,

which when encountering initial stages of glaucomatous tissue damage would then be susceptible to releasing IL-1 $\beta$  and further contributing to glaucomatous damage/disease progressions. Furthermore, the low level response in comparison with traditional inflammatory responses is compatible with the slow progressive nature of glaucomatous pathophysiology. It is however unknown if ATP mediated priming is acting as a direct stimulus for microglia, or whether IL-1 $\beta$  upregulation is as a result of paracrine detection of cellular/apoptotic debris, as intermediate ATP was previously shown to induce cytotoxicity in a subpopulation of resting microglia. Further investigation into the receptor subtype responsible would help clarify the exact mechanisms of ATP mediated microglial priming.

Reduced blood flow and consequential ischaemia of the retina and optic nerve head have also been proposed as mechanisms underlying glaucomatous pathophysiology. OGD was explored in relation to purinergic signalling and glaucoma pathophysiology. OGD was shown to have a significant cytotoxic effect on BV-2 microglia which appears to be P2X7 receptor dependent, which is in agreement with similar findings in BV-2 microglia (Eyo *et al*, 2013). Ischaemic events in glaucoma may therefore have a substantial impact on the ability of microglial cells to respond to resultant inflammatory situations. No significant upregulation of IL-1 $\beta$  was detected in OGD treated BV-2 cells which would imply that OGD treatment does not induce an M1 like phenotype in BV-2 cells. It would be interesting to explore the polarization state of OGD treated BV-2 cells further, as non-polarised and M2 phenotypic microglia have previously been shown to be protective against OGD induced cell death in organotypic brain slices (Girard *et al*, 2013), although due to the cytotoxicity of OGD in BV-2 cells themselves, there may be a limited capacity for microglia to respond.

In summary, changes to purinergic signalling, including increases in ocular ATP have been shown in patients with glaucoma (Zhang *et al*, 2007; Li *et al*, 2011) and ATP release has been demonstrated under simulated glaucomatous conditions in retinal tissue (Reigada *et al*, 2008). Furthermore purinergic stimulation has induced cell death in cultured RGCs via P2X7 (Zhang *et al*, 2005) implicating a direct mechanism for purinergic stimulation and P2X7 in the etiology of glaucoma.

However questions relating to indirect mechanisms of purinergic signalling involved in glaucomatous neuroinflammation and degeneration still remain. BzATP stimulation of HORCs has previously shown an upregulation of IL-1 $\beta$ , which was mediated by P2X7 (Niyadurupola *et al*, 2013). Here it was shown that P2X7 stimulation does not upregulate IL-1 $\beta$  BV-2 cells, but ATP stimulation via a different receptor does, linking ATP release under glaucomatous conditions with DAMP priming of microglia. P2X7 receptor stimulation was shown to be a strong mediator of IL-1 $\beta$  release, and therefore it is possible that multiple waves of extracellular ATP could cause IL-1 $\beta$  production and release from retinal microglia. The demonstration that astrocytes can mimic these results, albeit mediated by P2X7 (Albalawi *et al*, 2017), suggests that multiple retinal glial cells may contribute to the neuroinflammatory response in glaucoma.

The presented work in this thesis has helped provide insight into the role of the P2X7 receptor in microglia. Given the crucial part played by microglia in retinal homeostasis, it may also contribute to a greater understanding of the pathophysiology of the disease.

## Conclusions

- CRISPR gene editing was used to successfully generate a functional P2X7 receptor deficient BV-2 microglia cell line (Clone-14).
- Multiple purinergic receptors mediate ATP stimulated intracellular Ca<sup>2+</sup> responses in BV-2 microglia, including P2X7, P2X4 and P2Y2.
- Similarly, P2Y6 appears to play a role in ADP stimulated Ca<sup>2+</sup> responses in BV-2 microglia.
- Long term P2X7 stimulation induces apoptotic cell death followed by secondary necrosis/cell lysis in BV-2 microglia.
- Approximately 30% of a homogenous BV-2 population are also susceptible to purinergic stimulated apoptotic cell death, mediated by an unidentified receptor (possibly P2Y12).
- The P2X7 receptor activation mediates the release of intracellular IL-1 $\beta$  in BV-2 cells.
- A novel role for purinergic stimulation was demonstrated in the priming of IL-1 $\beta$ , not mediated by P2X7, albeit at far lower levels than the traditional priming agent LPS.
- P2X7 plays a role in the death of BV-2 cells following oxygen glucose deprivation.

## List of Abbreviations

$\alpha\beta$ meATP	$\alpha\beta$ -methylene ATP
$\beta\gamma$ meATP	L- $\beta\gamma$ methylene ATP
2MeSADP	2-methylthio-adenosine-5'-diphosphate
2MeSATP	2-methylthio-adenosine-5'-triphosphate
5-HT	5-hydroxytryptamine
Ach	Acetylcholine
ADP	Adenosine diphosphate
ADP $\beta$	Adenosine-5'-( $\beta$ -thio)-diphosphate
AMP	Adenosine monophosphate
ANOVA	Analysis of Variance
AP4A	Diadenosine tetraphosphate
Apaf1	Apoptotic protease activating factor-1
ASC	Apoptosis associated speck like protein
ATP	Adenosine triphosphate
BBG	Brilliant blue G
BDNF	Brain-derived neurotrophic factor
BzATP	Benzoyl-benzoyl adenosine 5'-triphosphate
CARD	Caspase recruitment domain
CASP	Caspase
CD	Cluster of differentiation
cDNA	Complimentary deoxyribonucleic acid
CNS	Central nervous system
CRISPR	Clustered regularly interspaced short palindromic repeats
CTP	Cytidine-5'-triphosphate

DAG	Diacylglycerol
DAMPs	Damage associated molecular patterns
DBI	Diazepam binding inhibitor
DISC	Death-inducing signalling complex
DMEM	Dulbecco's Minimum Essential Medium
DMSO	Dimethyl Sulfoxide
DNA	Deoxyribonucleic acid
dNTP	Deoxynucleotide triphosphate
DPBS	Dulbecco's Phosphate Buffered Saline
EC <sub>50</sub>	50% effective drug concentration
ELISA	Enzyme-linked Immunosorbant Assay
ER	Endoplasmic reticulum
FBS	Fetal bovine serum
FCRLS	Fc receptor-like scavenger S
GABA	Gamma-aminobutyric acid
GCL	Ganglion cell layer
GFP	Green fluorescent protein
Glu	Glutamate
GPCR	G protein-coupled receptor
GPMB	Glycosylated protein nmb
GSDM	Gasdermin
GTP	Guanosine-5'-triphosphate
HSP	Heat shock protein(s)
ICE	Interleukin converting enzyme
IL-13	Interleukin-13

IL-1 $\alpha$	Interleukin-1 alpha
IL-1 $\beta$	Interleukin-1 beta
IL-1RA	Interleukin-1 receptor antagonist
IL-1RAcP	Interleukin-1 receptor accessory protein
IL-4	Interleukin-4
INL	Inner nuclear layer
IOP	Intraocular pressure
IP <sub>3</sub>	Inositol 1,4,5-triphosphate
IPL	Inner plexiform layer
ITP	Ionisine-5'-triphosphate
K/O	Knockout
LDH	Lactate dehydrogenase
LGIC	Ligand gated ion channel
LPS	Lipopolysaccharide
LRR	Leucine-rich repeat
MHC	Major histocompatibility complex
MLKL	Mixed lineage kinase domain like pseudokinase
MPT	Mitochondrial permeability transition pore
mRNA	Messenger RNA
MTS	3-(4,5-dimethylthiazol-2-yl)-5-(3-carboxymethoxyphenyl)- 2-(4-sulphophenyl)-2H-tetrazolium
NACHT	Nucleotide-binding and oligomerization
NCX	Na <sup>+</sup> /Ca <sup>2+</sup> exchange transporter
NCXK	Na <sup>+</sup> /Ca <sup>2+</sup> -K <sup>+</sup> exchange transporter
NF- $\kappa$ B	Nuclear factor kappa B

NGF	Nerve growth factor
NLR	NOD-like receptor
NLRP3	Nacht, LRR and PYD domains-containing protein 3
NMDA	N-methyl D-aspartate
NODs	Nucleotide-binding oligomerization domains
NTG	Normal-tension glaucoma
NTPDase1	Ectonucleotidase triphosphate diphosphohydrolase-1
oATP	Oxidised ATP
OFL	Optic fiber layer
OGD	Oxygen glucose deprivation
ONH	Optic nerve head
ONL	Outer nuclear layer
PAM	Positive allosteric modulator
PAMPs	Pathogen associated molecular patterns
PBS	Phosphate buffered saline
PDL	Poly-D-Lysine
PI3K	Phosphoinositol-3 kinase
PLC	Phospholipase C
PMCA	Plasma membrane Ca <sup>2+</sup> ATPase
POAG	Primary open angle glaucoma
PRR	Pattern recognition receptor
PYD	Pyrin domain
qRT-PCR	Quantitative reverse transcription polymerase chain reaction
RB2	Reactive blue 2

RCD	Regulated cell death
RGCs	Retinal ganglion cells
RIPK	Receptor-interacting kinase
RNA	Ribonucleic acid
ROS	Reactive oxygen species
RPE	Retinal pigment epithelium
RyR	Ryanodine receptor
SAH	S-adenosylhomocysteine
SERCA	Smooth endoplasmic reticular Ca <sup>2+</sup> ATPase
siRNA	Small interfering Ribonucleic acid
SNARE	Soluble N-ethylmaleimide-sensitive factor attachment protein receptor
SNP	Single nucleotide polymorphism
SR	Sarcoplasmic reticulum
SRs	Scavenger receptors
TLRs	Toll-like receptors
TM	Transmembrane
TMEM119	Transmembrane protein 119
TNF- $\alpha$	Tumor necrosis factor alpha
TNP	Trinitro-phenyl
TrkB	Tropomyosin receptor kinase B
TRPM7	Transient receptor potential cation channel subfamily member 7
TUNEL	Terminal deoxynucleotidyl transferase dUTP nick endlabelling
TYRP1	Tyrosine-related protein-1

UDP	Uridine 5'-diphosphate
UTP	Uridine 5'-triphosphate
VGCC	Voltage gated calcium channel
VNUT	Vesicular nucleotide transporter
VR1	Vanilloid receptor
YO-PRO-1	Yohimbine-proline 1
ZBP1	Z-DNA binding protein 1 (ZBP1)

## References

- Abbracchio MP, Burnstock G, Boeynaems JM, Barnard EA, Boyer JL, Kennedy C, Knight GE, Fumagalli M, Gachet C, Jacobson KA, Weisman GA, (2006). Update on the P2Y G protein-coupled nucleotide receptors: from molecular mechanisms and pathophysiology to therapy. *Parmaicol Rev*, **58**, p281p341.
- Abbracchio MP, Burnstock G, Verkhratsky A, Zimmermann H, (2009). Purinergic signalling in the nervous system: an overview. *Trends Neurosci*, **32**, p19-29.
- Abdelrahman A, Namasivayam V, Hinz S, Schiedel AC, Kose M, Burton M, El-Tayeb A, Gillard M, Bajorath J, de Ryck M, Muller CE, (2017). Characterization of P2X4 receptor agonists and antagonist by calcium influx and radioligand binding studies. *Biochem Pharmacol*, **125**, p41-54.
- Abulafina DP, de Rivero Vaccari JP, Lozano JD, Lotocki G, Keane RW, Dietrich WD, (2009). Inhibition of the inflammasome complex reduces the inflammatory response after thromboembolic stroke in mice. *J Cereb Blood Flow Metab*, **29**, p534-544.
- Adamczak SE, de Rivero vaccari JP, Dale G, Brand FJ 3<sup>rd</sup>, Nonner D, Bullock MR, Dahl GP, Dietrich WD, Keane RW, (2014). Pyroptotic neuronal cell death mediated by the AIM2 inflammasome. *J Cereb Blood Flow Metab*, **34**, 621-629.
- Adinolfi E, Pizzirani C, Idzko M, Panther E, Norgauer J, Di Virgilio F, Ferrari D, (2005). P2X<sub>7</sub> receptor: Death or life? *Purinergic Signal*, **1**, p219-227.
- Adinolfi E, Raffaghello L, Giuliani AL, Cavazzini L, Capece M, Chiozzi P, Bianchi G, Kroemer G, Pistoia V, Di Virgilio F, (2012). Expression of P2X<sub>7</sub> receptor increases in vivo tumor growth. *Cancer res*, **72**, p2957-2969.
- Aghaei M, Panjehpour M, Karami-Tehrani F, Salami S, (2011). Molecular mechanisms of A3 adenosine receptor-induced G1 cell cycle arrest and apoptosis in androgen-dependent and independent prostate cancer cell lines: involvement of intrinsic pathway. *J Cancer Res Clin Oncol*, **137**, p1511-1523.
- Aglietti RA, Estevez A, Gupta A, Ramirez MG, Liu PS, Kayagaki, Ciferri C, Dixit VM, Dueber EC, (2016). GsdmD p30 elicited by caspase-11 during pyroptosis forms pores in membranes. *Proc Natl Acad Sci USA*, **113**, p7858-7863

- Albalawi F, Lu W, Beckel JM, Lim JC, McCaughey SA, Mitchell CH, (2017). The P2X7 Receptor Primes IL-1 $\beta$  and the NLRP3 Inflammasome in Astrocytes Exposed to Mechanical Strain. *Front Cell Neurosci*, **11**, 227.
- Alberto AV, Faria RX, Couto CG, Ferreira LG, Souza CA, Teixeira PC, Froes MM, Alves LA, (2013). Is pannexin the pore associated with the P2X7 receptor? *Naunyn Schmiedebergs Arch Pharmacol*, **386**, p775-787.
- Aldarwesh A, (2015), 'Oxygen and Glucose Deprivation on Human Müller Cells (MIO-M1) and Human Organotypic Retinal Cultures (HORCs) in Relation to Glaucoma, PhD Thesis, University of East Anglia, Norwich
- Ali S, Turner J, Fountain SJ, (2018). P2Y2 and P2Y6 receptor activation elicits intracellular calcium responses in human adipose-derived mesenchymal stromal cells. *Purinergic Signal*, **14**, p371-384.
- Allen IC, Scull MA, Moore CB, Holl EK, McElvania-TeKippe E, Taxman DJ, Guthrie EH, Pickles RJ, Ting JP, (2009). The NLRP3 inflammasome mediates in vivo innate immunity to influenza A virus through recognition of viral RNA. *Immunity*, **30**, 556-565.
- Amadiol S, Montilli C, Picconi B, Calabresi P, Volonte C, (2007). Mapping P2X and P2Y receptor proteins in striatum and substantia nigra: An immunohistological study. *Purinergic Signal*, **3**, p389-398.
- Ames A 3<sup>rd</sup>, (1992). Energy requirements of CNS cells as related to their function and to their vulnerability to ischaemia: a commentary based on studies on retina. *Can J Physiol Pharmacol*, **70**, suppl:S158-164.
- Anders C, Niewoehner O, Duerst A, Jinek M, (2014). Structural basis of PAM-dependent target DNA recognition by the Cas9 endonuclease. *Nature*, **513**, 569-573.
- Anderson CM, Nedergaard M, (2006). Emerging challenges of assigning P2X7 receptor function and immunoreactivity in neurons. *Trends Neurosci*, **29**, p257-262
- Anderson DR, Davis EB, (1975). Sensitivities of ocular tissues to acute pressure-induced ischemia. *Arch Ophthalmol*, **93**, p267-274
- Anderson MG, Smith RS, Hawes NL, Zabaleta A, Chang B, Wiggs JL, John SW, (2002). Mutations in genes encoding melanosomal

proteins cause pigmentary glaucoma in DBA/2J mice. *Nat Genet*, **30**, p81-85.

- Andrei C, Dazzi C, Lotti LV, Torrisi MR, Chimini G, Rubartelli A, (1999). The secretory route for the leaderless protein interleukin 1beta involves exocytosis of endolysosome-related vesicles. *Mol Biol Cell*, **10**, p1463-1475.
- Arbeloa J, Perez-Samartin A, Gottlieb M, Matute C, (2012). P2X7 receptor blockade prevents ATP excitotoxicity in neurons and reduces brain damage after ischemia. *Neurobiol Dis*, **45**, p954-961.
- Ashkenazi A, Dixit VM, (1998). Death receptors: signalling and modulation. *Science*, **281**, 1305-1308.
- Ashwell KW, Hollander H, Streit W, Stone J, (1989). The appearance and distribution of microglia in the developing retina of the rat. *Vis Neurosci*, **2**, p437-448.
- Askew K, Li K, Olmos-Alonso A, Garcia-Moreno F, Liang Y, Richardson P, Tipton T, Chapman M, Riecken K, Beccari S, Sierra A, Molnar Z, Cragg M, Garaschuk O, Perry VH, Gomez-Nicola D, (2017). Coupled Proliferation and Apoptosis Maintain the Rapid Turnover of Microglia in the Adult Brain. *Cell Rep*. **18**, p391-405.
- Auron PE, Webb AC, Rosenwass LJ, Mucci SF, Rich A, Wolff SM, (1984). Nucleotide sequence of human monocyte interleukin 1 precursor cDNA. *Proc Natl Acad Sci USA*, **81**, p7907-7911.
- Ayyanathan K, Naylor SL, Kunapuli SP, (1996). Structural characterization and fine chromosomal mapping of the human P2Y1 purinergic receptor gene (P2RY1). *Somat Cell Genet*, **22**, p419-424.
- Bailey MA, Imbert-Teboul M, Turner C, Srani SK, Burnstock G, Unwin RJ, (2001). Evidence for basolateral P2Y(6) receptors along the rat proximal tubule: functional and molecular characterization. *J Am Soc Nephrol*, **12**, p1640-1647.
- Baldelli P, Hernandez-Guijo JM, Carabelli V, Carbone E, (2005). Brain-derived neurotrophic factor enhances GABA release probability and nonuniform distribution of N- and P/Q-type channels on release sites of hippocampal inhibitory synapses. *J Neurosci*, **25**, p3358-3368.
- Balduini A, Di Buduo CA, Malara A, Lecchi A, Rebuzzini P, Currao M, Pallotta I, Jakubowski JA, Cattaneo M, (2012). Constitutively released adenosine diphosphate regulates proplatelet formation by human megakaryocytes. *Haematologica*, **97**, p1657-65.

- Balerini P, Ciccarelli R, Caciagli F, Rathbone MP, Werstiuk ES, Traversa U, Buccella S, Giuliani P, Jang S, Nargi E, Visini D, Santavenere C, Di Iorio P, (2005). P2X7 Receptro activation activation in rat brain cultured astrocytes increases the biosynthetic release of cysteinyl leukotrienes. *Int J Immunopathol Pharmacol*, **18**, 417-430.
- Ballerini P, Ciccarelli R, Caciagli F, Rathbone MP, Werstiuk ES, Travera U, Buccella S, Giuliani P, Jiang S, Nargi E, Visini D, Santavenere C, Di Iorio P, (2005). P2X7 receptro activation in rat brain cultured astrocytes increases the biosynthetic release of cysteinyl leukotrienes. *Int J Immunopath Ph*, **18**, p417-430
- Balogh J, Wihlborg AK, Isackson H, Joshi BV, Jacobson KA, Arner A, Erlinge D, (2005). Phospholipase C and cAMP-dependent positive inotropic effects of ATP in mouse cardiomyocytes via P2Y11-like receptors. *J Mol Cell Cardiol*, **39**, p223-230.
- Banks FC, Knight GE, Calvert RC, Thompson CS, Morgan RJ, Burnstock G, (2006). The purinergic component of human vas deferens contraction. *Fertil Steril*, **85**, p932-939
- Baqi Y, Hausmann R, Rosefort C, Rettinger J, Schmalzing G, Muller CE, (2011). Discovery of potent competitive antagonists and positive modulatos of the P2X2 receptor. *J Med Chem*, **54**, p817-830.
- Bar-Yehuda S, Stemmer SM, Madi L, Castel D, Ochaion A, Cohen S, Barer F, Zabutti A, Perez-Liz G, Del Valle L, Fishman P, (2008). The A3 adenosine receptor agonist CF102 induces apoptosis of hepatocellular carcinoma via de-regulation of the Wnt and NF-happaB signal transduction pathways. *Int J Oncol*, **33**, p287-295.
- Baraldi PC, Di Virgilio F, Romangnoli R, (2004). Agonists and antagonists acting at P2X7 receptor. *Curr Top Med Chem*, **4**, p1707-1717.
- Baricordi OR , Ferrari D, Melchiorri L, Chiozzi P, Hanau S, Chiari E, Rubini M, Di Virgilio F, (1996). An ATP-activated channel is involved in mitogenic stimulation of human T lymphocytes. *Blood*, **87**, p682-690.
- Barrett MO, Sesma JI, Ball CB, Jayasekara PS, Jacobson KA, Lazarowski ER, Harden TK, (2013). A Selective High-Affinity Antagonist of the P2Y14 Receptor Inhibits UDP-Glucose-Stimulated Chemotaxis of Human Neutrophils. *Mol Pharmacol*, **84**, p41-9.

- Beckel JM, Argall AJ, Lim JC, Xia J, Lu W, Coffey EE, Macarak EJ, Shahidullah M, Delamere NA, ZODE GS, Sheffield VC, Shestopalov VI, Laties AM, Mitchell CH. Mechanosensitive release of adenosine-5'-triphosphate through pannexin channels and mechanosensitive upregulation of pannexin channels in optic nerve head astrocytes: a mechanism for purinergic involvement in chronic strain. *Glia*, **62**, p1486-1501.
- Bell MD, Lopez-Gonzalez R, Lawson L, Hughes D, Fraser I, Gordon S, Perry VH, (1994). Upregulation of the macrophage scavenger receptor in response to different forms of injury in the CNS. *J Neurocytol*, **23**, p605-613.
- Bernier LP, Ase AR, Boue-Grabot E, Sequela P, (2012). P2X4 receptor channels form large noncytolytic pores in resting and activated microglia. *Glia*, **60**, p728-737.
- Berridge MJ, (1993). Inositol triphosphate and calcium signalling. *Nature*, **361**, p315-325
- Berridge MJ, (2016). The inositol triphosphate/calcium signaling pathway in health and disease. *Physiol Rev*, **96**, p1261-1296.
- Berridge MJ, Lipp P, Bootman MD, (2000). The versatility and universality of calcium signalling. *Nat Rev Mol Cell Biol*, **1**, p11-21.
- Berry DA, Barden JA, Balcar VJ, Keogh A, dos Remedios CG, (1999). Increase in expression of P2X1 receptors in the atria of patients suffering from dilated cardiomyopathy. *Electrophoresis*, **20**, p2059-64.
- Besada P, Shin DH, Costanzi S, Ko H, Mathé C, Gagneron J, Gosselin G, Maddileti S, Harden TK, Jacobson KA, (2006). Structure-activity relationships of uridine 5'-diphosphate analogues at the human P2Y6 receptor. *J Med Chem*, **49**, p5532-5543.
- Bezbradica JS, Coll RC, Schroder K, (2017). Sterile signals generate weaker and delayed macrophage NLRP3 inflammasome responses relative to microbial signals. *Cell Mol Immunol*, **14**, p118-126.
- Bhattacharya A, Wang Q, Ao H, Shoblock JR, Lord B, Aluisio L, Fraser I, Nepomuceno D, Neff RA, Welty N, Lovenberg TW, Bonaventure P, Wickenden AD, Letavic MA, (2013). Pharmacological characterization of a novel centrally permeable P2X7 receptor antagonist: JNJ-47965567. *Br J Pharmacol*, **170**, p624-640

- Bianchi ME, (2007). DAMPs, PAMPs and alarmins: all we need to know about danger. *J Leukoc Biol*, **81**, p1-5
- Bianchi BR, Lynch KJ, Touma E, Niforatos W, Burgard EC, Alexander KM, Park HS, Yu H, Metzger R, Kowaluk E, Jarvis MF, van Biesen T, (1999). Pharmacological characterization of recombinant human and rat P2X receptor subtypes. *Eur J Pharmacol*, **376**, p127-138.
- Bianco F, Ceruti S, Colombo A, Fumagalli M, Ferrari D, Pizzirani C, Matteoli M, Di Virgilio F, Abbracchio MP, Verderio C, (2006). A role for P2X7 in microglial proliferation. *J Neurochem*, **99**, 745-758.
- Bianco F, Fumagalli M, Pravettoni E, D'Ambrosi N, Volonte C, Matteoli M, Abbracchio MP, Verderio C, (2005). Pathophysiological roles of extracellular nucleotides in glial cells: differential expression of purinergic receptors in resting and activated microglia. *Brain Res Rev*, **48**, p144-156
- Bianco F, Perrotta C, Novellino L, Francolini M, Riganti L, Menna E, (2009). Acid Sphingomyelinase activity triggers microparticle release from glial cells. *EMBO J*, **28**, p1043-1054.
- Bianco F, Pravettoni E, Colombo A, Schenk U, Moller T, Matteoli M, (2005). Astrocyte-derived ATP induces vesicle shedding and IL-1 beta release from microglia. *J Immunol*, **174**, p7268-7277.
- Blackburn MR, Vance CO, Morschl E, Wilson CN, (2009). Adenosine receptors and inflammation. *Handb Exp Pharmacol*, **193**, p215-269.
- Blasi E, Barluzzi R, Bocchini V, Mazzolla R, Bistoni F, (1990). Immortalization of murine microglial cells by a v-raf/vmyc carrying retrovirus. *J Neuroimmunol*, **27**, 229-237.
- Bo X, Jiang LH, Wilson HL, Kim M, Burnstock G, Suprenant A, North RA, (2003). Pharmacological and biophysical properties of the human P2X5 receptor. *Mol Pharmacol*, **63**, p1407-1416.
- Bo X, Zhang Y, Nassar M, Burnstock G, Schoepfer R, (1995). A P2X purinoceptor cDNA conferring a novel pharmacological profile. *FEBS Lett*, **375**, p129-133.
- Bo X, Karoon P, Nori SL, Bardini M, Burnstock G, (1998). P2X purinoceptors in postmortem human cerebral arteries. *J Cardiovasc Pharmacol*, **31**, p794-799.

- Bodin P, Bailey D, Burnstock G, (1991). Increased flow-induced ATP release from isolated vascular endothelial cells but not smooth muscle cells. *Br J Pharmacol*, **103**, p1203-1205.
- Bodor ET, Waldo GL, Hooks SB, Corbitt J, Boyer JL, Harden TK, (2003). Purification and functional reconstitution of the human P2Y<sub>12</sub> receptor. *Mol Pharmacol*, **64**, 1210-1216.
- Bogdanov YD, Wildman SS, Clements MP, King BF, Burnstock G, (1998). Molecular cloning and characterization of rat P2Y<sub>4</sub> nucleotide receptor. *Br J Pharmacol*, **124**, p428-430.
- Boldt W, Klapperstuck M, Buttner C, Sadtler S, Schmalzing G, Markwardt F, (2003). Glu496Ala polymorphism of human P2X<sub>7</sub> receptor does not affect its electrophysical phenotype. *Am J Physiol Cell Physiol*, **284**, p749-756.
- Bootman MD, (2012). Calcium signaling. *Cold Spring Harb Perspect Biol*, **4**, ao11171.
- Bortner CD, Oldenburg NBE Oldenburg, Cidlowski JA, (1995). The role of DNA fragmentation in apoptosis. *Trends Cell Biol*, **5**, p21-26.
- Borz P, (2015). Immunology: Caspase target drives pyroptosis. *Nature*, **526**, p642-643.
- Bosch E, Horwitz J, Bok D (1993). Phagocytosis of outer segments by retinal pigment epithelium:phagosome-lysosome interaction. *J Histochem Cytochem*, **41**, p253-263
- Bosco A, Inman DM, Steele MR, Wu G, Soto I, Marsh-Armstrong N, Hubbard WC, Calkins DJ, Horner PJ, Vetter ML, (2008). Reduced retina microglial activation and improved optic nerve integrity with minocycline treatment in the DBA/2J mouse model of glaucoma. *Invest Ophthalmol Vis Sci*, **49**, p1437-446.
- Bosco A, Steele MR, Vetter ML, (2011). Early microglial activation in a mouse model of chronic glaucoma. *J Comp Neurol*, **519**, p599-620.
- Bouhenni RA, Dunmire J, Sewell A, Edward DP, (2012). Animal Models of glaucoma. *J Biomed Biotechnol*, **2012**, 692609.
- Boumechache M, Masin M, Edwardson JM, Gorecki DC, Murrell-Lagnado R, (2009). Analysis of assembly and trafficking of native P2X<sub>4</sub> and P2X<sub>7</sub> receptor complexes in rodent immune cells. *J Biol Chem*, **284**, p13446-13454.

- Bowler JW, Bailey RJ, North RA, Suprenant A, (2003). P2X4, P2Y1 and P2Y12 receptors on rat alveolar macrophages. *Br J Pharmacol*, **140**, p567-575.
- Boyer JL, Mohanram A, Camaioni E, Jacobson KA, Harden TK, (1998). Competitive and selective antagonism of P2Y<sub>1</sub> receptors by N<sup>6</sup>-methyl 2'-deoxyadenosine 3',5'-biphosphate. *Br J Pharmacol*, **124**, p1-3.
- Bradbury EJ, Burnstock G, McMahon SB, (1998). The expression of P2X3 purinoreceptors in sensory neurons: effects of axotomy and glial-derived neurotrophic factor. *Mol Cell Neurosci*, **12**, p256-268.
- Brake AJ, Wagenbach MJ, Julius D, (1994). New structural motif for ligand-gated ion channels defined by an ionotropic ATP receptor. *Nature*, **371**, p519-523
- Bratton DL, Fadok VA, Richter DA, Kailey JM, Guthrie LA, Henson PM, (1997). Appearance of phosphatidylserine on apoptotic cells requires calcium mediated nonspecific flip-flop and is enhanced by loss of the aminophospholipid translocase. *J Biol Chem*, **272**, p26159-26165.
- Braun N, Sevigny J, Robson SC, Enjoji Guckelberger O, Hammer K, Di Virgilio, Zimmermann H, (2000). Assignment of ecto-nucleoside triphosphate diphosphohydrolase-1 / *cd39* expression to microglia and vasculature of the brain. *Eur J Neurosci*, **12** p4357-4366.
- Breitwieser GE, (2008). Extracellular calcium as an integrator of tissue function. *Int J Biochem Cell Biol*, **40**, p1467-1480.
- Bringmann A, Iandiev T, Wurm A, Holloborn M, Wiedemann P, Osborne NN, Reichenbach A, (2009). Cellular signaling and factors involved in Muller cell gliosis: neuroprotective and detrimental effects. *Prog Retin Eye Res*, **28**, p423-451.
- Brinson AE, Harden TK, (2001). Differential Regulation of the Uridine Nucleotide-activated P2Y4 and P2Y6 Receptors. SER-333 AND SER-334 IN THE CARBOXYL TERMINUS ARE INVOLVED IN AGONIST-DEPENDENT PHOSPHORYLATION DESENSITIZATION AND INTERNALIZATION OF THE P2Y4. *J Biol Chem*, **276**, p11939-11948.
- Broadway DC, Drance SM, (1998). Glaucoma and vasospasm. *Br J Ophthalmol*, **82**, p862-870.

- Brough D, Le Feuvre RA, Iwakura Y, Rothwell NJ, (2002). Purinergic (P2X7) receptor activation of microglia induces cell death via an interleukin-1-independent mechanism. *Mol Cell Neurosci*, **19**, p272-280.
- Brown GC, Neher JJ, (2014). Microglial phagocytosis of live neurons. *Nat Rev Neurosci*, **15**, p209-216.
- Bruce-Keller AJ, (1999). Microglial-neuronal interactions in synaptic damage and recovery. *J Neurosci Res*, **58**, p191-201.
- Brumatti G, Salmanidis M, Ekert PG, (2010). Crossing paths: interactions between cell death machinery and growth factor survival signals. *Cell Mol Life Sci*, **67**, p1619-1630.
- Brunschweiler A, Muller CE, (2006). P2 receptors activated by uracil nucleotides—an update. *Curr Med Chem*, **13**, p289-312.
- Bruttger J, Karram K, Wortge S, Regen T, Marini F, Hoppmann N, Klein M, Blank T, Yona S, Wolf Y, Mack M, Pinteaux E, Müller W, Zipp F, Binder H, Bopp T, Prinz M, Jung M, Waisman A, (2015). Genetic Cell Ablation Reveals Clusters of Local Self-Renewing Microglia in the Mammalian Central Nervous System. *Immunity*, **43**, p92-106
- Bruzzone R, Barbe MT, Jakob NJ, Monyer H, (2005). Pharmacological properties of homomeric and heteromeric pannexin hemichannels expressed in *Xenopus* oocytes. *J Neurochem*, **92**, p1033-1043.
- Buell G, Lewis C, Collo G, North RA, Surprenant A, (1996). An antagonist-insensitive P2X receptor expressed in epithelia and brain. *EMBO J*, **15**, p55-62.
- Buell GN, Talabot F, Gos A, Lorenz J, Lai E, Morris MA, Antonarakis SE, (1998). Gene structure and chromosomal localization of the human P2X7 receptor. *Recept Channels*, **5**, p347-354.
- Bulanova E, Budagian V, Orinska Z, Hein M, Petersen F, Thon L, Adam D, Bulfone-Paus S, (2005). Extracellular ATP induces-cytokine expression and apoptosis through P2X7 receptor in murine mast cells. *J Immunol*, **174**, p3880-3890.
- Burnstock G, (1972). Purinergic nerves. *Pharmacol Rev*, **24**, p509-581
- Burnstock G, (1997). The past, present and future of purine nucleotides as signalling molecules. *Neuropharmacol*, **36**, p1127-1139

- Burnstock G, (1978). A basis for distinguishing two types of purinergic receptor. (Straub R W & Bolis L eds.) Cell membrane receptors for drugs and hormones: a multidisciplinary approach. *New York: Raven press*, p107-118.
- Burnstock G, (2007). Purine and pyrimidine receptors. *Cell Mol Life Sci*, **64**, 1471-1483.
- Burnstock G, Campbell G, Satchell D, Smythe A, (1970). Evidence that adenosine triphosphate or a related nucleotide is the transmitter substance released by non-adrenergic inhibitory nerves in the gut. *Br J Pharmacol*, **40**, p668-688.
- Burnstock G, Kennedy C, (1985). Is there a basis for distinguishing two types of P2-purinoceptor? *Gen Pharmacol*, **16**, p433-440.
- Burnstock G, Knight GE, (2004). Cellular distribution and functions of P2 receptor subtypes in different systems. *Int Rev Cytol*, **240**, p31-304.
- Butovsky O, Jedrychowski MP, Moore CS, Cialic R, Lanser A, Gabriely G, Keglsperger T, Dake B, Wu PM, Dooykan C, Fanek Z, Liu L, Chen Z, Rothstein JD, Ransohoff RM, Gygu SP, Antel JP, Weiner HL, (2014). Identification of a Unique TGF-  $\beta$  Dependent Molecular and Functional Signature in Microglia. *Nat Neurosci*, **17**, p131-143
- Cai Z, Jitkaew S, Zhao J, Chiang HC, Chocki S, Liu J, Ward Y, Wu LG, Liu ZG, (2014). Plasma membrane translocation of trimerized MKL protein is required for TNF-induced apoptosis. *Nat Cell Biol*, **16**, p55-65.
- Calovi S, Mut-Arbona P, Sperlagh B, (2019). Microglia and the Purinergic Signaling System. *Neuroscience*, **405**, 137-147.
- Carrillo-Jimenez A, Puigdellivol M, Vilalta A, Venero JL, Brown GC, StGeorge-Hyslop P, Burguillos MA, (2018). Effective knockdown of Gene Expression in Primary Microglia With siRNA and Magnetic Nanoparticles Without Cell Death or Inflammation. *Front Cell Neurosci*, **12**, 313.
- Carter DA, Dick AD, (2004). CD200 maintains microglial potential to migrate in the adult human retinal explant model. *Curr Eye Res*, **28**, p427-436.
- Carter RL, Fricks IP, Barrett MO, Burianek LE, Zhou Y, Ko H, Das A, Jacobson KA, Lazarowski ER, Harden TK, (2009). Quantification of Gi-mediated inhibition of adenylyl cyclase activity reveals that

UDP is a potent agonist of the human P2Y<sub>14</sub> receptor. *Mol Pharmacol.*, **76**, p1341-1348.

Cassel SL, Eisenbarth SC, Iyerr SS, Sadler JJ, Colegio OR, Tephly LA, Carter AB, Rothman PB, Flavell RA, Sutterwala FS, (2008). The Nalp3 inflammasome is essential for the development of silicosis. *Proc Natl Acad Sci USA*, **105**, p9035-9040.

Catterall WA, Swanson TM, (2015). Structural basis for pharmacology of voltage-gated sodium and calcium channels. *Mol Pharmacol*, **88**, p141-150.

Cavaliere F, Amadio S, Dinkel K, Reymann KG, Volonte C, (2007). P2 receptor antagonist trinitrophenyl-adenosine-triphosphate protects hippocampus from oxygen and glucose deprivation cell death. *J Pharmacol Exp Ther*, **323**, p70-77.

Cavaliere F, Amadio S, Sancesario G, Bernardi G, Volonte C, (2004). Synaptic P2X<sub>7</sub> and oxygen/glucose deprivation in organotypic hippocampal cultures. *J Cereb Blood Flow Metab*, **24**, p392-398.

Cekic C, Linden J, (2016). Purinergic regulation of the immune system. *Nat Rev Immunol*, **16**, p177-192.

Chafke Y, Seguin R, Antel JP, Morissette C, Malo D, Henderson D, Seguela P, (2002). ADP and AMP induce interleukin-1beta release from microglial cells through activation of ATP-Primed P2X<sub>7</sub> receptor channels. *J Neurosci*, **22**, p3061-3069.

Chambers JK, Macdonald LE, Sarau HM, Ames RS, Freeman K, Foley JJ, Zhu Y, McLaughlin MM, Murdock P, McMillan L, Trill J, Swift A, Aiyar N, Taylor P, Vawter L, Naheed S, Szekeres P, Hervieu G, Scott C, Watson JM, Murphy AJ, Duzic E, Klein C, Bergsma DJ, Wilson S, Livi GP, (2000). A G protein-coupled receptor for UDP-glucose. *J Biol Chem*, **275**, p10767-71.

Chang K, Hanaoka K, Kumada M, Takuwa Y, (1995). Molecular cloning and functional analysis of a novel P2nucleotide receptor. *J Biol Chem*, **270**, p26152-26158.

Chataigneau T, Lemoine D, Grutter T, (2013). Exploring the ATP-binding site of P2X receptors. *Front Cell Neurosci*, **7**, 273.

Chessell IP, Simon J, Hibell AD, Michel AD, Barnard EA, Humphrey PP, (1998). Cloning and functional characterisation of the mouse P2X<sub>7</sub> receptor. *FEBS Lett*, **439**, p26-30.

Chhatriwala M, Ravi RG, Patel RI, Boyer JL, Jacobson KA, Harden TK, (2004). Induction of novel agonist selectivity for the ADP-activated P2Y<sub>1</sub> receptor versus the ADP-activated P2Y<sub>12</sub> and

- P2Y<sub>13</sub> receptors by conformational constraint of an ADP analog. *J Pharmacol Exp Ther*, **311**, p1038-1043.
- Chen CC, Akopian AN, Sivilotti L, Colquhoun D, Burnstock G, Wood JN, (1995). A P2X purinoceptor expressed by a subset of sensory neurons. *Nature*, **377**, p428-431.
- Chen D, Yu J, Zhang L, (2016). Necroptosis: an alternative cell death program defending against cancer. *Biochim Biophys Acta* **1865**, p228-236.
- Chen G, Shaw MH, Kim YG, Nunez G, (2009). NOD-like receptors: role in innate immunity and inflammatory disease. *Annu Rev Pathol*, **4**, p365-398.
- Chen R, Zheng L, Zhu S, Liu J, Zeh HJ, Kroemer G, Wang H, Billiar TR, Jiang J, Tang D, Kang R, (2019). cAMP metabolism controls caspase-11 inflammasome activation and pyroptosis in sepsis. *Sci Advan*, **5**, eaav5562.
- Cheng RKY, Segala E, Robertson N, Deflorian F, Dore AS, Errey JC, Fiez-Vandal C, Marshall FH, Cooke RM, (2017). Structures of Human A<sub>1</sub> and A<sub>2A</sub> Adenosine Receptors with Xanthines Reveal Determinants of Selectivity. *Structure*, **25**, p1275-1285.
- Chi W, Li F, Chen H, Wang Y, Zhu Y, Yang X, Zhu J, Wu F, Ouyang H, Ge J, Weinreb RN, Zhang K, Zhuo Y, (2014). Caspase-8 promotes NLRP1.NLRP3 inflammasome activation and IL-1 $\beta$  production in acute glaucoma. *Proc Natl Acad Sci USA*, **111**, p11181-11186.
- Cho YS, Challa S, Moguin D, Genga R, Ray TD Guildford M, Chan FK, (2009). Phosphorylation-drive assembly of the RIP1-RIP3 complex regulates programmed necrosis and virus-induced inflammation. *Cell*, **137**, 1112-1123.
- Chua J, Vania M, Cheung CM, Ang M, Chee SP, Yang H, Li J, Wong TT, (2012). Expression profile of inflammatory cytokines in aqueous from glaucomatous eyes. *Mol Vis*, **18**, p431-438
- Clyne JD, Wang LF, Hume RI, (2002). Mutational analysis of the conserved cysteines of the rat P2X<sub>2</sub>purinoceptor. *J Neurosci*, **22**, p3873-3880
- Cocco L, Follo MY, Manzoli L, Suh PG, (2015). Phosphoinositide-specific phospholipase C in health and disease. *J Lipid Res*, **56**, p1853-1860.
- Collo G, North RA, Kawashima E, Merlo-Pich E, Neidhart S, Surprenant A, Buell G, (1996). Cloning of P2X<sub>5</sub> and P2X<sub>6</sub>

- receptors and the distribution and properties of an extended family of ATP-gated ion channels. *J Neurosci*, **16**, p2495-507.
- Collo G, Neidhart S, Kawashima E, Kosco-Vilbois M, North RA, Buell G, (1997). Tissue distribution of the P2X7 receptor. *Neuropharmacology*, **36**, p1277-1283.
- Communi D, Gonzalez NS, Detheux M, Brézillon S, Lannoy V, Parmentier M, Boeynaems JM, (2001). Identification of a novel human ADP receptor coupled to G(i). *J Biol Chem.*, **276**, p41479-41485.
- Communi D, Govaerts C, Parmentier M, Boeynaems JM, (1997). Cloning of a human purinergic P2Y receptor coupled to phospholipase C and adenylyl cyclase. *J Biol Chem*, **272**, 31969-73.
- Communi D, Parmentier M, Boeynaems JM. (1996) Cloning, functional expression and tissue distribution of the human P2Y6 receptor. *Biochem Biophys Res Commun*, **222**, p303-308.
- Communi D, Piroton S, Parmentier M, Boeynaems JM (1995). Cloning and functional expression of a human uridine nucleotide receptor. *J. Biol. Chem*, **270**, p30849-30852
- Communi D, Suarez-Huerta N, Dussosoy D, Savi P, Boeynaems JM, (2001). Cotranscription and intergenic splicing of human P2Y11 and SSF1 genes. *J Biol Chem*, **276**, p16561-16566.
- Communi D, Robaye B, Boeynaems JM, (1999). Pharmacological characterization of the human P2Y11 receptor. *Br. J. Pharmacol.*, **128**, p1199-1206.
- Compan V, Baroja-Mazo A, Lopez-Castejon G, Gomez AL, Martinez CM, Angosto D, Montero MT, Herranz AS, Bazan E, Reimers D, Mulero V, Pelegrin P, (2012). Cell volume regulation modulates NLRP3 inflammasome activation. *Immunity*, **37**, p487-500.
- Cong L, Ran FA, Cox D, Lin S, Barretto R, Habib N, Hsu Pd, Wu X, Jiang W, Marraffini LA, Zhang F, (2013). Multiplex genome engineering using CRISPR/Cas systems. *Science*, **339**, 819-823.
- Cordeaux Y, Ikzerman AP, Hill SJ, (2004). Coupling of the human A1 adenosine receptor to different heterotrimeric G proteins: evidence for agonist-specific G protein activation. *Br J Pharmacol*, **143**, p705-714.
- Costanzi S, Mamedova L, Gao ZG, Jacobson KA, (2004). Architecture of P2Y nucleotide receptors: structural comparison based on

- sequence analysis, mutagenesis, and homology modelling. *J Med Chem*, **47**, p5393-5404.
- Coull JA, Beggs S, Boudreau D, Boivin D, Tsuda M, Inoue K, Gravel C, Salter MW, De Koninck Y, (2005). BDNF from microglia causes the shift in neuronal anion gradient underlying neuropathic pain. *Nature*, **438**, p1017-1021
- Coutinho-Silva R, Ojcius DM, Gorecki DC, Pereschini PM, Bisaggio RC, Mendes AN, Marks J, Burnstock G, Dunn PM, (2005). Multiple P2X and P2Y receptor subtypes in mouse J774, spleen and peritoneal macrophages. *Biochem Pharmacol*, **69**, 641-655.
- Crain JM, Nikodemova M, Watters JJ, (2009). Expression of P2 nucleotide receptors varies with age and sex in murine brain microglia. *J Neuroinflammation*, **6**, 24
- Cunningham CL, Martinez-Cerdeno V, Noctor SC, (2013). Microglia regulate the number of neural precursor cells in the developing cerebral cortex. *J Neurosci*, **33**, p4216-4233.
- Czabotar PE, Lessene G, Strasser A, Adams JM, (2014). Control of apoptosis by the BCL-2 protein family: implications for physiology and therapy. *Nat Rev Mol Cell Biol*, **15**, p49-63.
- Dabrowska M, Juzwa W, Krzyzosiak W, Olenjniczak M, (2018). Precise Excision of the CAG Tract from the Huntingtin by Cas9 Nickases. *Front Neurosci*, **12**, 75.
- Dahl G, (2015). ATP release through pannexon channels. *Philos Trans R Soc Lond B Biol Sci*, **370**, 20140191.
- Davalos D, Grutzendler J, Yang G, Kim JV, Zuo Y, Jung S, Littman DR, Dustin ML, Gan WB, (2005). ATP mediates rapid microglial response to local brain injury in vivo. *Nat Neurosci*, **8**, p752-758
- de Hoz R, Gallego BI, Ramirez AI, Rojas B, Salazar JJ, Valiente-Soriano FJ, Aviles-Trigueros M, Villegas-Perez MP, Vidal-Sanz M, Trivino A, Ramirez JM, (2013). Rod-Like Microglia Are Restricted to Eyes with Laser-Induced Ocular Hypertension but Absent from the Microglial Changes in the Contralateral Untreated Eye. *PLoS One*, **8**, 83733
- DeMar JC, Rundle DR, Wensel TG, Anderson RE (1999). Heterogeneous N-terminal acylation of retinal proteins. *Prog Lipid Res*, **38**, p49-90
- Dhuna K, Felgate M, Bidula SM, Walpole S, Bibic L, Cromer BA, Angulo J, Sanderson J, Stebbing MJ, Stokes L, (2019).

- Ginsenosides Act As Positive Modulators of P2X4 Receptors. *Mol Pharmacol*, **95**, p210-221.
- Dhuriya YK, Sharma D, (2018). Necroptosis: a regulated inflammatory mode of cell death. *J Neuroinflamm*, **15**, 199.
- Di Virgilio F, (2007). Liasons dangereuses: P2X(7) and the inflammasome. *Trends Pharmacol Sci*, **28**, p465-472.
- Di Virgilio F, Bronte V, Collavo D, Zanovello P, (1989). Responses of mouse lymphocytes to extracellular adenosine 5'-triphosphate (ATP). Lymphocytes with cytotoxic activity are resistant to the permeabilizing effects of ATP. *J Immuno*, **143**, 1955-1960.
- Di Virgilio F, Chiozzi P, Falzoni S, Ferrari D, Sanz JM, Venketaraman V, Baricordi OR (1998). Cytolytic P2X purinoceptors. *Cell Death Differ*, **5**, p191-199.
- Di Virgilio F, Ferrari D, Adinolfi E, (2009). P2X(7) a growth-promoting receptor-implications for cancer. *Purinergic Signal*, **5**, p251-256.
- Diaz-Araya CM, Provis JM, Penfold PL, Billson FA, (1995a). Development of microglial topography in human retina. *J Comp Neurol*, **363**, p53-68
- Diaz-Araya CM, Provis JM, Penfold PL (1995b). Ontogeny and cellular expression of MHC and leucocyte antigens in human retina. *Glia*, **15**, p458-470.
- Dick AD, Carter D, Robertson M, Broderick C, Hughes E, Forrester JV, Liversidge J, (2003). Control of myeloid activity during retinal inflammation. *J Leukoc Biol*, **74**, p161-166.
- Domercq M, Perez-Samartin A, Aparicio D, Alberdi E, Pampliega O, Matute C, (2010). P2X7 Receptors mediate ischemic damage to oligodendrocytes. *Glia*, **58**, p730-740.
- Donnelly-Roberts DL, Namovic MT, Han P, Jarvis MF, (2009). Mammalian P2X7 receptor pharmacology: comparison of recombinant mouse, rat and human P2X7 receptors. *Br J Pharmacol*, **157**, 1203-1214.
- Dorsam RT, Kunapuli SP, (2004). Central role of the P2Y<sub>12</sub> receptor in platelet activation. *J Clin Invest*, **113**, p340-345.
- Drury AN, Szent-Gyorgyi A, (1929). The physiological activity of adenine compounds with especial reference to their action upon the mammalian heart. *J Physiol*, **68**, 213-237.

- Duann P, Ho TY, Desai BD, Kapoian T, Cowen DS, Lianos EA, (2005). Mesengial cell apoptosis induced by stimulation of the adenosine A3 receptor: signaling and apoptotic events. *J Investig Med*, **53**, p37-43.
- Dubyak GR, el-Moatassim C (1993). Signal transduction via P2-purinergic receptors for extracellular ATP and other nucleotides. *Am J Physiol*, **265**, p577-606.
- Dvorianchikova G, Ivanov D, Barakat D, Grinberg A, Wen R, Slepak VZ, Shestopalov VI, (2012). Genetic ablation of Pannexin1 protects retinal neurons from ischemic injury. *PLoS One*, **7**, e31991.
- Ebneter A, Casson RJ, Wood JP, Childlow G, (2010). Microglial activation in the visual pathway in experimental glaucoma: spatiotemporal characterization and correlation with axonal injury. *Invest Ophthalmol Vis Sci*, **51**, p6448-6460.
- Egan TM, Khakh BS, (2004). Contribution of calcium ions to P2X channel responses. *J Neurosci*, **24**, p3413-3420.
- El-Tayeb A, Muller CE, (2006). Synthesis and structureactivity relationships of uracil nucleotide derivatives and analogues as agonists at human P2Y2, P2Y4 and P2Y6 receptors. *J Med Chem*, **49**, p7076-7087.
- El-Tayeb A, Qi A, Nicholas RA, Muller CE, (2011). Structural modifications of UMP, UDP and UTP leading to subtype-selective agonists for P2Y2, P2Y4 and P2Y6 receptors. *J Med Chem*, **54**, p2878-2890.
- Ennion SJ, Evans RJ, (2002). Conserved cysteine residues in the extracellular loop of the human P2X<sub>1</sub> receptor form disulfide bonds and are involved in receptor trafficking to the cell surface. *Mol Pharmacol*, **61**, p303-311
- Ennion SJ, Hagan S, Evans RJ, (2000). The Role of Positively Charged Amino Acids in ATP Recognition by Human P2X<sub>1</sub> Receptors. *J Biol Chem*, **275**, 35656.
- Erb L, Garrad R, Wang Y, Quinn T, Turner JT, Weisman GA, (1995). Site-directed mutagenesis of P2U purinoceptors. Positively charged amino acids in transmembrane helices 6 and 7 affect agonist potency and specificity. *J Biol Chem*, **270**, p4185-4188.
- Erb L, Weisman GA, (2012). Coupling of P2Y receptors to G proteins and other signalling pathways. *Wiley Interdiscip Rev Membr Transp Signal*, **1**, p789-803.

- Erblich B, Zhu L, Etgen AM, Dobrenis K, Pollard JW, (2011). Absence of colony stimulation factor-1 receptor results in loss of microglia, disrupted brain development and olfactory deficits. *PLoS One*, **6**, e26317
- Evans RK, Lewis C, Buell G, Valera S, North RA, Suprenant A, (1995). Pharmacological characterization of heterologously expressed ATP-gated cation channels (P2x purinoceptors). *Mol Pharmacol*, **48**, p178-183.
- Evans RJ, Lewis C, Virginio C, Lundstrom K, Buell G, Suprenant A, North RA, (1996). Ionic permeability of, and divalent cation effects on, two ATP-gated cation channels (P2X receptors) expressed in mammalian cells. *J Physiol*, **497**, p413-422.
- Eyo UB, Dailey ME, (2012). Effects of oxygen-glucose deprivation on microglial mobility and viability in developing mouse hippocampal tissues. *Glia*, **60**, p1747-1760.
- Eyo UB, Milner SA, Ahlers KE, Wu LJ, Dailey ME, (2013). P2X7 receptor activation regulates microglial cell death during oxygen-glucose deprivation. *Neuropharmacology*, **73**, p311-319.
- Facci L, Barbierato M, Marinelli C, Argentini C, Skaper SD, Giusti P, (2014). Toll-like receptors 2, -3 and -4 prime microglia but not astrocytes across central nervous system regions for ATP-dependent interleukin-1 $\beta$  release. *Sci Rep*, **4**, 6824.
- Falzoni S, Munerati M, Ferrari D, Spisani S, Moretti S, Di Virgilio F, (1995). The purinergic P2Z receptor of human macrophage cells. Characterization and possible physiological role. *J Clin Invest*, **95**, p1207-1216.
- Fan Y, Xie L, Chung CY, (2017). Signalling Pathways Controlling Microglia Chemotaxis. *Mol Cells*, **40**, p163-168.
- Feoktistov I, Biaggioni I, (1995). Adenosine A2b receptors evoke interleukin-8 secretion in human mast cells. An enprofylline-sensitive mechanism with implications for asthma. *J Clin Invest*, **96**, p-1979-1986.
- Ferguson DR, Kennedy I, Burton TJ, (1997). ATP is released from rabbit urinary bladder epithelial cells by hydrostatic pressure changes—a possible sensory mechanism? *J Physiol*, **505**, p503-511.
- Fernando SL, Saunders BM, Sluyter R, Skarratt KK, Wiley JS, Britton WJ, (2005). Gene dosage determines the negative effects of polymorphic alleles of the P2X7 receptor on adenosine

triphosphate-mediated killing of mycobacteria by human macrophages. *J Infect Dis*, **192**, p149-155.

Ferrari D, Chiozzi P, Falzoni S, Dal Susino M, Collo G, Buell G, Di, Virgilio F, (1997a). ATP-mediated cytotoxicity in microglial cells. *Neuropharmacology*, **36**, p1295-301.

Ferrari D, Chiozzi P, Falzoni S, Dal Susino M, Melchiorri L, Baricodri OR, Di Virgilio F, (1997b). Extracellular ATP triggers IL-1beta release by activating the purinergic P2Z receptor of human macrophages. *Immunol*, **159**, p1451-1458.

Ferrari D, Pizzirani C, Adinolfi E, Lemoli RM, Curti A, Idzko M, Panther E, Di Virgilio F, (2006). The P2X7 receptor: a key player in IL-1 processing and release. *J Immunol*, **176**, p387-3883.

Ferrari D, Villalba M, Chiozzi P, Falzoni S, Ricciardi-Castagnoli P, Di Virgilio F, (1996). Mouse microglial cells express a plasma membrane pore gated by extracellular ATP. *J Immuno*, **156**, p1531-1539.

Ferrari D, Los M, Bauer MK, Vandenabeele P, Wesselborg S, Schulze-Osthoff K, (1999). P2Z purinoreceptor ligation induces activation of caspases with distinct roles in apoptotic and necrotic alterations of cell death. *FEBS Lett*, **447**, p71-75.

Filippov AK, Choi RC, Simon J, Bernard EA, Brown DA, (2006). Activation of P2Y1 nucleotide receptors induces inhibition of the M-type K<sup>+</sup> current in rat hippocampal pyramidal neurons. *J Neurosci*, **26**, p9340-9348.

Fink SL, Cookson, BT, Caspase-dependent pore formation during pyroptosis leads to osmotic lysis of infected host macrophages. *Cell Microbiol*, **8**, p1812-1825

Fischer W, Zadori Z, Kullnick Y, Groger-Arndt H, Franke H, Wirkner K, Illes P, Mager PP, (2007). Conserved lysine and arginine residues in the extracellular loop of P2X(3) receptors are involved in agonist binding.

Flaxman SR, Bourne RRA, Resnikoff S, Ackland P, Braithwaite T, Cicinelli MCV, Das A, Jonas JB, Keefe J, Kempen JH, Leasher J, Limburg H, Naidoo K, Pesudvos K, Silvester A, Stevens GA, Thahhan N, Wong T, Taylor HR, (2017). Global causes of blindness and distance vision impairment 1990-2020: a systematic review and meta-analysis. *Lancet Global Health*, **5**, p1221-1234

- Frade JM, Barde YA, (1998). Microglia-derived nerve growth factor causes cell death in the developing retina. *Neuron*, **20**, 35-41
- Francheschi C, Abbrachio MP, Barbieri D, Ceruti S, Ferrari D, Iliou JP, Rounds S, Schubert P, Schulze-Lohoff, Rassendren FA, Staub M, Volonte C, Wakade AR, Burnstock G, (1996). Purines and cell death. *Drug Devel Res*, **39**, 442-449.
- Franke H, Bringmann A, Pannicke T, Krugel U, Grosche J, Reichenbach, Illes P, (2001). P2 receptors on macroglial cells: Functional implications for gliosis. *Drug Devel Res*, **53**, p140-147.
- Fredholm BB, Ijzerman AP, Jacobson KA, Klotz KN, Linden J, (2001). International Union of Pharmacology. XXV. Nomenclature and classification of adenosine receptors. *Pharmacol Rev*, **53**, p527-552.
- Fredriksson R, Lagerstrom MC, Lundin LG, Schioth HB, (2003). The G-protein-coupled receptors in the human genome from five main families. Phylogenetic analysis, paralogon groups, and fingerprints. *Mol Pharmacol*, **63**, p1256-1272.
- Freeman K, Tsui P, Moore D, Emson PC, Vawter L, Naheed S, Lane P, Bawagan H, Herrity N, Murphy K, Sarau HM, Ames RS, Wilson S, Livi GP, Chambers JK, (2001). Cloning, pharmacology, and tissue distribution of G-protein-coupled receptor GPR105 (KIAA0001) rodent orthologs. *Genomics*, **78**, p124-8.
- Frenguelli BG, Wigmore G, Lladet E, Dale N, (2007). Temporal and mechanistic dissociation of ATP and adenosine release during ischemia in the mammalian hippocampus. *J Neurochem*, **101**, p1400-1413.
- Frerking M, Malenka RC, Nicoll RA, (1998). Brain-derived neurotrophic factor (BDNF) modulates inhibitory, but not excitatory, transmission in the Ca1 region of the hippocampus. *J Neurophysiol*, **80**, p3383-3386.
- Fricks IP, Carter RL, Lazarowski ER, Harden TK, (2009). Gi-dependent cell signaling responses of the human P2Y14 receptor in model cell systems. *J Pharmacol Exp Ther*, **330**, 162-168.
- Fricks IP, Maddileti S, Carter RL, Lazarowski ER, Nicholas RA, Jacobson KA, Harden TK, (2008). UDP is a competitive antagonist at the human P2Y14 receptor. *J Pharmacol Exp Ther*, **325**, p588-94.

- Fries JE, Goczalik IM, Wheeler-Schiling TH, Kohler K, Guenther E, Wold S, Wiedemann P, Bringmann A, Reichenbach A, Francke M, Pannicke T, (2005). Identification of P2Y receptor subtypes in human muller glial cells by physiology, single cell RT-PCR and immunohistochemistry. *Invest Ophthalmol Vis Sci*, **46**, p3000-3007.
- Fu Y, Yang MS, Jiang J, Ganesh T, Joe E, Dingledine R, (2015). EP2 Receptor Signaling regulates Microglial Cell Death. *Mol Pharmacol*, **88**, 161-170.
- Fuchsjaeger-Mayrl G, Wally B, Georgopoulos M, Rainer G, Kircher K, Buehl W, Amoajo-Mensah T, Eichler HG, Vass C, Schmetterer L, (2004). Ocular blood flow and systemic blood pressure in patients with primary open-angle glaucoma and ocular hypertension. *Invest Ophthalmol Vis Sci*, **45**, p834-839.
- Fukumoto Y, Tanaka KF, Parajuli B, Shibata K, Yoshioka H, Kanemaru K, Gachet C, Ikenaka K, Koizumi S, Kinouchi H, (2018). Neuroprotective effects of microglial P2Y<sub>1</sub> receptors against ischemic neuronal injury. *J Cereb Blood Flow Metab*
- Fumagalli M, Brambilla R, D'Ambrosi N, Volonte C, Matteoli M, Verderio C, Abbracchio MP, (2003). Nucleotide-mediated calcium signaling in rat cortical astrocytes: role of P2X and P2Y receptors. *Glia*, **43**, p218-230.
- Fumagalli M, Trincavelli L, Lecca D, Martini C, Ciana P, Abbracchio MP, (2004). Cloning, pharmacological characterisation and distribution of the rat G-protein-coupled P2Y(13) receptor. *Biochem Pharmacol*, **68**, p113-24.
- Furuichi T, Yoshikawa S, Miyawaki A, Wada K, Maeda N, Mikoshiba K, (1989). Primary structure and functional expression of the inositol 1,4,5-triphosphate-binding protein P400. *Nature*, **342**, p32-38.
- Gallego BI, SalazarrJJ, de HozR, Rojas B, Ramirez AI, Salinas-Navarro M, Ortin-Martinez A, Valiente-Soriano FJ, Aviles-Trigueros M, Villegas-Perez MP, Vidal-Sanz M, Trivino A, Ramirez JM, (2012). IOP induces upregulation of GFAP and MHC-II and microglia reactivity in mice retina contralateral to experimental glaucoma. *J Neuroinflammation*, **9**, 92
- Gallina D, Zelinka CP, Cebulla CM, Fischer AJ, (2015). Activation of glucocorticoid receptors in Müller glia is protective to retinal neurons and supresses microglial reactivity. *Exp Neurol*, **273**, p114-125.

- Galvao J, Elvas F, Martins T, Cordeiro MF, Ambrosio AF, Santiago AR, (2015). Adenosine A3 receptor activation is neuroprotective against retinal neurodegeneration. *Exp Eye Res*, **140**, p65-74.
- Garcia-Guzman M, Soto F, Laube B, Stühmer W, (1996). Molecular cloning and functional expression of a novel rat heart P2X purinoceptor. *FEBS Lett*, **388**, p123-127.
- Garcia-Guzman M, Stühmer W, Soto F, (1997a). Molecular characterization and pharmacological properties of the human P2X3 purinoceptor. *Brain Res. Mol. Brain Res.*, **47**, p59-66.
- Garcia-Guzman M, Soto F, Gomez-Hernandez JM, Lund PE, Stühmer W, (1997b). Characterization of recombinant human P2X4 receptor reveals pharmacological differences to the rat homologue. *Mol Pharmacol*, **51**, p109-118.
- Gartland A, Hipkind RA, Gallagher JA, Bowler WB, (2001). Expression of a P2X7 receptor by a subpopulation of human osteoblasts. *J Bone Miner Res*, **16**, p846-856.
- Gever J, Cockayne DA, Dillon MP, Burnstock G, Ford AP (2006). Pharmacology of P2X channels *Pflugers Arch*, **452**, 513-537.
- Gibert B & Mehlen (2015). Dependence Receptors and Cancer: Addiction to Trophic ligands. *Cancer Res*, **75**, p5171-5175.
- Ginhoux F, Greter M, Leboeuf M, Nandi S, See P, Gokhan S, Mehler MF, Conway SJ, Ng LG, Stanley ER, Samokhvalov IM, Merad M, (2010). Fate mapping analysis reveals that adult microglia derive from primitive macrophages. *Science*, **330**, p841-845.
- Ginhoux F, Lim S, Hoeffel G, Low D, Huber T, (2013). Origin and differentiation of microglia. *Front Cell Neurosci*, **7**, 45.
- Girard S, Brough D, Lopez-Castejon G, Giles J, Rothwell NJ, Allan SM, (2013). Microglia and macrophages differentially modulate cell death after brain injury caused by oxygen-glucose deprivation in organotypic brain slices. *Glia*, **61**, p813-824.
- Girkin CA, McGwin G Jr, Morris R, Kuhn F, (2005). Glaucoma following penetrating ocular trauma: a cohort study of the United States Eye Injury Registry. *Am J Ophthalmol*, **139**, p100-105.
- Grahames CB, Michel AD, Chessel IP, Humphrey PP, (1999). Pharmacological characterization of ATP and LPS-induced IL-1beta release in human monocytes. *Br J Pharmacol*, **127**, 1915-1921.

- Greenfeder SA, Nunes P, Kwee L, Labow M, Chizzonite RA, Ju G, (1995). Molecular cloning and characterization of a second subunit of the interleukin 1 receptor complex. *J Biol Chem*, **270**, p13757-13765.
- Grootjans S, Vanden Berghe T, Vandenabeele (2017). Initiation and execution mechanisms of necroptosis: an overview. *Cell Death Differ*, **24**, p1184-1195.
- Gross O, Poeck H, Bscheider M, Dostert C, Hanneschlager N, Endres S, Hartmann G, Tardivel A, Schweighoffer E, Tybulecicz V, Mocsai A, Tschopp J, Ruland J, (2009). Syk kinase signalling couple to the Nlrp3 inflammasome for anti-fungal host defence. *Nature*, **459**, p433-436.
- Gu BJ, Zhang WY, Bendall LJ, Chessell IP, Buell GN, Wiley JS, (2000). Expression of P2X(7) purinoceptors on human lymphocytes and monocytes: evidence for non-functional P2X(7) receptors. *Am J Physiol Cell Physiol*, **279**, p1189-1197.
- Gu BJ, Zhang WY, Worthington RA, Sluyter R, Dao-Ung P, Petrou S, Barden JA, Wiley JS, (2001). A Glu-496 to Ala polymorphism leads to loss of function of the human P2X7 receptor. *J Biol Chem*, **276**, p11135-11142.
- Gustin A, Kirchmeyer M, Konicina E, Felten P, Losciuto S, Heurtaux T, Tardivel A, Heuschling P, Dostert C, (2015). NLRPS inflammasome is expressed and functional in mouse brain microglia but not astrocytes. *PLoS One*, **10**, e0130624.
- Haas M, Shaaban A, Reiser G, (2014). Alanine-(87)-threonine polymorphism impairs signalling and internalization of the human P2Y11 receptor, when co-expressed with the P2Y1 receptor. *J Neurochem*, **129**, p602-613.
- Halle A, Hornung V, Petzold GC, Stewart CR, Monks, BG, Reinheckel T, Fitzgerald KA, Latz E, Moore KJ, Golenbock DT, (2008). The NALP3 inflammasome is involved in innate immune response to amyloid-beta. *Nat Immuno*, **9**, p857-865.
- Hamard P, Hamard H, Dufaux J, Quesnot S, (1994). Optic nerve head blood flow using a laser Doppler velocimeter and haemorheology in primary open angle glaucoma and normal pressure glaucoma. *Br J Ophthalmol*, **78**, p449-453.
- Hammarberg C, Schulte G, Fredholm BB, (2003). Evidence for functional adenosine A3 receptors in microglial cells. *J Neurochem*, **86**, p1051-1054.

- Hangai M, Yoshimura N, Yoshida M, Yabuuchi K, Honda Y, (1995). Interleukin-1 gene expression in transient retinal ischemia in the rat. *Invest Ophthalmol Vis Sci*, **36**, p571-578.
- Hasko G, Linden J, Cronstein B, Pacher P, (2008). Adenosine receptors: therapeutic aspects for inflammatory and immune diseases. *Nat Rev Drug Discov*, **7**, 759-770.
- Hattori M, Gouaux E, (2012). Molecular mechanism of ATP binding and ion channel activation in P2X receptors. *Nature*, **485**, p207-210
- Haynes SE, Hollopeter G, Yang G, Kurpius D, Dailey ME, Gan WB, Julius D, (2006). The P2Y<sub>12</sub> receptor regulates microglial activation by extracellular nucleotides. *Nat Neurosci*, **9**, p1512-1519.
- He Y, Taylor N, Fourgeaud L, Bhattacharya A, (2017). The role of microglial P2X<sub>7</sub>: modulation of cell death and cytokine release. *J Neuroinflammation*, **14**, p135.
- Heine P, Braun N, Sevigny J, Robson SC, Servos J, Zimmermann H, (2001). The C-terminal cysteine-rich region dictates specific catalytic properties in chimeras of the ectonucleotidases NTPDase1 and NTPDase2. *Eur J Biochem*, **268**, p364-373.
- Helliwell RM, ShioukHuey CO, Dhuna K, Molero JC, Ye JM, Xue CC, Stokes L, (2015). Selected ginsenosides of the protopanaxidol series are novel positive allosteric modulators of P2X<sub>7</sub> receptors. *Br J Pharmacol*, **172**, p3326-3340.
- Henn A, Lund S, Hedtjarn M, Schrattenholz A, Porzgen P, Leist M, (2009). The suitability of BV2 cells as alternative model system for primary microglia cultures or for animal experiments examining brain inflammation. *ALTEX*, **26**, 83-94.
- Herbert JM, Savi P, (2003). P2Y<sub>12</sub>, a new platelet ADP receptor, target of clopidogrel. *Semin Vasc Med*, **3**, p113-122.
- Hibell AD, Kidd EJ, Chessell IP, Humphrey PP, Michel AD, (2000). Apparent species differences in the kinetic properties of P2X<sub>7</sub> receptors. *Br J Pharmacol*, **130**, p167-173.
- Ho T, Vessey KA, Fletcher EL, (2014). Immunolocalization of the P2X<sub>4</sub> receptor on neurons and glia in the mammalian retina. *Neuroscience*, **277**, p55-71.
- Hoffmann K, Baqi Y, Morena MS, Glänzel M, Müller CE, von Kügelgen I, (2009). Interaction of new, very potent non-nucleotide

- antagonists with Arg256 of the human platelet P2Y<sub>12</sub> receptor. *J Pharmacol Exp Ther*, **331**, p648-55.
- Hogquist KA, Nett MA, Unanue ER, Chaplin DD, (1991a). Interleukin 1 is processed and released during apoptosis. *Proc Nat Acad Sci USA*, **88**, p8485-8489.
- Hogquist KA, Unanue ER, Chaplin DD, (1991b). Release of IL-1 from mononuclear phagocytes. *J Immunol*, **147**, p2181-2186.
- Hollopeter G, Jantzen HM, Vincent D, Li G, England L, Ramakrishnan V, Yang RB, Nurden P, Nurden A, Julius D, Conley PB, (2001). Identification of the platelet ADP receptor targeted by antithrombotic drugs. *Nature*, **409**, p202-207.
- Holton P, (1959). The liberation of adenosine triphosphate on antidromic stimulation of sensory nerves. *J Physiol*, **145**, p494-504.
- Honda S, Sasaki Y, Ohsawa K, Imai Y, Nakamura Y, Inoue K, Kohsaka S, (2001). Extracellular ATP or ADP induce chemotaxis of cultured microglia through Gi/o-coupled P2Y receptors. *J Neurosci*, **21**, p1975-1982.
- Hoogland IC, Houbolt C, van Westerloo DJ, van Gool WA, van de Beek D, (2015). Systemic inflammation and microglial activation: systematic review of animal experiments. *J Neuroinflammation*, **12**, 114.
- Howell GR, Macalinao DG, Sousa GL, Walden M, Soto I, Kneeland SC, Barbay JM, King BL, Marchant JK, Hibbs M, Stevens B, Barres BA, Clark AF, Libby RT, John SW, (2011). Molecular clustering identifies complement and endothelin induction as early events in a mouse model of glaucoma. *J Clin Invest*, **121**, p1429-1444.
- Hu, H, Lu W, Laites AM, Mitchell CH, (2008). Stimulation of P2X<sub>7</sub> receptor kills rat retinal ganglion cells in vivo. *Invest Ophthalmol Vis Sci*, **49**, 2063
- Hu H, Wennan L, Zhang M, Zhang X, Argall AJ, Patel A, Lee GE, Kim Y, Jacobson KA, Laites AM, Mitchell CH, (2010). Stimulation of P2X<sub>7</sub> receptor kills rat retinal ganglion cells in vivo. *Exp Eye Res*, **91**, p425-432.
- Hu Q, Wu D, Chen W, Yan Zhen, Yan C, He T, Liang Q, Shi Y (2014). Molecular determinants of caspase-9 activation by the Apaf-1 apoptosome. *PNAS* **111**, p16254-16261.

- Hu X, Li P, Guo Y, Wang H, Leak RK, Chen S, Gao Y, Chen J, (2012). Microglia/macrophage polarization dynamics reveal novel mechanism of injury expansion after focal cerebral ischemia. *Stroke*, **43**, p3063-3070.
- Huang L, Xu W, Xu G, (2013). Transplantation of CX3CL1-expressing mesenchymal stem cells provides neuroprotective and immunomodulatory effects in a rat model of retinal degeneration. *Ocul Immunol Inflamm*, **21**, p276-285.
- Huang Z, Zhou T, Sun X, Zheng Y, Cheng B, Li M, Liu X, He C, (2018). Necroptosis in microglia contributes to neuroinflammation and retinal degeneration through TLR4 activation. *Cell Death Differ*, **25**, 180-189.
- Hulsmann M, Nickel P, Kassack M, Schmalzing G, Lambrecht G, Markwardt F, (2003). NF449, a novel picomolar potency antagonist at human P2X1 receptors. *Eur J Pharmacol*, **470**, p1-7
- Hume DA, Perry VH, Gordon S, (1983). Immunohistochemical localization of a macrophage-specific antigen in developing mouse retina: phagocytosis of dying neurons and differentiation of microglial cells to form a regular array in the plexiform layers. *J Cell Biol*, **97**, p253-257.
- Humphreys BD, Rice J, Kertsey SB, Dubyak GR, (2000). Stress-activated protein kinase/JNK activation and apoptotic induction by the macrophage P2X7 nucleotide receptor. *J Biol Chem*, **275**, p26972-26798.
- Inoue K, (2006). The function of microglia through purinergic receptors: neuropathic pain and cytokine release. *Pharmacol Ther*, **109**, p210-226.
- Inoue K, Hosoi J, Denda M, (2007). Extracellular ATP has stimulatory effects on the expression and release of IL-6 via purinergic receptors in normal human epidermal keratinocytes. *J Invest Dermatol*, **127**, p362-371.
- Irino Y, Nakamura Y, Inoue K, Kohsaka S, Ohsawa K, (2008). Akt activation is involved in P2Y12 receptor-mediated chemotaxis of microglia. *J Neurosci Res*, **86**, p1511-1519.
- Ivanov AA, Ko H, Cosyn L, Maddileti S, Besada P, Fricks I, Costanzi S, Harden TK, Calenbergh SV, Jacobson KA, (2007). Molecular modelling of the human P2Y2 receptor and design of a selective agonist, 2'-amino-2'-deoxy-2-thiouridine 5'-triphosphate. *J Med Chem*, **50**, p1166-1176.

- Jabs R, Guenther E, Marquardt K, Wheeler-Schilling TH, (2000). Evidence for P2X<sub>3</sub>, P2X<sub>4</sub>, P2X<sub>5</sub>, but not for P2X<sub>7</sub> containing purinergic receptors in Müller cells of the rat retina. *Mol Brain Res*, **76**, p205-210.
- Jacobson KA, Costanzi S, Deflorian F, (2013). Probing GPCR Structure: Adenosine and P2Y Nucleotide Receptors. *Methods Enzymol*, **520**, p199-217.
- Jacobson KA, Ivanov AA, de Castro S, Harden TK, Ko H, (2009). Development of selective agonists and antagonists of P2Y receptors. *Purinergic Signal*, **5**, 75-89.
- Jacobson KA, Jarvis MF, Williams M, (2002). Purine and pyrimidine (P2) receptors as drug targets. *J Med Chem*, **45**, p4057-4093.
- Jacobson KA, Kim YC, Wildman SS, Mohanram A, Harden TK, Boyer JL, King BF, Burnstock G, (1998). A pyridoxine cyclic phosphate and its 6-azoaryl derivative selectively potentiate and antagonize activation of P2X<sub>1</sub> receptors. *J Med Chem*, **41**, p2201-2206.
- Jacobson KA, Muller CE, (2015). Medicinal Chemistry of Adenosine, P2Y and P2X Receptors, *Neuropharmacology*, **104**, p31-49.
- James G, Butt A, (2002). P2Y and P2X purinoceptor mediated Ca<sup>2+</sup> signalling in glial cell pathology in the central nervous system. *Eur J Pharmacol*, **447**, 247-260
- Janssens R, Paindavoine P, Parmentier M, Boeynaems JM, (1999). Human P2Y<sub>2</sub> receptor polymorphism: identification and pharmacological characterization of two allelic variants. *Br J Pharmacol*, **127**, p709-716.
- Jarvis MF, Burgand EC, McGaraughty S, Honore P, Lynch K, Brennan TJ, Subieta A, Van Biesen T, Cartmell J, Bianchi B, Niforatos W, Kage K, Yu H, Mikusa J, Wismer CT, Zhu CZ, Chu K, Lee CH, Stewart AO, Polakowski J, Cox BF, Kowaluk E, Williams M, Sullivan J, Faltynek C, (2002). A-317491, a novel potent and selective non-nucleotide antagonist of P2X<sub>3</sub> and P2X<sub>2/3</sub> receptors, reduces chronic inflammatory and neuropathic pain in the rat. *Proc Natl Acad Sci USA*, **99**, p17179-17184.
- Jarvis MF, Khakh BS, (2009). ATP-gated P2X cation-channels. *Neuropharmacology*, **56**, p208-215.
- Jiang LH, Kim M, Spelta V, Bo X, Suprenant A, North RA, (2003). Subunit arrangement in P2X receptors. *J Neurosci*, **23**, p8903-8910

- Jiang R, Taly A, Lemione D, Martz A, Cunrath O, Grutter T, (2012). Tightening of the ATP-binding sites induces the opening of P2X receptor channels. *EMBO J*, **31**, p2134-2143.
- Jin M, Kim BW, Koppula S, Kim IS, Park JH, Kumar H, Choi DK, (2012). Molecular effects of activated BV-2 microglia by mitochondrial toxin 1-methyl-4-phenylpyridinium *Neurotoxicology*, **33**, 147-155.
- Johnson EC, Morrison JC, (2009). Friend or Foe? Resolving the Impact of Glial Responses in Glaucoma. *J Glaucoma*, **18**, p341-353.
- Jonas JB, Müller-Bergh JA, Schlötzer-Schrehardt UM, Naumann GO (1990). Histomorphometry of the human optic nerve. *Invest Ophthalmol Vis Sci*, **31**, p736-744.
- Jorgensen I, Miao EA, (2015). Pyroptotic cell death defends against intracellular pathogens. *Immunol Rev*, **265**, p130-142.
- Jung DY, Lee H, Jung BY, Ock J, Lee MS, Lee WH, Suk K, (2005). TLR4 but not TLR2 signals autoregulatory apoptosis of cultured microglia: a critical role of IFN- $\beta$  as a decision maker. *J Immunol*, **174**, 6467-6476.
- Juranyi Z, Sperlagh B, Vizi ES, (1999). Involvement of P2 purinoceptors and the nitric oxide pathway in [3H]purine outflow evoked by short-term hypoxia and hypoglycaemia in rat hippocampal slices. *Brain Res*, **823**, p183-190.
- Kaczmarek-Hajek K, Lorinczi E, Hausmann R, Nicke A, (2012). Molecular and functional properties of P2X receptors—recent progress and persisting challenges. *Purinergic Signal*, **8**, 375-417.
- Kaczmarek A, Vandenabeele P, Krysko DV, (2013). Necroptosis: the release of damage-associated molecular patterns and its physiological relevance. *Immunity*, **38**, p209-223.
- Kagayaki N, Stowe IB, Lee BL, O'Rourke K, Anderson K, Warming S, Cuellar T, Haley B, (2015). Caspase-11 cleaves gasdermin D for non-canonical inflammasome signalling. *Nature*, **526**, p666-671.
- Kahlenberg JM, Dubyak GR, (2004). Mechanisms of caspase-1 activation by P2X7 receptor mediated K<sup>+</sup> release. *Am J Physiol Cell Physiol*, **286**, c1100-8
- Kannengati TD, Lamkanfi M, Kim YG, Chen G, Park JH, Franchi L, Vandenabeele P, Nunez G, (2007). Pannexin-1-mediated

recognition of bacterial molecules activates the cryopyrin inflammasome independent of Toll-like receptor signalling. *Immunity*, **26**, p433-443.

- Kanneganti TD, Body-Malapel M, Amer A, Park JH, Whitfield J, Franchi L, Taraporewala ZF, Miller D, Patton JT, Inohara N, Nunez G, (2006). Critical role for Cryopyrin/Nalp3 in activation of caspase-1 in response to viral infection and double-stranded RNA. *J Biol Chem*, **281**, p36560-36568.
- Karlsetter M, Scholz R, Rutar M, Wong WT, Provis JM, Langmann T, (2015). Retinal microglia: just bystander or target for therapy? *Prog Retin Eye Res*, **45**, p30-57.
- Kato K, Nishimasu H, Okudaira S, Mihara E, Ishitani R, Takagi J, Aoki J, Nureki O, (2012). Crystal structure of Enpp1, an extracellular glycoprotein involved in bone mineralization and insulin signalling. *Proc Natl Acad Sci USA*, **109**, p16876-16881.
- Kato G, Inada H, Wake H, Akiyoshi R, Miyamoto A, Eto K, Ishikawa T, Moorhouse AJ, Strassman AM, Nabekura J, (2016) Microglial Contact Prevents excess depolarization and rescues neurons from excitotoxicity. *eNeuro*, **3**,
- Kawate T, Michel JC, Birdsong WT, Gouaux E, (2009). Crystal structure of the ATP-gated P2X4 ion channel in the closed state. *Nature*, **460**, p592-598.
- Kazui M, Nishiya Y, Ishizuka T, Hagihara K, Farid NA, Okazaki O, Ikeda T, Kurihara A, (2010). Identification of the human cytochrome P450 enzymes involved in the two oxidative steps in the bioactivation of clopidogrel to its pharmacologically active metabolite. *Drug Metab Dispos*, **38**, p92-99.
- Kemp PA, Sugar RA, Jackson AD, (2004). Nucleotide-mediated mucin secretion from differentiated human bronchial epithelial cells. *Am J Respir Cell Mol Biol*, **31**, p446-455.
- Kennedy C, Chootip K, Mitchell C, Syed NI, Tengah A, (2013). P2X and P2Y nucleotide receptors as targets in cardiovascular disease. *Future Med Chem*, **5**, p431-49.
- Kennedy C, Qi AD, Herold CL, Harden TK, Nicholas RA. (2000) ATP, an agonist at the rat P2Y(4) receptor, is an antagonist at the human P2Y(4) receptor. *Mol Pharmacol*, **57**, p926-931.
- Kerr JF, Wyllie AH, Currie AR, (1972). Apoptosis: a basic biological phenomenon with wide –ranging implications in tissue kinetics. *Br J Cancer*, **26**, p239-257.

- Kerr J, Nelson P, O'Brien C, (1998). A comparison of ocular blood flow in untreated primary open-angle glaucoma and ocular hypertension. *Am J Ophthalmol*, **126**, p42-51.
- Kettenmann H, Hanisch UK, Noda M, Verkhratsky A, (2011). Physiology of microglia. *Physiol Rev*, **91**, p461-553.
- Kettenmann H, Kirchhoff F, Verkhratsky A, (2013). Microglia: New Roles for the Synaptic Stripper. *Neuron*, **77**, p10-18.
- Kezic JM, Chrysostomou V, Trounce IA, McMenemy PG, Crowston JG, (2013). Effect of anterior chamber cannulation and acute IOP elevation on retinal macrophages in the adult mouse. *Invest Ophthalmol Vis Sci*, **54**, p3028-3036.
- Khadra A, Tomic M, Yan Z, Zemkova H, Sherman A, Stojilkovic SS, (2013). Dual gating mechanism and function of P2X7 receptor channels. *Biophys J*, **104**, 2612-2621.
- Khakh BS, Bao XR, Labarca C, Lester HA, (1999a). Neuronal P2X transmitter-gated cation channels change their ion selectivity in seconds. *Nat Neurosci*, **2**, p322-330.
- Khakh BS, Proctor WR, Dunwiddie TV, Labarca C, Lester HA, (1999b). Allosteric control of gating and kinetics at P2X(4) receptor channels. *J Neurosci*, **19**, p7289-7299.
- Kierdorf K, Emy D, Goldmann T, Sander V, Schulz C, Perdiguero EG, Wieghofer P, Heinrich A, Riemke P, Holscher C, Müller DN, Luckow B, Brocker T, Debowski K, Fritz G, Opdenakker G, Diefenbach A, Biber K, Heikenwalder M, Geissmann F, Rosenbauer F, Prinz M, (2013). Microglia emerge from erythromyeloid precursors via Pu.1- and Irf8-dependent pathways. *Nat Neurosci*, **16**, p273-280.
- Kielian T, (2006). Toll-Like Receptors in Central Nervous System Glial Inflammation and Homeostasis. *J Neurosci Res*, **83**, p711-730.
- Kim YC, Lee JS, Sak K, Marteau F, Mamedova L, Boeynaems JM, Jacobson KA, (2005). Synthesis of pyridoxal phosphate derivatives with antagonist activity at the P2Y13 receptor. *Biochem Pharmacol.*, **70**, p266-274.
- King BF, Burnstock G, Boyer JL, Boeynaems JM (2000). P2Y receptors. IUPHAR Compendium of Receptor Characterization and Classification.
- Kischkel FC, Hellbardt S, Behrmann I, Germer M, Pawlita M, Krammer Ph, Peter ME, (1995). Cytotoxicity-dependent APO-1 (Fas/CD95)-

associated proteins form a death inducing signaling complex (DISC) with the receptor. *EMBO J*, **14**, p5579-5588

Kitaoka Y, Munemasa Y, Nakazawa T, Ueno S, (2007). NMDA-induced interleukin-1beta expression is mediated by nuclear factor-kappa Bp65 in the retina. *Brain Res*, **20**, p247-255.

Klapperstuck M, Buttner C, Schmalzing G, Markwardt F, (2001). Functional evidence of distinct ATP activation sites at the human P2X<sub>7</sub> receptor. *J Physiol*, **534**, p23-35.

Ko H, Carter RL, Cosyn L, Petrelli R, de Castro S, Besada P, Zhou Y, Cappellacci L, Franchetti P, Grifantini M, Van Calenbergh S, Harden TK, Jacobson KA, (2008). Synthesis and potency of novel uracil nucleotides and derivatives as P2Y<sub>2</sub> and P2Y<sub>6</sub> receptor agonists. *Bioorg Med Chem*, **16**, 6319-6332.

Kobayashi K, Yamanaka H, Fukuoka T, Dai Y, Obata K, Noguchi K, (2012). P2Y<sub>12</sub> receptor upregulation in activated microglia is a gateway of p38 signalling and neuropathic pain. *J Neurosci*, **28**, p2892-2902.

Kohno H, Chen Y, Kevany BM, Pearlman E, Miyagi M, Maeda T, Palczewski K, Maeda A (2013). Photoreceptor proteins initiate microglial activation via Toll-like receptor 4 in retinal degeneration mediated by all-trans-retinal. *J Biol Chem*, **288**, p15326-15341.

Koizumi S, Shigemoto-Mogami Y, Nasu-Tada K, Shinozaki Y, Ohsawa K, Tsuda M, Joshi BV, Jacobson KA, Kohsaka S, Inoue K, (2007). UDP acting at P2Y<sub>6</sub> receptors is a mediator of microglial phagocytosis. *Nature*, **446**, p1091-1095.

Kolb H, Fernandez E, Schouten J, Ahnelt P, Linberg KA, Fisher SK (1994). Are there three types of horizontal cell in the human retina? *J Comp Neurol*, **343**, p370-386

Kong H, Omran A, Ashhab MU, Gan N, Peng J, He F, Wu L, Deng X, Yin F, (2014). Changes in microglial inflammation-related and brain-enriched MicroRNAs expressions in response to in vitro oxygen-glucose deprivation. *Neurochem Res*, **39**, p233-243.

Kosicki M, Tomberg K, Bradley A, (2018). Repair of double-strand breaks induced by CRISPR-Cas9 leads to large deletions and complex rearrangements. *Nat Biotechnol*, **36**, p765-771.

Hidetoshi TS, Makoto T, Inoue K, (2012). P2Y receptors in microglia and neuroinflammation. *Wiley Interdiscip Rev Membr Transp Signal*, **4**, p493-501.

- Kreutzberg GW, (1996). Microglia: a sensor for pathological events in the CNS. *Trends Neurosci*, **19**, 312-318.
- La-Sala A, Ferrari D, Di Virgilio F, Idzko M, Norgauer J, Girolomoni G, (2003). Alerting and tuning the immune response by extracellular nucleotides. *J Leukoc Biol*, **73**, 339-343.
- Laflamme N, Rivest S, (2001). Toll-like receptor 4: the missing link of the cerebral innate immune response triggered by circulating gram-negative bacterial cell wall components. *FASEB J*, **15**, p155-163.
- Lagerstrom MC, Schioth HB, (2008). Structural diversity of G-protein-coupled receptors and significance for drug discovery. *Nat Rev Drug Discov*, **7**, p339-357.
- Lang D, Knop J, Wesche H, Raffetseder U, Kurrle R, Boraschi D, Martin MU, (1998). The type II IL-1 receptor interacts with the IL-1 receptors accessory protein: a novel mechanism of regulation of IL-1 responsiveness. *J Immunol*, **161**, p6871-6877.
- Langmann T, (2007). Microglia activation in retinal degeneration. *J Leukoc Biol*, **81**, 1345-1351.
- Lanner JT, Georgiou DK, Joshi AD, Hamilton SL, (2010). Ryanodine receptors: structure, expression, molecular details and function in calcium release. *Cold Spring Harb Perspect Biol*, **2**, a003996
- Latini S, Pedata F, (2001). Adenosine in the central nervous system: release mechanisms and extracellular concentrations. *J Neurochem*, **79**, p463-484.
- Lauro C, Cipriani R, Catalano M, Trettel F, Chece G, Brusadin V, Antonilli L, van Rooijen N, Eusebi F, Fredholm BB, Limatola C, (2010). Adenosine A<sub>1</sub> Receptors and Microglial Cells Mediate CX3CL1-Induced Protection of Hippocampal Neurons Against Glu-Induced Death. *NEUROPSYCHOPHARMACOL*, **35**, p1550-1559.
- Lauro C, Di Angelantonio S, Cipriani R, Sobrero F, Antonilli L, Brusadin V, Ragozzino D, Limatola C, (2008). Activity of adenosine receptors type 1 is required for CX3CR1-mediated neuroprotection and neuromodulation in hippocampal neurons. *J Immunol*, **180**, p7590-7596.
- Lawson LJ, Perry VH, Gordon S, (1992). Turnover of resident microglia in the normal adult mouse brain. *Neuroscience*, **48**, p405-415.

- Layhadi JA, Fountain SJ, (2017). P2X4 Receptor-Dependent Ca<sup>2+</sup> Influx Model Human Monocytes and Macrophages. *Int J Mol Sci*, **18**, E2261
- Lazarowski ER, Rochelle LG, O'Neal WK, Ribeiro CM, Grubb BR, Zhang V, Harden TK, Boucher RC, (2001). Cloning and functional characterization of two murine uridine nucleotide receptors reveal a potential target for correcting ion transport deficiency in cystic fibrosis gallbladder. *J Pharmacol Exp Ther*, **297**, p43-49.
- Lazarowski ER, Watt WC, Stutts MJ, Boucher RC, Harden TK, (1995). Pharmacological selectivity of the cloned human P2U-purinoceptor: potent activation by diadenosine tetraphosphate. *Br J Pharmacol*, **116**, p1619-1627.
- Lê KT, Paquet M, Nouel D, Babinski K, Séguéla P, (1997). Primary structure and expression of a naturally truncated human P2X ATP receptor subunit from brain and immune system. *FEBS Lett*, **418**, p195-199.
- Le Rhun A, Escalera-Maurer A, Bratovic M, Charpentier E, (CRISPR-Cas in *Streptococcus pyogenes*. *RNA Biol*, **16**, 380-389.
- Lecut C, Frederix K, Johnson DM, Deroanne C, Thiry M, Faccinnetto C, Maree R, Evans RJ, Volders PG, Oury C, (2009). P2X1 ion channels promote neutrophil chemotaxis through Rho kinase activation. *J Immunol*, **183**, p2801-2809.
- Lee SW, de Rivero Vaccari JP, Truettner JS, Dietrich WD, Keane RW, (2019). The role of microglia inflammasome activation in pyroptotic cell death following penetrating traumatic brain injury. *J Neuroinflammation*, **16**, 27.
- Lees MP, Fuller SJ, McLeod R, Boutler NR, Miller CM, Zakrzewski AM, Mui EJ, Witola WH, Coyne JJ, Hargrave AC, Jamieson SE, Blackwell JM, Wiley JS, Smith NC, (2010). P2X7 receptor-mediated killing of an intracellular parasite, *Toxoplasma gondi*, by human and murine macrophages. *J Immunol*, **184**, p7040-7046.
- Li J, Feng Y, Sung MS, Lee TH, Park SW, (2017). Association of interleukin-1 gene clusters polymorphisms with primary open-angle glaucoma: a meta-analysis. *BMC Ophthalmol*, **17**, 218.
- Li A, Zhang X, Zheng D, Ge J, Laties AM, Mitchell CH, (2011). Sustained elevation of extracellular ATP in aqueous humor from humans with primary chronic angle-closure glaucoma. *Exp Eye Res*, **93**, p528-533.

- Liang KJ, Lee JE, Wand YD, Ma W, Fontainhas AM, Fariss RN, Wong WT, (2009). Regulation of dynamic behaviour of retinal microglia by CX3CR1 signaling. *Invest Ophthalmol Vis Sci*, **50**, p4444-4451.
- Libert F, Schiffmann Sn, Lefort A, Parmentier M, Gerard C, Dumont JE, Vanderhaeghen JJ, Vassart G, (1991). The orphan receptor cDNA RDC7 encodes an A1 adenosine receptor. *EMBO J*, **10**, p1677-1682.
- Libby RT, Anderson MG, Pang, IH, Robinson ZH, Savinova OV, Cosma IM, Snow A, Wilson LA, Smith RS, Clark AF, John SW, (2005). Inherited glaucoma in DBA/2J mice: pertinent disease features for studying the neurodegeneration. *Vis Neurosci*, **22**, p637-648.
- Lieber MR, (2010). The mechanism of double strand DNA break repair by the nonhomologous DNA end-joining pathway. *Annu Rev Biochem*, **79**, p181-211.
- Light AR, Wu Y, Huguen RW, Guthrie PB, (2006). Purinergic receptors activating rapid intracellular Ca<sup>2+</sup> increases in microglia. *Neuron Glia Biol*, **2**, p125-138.
- Lim SH, ark E, You B, Jung Y, Park AR, Park SG, Lee JR, (2013). Neuronal synapse formation induced by microglia and interleukin 10. *PLoS One*, **8**, 1-13.
- Lin HJ, Tsai SC, Tsai FJ, Chen WC, Tsai JJ, Hsu CD, (2003). Association of interleukin 1beta and receptor antagonist gene polymorphisms with primary open-angle glaucoma. *Ophthalmologica*, **217**, p358-364.
- Linkermann A, Green DR, (2014). Necroptosis. *N Engl J Med*, **370**, p455-465.
- Lister MF, Sharkey J, Sawatzky DA, Hodgkiss JP, Davidson DJ, Rossi AG, Finlayson K, (2007). The role of the purinergic P2X7 receptor in inflammation. *J Inflamm (Lond)*, **4**, 5
- Liu S, Li ZW, Weinreb RN, Xu G, Lindsey JD, Ye C, Yung WH, Pang CP, Lam DS, Leung CK, (2012). Tracking retinal microgliosis in models of retinal ganglion cell damage. *Invest Ophthalmol Vis Sci*, **53**, p6254-6262.
- Liu X, Quan N, (2018). Microglia and CNS Interleukin-1: Beyond Immunological Concepts. *Front Neurol*, **9**, 8.
- Liversidge J, Grabowski P, Ralston S, Benjamin N, Forrester JV, (1994). Rat retinal pigment epithelial cells express an inducible

form of nitric oxide synthase and produce nitric oxide in response to inflammatory cytokines and activated T cells. *Immunology*, **83**, p404-409.

Lloyd HG, Deussen A, Wuppermann H, Schrader J, (1988). The transmethylation pathway as a source of adenosine in the isolated guinea-pig heart. *Biochem J*, **252**, p489-494.

Locksley RM, Killeen N, Lenardo MJ, (2001). The TNF and TNF receptor superfamilies: integrating mammalian biology. *Cell*, **104**, p487-501.

Locovei S, Wang J, Dahl H, (2006). Activation of pannexin 1 channels by ATP through P2Y receptors and by cytoplasmic calcium. *FEBS Lett*, **580**, p239-244.

Locovei S, Scemes E, Qiu F, Spray DC, Dahl G, (2007). Pannexin1 is part of the pore forming unit of the P2X(7) receptor death complex. *FEBS Lett*, **581**, p483-488.

Longhurst PA, Schwegel T, Folander K, Swanson R, (1996). The human P2x1 receptor: molecular cloning, tissue distribution, and localization to chromosome 17. *Biochim Biophys Acta*, **1308**, p185-188.

Lu W, Hu H, Sevigny J, Gabelt BT, Kaufman PL, Johnson EC, Morrison JC, Zode GS, Sheffield VC, Zhang X, Laties AM, Mitchell CM, (2015). Rat, mouse and primate models of chronic glaucoma show sustained elevation of extracellular ATP and altered purinergic signalling in the posterior eye. *Invest Ophthalmol Vis Sci*, **56**, p3075-3083.

Lu YC, Yeh WC, Ohashi PS, (2008). LPS/TLR4 signal transduction pathway. *Cytokine*, **42**, p145-151.

Luheshi NM, Giles JA, Lopez-Castejon G, Brough D, (2012). Shpingosine regulates the NLRP3-inflammasome and IL-1b release from macrophages. *Eur J Immunol*, **42**, p716-725.

Lund S, Christensen KV, Hedtjarn M, Mortensen AL, Hagberg H, Falsig J, Hasseldam H, Schrattenholz A, Porzgen P, Leist M, (2006). The dynamics of the LPS triggered inflammatory response of murine microglia under different culture and in vivo conditions. *J Neuroimmunol*, **180**, p71-87.

Luo C, Yang X, Kain A, Powell D, Kuehn MH, Tezel G, (2010). Glaucomatous Tissue Stress and the Regulation of Immune Response through Glial Toll-Like Receptor Signaling. *Invest Ophthalmol Vis Sci*, **51**, p5697-5707.

- Lustig KD, Shiau AK, Brake AJ, Julius D, (1993). Expression cloning of an ATP receptor from mouse neuroblastoma cells. *Proc Natl Acad Sci USA*, **90**, p5113-5117.
- Lynch KJ, Touma E, Niforatos W, Kage KL, Burgard EC, van Biesen T, Kowaluk EA, Jarvis MF, (1999). Molecular and functional characterization of human P2X(2) receptors. *Mol Pharmacol*, **56**, 1171-1181.
- Lyons SA, Kettenmann H, (1998). Oligodendrocytes and microglia are selectively vulnerable to combined hypoxia and hypoglycaemia. *J Cereb Blood Flow Metab*, **18**, p521-530.
- Lyubchenko T, Woodward H, D Veo K, Burns N, Nijmeh H, Liubchenko GA, Stenmark KR, Gerasimovskaya EV, (2011). P2Y1 and P2Y13 purinergic receptors mediate Ca<sup>2+</sup> signaling and proliferative responses in pulmonary artery vasa vasorum endothelial cells. *Am J Cell Physiol*, **300**, 266-275.
- MacKenzie A, Wilson HL, Kiss-Toth E, Dower SK, North RA, Suprenant A, (2001). Rapid secretion of interleukin-1beta by microvesicle shedding. *Immunity*, **15**, p825-835.
- MacKenzie A, Young MT, Adinolfi E, Suprenant A, (2005). Pseudoapoptosis induced by brief activation of ATP-gated P2X7 receptors. *J Biol Chem*, **280**, 33968-33976.
- Madeira MH, Boia R, Elvas F, Martins T, Cunha RA, Ambrosio AF, Santiago AR, (2015). Selective A2A receptor antagonist prevents microglia-mediated neuroinflammation and protects retinal ganglion cells from high intraocular pressure-induced transient ischemic injury. *Transl Res*, **169**, p112-128.
- Maderna P, Godson C, (2003). Phagocytosis of apoptotic cells and the resolution of inflammation. *Biochim Biophys Acta*, **1639**, 141-151.
- Mamedova LK, Joshi BV, Gao ZG, von Kügelgen I, Jacobson KA, (2004). Diisothiocyanate derivatives as potent, insurmountable antagonists of P2Y6 nucleotide receptors. *Biochem Pharmacol*, **67**, 1763-1770.
- Man SM, Karki R, Kanneganti TD, (2017). Molecular mechanisms and functions of pyroptosis, inflammatory caspases and inflammasomes in infectious diseases. *Immunol Rev*, **277**, p61-75.
- Maneu V, Yanez A, Murciano C, Molina A, Gil ML, Gozalbo D, (2011). Dectin-1 mediates in vitro phagocytosis of *Candida albicans*

- yeast cells by retinal microglia. *FEMS Immunol Med Microbiol*, **63**, p148-150.
- Mansfield KJ, Hughes JR, (2014). P2Y Receptor Modulation of ATP Release in the Urothelium. *Biomed Res Int*, 830374.
- Mansoor SE, Lu W, Oosterheert W, Shekhar M, Tajkhorshid E, Gouaux E, (2016). X-ray structure define human P2X(3) receptor gating cycle and antagonist action. *Nature*, **538**, p66-77.
- Mariathasan S, Weiss DS, Newton K, McBride J, O'Rourke K, Roose-Girma M, Lee WP, Weinrauch Y, Monack DM, Dixit VM, (2006). Cryopyrin activates the inflammasome in response to toxins and ATP. *Nature*, **440**, p228-232.
- Marino G, Kroemer G, (2013). Mechanisms of apoptotic phosphatidylserine exposure. *Cell Res*, **23**, p1247-1248.
- Marmour M, (1993). Chapter 8 mechanisms of retinal adhesion. *Prog Retin Eye Res*. **12**, p179-204.
- Marquez-Klaka B, Rettinger J, Bhargava Y, Eisele T, Nicke A, (2007). Identification of an intersubunit cross-link between substituted cysteine residues located in the putative ATP binding site of the P2X1 receptor. *J Neurosci*, **27**, p1456-1466.
- Marteau F, Le Poul E, Communi D, Communi D, Labouret C, Savi P, Boeynaems JM, Gonzalez NS, (2003). Pharmacological characterization of the human P2Y13 receptor. *Mol Pharmacol*, **64**, p104-112.
- Martinon F, Burns K, Tschopp J, (2002). The inflammasome: a molecular platform triggering activation of inflammatory caspases and processing of proIL-beta. *Mol Cell*, **10**, p417-426.
- Martins I, Wang Y, Michaud M, Ma Y, Sukkurwala AQ, Shen S, Kepp O, Metivier D, Galluzzi L, Perfettini JL, Zitvogel L, Kroemer G, (2014). Molecular mechanisms of ATP secretion during immunogenic cell death. *Cell Death Differ*, **21**, p79-91.
- Maruoka H, Barrett MO, Ko H, Tosh DK, Melman A, Burianek LE, Balasubramanian R, Berk B, Costanzi S, Harden TK, Jacobson KA, (2010) Pyrimidine ribonucleotides with enhanced selectivity as P2Y(6) receptor agonists: novel 4-alkyloxyimino, (S)-methanocarba, and 5'-triphosphate gamma-ester modifications. *J Med Chem*, **53**, p4488-4501.
- Maruoka H, Jayasekara MP, Barrett MO, Franklin DA, de Castro S, Kim N, Costanzi S, Harden TK, Jacobson KA, (2011). Pyrimidine

nucleotides with 4-alkoxyimino and terminal tetraphosphate  $\delta$ -ester modifications as selective agonists of the P2Y(4) receptor. *J Med Chem.*, **54**, p4018-4033.

McCarter Jc, (1940). A silver carbonate staining method for oligodendrocytes and microglia for routine use. *Am J Pathol*, **16**, p233-235.

Meis S, Hamacher A, Hongwiset D, Marzian C, Wiese M, Eckstein N, Royer HD, Communi D, Boeynaems JM, Hausmann R, Schmalzing G, Kassack MU, (2010). NF546 [4,4'-(carbonylbis(imino-3,1-phenylene-carbonylimino-3,1-(4-methylphenylene)-carbonylimino))-bis(1,3-xylene-alpha,alpha'-diphosphonic acid) tetrasodium salt] is a non-nucleotide P2Y11 agonist and stimulates release of interleukin-8 from human monocyte-derived dendritic cells. *J Pharmacol Exp Ther*, **332**, p238-247.

Messenger SW, Falkowski MA, Groblewski GE, (2014). Ca<sup>2+</sup>-regulated secretory granule exocytosis in pancreatic and parotid acinar cells. *Cell Calcium*, **55**, p369-375.

Miao EA, Rajan JV, Aderem A, (2011). Caspase-1 induced pyroptotic cell death. *Immuno Rev*, **243**, p206-214.

Michel AD, Chambers LJ, Walter DS, (2008). Negative and positive allosteric modulators of the P2X(7) receptor. *Br J Pharmacol*, **153**, p737-750.

Micklewright JJ, Layhadi JA, Fountain SJ, (2018). P2Y<sub>12</sub> receptor modulation of ADP-evoked intracellular Ca<sup>2+</sup> signalling in THP-1 human monocytic cells. *Br J Pharmacol*, **175**, p2483-2491.

Mitchell CH, Lu W, Hu H, Zhang X, Reigada D, Zhang M, (2009). The P2X(7) receptor in retinal ganglion cells: A neuronal model of pressure-induced damage and protection by a shifting purinergic balance. *Purinergic Signal*, **5**, p241-249

Mizogucji Y, Monji A, (2017). Microglial Intracellular Ca<sup>2+</sup> signalling in Synaptic Development and its Alterations in Neurodevelopmental Disorders. *Front Cell Neurosci*, **11**:69.

Moore CS, Ase AR, Kinsara A, Rao VT, Michell-Robinson M, Leong SY, Butovsky O, Ludwin SK, Seguela P, Bar-Or A, Antel JP, (2015). P2Y<sub>12</sub> expression and function in alternatively activated human microglia. *Neruol Neuroimmunol Neuroinflamm*, **2**, e80

Moore DJ, Chambers JK, Wahlin JP, Tan KB, Moore GB, Jenkins O, Emson PC, Murdock PR, (2001). Expression pattern of human

- P2Y receptor subtypes: a quantitative reverse transcription-polymerase chain reaction study. *Biochim Biophys Acta*, **1521**, p107-119.
- Mozaffarieh M, Grieshaber MC, Flammer J, (2008). Oxygen and blood flow: players in the pathogenesis of glaucoma. *Mol Vis*, **14**, p224-233.
- Mulryan K, Gitterman DP, Lewis CJ, Vial C, Leckie BJ, Cobb AL, Brown JE, Conley EC, Buell G, Pritchard CA, Evans RJ, (2000). Reduced vas deferens contraction and male infertility in mice lacking P2X1 receptors. *Nature*, **403**, p86-89.
- Murgia M, Hanau S, Pizzo P, Ripa M, Di Virgilio F, (1993). Oxidized ATP. An irreversible inhibitor of the macrophage purinergic P2Z receptor. *J Biol Chem*, **268**, p8199-203.
- Murphy JM, Czabotar PE, Hildebran JM, Lucet IS, Zhang JG, Alvarez-Diaz S, Leis R, Lalaoui N, (2013). The Pseudokinase MLKL mediates necroptosis via a molecular switch mechanism. *Immunity*, **39**, p443-453.
- Nadal-Nicolas FM, Galindo-Romero C, Valiente-Soriano FJ, Barbera-Cremades M, de Torre-Minguela C, Salinas-Navarro M, Pelegrin P, Agudo-Barriuso M, (2016). Involvement of P2X7 receptor in neuronal degeneration triggered by traumatic injury.
- Nagaya N, Tittle RK, Saar N, Dellal SS, Hume RI, (2005). An intersubunit zinc binding site in rat P2X2 receptors. *J Biol Chem*, **280**, p25982-25993.
- Nakajima K, Kohsaka S, (1993). Functional role of microglia in the brain. *Neurosci Res*, **17**, p187-203.
- Namasivayam V, Lee SY, Muller CE, (2017). The promiscuous ectonucleotidase NPP1: molecular insights into substrate binding and hydrolysis. *Biochem Biophys Acta Gen Subj*, **186**, p603-614
- Naskar R, Wissing M, Thanos S, (2002). Detection of early neuron degeneration and accompanying microglial responses in the retina of a rat model of glaucoma. *Invest Ophthalmol Vis Sci*, **43**, p2962-2968.
- Nawa G, Urano T, Tokino T, Ochi T, Miyoshi Y, (1998). Cloning and characterization of the murine P2XM receptor gene. *J Hum Genet*, **43**, p262-267.

- Neufeld AH, (1999). Microglia in the optic nerve head and the region of parapapillary chorioretinal atrophy in glaucoma. *Arch Ophthalmol*, **117**, p1050-1056.
- Newman EA, (2003). Glial cell inhibition of neurons by release of ATP. *J Neurosci*, **23**, p1659-1666.
- Newman EA, (2004). Glial Modulation of Synaptic Transmission in the retina. *Glia*, **47**, p268-274.
- Nguyen T, Erb L, Weisman GA, Marchese A, Heng HH, Garrad RC, George SR, Turner JT, O'Dowd BF (1995). Cloning, expression, and chromosomal localization of the human uridine nucleotide receptor gene. *J Biol Chem.*, **270**, p30845-30848.
- Nguyen-Legros J, Hicks D (2000). Renewal of photoreceptor outer segments and their phagocytosis by the retinal pigment epithelium. *Int Rev Cytol*, **196**, p245-313.
- Nicke A, (2008). Homotrimeric complexes are the dominant assembly state of native P2X7 subunits. *Biochem Biophys Res Commun*, **377**, p803-808.
- Nicke A, Kuan YH, Masin M, Rettinger J, Marquez-Klaka B, Bender O, Gorecki DC, Murrell-Lagnado RD, Soto F, (2009). A functional P2X7 splice variant with an alternative transmembrane domain 1 escapes gene inactivation in P2X7 knock-out mice. *J Biol Chem*, **284**, 25813-25822.
- Nimmerjahn A, Kirchhoff F, Helmchen F, (2005). Resting microglial cells are highly dynamic surveillants of brain parenchyma in vivo. *Science*, **308**, p1314-1318
- Nishida M, Sato Y, Uemura A, Narita Y, Tozaki-Saitoh H, Nakaya M, Ide T, Suzuki K, Inoue K, Nagao T, Kurose H, (2008). P2Y6 receptor-Galpha12/13 signalling in cardiomyocytes triggers pressure overload-induced cardiac fibrosis. *EMBO J*, **27**, 3104-3115.
- Niyadurupola, N (2009), 'The Development of Human Organotypic Retinal Cultures for Glaucoma Research: P2X7 receptor stimulation and interleukin-1b regulation in relation to retinal ganglion cell death', MD thesis, University of East Anglia, Norwich
- Niyadurupola N, Sidaway P, Ma N, Rhodes JD, Broadway DC, Sanderson J, (2013). P2X7 receptor activation mediates retinal ganglion cell death in a human retina model of ischemic neurodegeneration. *Invest Ophthalmol Vis Sci*, **54**, p2163-2170.

- Niyadurupola N, Sidaway P, Osborne A, Broadway DC, Sanderson J, **95**, p720-726.
- Nobile M, Monaldi I, Alloisio S, Cugnoli C, Ferroni S, (2003). ATP-induced, sustained calcium signalling in cultured rat cortical astrocytes: evidence for a non-capacitave, P2X7-like –mediated calcium entry. *FEBS L*, **538**, p71-76.
- Nomura N, Miyajima N, Sazuka T, Tanaka A, Kawarabayasi Y, Sato S, Nagase T, Seki N, Ishikawa K, Tabata S, (1994). Prediction of the coding sequences of unidentified human genes. I. The coding sequences of 40 new genes (KIAAA0001-KIAA0040) deduced by analysis of randomly sampled cDNA clones from human immature myeloid cell line KG-1. *DNA Res*, **1**, p27-35.
- Norenberg W, Sobottka H, Hempel C, Plotz T, Fischer W, Schmalzing G, Schaefer M, (2012). Positive allosteric modulation by ivermectin of human but not murine P2X7 receptors. *Br J Pharmacol*, **167**, p48-66.
- North RA, (2002). Molecular physiology of P2X receptors. *Physiol Rev*, **82**, 1013-1067.
- North RA, Jarvis MF, (2013), P2X receptors as drug targets. *Mol Pharmacol*, **83**, p759-769.
- Nunez G, London L, Hockenbery D, Alexander M, McKearn JP, Korsmeyer SJ, (1990). Deregulated BCl-2 gene expression selectively prolongs survival of growth factor-deprived hemopoietic cell lines. *J Immuno*, **144**, p3602-3610.
- Ock J, Lee H, Kim S, Lee WH, Choi DK, Park EJ Kim SH, Kim IK, Suk K, (2006). Induction of microglial apoptosis by corticotropin-releasing hormone. *J Neurochem*, **98**, p962-972.
- Ogata T, Schubert P, (1996). Programmed cell death in rat microglia is controlled by extracellular adenosine. *Neurosci Lett*, **218**, p91-94.
- Ohsawa K, Iino Y, Nakamura Y, Akazawa C, Inoue K, Kohsaka S, (2007). Involvement of P2X4 and P2Y12 receptors in ATP-induced microglial chemotaxis. *Glia*, **55**, p604-616.
- Olah ME, (1997). Identification of A2a adenosine receptor domains involved in selective coupling to Gs. Analysis of chimeric A1/A2a adenosine receptors. *J Biol Chem*, **272**, p337-344.

- Olah M, Amor S, Brouwer N, Binet K, Eggen B, Biber K, Boddeke HW, (2012). Identification of a microglia phenotype supportive of remyelination. *Glia*, **60**, p306-321.
- Orrenius S, Zhivotovsky B, Nicotera P, (2003). Regulation of cell death: the calcium-apoptosis link. *Nat Rev Mol Cell Biol*, **4**, p552-565.
- Osterberg G (1935). Topography of the layer of rods and cones in the human retina. *Acta Ophthalmol Suppl*, **6**, p1-103
- Otsu H, Yamamoto A, Maeda N, Mikoshiba K, Tashiro Y, (1990). Immunogold localization of Inositol 1, 4, 5-triphosphate (InP<sub>3</sub>) receptor in mouse cerebellar purkinje cells using three monoclonal antibodies. *Cell Struct Funct*, **15**, 163-173.
- Ottensmeyer PF, Wilzler M, Schulze M, Tobiasch E, (2018). Small Molecules Enhance Scaffold-Based Bone Grafts via Purinergic Receptor Signalling in Stem Cells. *Int J Mol Sci*, **19**, E3601.
- Pagani F, Paolicelli RC, Murana E, Cortese B, Di Angelantonio S, Zurolo E, Guiducci E, Ferreira TA, Garfalo S, Catalano M, D'Alessandro G, Porzia A, Peruzzi G, Mainiero F, Limatola C, Gross CT, Ragozzino D, (2015). Defective microglial development in the hippocampus of Cx3cr1 deficient mice. *Front Cell Neurosci*, **9**, 111.
- Palmer RK, Boyer JL, Schachter JB, Nicholas RA, Harden TK, (1998). Agonist action of adenosine triphosphates at the human P2Y<sub>1</sub> receptor. *Mol Pharmacol*, **54**, p1118-1123.
- Panel WC, Holland GN, Lee DA, Christensen RE, (1990). Glaucoma in patients with uveitis. *Br J Ophthalmol*, **74**, p223-227
- Pang IH, Clark AF, (2007). Rodent models for glaucoma retonopathy and optic neuropathy. *J Glaucoma*, **16**, p483-505.
- Paolicelli RC, Bolasco G, Pagani F, Maggi L, Scianni M, Panzanelli P, Giustetto M, Ferreira TA, Guiducci E, Dumas L, Ragozzino D, Gross CT, (2011). Synaptic pruning by microglia is necessary for normal brain development. *Science*, **333**, p1456-1458.
- Parr CE, Sullivan DM, Paradiso AM, Lazarowski ER, Burch LH, Olsen JC, Erb L, Weisman GA, Boucher RC, Turner JT, (1994). Cloning and expression of a human P2U nucleotide receptor, a target for cystic fibrosis pharmacotherapy. *Proc. Natl. Acad. Sci. USA*, **91**, p3275-3279.
- Parvathani LK, Tertysnikova S, Greco CR, Roberts SB, Roberston B, Posmantur R, (2003). P2X<sub>7</sub> mediates superoxide production

- in primary microglia and is up-regulated in a transgenic mouse model of Alzheimer's disease. *J Biol Chem*, **278**, 13309-13317.
- Patel AS, Reigada D, Mitchell CH, Bates SR, Marquiles SS, Koval M, (2005). **289**, 489-496.
- Pausch MH, Lai M, Tseng E, Paulsen J, Bates B, Kwak S, (2004). Functional expression of human and mouse P2Y<sub>12</sub> receptors in *Saccharomyces cerevisiae*. *Biochem Biophys Res Commun*, **324**, p171-177.
- Payne J, Maher F, Simpson I, Mattice L, Davies P, (1997). Glucose transporter Glut 5 expression in microglial cells. *Glia*, **21**, p327-331.
- Pelegri P, Suprenant A, (2006). Pannexin-1 mediates large pore formation and interleukin-1 $\beta$  release by the ATP-gated P2X<sub>7</sub> receptor. *EMBO J*, **25**, p5071-5082.
- Peng PH, Huang H, Lee Y, Chen Y, Ma M, (2009). Novel role for the delta-opioid receptor in hypoxic preconditioning in rat retinas. *J Neurochem*, **108**, 741-754.
- Perego C, Fumagalli S, De Simoni MG, (2011). Temporal pattern of expression and colocalization of microglia/macrophage phenotype markers following brain ischemic injury in mice. *J Neuroinflammation*, **8**, 174.
- Perez de Lara M, Guzman-Aranquez A, de la Villa P, Diaz-Hernandez JI, Miras-Protugal MT, Pintor J, (2015). Increased levels of extracellular ATP in glaucomatous retinas: Possible role of the vesicular nucleotide transporter during the development of pathology. *Mol Vis*, **21**, p1060-1070.
- Pidlaoan LV, Jin J, Sandhu AK, Athwal RS, Kunapuli SP, (1997). Colocalization of P2Y<sub>2</sub> and P2Y<sub>6</sub> receptor genes at human chromosome 11q13.3-14.2. *Somat Cell Mol Genet*, **23**, p291-296.
- Pihan P, Carreras-Sureda A, Hetz C, (2017). BCL-2 family: integrating stress responses at the ER to control cell demise. *Cell Death Differ*, **24**, p1478-1487
- Pizzirani C, Ferrari D, Chiozzi P, Adinolfi E, Sandona D, Savaglio E, (2007). Stimulation of P2 receptors causes release of IL-1 $\beta$ -loaded microvesicles from human dendritic cells. *Blood*, **109**, p3856-3864.
- Pociot F, Molvig J, Wogensen L, Worsaae H, Nerup J, (1992). A TaqI polymorphism in the human interleukin-1 beta (IL-1 beta) gene

- correlates with IL-1 beta secretion in vitro. *Eur J Clin Invest*, **22**, p396-402.
- Porter AG, Janicke RU, (1999). Emerging roles of caspase-3 in apoptosis. *Cell Death Differ*, **6**, p99-104
- Praetorius HA, Leipziger J, (2009). ATP release from non-excitabile cells. *Purinergic Signal*, **5**, p433-446.
- Prakriya M, Lewis RS, (2010). Store-operated Calcium Channels. *Physiol Rev*, **95**, p1383-1436.
- Przybyla T, Sakowicz-Burkiewicz M, Pawelczyk T, (2018). Purinergic signalling in B cells. *Acta Biochem Pol*, **65**, p1-7
- Punkratov Y, Lalo U, (2015). Role for astroglial  $\alpha$ 1-adrenoreceptors in gliotransmission and control of synaptic plasticity in the neocortex. *Front Cell Neurosci*, **9**, 230.
- Puthussery T, Flethcer EL, (2007). Neuronal expression of P2X3 purinoceptors in the rat retina. *Neuroscience*, **146**, p403-414
- Puyang Z, Feng L, Chen H, Liang P, Troy JB, Liu X, (2016). Retinal ganglion cell loss is delayed following optic nerve crush in NLRP3 knockout mice. *Sci Rep*, **6**, 20998
- Qi AD, Kennedy C, Harden TK, Nicholas RA, (2001). Differential coupling of the human P2Y(11) receptor to phospholipase C and adenylyl cyclase. *Br J Pharmacol*, **132**, p318-326.
- Qu Y, Franchi L, Nunez G, Dubyak GR, (2007). Nonclassical IL-1 beta secretion stimulated by P2X7 receptors is dependent on inflammasome activation and correlated with exosome release in murine macrophages. *J Immunol*, **179**, p1913-1925.
- Qu Y, Misaghi S, Newton K, Gilmour LL, Louie S, Cupp JE, Dubyak GR, Hackos D, Dixit VM. Pannexin-1 is required for ATP release during apoptosis but not for inflammasome activation. *J Immunol*, **186**, p6553-6561.
- Qureshi OS, Paramasivam A, Yu JC, Murrell-Lagnado RD, (2007). Regulation of P2X4 receptors by lysosomal targeting, glycan protection and exocytosis. *J Cell Sci*, **120**, p3838-3849.
- Raas Q, Saih FE, Gondcaille C, Tromprier D, Hamon Y, Leoni V, Caccia C, Nasser B, Jadot M, Menetrier F, Lizard G, Cherkakaoui, M, Andreoletti P, Savary S, (2019). A microglial cell model for acyl-CoA oxidase 1 deficiency. *Biochim Biophys Acta Mol Cell Biol Lipids*. **1864**, p567-576.

- Rafehi M, Malik EM, Neumann A, Albdelrahman A, Hanck T, Namasivayam V, Muller CE, Bagi Y, (2017). Development of Potent and Selective Antagonists for the UTP-Activated P2Y<sub>4</sub> Receptor. *J Med Chem*, **60**, p3020-3038.
- Ransford GA, Fregien N, Qiu F, Dahl G, Conner Gem Salathe M, (2009). Pannexin 1 contributes to ATP release in airway epithelia. *Am J Respir Cell Mol Biol*, **41**, p525-534.
- Ransohoff RM, Perry VH, (2009). Microglial physiology: unique stimuli, specialized responses. *Annu Rev Immunol*, **27**, p119-145.
- Rao S, Morales AA, Pearse DD, (2015). The comparative Utility of Viromer RED and Lipofectamine for Transient Gene Introduction into Glial Cells. *Hindawi*, 458624
- Raouf R, Chabot-Dore AJ, Ase AR, Blais D, Sequela P, (2007). Differential regulation of microglial P2X<sub>4</sub> and P2X<sub>7</sub> ATP receptors following LPS-induced activation. *Neuropharmacology*, **53**, p496-504.
- Rassendren F, Buell GN, Virginio C, Collo G, North RA, Surprenant A, (1997). The permeabilizing ATP receptor, P2X<sub>7</sub>. Cloning and expression of a human cDNA. *J Biol Chem*, **272**, p5482-5486.
- Rayamajhi M, Zhang Y, Miao EA, (2013). Detection of pyroptosis by measuring released lactate dehydrogenase activity. *Methods Mol Biol*, **1040**, p85-90.
- Record M, Subra C, Silvente-Poirot S, Poirot M, (2011). Exosomes as intracellular signalosomes and pharmacological effectors. *Biochem Pharmacol*, **81**, p1171-1182.
- Reigada D, Lu W, Zhang M, Mitchell CH, (2008). Elevated pressure triggers physiological release of ATP from the retina: Possible role for pannexin hemichannels. *Neuroscience*, **157**, p396-404.
- Reigada D, Mitchell CH, (2005). Release of ATP from retinal pigment epithelial cells involves both CFTR and vesicular transport. *Am J Physiol Cell Physiol*, **288**, p132-140.
- Riedl SJ, Salvesen GS (2007). The apoptosome: signalling platform of cell death. *Nat Rev Mol Cell Biol*, **8**, p405-413.
- Roberts JA, Evans RJ, (2007). Cysteine Substitution Mutants Give Structural Insight and Identify ATP Binding and Activation Sites at P2X Receptors. *J Neurosci*, **27**, p4072-4082

- Rodrigues-Neves AC, Aires ID, Vindeirinho J, Boia R, Madeira MH, Goncalves FQ, Cunha RA, Santos PF, Ambrosio AF, Santiago AR, (2018). Elevated Pressure Changes the Purinergic System of Microglial Cells. *Front Pharmacol*, **9**, 16
- Rogers C, Fernandes-Alnemri T, Mayes L, Alnemri D, Cingolani G, Alnemri ES, (2017). Cleavage of DFNA5 by caspase-3 during apoptosis mediates progression to secondary necrotic/pyroptotic cell death. *Nat Commun*, **8**, 14128.
- Rogers JT, Morganti JM, Bachstetter AD, Hudson CE, Peters MM, Grimming BA, Weeber EJ, Bickford PC, Gemma C, (2011). CX3CR1 Deficiency Leads to Impairment of Hippocampal Cognitive Function and Synaptic Plasticity. *J Neurosci*, **31**, p16241-16250.
- Rojas B, Gallego BI, Ramirez AI, Salazarr JJ, de Hoz R, Valiente-Soriano FJ, Aviles-Trigueros M, Villegas-Perez MP, Vidal-Sanz M, Trivino A, Ramirez JM, (2014). Microglia in mouse retina contralateral to experimental glaucoma exhibit multiple signs of activation in all retinal layers. *J Neuroinflammation*, **11**, 133.
- Rokic MB, Tvrdonova V, Vavra V, Jindrichova M, Obsil T, Stojilkovic SS, Zemkova H, (2010). Roles of conserved ectodomain cysteines of the rat P2X<sub>4</sub> purinoreceptor in agonist binding and channel gating. *Physiol Res*, **59**, p927-936.
- Roos WP, Thomas AD, Karina B, (2016). DNA damage and the balance between survival and death in cancer biology. *Nat Rev Cancer*, **16**, p20-33.
- Rubartelli A, Cozzolino F, Talio M, Sitia R, (1990). A novel secretory pathway for interleukin-1 beta, a protein lacking a signal sequence. *EMBO J*, **9**, p1503-1510.
- Ruppelt A, Ma W, Borchardt K, Silberberg SD, Soto F, (2001). Genomic structure, developmental distribution and functional properties of the chicken P2X<sub>5</sub> receptor. *J Neurochem*, **77**, p1256-1265.
- Russo R, Cavaliere F, Watanabe C, Nucci C, Bagetta G, Corasaniti MT, Sakurada S, Morrone LA, (2008). 17Beta-estradiol prevents retinal ganglion cell loss induced by acute rise of intraocular pressure in rat. *Prog Brain Res*, **173**, p583-590.
- Saelens X, Festjens N, Vande Walle L, van Gurp M, van Loo G, Vandenabeele P, (2004). Toxic proteins released from mitochondria in cell death. *Oncogene*, **23**, p2861-2874.

- Sanderson J, Dartt DA, Trinkaus-Randall V, Pintor J, Civan MM, Delamere NA, Fletcher EL, Salt TE, Grosche A, Mitchell CH, (2014). Purines in the eye: recent evidence for the physiological and pathological role of purines in the RPE, retinal neurons, astrocytes, Muller cells, lens, trabecular meshwork, cornea and lacrimal gland. *Exp Eye Res*, **127**, p270-279.
- Santos AM, Calvente R, Tassi M, Carrasco MC, Martin-Oliva D, Marin-Teva JL, Navascues J, Cuadros MA, (2008). Embryonic and postnatal development of microglial cells in the mouse retina. *J Comp Neurol*, **10**, p224-239.
- Santos-Carvalho A, Ivaro AR, Martins J, Ambrosio AF, Cavadas C (2014). Emerging novel roles of neuropeptide Y in the retina: from neuromodulation to neuroprotection. *Prog Neurobiol*, **112**, p70-79.
- Sanz JM, Chiozzi P, Ferrari D, Colaianna M, Idzko M, Falzoni S, Fellin R, Trabace L, Di Virgilio F, (2009). Activation of microglia by amyloid {beta} requires P2X7 receptor expression. *J Immunol*, **182**, p4378-4385.
- Sanz JM, Di Virgilio F, (2000). Kinetics and mechanism of ATP-dependent IL-1 beta release from microglial cells. *J Immunol*, **164**, p4893-4898.
- Sasaki Y, Hoshi M, Akazawa C, Nakamura Y, Tsuzuki H, Inoue K, Kohsaka S, (2003). Selective expression of Gi/o-coupled ATP receptor P2Y12 in microglia in rat brain. *Glia*, **44**, p242-250.
- Satoh J, Kino Y, Asahina N, Takitani M, Miyoshi J, Ishida T, Saito Y, (2016). TMEM119 marks a subset of microglia in the human brain. *Neuropathology*, **36**, p39-49.
- Saul A, Hausmann R, Kless A, Nicke A, (2013). Heteromeric assembly of P2X subunits. *Front Cell Neurosci*, **7**, 250.
- Savage CD, Lopez-Castejon G, Denes A, Brough D, (2012). NLRP3-Inflammasome Activating DAMPs Stimulate an Inflammatory Response in Glia in the Absence of Priming Which Contributes to Brain Inflammation after injury. *Front Immunol*, **3**, 288.
- Savi P, Pereillo JM, Uzabiaga MF, Combalbert J, Picard C, Maffrand JP, Pascal M, Herbert JM, (2000). Identification and biological activity of the active metabolite of clopidogrel. *Thromb Haemost*, **84**, p891-896.

- Sawada K, Echigo N, Juge N, Miyaji T, Otsuka M, Omote H, Yamamoto A, Moriyama Y, (2008). Identification of a vesicular nucleotide transporter. *Proc Natl Acad Sci USA*, **105**, p5683-5686.
- Sawynok J, (2016). Adenosine receptor targets for pain. *Neuroscience*, **338**, p1-18.
- Scanlon ST, (2018). Caspase-8 is a player in pyroptosis. *Science*, **362**, p1014-1016.
- Scase TJ, Heath MF, Allen JM, Sage SO, Evans RJ, (1998). Identification of a P2X1 purinoceptor expressed on human platelets. *Biochem Biophys Res Commun*, **242**, p525-528
- Schafer DP, Lehrman EK, Kautzman AG, Koyama R, Mardinly AR, Yamasaki R, Ransohoff RM, Greenberg ME, Barres BA, Stevens B, (2012). Microglia sculpt postnatal neural circuits in an activity and complement-dependent manner. *Neuron*, **74**, p691-705.
- Schmid-Brunclik N, Burgi-Taboada C, Antoniou X, Gassmann M, Ogunshola OO, (2008). Astrocyte responses to injury: VEGF simultaneously modulates cell death and proliferation. *Am J Physiol Regul Integr Comp Physiol*, **295**, p864-873.
- Schmidt P, Ritscher L, Dong EN, Hemsdorf T, Coster M, Wittkopf D, Meiler J, Schoneberg T, (2013). Identification of Determinates Required for Agonistic and Inverse Agonistic Ligand Properties at the ADP Receptor P2Y<sub>12</sub>. *Mol Pharmacol*, **83**, p256-266.
- Schroder K, Tschopp J, (2010). The inflammasomes. *Cell*, **140**, p821-832.
- Schuetz E, Thanos S, (2004). Neuro-glial interactions in the adult rat retina after reaxotomy of ganglion cells: examination of neuron survival and phagocytic microglia using fluorescent tracers. *Brain Res Bull*, **62**, p391-396.
- Sebbagh M, Renvoize C, Hamelin J, Riche N, Bertoglio J, Breard J, (2001). Caspas-3-mediated cleavage of ROCK I induces MLC phosphorylation and apoptotic membrane blebbing. *Nat Cell Biol*, **3**, 346-352.
- Séguéla P, Haghghi A, Soghomonian JJ, Cooper E, (1996). A novel neuronal P2x ATP receptor ion channel with widespread distribution in the brain. *J Neurosci*, **16**, p448-455.
- Sekar P, Huang DY, Hsieh SL, Chang SF, Lin WW, (2018). AMPK-dependent and independent actions of P2X7 in regulation of mitochondrial and lysosomal functions in microglial. *Cell Commun Signal*, **16**, 83.

- Seo DR, Kim KY, Lee YB, (2004). Interleukin-10 expression in lipopolysaccharide-activated microglia is mediated by extracellular ATP in an autocrine fashion. *Neuroreport*, **15**, p1157-1167.
- Seo DR, Kim SY, Kim KY, Lee HG, Moon JH, Lee JS, Lee SH, Kim SU, Lee YB, (2008). Cross talk between P2 purinergic receptors modulates extracellular ATP-mediated interleukin-10 production in rat microglial cells. *Exp Mol Med*, **40**, p19-26.
- Shi J, Zhao Y, Wang Y, Gao W, Ding J, Li P, Hu L, Shao F, (2014). Inflammatory caspases are innate immune receptors for intracellular LPS. *Nature*, **514**, 187-192.
- Shieh CH, Heinrich A, Serchov T, van Calker D, Biber K, (2014). P2X7-dependent, but differently regulated release of IL-6, CCL2 and TNF-alpha in cultured mouse microglia. *Glia*, **62**, 592-607.
- Shigematsu Y, Shimoda Y, Kaneda M, (2007). Distribution of immunoreactivity for P2X3, P2X5, and P2X6-purinoceptors in mouse retina. *J Mol Histol*, **38**, p369-371.
- Shin WH, Lee DY, Park KW, Kim SU, Yang MS, Joe EH, Jin BK, (2004). Microglia expressing interleukin-13 undergo cell death and contribute to neuronal survival in vivo.
- Sierra A, Encinas JM, Deudero JJ, Chancey JH, Enikolopov G, Overstreet-Wadiche LS, Tsirka SE, Maletic-Savatic M, (2010). Microglia shape adult hippocampal neurogenesis through apoptosis-coupled phagocytosis. *Cell Stem Cell*, **7**, p483-495.
- Silinsky EM, (1975). On the association between transmitter secretion and the release of adenine nucleotides from mammalian motor nerve terminals. *J Physiol*, **247**, p145-162.
- Singer II, Scott S, Hall GL, Limjuco G, Chin J, Schmidt JA, (1988). Interleukin 1 beta is localized in the cytoplasmic ground substance but is largely absent from the Golgi apparatus and plasma membranes of stimulated human monocytes. *J Exp Med*, **167**, p389-407.
- Silva MT, (2010). Secondary necrosis: The natural outcome of the complete apoptotic program. *FEBS Lett*, **584**, p4491-4499.
- Silver IA, Deaa J, Erecinska M, (1997). Ion homeostasis in brain cells: differences in intracellular ion responses to energy limitation between cultured neurons and glial cells. *Neuroscience*, **78**, p589-601

- Simon J, Filippov AK, Göransson S, Wong YH, Frelin C, Michel AD, Brown DA, Barnard EA, (2002). Characterization and channel coupling of the P2Y(12) nucleotide receptor of brain capillary endothelial cells. *J Biol Chem*, **277**, p31390-31400.
- Sim JA, Park CK, Oh SB, Evans RJ, North RA, (2007). P2X1 and P2X4 receptor currents in mouse macrophages. *Br J Pharmacol*, **152**, 1283-1290.
- Sierra A, Abiega O, Shahraz A, Neumann H, (2013). Janus-faced microglia: beneficial and detrimental consequences of microglial phagocytosis. *Front Cell Neurosci*, **7**, 6
- Sluyter R, Barden JA, Wiley JS, (2001). Detection of P2X purinergic receptors on human B lymphocytes. *Cell Tissue Res.*, **304**, p231-236.
- Sluyter R, Stokes L, (2011). Significance of P2X7 receptor variants to human health and disease. *Recent Pat DNA Gene Seq*, **5**, p41-45.
- Smart ML, Gu B, Panchal RG, Wiley J, Cromer B, Williams DA, Petrou S, (2003). P2X7 receptor cell surface expression and cytolytic pore formation are regulated by distal C-terminal region. *J Biol Chem*, **278**, p8853-8860.
- Smolders S, Kessels S, Smolders SM, Poulhes F, Zelphati O, Sapet C, Brone B, (2018). Magnetofection is superior to other chemical transfection to other chemical transfection methods in microglial cell line. *J Neurosci Methods*, **293**, 169-173.
- Smith SM, Mitchell GS, Friedle SA, Sibigtroth CM, Vinit S, Watters JJ, (2013). Hypoxia Attenuates purinergic P2X Receptor-Induced Inflammatory Gene Expression in Brainstem Microglia. *Hypoxia (Auckl)*, **1**
- Solini A, Chiozzi P, Morelli A, Fellin R, Di Virgilio F, (1999). Human primary fibroblasts in vitro express a purinergic P2X7 receptor coupled to ion fluxes, microvesicle formation and IL-6 release. *J Cell Sci*, **112**, p297-305.
- Soto F, Garcia-Guzman M, Gomez-Hernandez JM, Hollmann M, Karschin C, Stühmer W, (1996a). P2X4: an ATP-activated ionotropic receptor cloned from rat brain. *Proc Natl Acad Sci USA*, **93**, 3684-3688.
- Soto F, Garcia-Guzman M, Karschin C, Stuhmer W, (1996). Cloning and tissue distribution of a novel P2X receptor from rat brain. *Biochem Biophys Res Commun*, **223**, p-456-460.

- Sperligh B, Illes P, (2007). Purinergic modulation of microglial cell activation. *Purinergic Signal*, **3**, p117-127
- Sperligh B, Vizi ES, Wirkner K, Illes P, (2006). P2X7 receptors in the nervous system. *Prog Neurobiol*, **78**, p327-346.
- Stansley B, Post J, Hensley K, (2012). A comparative review of cell culture systems for the study of microglial biology in Alzheimer's disease. *J Neuroinflammation*, **9**, 115.
- Steinberg SH (1985). Interactions between the retinal pigment epithelium and neural retina. *Doc Ophthalmol*, **60**, p327-346.
- Stevens B, Allen NJ, Vazquez LE, Howell GR, Christopherson KS, Nouri N, Micheva KD, Mehalow AK, Huberman AD, Stafford B, Sher A, Litke AM, Lambris JD, Smith SJ, John SW, Barres BA, (2007). The classical complement cascade mediates CNS synapse elimination. *Cell*, **131**, p1164-1178.
- Stojilkovic SS, Tomic M, He ML, Yan Z, Koshimizu TA, Zemkova H, (2005). Molecular dissection of purinergic P2X receptor channels. *Ann N Y Acad Sci*, **1048**, p116-130.
- Stokes L, Fuller SJ, Sluyter R, Skarratt KK, Gu BJ, Wiley JS, (2010). Two haplotypes of the P2X(7) receptor containing the Ala-348 to Thr polymorphism exhibits a gain-of-function effect and enhanced interleukin-1beta secretion. *FASEB J*, **24**, p2916-2927
- Stokes L, Layhadi JA, Bibic L, Dhuna Kshitija, Fountain S, (2017). P2X4 Receptor Function in the Nervous System and Current Breakthroughs in Pharmacology. *Front Pharmacol*, **8**, 291.
- Stokes L, Scurrah K, Ellis JA, Cromer BA, Skarratt KK, Gu BJ, Harrap SB, Wiley JS, (2011). A loss-of-function polymorphism in the human P2X4 receptor is associated with increased pulse pressure. *Hypertension*, **58**, p1086-1092.
- Stokes L, Suprenant A, (2009). Dynamic regulation of the P2X4 receptor in alveolar macrophages by phagocytosis and classical activation, *Eur J Immunol*. **39**, p986-995.
- Stoop R, Suprenant A, North RA, (1997). Different sensitivities to pH of ATP-induced currents at four cloned P2X receptors. *J Neurophysiol*, **78**, p1837-1840.
- Streit WJ, Walter SA, Pennell NA, (1999). Reactive microgliosis. *Prog Neurobiol*, **57**, p563-581.

- Sudhof TC, Rothman JE, (2009). Membrane fusion: grappling with SNARE and SM proteins. *Science*, **323**, p474-477.
- Sugiyama T, Lee SY, Horie T, Oku H, Takai S, Tanioka H, Kuriki Y, Kojima S, Ikeda T, (2013). P2X7 receptor activation may be involved in neuronal loss in the retinal ganglion cell layer after acute elevation of intraocular pressure in rats. *Mol Vis*, **19**, p2080-2091.
- Sugiyama T, Oku H, Shibata M, Fukuhara M, Yoshida H, Ikeda T, (2010). Involvement of P2X7 receptors in the hypoxia-induced death of rat retinal neurons. *Invest Ophthalmol Vis Sci*, **51**, p3236-3243.
- Summersgill H, England H, Lopez-Castejon G, Lawrence CB, Luheshi NM, Pahle J, Mendes P, Brough D, (2014). Zinc depletion regulates the processing and secretion of IL-1b. *Cell Death Dis*, **30**, e1040.
- Suplat D, Krzeminski P, Pomorski P, Baranska J, (2007). P2Y(1) and P2Y(12) receptor cross-talk in calcium signalling: Evidence from nonstarved and long term serum-deprived glioma C6 cells. *Purinergic Signal*, **3**, p221-230.
- Suprenant A, Rassendren F, Kawashima E, North RA, Buell G, (1996). The cytolytic P2Z receptor for extracellular ATP identified as a P2X receptor (P2X7). *Science*, **272**, p735-738.
- Syed N, Kennedy C, (2012). Pharmacology of P2X receptors. *WIREs WIREs Membr Transp Signal*, **1**, p16-30.
- Tait SW, Green DR, (2010). Mitochondria and cell death: outer membrane permeabilization and beyond. *Nat Rev Cell Biol*, **11**, 621-632.
- Takai Y, Tanito M, Ohira A, (2012). Multiplex cytokine analysis of aqueous humor in eyes with primar open-angle glaucoma, exfoliation glaucoma, and cataract. *Invest Ophthalmol Vis Sci*, **53**, 241-247.
- Takasaki J, Kamohara M, Saito T, Matsumoto M, Matsumoto S, Ohishi T, Soga T, Matsushime H, Furuichi K, (2001). Molecular cloning of the platelet P2T(AC) ADP receptor: pharmacological comparison with another ADP receptor, the P2Y(1) receptor. *Mol Pharmacol*, **60** p432-439.
- Takenouchi T, Sekiyama K, Sekigawa A, Futija M, Maragai M, Sugama S, Iwamaru Y, Kitani H, Hashimoto M, (2010). P2X7 receptor

signaling pathway as a therapeutic target for neurodegenerative diseases. *Arch Immunol Ther Exp (Warsz)*, **58**, p91-96.

Tanaka T, Saito H, Matsuki N, (1997). Inhibition of GABA<sub>A</sub> synaptic responses by brain-derived neurotrophic factor (BDNF) in rat hippocampus. *J Neurosci*, **17**, p2959-2966.

Taylor S, Calder CJ, Albon J, Erichsen JT, Boulton ME, Morgan JE, (2011). Involvement of the CD200 receptor complex in microglia activation in experimental glaucoma. *Exp Eye Res*, **92**, p338-343.

Thanos S, (1991). The relationship of microglial cells to dying neurons during natural neuronal cell-death and axotomy-induced degeneration of the rat retina. *Eur J Neurosci*, **3**, p1189-1207.

Thornberry NA, Bull HG, Calaycay JR, Chapman KT, Howard D, Kostura MJ, Miller DK, Molineaux SM, Weidner JR, Aunins J (1992). A novel heterodimeric cysteine protease is required for interleukin-1 beta processing in monocytes. *Nature*, **356**, p768-774.

Tokuyama Y, Hara M, Jones EMC, Fan Z, Bell GI, (1995). Cloning of Rat and Mouse P-2Y Purinoceptors. *Biochem Biophys Res Commun*, **211**, p211-218.

Torres GE, Egan TM, Voigt MM, (1999). Hetero-oligomeric assembly of P2X receptor subunits. Specificities exist with regard to possible partners. *J Biol Chem*, **274**, p6653-6659.

Tovell VE, Sanderson J, (2008). Distinct P2Y receptor subtypes regulate calcium signalling in human retinal pigment epithelial cells. *Invest Ophthalmol Vis Sci*, **49**, p350-357.

Tozaki-Saitoh H, Tsuda M, Inou K, (2012). P2Y receptors in microglia and neuroinflammation. *WIREs Membr Transp Signal*, **1**, p493-501.

Tozzi M, Larsem A, Lange SC, Giannuzzo A, Andersen MN, Novak, I, (2018). The P2X7 receptor and pannexin-1 are involved in glucose-induced autocrine regulation in BETA-cells.

Tremblay ME, Lowery RL, Majewska AK, (2010). Microglial interactions with synapses are modulated by visual experience. *PLoS Biol*, **8**, e1000527

Tsuda M, Shigemoto-Mogami Y, Koizumi S, Mizokoshi A, Kohsaka S, Salter MW, Inoue K, (2003). P2X4 receptors induced in spinal

- microglia gate tactile allodynia after nerve injury. *Nature*, **424**, p778-783.
- Ulmann L, Hatcher JP, Hughes JP, Chaumont S, Green PJ, Conquet F, Buell GN, Reeve AJ, Chessell IP, Rassendren F, (2008). Up-regulation of P2X4 receptors in spinal microglia after peripheral nerve injury mediates BDNF release and neuropathic pain. *J Neurosci*, **28**, p11263-11268.
- Ulvestad E, Williams K, Matre R, Nayland H, Olivier A, Antel J, (199) Fc receptors for IgG on cultured human microglia mediate cytotoxicity and phagocytosis of antibody-coated targets. *J Neuropathol Exp Neurol*, **53**, p27-36.
- Unsworth CD, Johnson RG jr, (1990). ATP compartmentation in neuroendocrine secretory vesicles. *Ann N Y Acad Sci*, **603**, p353-365.
- Urano T, Nishimori H, Han H, Furuhashi T, Kimura Y, Nakamura Y, Tokino T, (1997). Cloning of P2XM, a novel human P2X receptor gene regulated by p53. *Cancer Res*, **57**, p3281-3287.
- Vajjhala PR, Mirams RE, Hill JM, (2012). Multiple binding sites on the pyrin domain of ASC protein allow self-association and interaction with NLRP3 protein. *J Biol Chem*, **287**, p41732-41743.
- Valera S, Hussy N, Evans RJ, Adami N, North RA, Surprenant A, Buell G, (1994). A new class of ligand-gated ion channel defined by P2x receptor for extracellular ATP. *Nature*, **371**, p516-519.
- van Overbeek M, Capurso D, Carter MM, Thompson MS, Frias E, Russ C, Reece-Hoyes JS, Nye C, Gradia S, Vidal B, Zheng J, Hoffman GR, Fuller CK, May AP (2016). DNA repair Profiling Reveals Nonrandom Outcomes at Cas9-Mediated Breaks. *Mol Cell*, **63**, p633-646.
- Vandenabeele P, Galluzzi L, Vanden Berghe T, Kroemer G, (2010). Molecular mechanism of necroptosis: an ordered cellular explosion. *Nat Rev Mol Cell Biol* **11**, p700-714.
- Vazquez-Villoldo N, Domercq M, Martin A, Llop J, Gomez-Vallejo V, Matute C, (2014). P2X4 receptors control the fate and survival of activated microglia. *Glia*, **62**, p171-184.
- Vecino E, Acera A, (2015). Development and programmed cell death in the mammalian eye. *Int J Dev Biol*, **59**, p63-71.

- Vecino E, Rodriguez F, Ruzafa N, Pereiro X, Sharma SC, (2016). Glia-neuron interactions in the mammalian retina. *Prog Retin Eye Res*, **51**, p1-40.
- Vercammen D, Brouckaert G, Denecker G, G, Van de Cran M, Declercq W, Fiers W, Vandenabeele, (1998). Dual signalling of the Fas receptor: initiation of both apoptotic and necrotic cell death pathways. *J Exp Med*, **188**, p919-930.
- Vercammen D, Vandenabeele P, Beyaert R, Declercq W, Fiers W, (1997). Tumour necrosis factor-induced necrosis versus anti-Fas-induced apoptosis in L929 cells. *Cytokine*, **9**, 801-808.
- Vial C, Evans RJ, (2000). P2X receptor expression in mouse urinary bladder and the requirement of P2X(1) receptors for functional P2X receptor responses in the mouse urinary bladder smooth muscle. *Br J Pharmacol*, **131**, p1489-1495.
- Vial C, Evans RJ, (2001). Smooth muscle does not have a common P2x receptor phenotype: expression, ontogeny and function of P2x1 receptors in mouse ileum, bladder and reproductive systems. *Auton Neurosci*, **92**, p56-64.
- Vial C, Evans RJ, (2002). P2X(1) receptor-deficient mice establish the native P2X receptor and a P2Y6-like receptor in arteries. *Mol Pharmacol*, **62**, p1438-1445
- Vial C, Hechler B, Léon C, Cazenave JP, Gachet C, (1997). Presence of P2X1 purinoceptors in human platelets and megakaryoblastic cell lines. *Thromb. Haemost*, **78**, p1500-1504.
- Virginio C, MacKenzie A, North RA, Surprenant A, (1999). Kinetics of cell lysis dye uptake and permeability changes in cells expressing the rat P2X7 receptor. *J Physiol*, **519**, p335-346.
- Virginio C, Robertson G, Surprenant A, North RA, (1998). Trinitrophenyl-substituted nucleotides are potent antagonists selective for P2X1, P2X3, and heteromeric P2X2/3 receptors. *Mol Pharmacol*, **53**, p969-973.
- Visentin S, Renzi M, Frank C, Greco A, Levi G, (1999). Two different ionotropic receptors are activated by ATP in rat microglia. *J Physiol*, **519**, 723-736.
- Visentin S, Nuccio CD, Bellenchi GC, (2006). Different patterns of Ca<sup>2+</sup> signals are induced by low compared to high concentrations of P2Y agonists in microglia. *Purinergic Signal*, **2**, p605-617.

- von Kugelen I, (2019). Pharmacology of P2Y receptors. *Brain Res Bull*, **151**, p-12-24.
- von Kugelgen I, Hoffmann K, (2016). Pharmacology and structure of P2Y receptors. *Neuropharmacology*, **104**, p50-61.
- Waldo GL, Corbitt J, Boyer JL, Ravi G, Kim HS, Ji XD, Lacy J, Jacobson KA, Harden TK, (2002). Quantitation of the P2Y<sub>1</sub> Receptor with a High Affinity Radiolabeled Antagonist. *Mol Pharmacol*, **62**, p1249-1257.
- Walker JE, Saraste M, Runswick MJ, Gay NJ, (1982). Distantly related sequences in the alpha- and beta-subunits of ATP synthase, myosin, kinases and other ATP-requiring enzymes and a common nucleotide binding fold. *EMBO J*, **1**, p945-951.
- Walton NM, Sutter BM, Laywell ED, Levkoff LH, Kearns SM, Marshall GP 2<sup>nd</sup>, Scheffler B, Steindler DA, (2006). Microglia instruct subventricular zone neurogenesis. *Glia*, **54**, p815-824.
- Walz W, Ilschner S, Ohlemeyer C, Banati R, Kettenmann H, (1993). Extracellular ATP activates a cation conductance and a K<sup>+</sup> conductance in cultured microglial cells from mouse brain. *J Neurosci*, **13**, p4403-4411.
- Wang CZ, Namba N, Gono T, Inagaki N, Seino S, (1996). Cloning and pharmacological characterization of a fourth P2X receptor subtype widely expressed in brain and peripheral tissues including various endocrine tissues. *Biochem Biophys Res Commun*, **220**, p196-202.
- Wang L, Jacobsen SE, Bengtsson A, Erlinge D, (2004). P2 receptor mRNA expression profiles in human lymphocytes, monocytes and CD34<sup>+</sup> stem and progenitor cells. *BMC Immunol*, **5**, 16.
- Wang L, Karlsson L, Moses S, Hultgårdh-Nilsson A, Andersson M, Bornha C, Gudbjartsson T, Jern S, Erlinge D, (2002). P2 receptor expression profiles in human vascular smooth muscle and endothelial cells. *J Cardiovasc Pharmacol*, **40**, p841-853.
- Wang MH, Wang X, Zhao L, Ma WX, Rodriguez IR, (2014). Macroglia-Microglia Interactions via TSPO Signalling Regulates Microglial Activation in the Mouse Retina. *J Neurosci*, **34**, p3793-3806.
- Wang MH, Wong WT, (2014). Microglia-Müller cell interactions in the retina. *Adv Exp Med Biol*, **801**, p333-338.
- Wareham K, Vial C, Wykes RC, Bradding P, Seward EP, (2009). Functional evidence for the expression of P2X<sub>1</sub>, P2X<sub>4</sub>

- and P2X7 receptors in human lung mast cells. *Br J Pharmacol*, **157**, p1215-1224.
- Webb TE, Simon J, Krishek BJ, Bateson AN, Smart TG, King BF, Burnstock G, Barnard EA, (1993). Cloning and functional expression of a brain G-protein-coupled ATP receptor. *FEBS Lett*, **324**, p219-225.
- Weinhard L, Bartolomei G, Bolasco G, Machado P, Schieber NL, Neniskyte U, Exiga M, Vadasiute A, Raggioli A, Schertel A, Schwab Y, Gross CT, (2018). Microglia remodel synapses by presynaptic trogocytosis and spine head filopodia induction. *Nat Commun*, **9**, 1228.
- White PJ, Webb TE, Boarder MR, (2003). Characterization of a Ca<sup>2+</sup> response to both UTP and ATP at human P2Y11 receptors: evidence for agonist-specific signaling. *Mol Pharmacol*, **63**, p1356-1363.
- Wheeler-Schilling TH, Marquardt K, Kohler K, Jabs R, Guenther E, (2000). Expression of purinergic receptors in bipolar cells of the rat retina. *Brain Res Mol Brain Res*, **76**, p415-418.
- Wildman SS, King BF, Burnstock G, (1998). Zn<sup>2+</sup> modulation of ATP-responses at recombinant P2X2 receptors and its dependence on extracellular pH. *Br J Pharmacol*, **123**, p1214-1220.
- Wilkinson WJ, Jiang LH, Suprenant A, North RA, (2006). Role of ectodomain lysines in the subunits of the heteromeric P2X2/3 receptor. *Mol Pharmacol*, **70**, p1159-1163.
- Willoughby CE, Ponzin D, Ferrari S, Lobo A, Landau K, Omidy Y (2010). Anatomy and physiology of the human eye: effects of mucopolysaccharidoses disease on structure and function – a review. *J Clin Exp Ophthalmol*, **38**, p2-11.
- Winkler B, Arnold M, Brassell M, Puro D, (2000). Energy Metabolism in Human Müller Cells. *Invest Ophthalmol Vis Sci*, **41**, p3183-3190.
- Wittenberger T, Schaller HC, Hellebrand S, (2001). An expressed sequence tag (EST) data mining strategy succeeding in the discovery of new G-protein coupled receptors. *J Mol Biol*, **307**, p799-813.
- Wurm A, Erdmann I, Bringmann A, Reichenbach A, Pannicke T, (2009). Expression and function of P2Y receptors on Müller cells of the postnatal rat retina. *Glia*, **57**, p1680-90.

- Xiang Z, Burnstock G, (2005). Expression of P2X receptors on rat microglial cells during early development. *Glia*, **52**, p119-126.
- Xue Y, Xie Y, Xue B, Hu N, Zhang G, Guan H, Ji M, (2016). Activated Muller cells involved in ATP-induced upregulation of P2X7 receptor expression and retinal ganglion cell death. *Biomed Res Int*, 9020715.
- Yao J, Keri JE, Taffs RE, Colton CA, (1992). Characterization of interleukin-1 production by microglia in culture. *Brain Res*, **591**, p88-93.
- Yang D, He Y, Munoz-Planillo R, Liu Q, Nunez G. (2015). Caspase-11 requires the pannexin-1 channel and the purinergic P2X7 pore to mediate pyroptosis and endotoxin shock. *Immunity*, **43**, 923-932.
- Yang Z, Zhong L, Zhong S, Xian R, Yuan B, (2015b). Hypoxia induces microglia autophagy and neural inflammation injury in focal cerebral ischemia model. *Exp Mol Pathol*, **98**, p219-224.
- Yang MS, Ji KA, Jeon SB, Jin BK, Kim SU, Jou I Joe E, (2006). Interleukin-13 enhances cyclooxygenase-2 expression in activated rat brain microglia: implications for death of activated microglia. *J Immunol*, **177**, 1323-1329.
- Yang MS, Park EJ, Sohn S, Kwon HJ, Shin WH, Pyo HK, Jin B, Choi KS, Jou I, Joe H, (2002). Interleukin-13 and -4 induce death of activated microglia. *Glia*, **38**, 273-280.
- Yenari MA, Giffard RG, (2001). Ischemic vulnerability of primary murine microglial cultures. *Neurosci Lett*, **298**, p5-8.
- Yin J, Valin KL, Dixon ML, Leavenworth JW, (2017). The Role of Microglia and macrophages in CNS Homeostasis, Autoimmunity and Cancer. *J Immunol Res*, 5150678.
- Yoneda S, Tanihara H, Kido N, Honda Y, Goto W, Hara H, Miyawaki N, (2001). Interleukin-1 $\beta$  mediates ischemic injury in the rat retina. *Exp Eye Res*, **73**, p661-667.
- Yu DY, Cringle SJ (2001). Oxygen distribution and consumption within the retina in vascularised and avascular retinas and in animal models of retinal disease. *Prog Retin Eye Res*, **20**, p175-208.
- Yu J, Ciancetta A, Dudas S, Duca S, Lottermoser J, Jacobson KA. (2018) Structure-Guided Modification of Heterocyclic Antagonists of the P2Y<sub>14</sub> Receptor. *J Med Chem*, **61**, p4860-4882.

- Yuan J, Najafov A, Py BF, (2016). Roles of caspases in necrotic cell death. *Cell*, **167**, p1693-1704.
- Yuan T, Liang Y, Peng B, Lin B, So K, (2015). Local proliferation is the main source of rod microglia after optic nerve transection. *Sci Rep*, **5**, 10788.
- Yuan L, Neufeld AH, (2000). Tumor necrosis factor-alpha: A potentially neurodestructive cytokine produced by glia in the human glaucomatous optic nerve head. *Glia*, **32**, p42-50.
- Yuan L, Neufeld AH, (2001). Activated microglia in the human glaucomatous optic nerve head. *J Neurosci Res*, **64**, p523-532.
- Zanovello P, Bronte P, Rosato A, Pizzo P, Di Virgilio F, (1990). Responses of mouse lymphocytes to extracellular ATP. II. Extracellular ATP causes cell type –dependent lysis and DNA fragmentation. *J Immunol*, **145**, p1545-1550.
- Zhan Y, Paolicelli RC, Sforazzini F, Weinhard L, Bolasco G, Pagani F, Vyssotski AL, Bifone A, Gozzi A, Ragozzino D, Gross CT, (2014). Deficient neuron-microglia signalling results in impaired functional brain connectivity and social behaviour. *Nat Neurosci*, **17**, p400-406.
- Zhang X, Chintala SK, (2004). Influence of interleukin-1 beta induction and mitogen-activated protein kinase phosphorylation on optic nerve ligation-induced matrix metalloproteinase-9 activation in the retina. *Exp Eye Res*, **78**, 849-860.
- Zhang X, Li A, Ge J, Reigada D, Laties AM, Mitchell CH, (2007). Acute increase of ocular pressure releases ATP into the anterior chamber. *Exp Eye Res*, **85**, p637-643.
- Zhang D, Gao ZG, Zhang K, Kiselev E, Crane S, Wang J, Paoletta S, Yi C, Ma L, Zhang W, Han GW, Liu H, Cherezov V, Katritch V, Jiang H, Stevens RC, Jacobson KA, Zhao Q, Wu B, (2015). Two disparate ligand-binding sites in the human P2Y<sub>1</sub> receptor. *Nature*, **520**, p317-321.
- Zhang FL, Luo L, Gustafson E, Palmer K, Qiao X, Fan X, Yang S, Laz TM, Bayne M, Monsma Jr F, (2002). P2Y<sub>13</sub>: identification and characterization of a novel G<sub>α</sub>hi-coupled ADP receptor from human and mouse. *J Pharmacol Exp Ther*, **301**, p705-713.
- Zhang J, Zhang K, Gao ZG, Paoletta S, Zhang D, Han GW, Li T, Ma L, Zhang W, Muller CE, Yang H, Jiang H, Cherezov V, Katritch V, Jacobson K, Stevens RC, Wu B, Zhao Q, (2014a). Agonist-bound structure of the human P2Y<sub>12</sub> receptor. *Nature*, **509**, p119-122.

- Zhang K, Zhang J, Gao ZG, Zhang D, Zhu L, Han GW, Moss SM, Paoletta S, Kiselev E, Lu W, Fenalti G, Zhang W, Muller CE, Yang H, Jiang H, Cherezov V, Katrich V, Jacobson KA, Stevens RC, Wu B, Zhao Q, (2014b), Structure of the human P2Y<sub>12</sub> receptor in complex with an antithrombotic drug. *Nature*, **509**, p115-118.
- Zhang L, Dong LY, Li YJ, Hong Z, Wei WS, (2012). miR-21 Represses FasL in Microglia and Protects Against Microglial-Mediated Neuronal Cell Death Following Hypoxia/Ischemia. *Glia*, **60**, 1888-1895.
- Zhang Xm Zhang M, Laties AM, Mitchell CH, (2005). Stimulation of P2X<sub>7</sub> receptors elevates Ca<sup>2+</sup> and kills retinal ganglion cells. *Invest Ophthalmol Vis Sci*, **46**, p2183-2191.
- Zhang Xm Zhang M, Laties AM, Mitchell CH, (2005). Balance of purines may determine life or death in retinal ganglion cells as A<sub>3</sub> receptors prevent loss following P2X<sub>7</sub> receptor stimulation. *J Neurochem*, **98**, p566-575.
- Zhou QY, Li C, Olah ME, Johnson RA, Stiles GL, Civelli O, (1992). Molecular cloning and characterization of an adenosine receptor: the A<sub>3</sub> adenosine receptor. *Proc Natl Acad Sci USA*, **89**, p7432-7436.
- Zhu C, Kros JM, van der Weiden M, Zheng P, Cheng C, Mustafa DAM, (2017). Expression site of P2RY<sub>12</sub> in residential microglial cells in astrocytomas correlates with M1 and M2 marker expression and tumor grade. *Acta neuropathol Commun*, **5**, 4.